SHEAR BEHAVIOUR AND STIFFNESS OF NATURALLY CEMENTED SANDS

by

Teresa Cuccovillo

A thesis submitted for the degree of
Doctor of Philosophy

Geotechnical Engineering Research Centre
City University
London

December 1995

CONTENTS

LIST OF TABLES 5

LIST OF FIGURES 6

ACKNOWLEDGEMENTS 16

DECLARATION 17

ABSTRACT 18

NOMENCLATURE 19

1. INTRODUCTION 22

2. LITERATURE REVIEW 27
- 2.1 INTRODUCTION 27
- 2.2 THE BEHAVIOUR OF NATURAL CLAYS 28
  - 2.2.1 One-dimensional compression 28
  - 2.2.2 Shearing 32
- 2.3 THE SHEAR BEHAVIOUR OF SANDS 35
- 2.4 STRUCTURE IN NATURALLY CEMENTED SANDS 40
- 2.5 THE BEHAVIOUR OF CEMENTED SANDS AND WEAK ROCKS 43

3. LABORATORY EQUIPMENT AND PROCEDURES 50
- 3.1 INTRODUCTION 50
- 3.2 THE TRIAXIAL SYSTEM 51
  - 3.2.1 Low pressure system 51
  - 3.2.2 High pressure systems 52
  - 3.2.3 Instrumentation 56
  - 3.2.4 Computer and interface system 58
  - 3.2.5 Accuracy of measurements and calibration of transducers 60
- 3.3 MEASUREMENTS OF SMALL STRAIN STIFFNESS 62
  - 3.3.1 Limitations of external axial strain measurements 63
  - 3.3.2 Local axial strain instrumentation and improvement of the output signal 65
  - 3.3.3 Limitations of the apparatus 70
  - 3.3.4 Design of the sample-load cell connection 73
- 3.4 EXPERIMENTAL PROCEDURES AND MODIFICATIONS 75
  - 3.4.1 Preparation of intact samples 75
  - 3.4.2 Preparation of reconstituted samples 76
  - 3.4.3 Sample saturation and standard setting up procedures 78
  - 3.4.4 Modifications of the setting up procedures 80

4. EXPERIMENTAL WORK ON THE ARTIFICIAL SOIL 83

4.1 REVIEW OF PREVIOUS WORK 83
4.2 PREPARATION OF THE WEAKLY CEMENTED SAMPLES 86
4.3 TESTING PROGRAMME 87
4.4 PRELIMINARY CALCULATIONS 87
4.5 ISOTROPIC COMPRESSION 89
4.6 SHEARING 91
4.7 NORMALIZED STRESS PATHS 96

5. EXPERIMENTAL WORK ON THE CALCARENITE 100

5.1 SOIL DESCRIPTION 100
5.2 TESTING PROGRAMME 102
5.3 PRELIMINARY CALCULATIONS 104
5.4 ISOTROPIC COMPRESSION 106
5.5 SHEARING 110
5.6 STIFFNESS 114
5.6.1 Introduction 114
5.6.2 Intact soil 117
5.6.3 Reconstituted soil 120
5.7 NORMALIZED STRESS PATHS 122

6. EXPERIMENTAL WORK ON THE SILICA SANDSTONE 127

6.1 GEOLOGICAL STUDY FOR THE SELECTION OF THE SILICA SANDSTONE 127
6.2 SOIL SAMPLING AND THIN SECTIONS 131
6.3 TESTING PROGRAMME 132
6.4 PRELIMINARY CALCULATIONS 134
6.5 ISOTROPIC COMPRESSION 134
6.6 SHEARING 136
6.7 STIFFNESS 140
6.7.1 Introduction 140
6.7.2 Stiffness of the intact soil in drained shearing 142
6.7.3 Stiffness and effective stress paths of the intact soil in undrained shearing 146
6.7.4 Pore pressure response of the intact soil 149
6.7.5 Comparison between G_{max} determined from drained and undrained tests 154
6.7.6 Stiffness of the reconstituted soil 156

7. DISCUSSION 159

7.1 THE SHEAR BEHAVIOUR OF THE CEMENTED CARBONATE SANDS 159
7.1.1 Introduction 159
7.1.2 New method of normalization 161
7.1.3 Yielding of the cemented carbonate sands during shearing 163
7.1.4 The shear behaviour of the cemented carbonate sands after yielding 167

7.2 THE SHEAR BEHAVIOUR OF THE CEMENTED SILICA SAND 169
7.2.1 Introduction 169
7.2.2 Normalized stress paths 170
7.2.3 Stress-dilatancy 171
7.3 COMPARISONS BETWEEN THE SHEAR BEHAVIOUR OF THE CEMENTED CARBONATE AND SILICA SANDS 178
7.4 STIFFNESS OF THE CALCARENITE AND SILICA SANDSTONE 184

8. CONCLUSIONS 189
8.1 INTRODUCTION 189
8.2 GENERAL FEATURES OF BEHAVIOUR 190
8.2.1 Isotropic compression 190
8.2.2 Shearing 191
8.3 STIFFNESS AND YIELDING OF NATURALLY CEMENTED SANDS 192
8.3.1 Developments of laboratory techniques 192
8.3.2 Test results 193
8.4 INFLUENCE OF V, P' AND BOND STRENGTH ON THE SHEAR BEHAVIOUR OF THE CEMENTED SANDS 194
8.5 CORRELATION BETWEEN SHEAR BEHAVIOUR AND MATERIAL PROPERTIES 196
8.6 IMPLICATIONS OF THE RESEARCH 197
8.7 RECOMMENDATIONS FOR FUTURE WORK 199

REFERENCES 200

TABLES

FIGURES

LIST OF TABLES

Table 3.1 Characteristics of the load cells and pore pressure transducers.

Table 3.2 Characteristics of the displacement transducers and volume gauges.

Table 4.1 Testing programme for the artificially cemented samples prepared using method B.

Table 4.2 Testing programme for the artificially cemented samples prepared using method A.

Table 5.1 Depth of retrieval of calcarenite samples and initial specific volumes.

Table 5.2 Testing programme for intact samples of calcarenite.

Table 5.3 Testing programme for reconstituted samples of calcarenite.

Table 5.4 Testing programme for the undrained loading-unloading probes performed on an intact sample of calcarenite.

Table 5.5 Testing programme for the undrained loading-unloading probes performed on a reconstituted sample of calcarenite.

Table 5.6 Testing programme performed by Coop and Atkinson (1993) on intact samples of calcarenite.

Table 6.1 Testing programme for intact samples of silica sandstone.

Table 6.2 Testing programme for reconstituted samples of silica sandstone.

Table 6.3 Testing programme for the undrained loading-unloading probes performed on an intact sample of silica sandstone.

LIST OF FIGURES

CHAPTER 2

Figure 2.1 One-dimensional compression for a reconstituted sample, a good quality undisturbed sample and a natural clay in situ. (after Tavenas and Leroueil, 1987).

Figure 2.2 Schematic description of the consolidation of a natural clay deposit (after Tavenas and Leroueil, 1987).

Figure 2.3 One-dimensional compression of Mexico City clay (after Mesri et al., 1975).

Figure 2.4 One-dimensional compression of the Grande Baleine clay (after Locat and Lefebvre, 1985).

Figure 2.5a One-dimensional compression of Winnipeg clay (after Graham and Li, 1985).

Figure 2.5b Loci of isotropic and one-dimensional preconsolidation pressures (σ'_{vc} in Figure 2.5a) and critical states for Winnipeg clay (after Graham and Li, 1985).

Figure 2.6 One-dimensional compression of Boom clay (after Coop et al., 1995).

Figure 2.7 Normalized one-dimensional compression curves of reconstituted clays (after Burland, 1990).

Figure 2.8 Sedimentation and intrinsic compression lines for normally consolidated clays (after Burland, 1990).

Figure 2.9 Examples of clays having in situ states which are above and below the sedimentation compression line (after Burland, 1990).

Figure 2.10 State boundary surfaces for intact and destructured clays (after Tavenas and Leroueil, 1987).

Figure 2.11 Yield states from drained and undrained triaxial tests on Winnipeg clay in: (a) stress space; (b) normalized stress space.

Figure 2.12 Comparison between natural and reconstituted Vallerica clay: (a) isotropic compression; (b) stress-volume paths during shearing ; (c) peak states normalized by a p_e' taken on the reconstituted NCL; (d) peak states normalized by a p_e' taken on the appropriate NCL (after Rampello et al., 1993).

Figure 2.13 Normalized stress paths for Boom clay in triaxial compression and extension tests (after Coop et al., 1995).

Figure 2.14 Variation of the peak angle of friction with mean effective stress and relative density I_D for initially loose (○) and dense (•) samples of Chattahoochee River sand (after Vesic and Clough, 1968).

Figure 2.15 Variation of the peak angle of friction of sands with the state parameter ψ_i (after Been and Jefferies, 1985).

Figure 2.16 Normalized stress paths for Dog's Bay sand: (a) drained tests; (b) undrained tests (after Coop, 1990).

Figure 2.17 Stress paths for compacted and overconsolidated samples of a carbonate sand in undrained triaxial tests (after Coop, 1990).

Figure 2.18 Intergranular fabric classification (after Dusseault and Morgenstern, 1979).

Figure 2.19 Unconfined compressive strength as a function of the tangential index (TI %) for a group of locked sands from the U.K. (after Dobereiner and De Freitas, 1986).

Figure 2.20 A comparison between the rate of dilation at failure for shear box tests on locked sands (oil sands) and Ottawa sand (after Dusseault and Morgenstern, 1979).

Figure 2.21 Some classification systems of soils and rocks (after Dobereiner and De Freitas, 1986).

Figure 2.22 One-dimensional compression for three samples of an artificially cemented soil with the same grading and degree of bonding but different initial void ratios (after Maccarini, 1987).

Figure 2.23 One-dimensional compression for samples of chalk with different initial void ratios: (a) after Leddra, 1990; (b) after Petley et al., 1993.

Figure 2.24 One-dimensional compression for intact and reconstituted samples of a fine grained tuff (after Aversa et al., 1990).

Figure 2.25 Relationship between compression index and initial void ratio in one-dimensional compression (after Vaughan, 1988).

Figure 2.26 Shear behaviour in drained triaxial compression for a naturally cemented sand: (a) moderately cemented; (b) weakly cemented (after Clough et al., 1981).

Figure 2.27 Peak strength envelopes (after Clough et al., 1981): (a) artificially cemented sand; (b) naturally cemented sand with stronger bonding (SLAC-1) and weaker bonding (PCA-1 and PCA-2).

Figure 2.28 Comparison between the shear behaviour of an artificially cemented and an uncemented carbonate sand: (a) at high confining pressures; (b) at intermediate confining pressures; (c) at low confining pressures (after Coop and Atkinson, 1993).

Figure 2.29 Idealized shear behaviour of cemented soils: (a) stress paths; (b) stress-strain behaviour (after Coop and Atkinson, 1993).

Figure 2.30 Stress paths for drained triaxial tests on a marl from the Corinth Canal (Anagnostopoulos et al., 1991).

Figure 2.31 Determinations of the yield point for an oolitic limestone (after Elliott and Brown, 1985).

Figure 2.32 Stresses at yield for an oolitic limestone (after Elliott and Brown, 1985).

Figure 2.33 Drained triaxial tests on a residual soil from basalt (after Maccarini, 1987).

Figure 2.34 Variation of Young's moduli E_{sec}, E_{tan} and E_{eq} with: (a) and (b) q/q_{max}; (c) and (d) axial strains (after Kim et al., 1994).

Figure 2.35 Variation of initial Young's modulus with depth for chalk at three different sites obtained from surface wave geophysics (Clayton, 1989).

CHAPTER 3

Figure 3.1 Schematic diagram of the high pressure system.

Figure 3.2 Schematic diagram of the axial loading system.

Figure 3.3 Schematic diagram of the 10 MPa triaxial system after modifications.

Figure 3.4 Arrangement of LVDTs and radial strain belt in the 70 MPa apparatus.

Figure 3.5 Errors affecting external axial strain measurements.

Figure 3.6 Arrangement of LVDTs in the 10 MPa apparatus.

Figure 3.7 Noise from (a) LVDTs and (b) internal load cell.

Figure 3.8 Stress-strain data showing non-uniformity of strains prior to changing the setting up and testing procedures.

Figure 3.9 Connections between sample and load cell (after Baldi et al., 1988).

Figure 3.10 Conical connection between the sample and the internal load cell.

Figure 3.11 Redesigned connection between the sample and the internal load cell.

Figure 3.12 Variation of deviator stress with time for a dummy sample using the redesigned connection with (a) the initial and (b) final configurations.

Figure 3.13 Mould for trimming the ends of the sample.

Figure 3.14 Device for the saturation of the sample.

Figure 3.15 Device to check the sample centrality with respect to the apparatus axis.

Figure 3.16 Device to check the perpendicularity of the ends of the sample with respect to the apparatus axes.

Figure 3.17 Installation of the sample in the 10 MPa apparatus.

Figure 3.18 Configuration of 'O'-rings to seal the sample.

CHAPTER 4

Figure 4.1a Grading curve of Dog's Bay sand (after Coop, 1990).

Figure 4.1b Thin sections of Dog's Bay sand under cross-polarised light.

Figure 4.2 Thin section of the artificially cemented sand under: (a) plain white light; (b) cross-polarised light.

Figure 4.3a Isotropic compression of the weakly cemented sand prepared using method B and of the uncemented sand.

Figure 4.3b Isotropic compression of the weakly cemented sand prepared using method A and of the uncemented sand.

Figure 4.4 Isotropic compression of the strongly cemented sand.

Figure 4.5 Stress-strain curves of the weakly cemented sand prepared using method B: (a) at low confining pressures; (b) at high confining pressures.

Figure 4.6 Stress-strain curves of the weakly cemented sand prepared by method A: (a) at low confining pressures; (b) at high confining pressures.

Figure 4.7 Ultimate states for the uncemented, weakly and strongly cemented samples.

Figure 4.8 Stress ratios during shearing for all the weakly cemented samples prepared using method B.

Figure 4.9 Stress ratios during shearing for all the weakly cemented samples prepared using method A.

Figure 4.10 States at the end of shearing for uncemented, weakly and strongly cemented samples.

Figure 4.11 Shear behaviour of the weakly cemented samples (type B) and uncemented samples tested from similar initial values of p'/p'_{cs} at intermediate and high confining pressures.

Figure 4.12 Shear behaviour of the strongly cemented and uncemented samples tested from similar initial values of p'/p'_{cs} at intermediate and high confining pressures.

Figure 4.13 Shear behaviour of the strongly cemented, weakly cemented (type B) and uncemented samples tested from similar initial values of p'/p'_{cs} at low confining pressures.

Figure 4.14 Normalized stress paths for the weakly cemented samples prepared using method B compared with those for the uncemented samples.

Figure 4.15 Normalized stress paths for the strongly cemented samples (after Coop and Atkinson, 1993).

Figure 4.16 Normalized stress paths for the weakly cemented samples prepared using method A compared with those for the uncemented samples.

CHAPTER 5

Figure 5.1 Thin sections under cross-polarised light for two calcarenite samples retrieved from borehole B2-6 at (a) 132.5 m and (b) 139.2 m depth below the sea bed.

Figure 5.2 Grading curve determined for the reconstituted calcarenite.

Figure 5.3 Isotropic compression of intact and reconstituted samples of calcarenite.

Figure 5.4 Stress-strain curves from an undrained test performed on the calcarenite at low confining pressures: (a) complete test; (b) local axial strains (ε_{al}) up to 0.5 %.

Figure 5.5 Stress-strain curve from a drained constant p' test performed on the calcarenite at low confining pressures (after Coop and Atkinson, 1993).

Figure 5.6 Stress-strain curve from a drained constant p' test performed on the calcarenite at intermediate confining pressures (after Coop and Atkinson, 1993).

Figure 5.7 Stress-strain curves from a drained constant p' test performed on the calcarenite at intermediate confining pressures for: (a) the complete test; (b) external axial strains up to 0.5 %.

Figure 5.8 Stress-strain curve from a drained constant p' tests performed on the calcarenite at high confining pressures.

Figure 5.9 Stress-strain curve from a drained constant p' tests performed on the calcarenite at very high confining pressures.

Figure 5.10 Stress-strain curve from a drained constant p' tests performed on reconstituted soil of calcarenite at low confining pressures.

Figure 5.11 Stress-strain curve from a drained constant p' tests performed on reconstituted soil of calcarenite at high confining pressures.

Figure 5.12 Ultimate states of intact and reconstituted samples of calcarenite.

Figure 5.13 Ultimate states and peak states of intact and reconstituted samples of calcarenite.

Figure 5.14 States at the end of shearing for intact and reconstituted samples of calcarenite.

Figure 5.15 Shear behaviour of intact (after Coop and Atkinson, 1993) and reconstituted samples of calcarenite tested from similar initial values of p'/p'_{cs} at low confining pressures (constant p' tests).

Figure 5.16 Shear behaviour of reconstituted and intact samples of calcarenite which yielded in isotropic compression (constant p' tests).

Figure 5.17 Pre-yield stress-strain relationships for undrained cycles performed on the calcarenite.

Figure 5.18 Pre-yield tangent shear moduli in two series of undrained cycles performed at low values of p'.

Figure 5.19a Stress-strain relationships for undrained cycles performed on the calcarenite at intermediate values of p'.

Figure 5.19b Variation of the tangent shear moduli with deviator stress for undrained loading probes performed on the calcarenite at intermediate values of p'.

Figure 5.20 Variation of the tangent shear moduli with deviator stress for undrained loading probes performed on the calcarenite at intermediate values of p'.

Figure 5.21 Variation of the tangent shear moduli with deviator stress for undrained loading probes performed on the calcarenite at high values of p'.

Figure 5.22 Effective stress paths for undrained cycles performed on the calcarenite for different values of p'.

Figure 5.23 Variation of the tangent shear moduli with deviator stress from undrained loading probes on a reconstituted sample of calcarenite performed for different values of p'.

Figure 5.24 Normalized stress paths for the calcarenite: (a) reconstituted samples; (b) intact samples which yielded in isotropic compression; (c) intact samples which did not yield in isotropic compression and comparison with to some of the tests in (b).

CHAPTER 6

Figure 6.1 Section of the Lower Greensand at Redcliff (after Osborne Wight, 1921).

Figure 6.2 Grading curve of the reconstituted soil obtained from the silica sandstone.

Figure 6.3 Thin section of the silica sandstone under plain white light.

Figure 6.4 Thin sections of the silica sandstone under: (a) plain white light; (b) plain polarised light

Figure 6.5 Scanning electron micrographs of the silica sandstone with different degrees of magnification: (a) and (c) samples with unpolished surfaces; (b) polished thin section.

Figure 6.6 Isotropic compression of intact and reconstituted samples of silica sandstone.

Figure 6.7 Stress-strain curves from drained constant p' tests performed on the silica sandstone at relatively low confining pressures.

Figure 6.8 Stress-strain curves from drained constant p' tests performed on the silica sandstone at high confining pressures.

Figure 6.9 Stress-strain curves from drained constant p' tests performed on reconstituted samples of silica sandstone (a) at the lowest and (b) at the highest confining pressures.

Figure 6.10 Ultimate states of intact and reconstituted samples of silica sandstone.

Figure 6.11 Ultimate states and peak states of intact and reconstituted samples of silica sandstone.

Figure 6.12 States at the end of shearing for intact and reconstituted samples of silica sandstone.

Figure 6.13 Shear behaviour of intact and reconstituted samples of silica sandstone tested from similar initial values of p'/p'_{cs} at (a) relatively low and (b) high confining pressures (constant p' tests).

Figure 6.14 Tangent shear modulus as a function of (a) deviator stress and (b) shear strain for a constant p' test performed at relatively low confining pressures.

Figure 6.15 Tangent shear modulus as a function of deviator stress for a constant p' stress path test performed at intermediate confining pressures.

Figure 6.16 Tangent shear modulus as a function of deviator stress for a constant p' stress path tests performed at high confining pressures.

Figure 6.17 Tangent shear modulus as a function of deviator stress for a constant p' stress path tests performed at very high confining pressures.

Figure 6.18 Pre-yield stress-strain relationships for undrained cycles performed on the silica sandstone.

Figure 6.19 Tangent shear moduli as a function of (a) axial strain and (b) deviator stress obtained from undrained loading probes performed on the silica sandstone (q_{max} = 800 kPa).

Figure 6.20 Tangent shear modulus from undrained probes performed on the silica sandstone (q_{max} = 2100 kPa).

Figure 6.21 Stress-strain relationships from undrained loading probes performed on the silica sandstone (q_{max} = 4200 kPa).

Figure 6.22 Tangent shear moduli from undrained loading probes performed on the silica sandstone (q_{max} = 4200 kPa).

Figure 6.23 Tangent shear moduli from undrained probes performed on the silica sandstone (q_{max} = 6000 kPa).

Figure 6.24 Effective stress paths for undrained cycles performed on the silica sandstone from the same isotropic state but up to different maximum deviator stresses.

Figure 6.25 Comparison between the volumetric strains measured by the volume gauge and those determined from the local axial transducers in isotropic compression.

Figure 6.26 Variation of the bulk modulus of the silica sandstone with mean effective stress.

Figure 6.27 Tangent shear modulus as a function of shear strain for an overconsolidated reconstituted sample of the silica sandstone sheared at a constant value of p'.

CHAPTER 7

Figure 7.1 Isotropic boundary for the intact samples of calcarenite.

Figure 7.2 Isotropic boundary for the artificially cemented carbonate sand with strong bonding.

Figure 7.3 Isotropic boundary for the artificially cemented carbonate sand with weak bonding.

Figure 7.4 Yield surface for the artificially cemented carbonate sand.

Figure 7.5 Stress states at yield for the artificially cemented carbonate sand with strong bonding (after Coop and Atkinson, 1993).

Figure 7.6 Isotropic boundary for the intact samples of calcarenite with weaker bonding.

Figure 7.7 Yield surface for the calcarenite.

Figure 7.8a Normalized stress paths for reconstituted and intact samples of calcarenite with stronger bonding sheared after isotropic yielding.

Figure 7.8b Normalized stress paths for intact samples of calcarenite with weaker and stronger bonding sheared after isotropic yielding.

Figure 7.9 Shear behaviour of the calcarenite with identification of the yield surface, outer intact state boundary surface and intrinsic state boundary surface.

Figure 7.10 Shear behaviour of the artificially cemented carbonate sand: (a) normalized stress paths for samples sheared after isotropic yielding; (b) identification of the yield surface, outer intact state boundary surface and intrinsic state boundary surface.

Figure 7.11 Normalized stress paths for intact and reconstituted samples of silica sandstone.

Figure 7.12 Magnification of Figure 7.11 showing the yield surface for the silica sandstone.

Figure 7.13 Stress-dilatancy relationships for constant p' tests performed on intact and reconstituted samples of silica sandstone with similar initial values of p'/p'_{cs}.

Figure 7.14 Stress-dilatancy relationship for an intact sample of silica sandstone sheared at a constant p' from a low value of p'/p'_{cs}.

Figure 7.15 Peak stress ratio as function of maximum rate of dilation for intact and reconstituted silica sandstone.

Figure 7.16 Normalized states at peak for reconstituted and intact samples of silica sandstone referred to the CSL of the reconstituted soil.

Figure 7.17 Normalized states at peak for reconstituted and intact samples of silica sandstone referred to the appropriate CSLs.

Figure 7.18 Comparison between the stress-dilatancy relationships of intact and reconstituted samples of silica sandstone sheared at different mean effective stresses.

Figure 7.19 Shear behaviour of the reconstituted and intact silica sandstone referring the normalization of the intact soil to the CSL of the reconstituted soil.

Figure 7.20 Shear behaviour of the reconstituted and intact silica sandstone referring the normalization of the intact soil to a CSL as indicated by Figure 7.16.

Figure 7.21 Transmitter and receiver signals for a bender element test performed on the silica sandstone at low confining pressures.

Figure 7.22 G_{max} for intact and reconstituted calcarenite as a function of (a) mean effective stress and (b) specific volume.

Figure 7.23 G_{max} for intact and reconstituted calcarenite as a function of the normalized state p'/p'_{IB}.

Figure 7.24 Comparison between the normalized maximum shear moduli of intact and reconstituted calcarenite as a function of the normalized state p'/p'_{IB}.

ACKNOWLEDGEMENTS

The research was funded by an EPSRC contract and was performed at the Geotechnical Engineering Research Centre of City University, London. I am most grateful to my advisor Dr Matthew Coop for his invaluable comments and constant encouragement throughout the research. With his skilful management of the laboratory I was able to work in an efficient environment where the experiments could be run smoothly.

My discussions with Professor John Atkinson were always very useful and enjoyable. I would like to thank Dr Neil Taylor for his advice during the research. Dr Kevin O'Connor gave me invaluable help in identifying one of the materials tested and in solving a number of experimental difficulties. A special thought goes to Dr Akitoshi Mochizuki from Osaka City University in Japan for his comments on my work and our many enjoyable discussions. Dr Sarah Stallebrass and my colleagues of the Geotechnical Engineering Research Centre also gave helpful contributions and made the working environment stimulating. Keith Osborne, Lloyd Martika, Harvey Skinner and Reg Allen provided a technical support in the laboratory which was unique, swiftly solving any problems and creating a jovial atmosphere.

Information and advice on the geological aspects of the research were kindly provided by Professor Peter Fookes, Dr Colin Warren and Mr John Farnaby. My thanks also go to Sean Holding of University College, London who prepared the thin sections which were then examined by Dr Tucker and Robin Baldwin of Geomaterials Research Services Ltd, Basildon. The scanning electron micrographs which appear in this thesis were kindly performed by the Department of Geology at Queen Mary and Westfield College, London. I would also like to acknowledge the Department of Civil Engineering at Surrey University for lending a loading frame which was used for some of the experiments.

The support that I have received form my family was essential for me. My father Angelo and my mother Enza were always interested in the progress of my work giving me encouragement and determination. The visits of my sister Alessandra made the breaks from my work particularly enjoyable. In this respect significant contributions have been made by my brother Elio and by Anna and Paolo.

DECLARATION

I grant powers of discretion to the University Librarian to allow this thesis to be copied in whole or part without further reference to me. This permission covers only single copies for study purposes subject to normal conditions of acknowledgement.

ABSTRACT

The behaviour of natural soils is highly influenced by structural features arising from their geological history and was recognised to lie outside current frameworks which account only for the stress-volume state of the soil. The objective of the research was to compare the shear behaviour and stiffness of two naturally cemented sands: a calcarenite with relatively low densities, weak particles and strong bonding and a silica sandstone with high densities, strong particles and weak bonding. Comparative studies were also undertaken on their corresponding reconstituted soils and on an artificially cemented carbonate sand.

Testing was performed in stress path controlled triaxial systems over a wide range of confining pressures. Identification of the yield surface was found to be an essential feature to describe the shear behaviour of the soils examined. The determination of the yield points of such stiff soils required internal measurements of stresses and strains, with an accuracy higher than currently achieved in soil testing. For reliable determinations of stiffness and yielding the uniformity of strains in the samples had to be guaranteed. Therefore several parts of the equipment were redesigned or modified and new sample preparation and setting up procedures were developed.

Comparison of results from natural and reconstituted soils showed that bonding increased the stiffness and the stress-strain linearity. For the naturally cemented sands the maximum shear modulus was found to vary with state only when the soils were sheared after isotropic yielding. Undrained loading-unloading probes showed that the linear behaviour was reversible and that plastic strains were accompanied by a progressive deterioration of bonding resulting initially in a reduction of the yield stresses and finally, after sufficient cycling in a decrease of the maximum shear modulus.

The combined influence of bond strength and specific volume on yielding could be accounted for when normalizing the yield stresses by an equivalent pressure taken on the state boundary in isotropic compression. This type of normalization also allowed the full state boundary to be identified. The yield surface was found to be the boundary limiting the domain governed by bonding and for the calcarenite occupied a larger portion of the permissible states than for the silica sandstone. States between the yield surface and the state boundary surface were controlled by bond degradation and either particle crushing for the calcarenite or dilation for the silica sandstone.

After accounting for differences in states, both naturally cemented sands showed peak strengths which were higher than those for the reconstituted soils. For the calcarenite the peak strengths simply resulted from cohesion, as the peak stress ratios were reached on the yield surface. Only when stress ratios at yielding were lower than the critical state stress ratio the strength was truly frictional and coincident with the critical state. For the silica sandstone, in contrast, the peak strengths were found to be frictional except at the lowest confining pressures. The peak stress ratios were reached at states above the yield surface and were associated with a maximum rate of dilation. The dilatancy and strength of the intact soil were higher than those of the reconstituted soil at comparable states and were interpreted as resulting from differences in fabric and from the delayed volumetric response induced by the presence of bonding at the early stages of shearing. The case of the silica sandstone showed that only when density is a predominant factor in comparison with bonding then different modes of shear behaviour follow the theory of Critical State Soil Mechanics.

NOMENCLATURE

SYMBOLS

A_a	Area of actuator
A_c	Current area of sample
A_i	Initial area of sample
A_r	Area of ram
A_s	Area of sample
B	Pore pressure coefficient
C	Compressibility of the soil skeleton
C_L	Compressibility of the pore water drainage lines
C_M	Compressibility of the pore water measuring device
C_S	Compressibility of the soil particles
C_w	Compressibility of the pore water
C^*_c	Compression index for reconstituted soils
c'	Cohesion intercept
c_u	Undrained shear strength
D_r	Relative density
d	Rate of dilation (or dilatancy)
d_{max}	Maximum rate of dilation (or dilatancy)
d_{50}	Diameter for which 50% by weight of the soil has particles with a smaller diameter
E	Young's modulus
E_{eq}	Equivalent Young's modulus
E_{max}	Maximum Young's modulus
E_{sec}	Secant Young's modulus
E_{tan}	Tangent Young's modulus
e	Void ratio
e^*_{100}	Void ratio at a vertical effective stress of 100 kPa for reconstituted soils
e^*_{1000}	Void ratio at a vertical effective stress of 1000 kPa for reconstituted soils
f_m	Membrane flexibility
G_s	Specific gravity
G	Tangent shear modulus
G^u_{cor}	Corrected maximum shear modulus for undrained tests
G_{max}	Maximum shear modulus
$G^{p'}_{max}$	Maximum shear modulus for drained tests at a constant mean effective stress
G^u_{max}	Maximum shear modulus for undrained tests
I_v	Void index
J	Cross anisotropic modulus
ln	Natural logarithm
log	Logarithm to the base 10
K	Bulk modulus
K_o	Coefficient of lateral earth pressure at rest
n	Porosity
p	Mean total stress
p_c	Pressure in the axial hydraulic cylinder

p'	Mean effective stress
p'_e	Equivalent pressure
p'_{cs}	Equivalent pressure taken on critical state
$(p'/p'_{cs})_i$	Initial value of p'/p'_{cs}
$(p'/p'_{cs})_p$	Initial value of p'/p'_{cs} at peak stress ratio
p'_i	Initial mean effective stress at the start of shearing
p'_{IB}	Equivalent pressure taken on the intact isotropic boundary
p_r	Reference pressure
q	Deviator stress
q_{max}	Maximum deviator stress
u	Pore pressure
V	Current volume of sample
V_i	Initial volume of sample
V_L	Volume of water in pore water drainage lines
v	Current specific volume
v_{cs}	Reference value of specific volume at the critical state for a given mean effective stress
v_f	Specific volume at the end of test
v_i	Initial specific volume at the start of the test
v_1	Specific volume at start of shearing
v_{max}	Maximum specific volume
v_{min}	Minimum specific volume
v_λ	Intercept at $p' = 1$ kPa of a line with slope λ passing through a state at a specific volume v and mean effective stress p'
$v_{\lambda i}$	Initial value of v_λ
W	Dry weight of sample at end of test
ΔW	Total work
ΔW_{fric}	Work dissipated as friction
ΔW_{bon}	Work dissipated in disrupting bonding
Δw_{bon}	Work per unit volume dissipated in disrupting bonding
w_i	Water content at the start of test
w_f	Water content at end of test
α	Coefficient of stress-dilatancy relationship
Γ	Specific volume of soil at critical state with $p' = 1$ kPa
γ_w	Unit weight of water
γ_{di}	Dry unit weight at the start of test
γ_{ti}	Total unit weight at the start of test
Δ	Large increment
δ	Small increment
ε_a	Axial strain measured externally
ε_{al}	Axial strain measured locally
ε_s	Shear strain
ε_v	Volumetric strain
ε_{vf}	Overall volumetric strain at end of test
ε_a^e	Elastic axial strain
ε_v^e	Elastic volumetric strain
ε_a^p	Plastic axial strains
ε_s^p	Plastic shear strains
ε_v^p	Plastic volumetric strain

η	Stress ratio equal to q/p'
η_y	Stress ratio at yield
η_p	Peak stress ratio
λ	Slope of normal compression line and critical state line
M	Slope of critical state line in q : p' plane
N	Specific volume of isotropically normally consolidated soil at a mean effective stress of 1kPa
ν	Angle of friction to the horizontal in the saw-blade model
ν_{max}	Maximum value of ν
σ	Isotropic stress
σ_r	Radial stress, also cell pressure
σ_a	Total axial stress
σ'_a	Axial effective stress
σ_r	Total radial stress
σ'_r	Radial effective stress
σ'_v	Vertical effective stress
σ'_{vc}	Effective preconsolidation pressure in one-dimensional compression
σ'_{vo}	In situ vertical effective stress
ϕ'	Mobilised angle of friction
ϕ'_c	Angle of friction along the inclined planes in the saw-blade model
ϕ'_{cs}	Critical state angle of friction
ϕ'_f	Angle of friction in Rowe's stress-dilatancy relationship
ϕ'_p	Peak angle of friction
ϕ'_μ	Inter particle friction angle
ψ_i	Initial state parameter for sands equal to $v_{\lambda i} - \Gamma$

ABBREVIATIONS

AC	Alternating current
A/D	Analogue to Digital
CS	Critical state
CSL	Critical state line
D/A	Digital to analogue
DC	Direct current
IB	Isotropic boundary
ICL	Intrinsic compression line
ISBS	Intrinsic state boundary surface
LDT	Local deformation transducer
LL	Liquid limit (also w_L after Burland 1990)
LVDT	Linear variable differential transformer
NCL	Normal compression line
PYCL	Post-yield compression line
SBS	State boundary surface
SCL	Sedimentation compression line
TI	Tangential index

1. INTRODUCTION

In the last decade much of the research on the fundamental behaviour of soils has focused on the study of saturated natural soils. When compared to their corresponding reconstituted soils, many natural soils show patterns of behaviour which do not conform to the conceptual framework of Critical State Soil Mechanics (Roscoe et al., 1958; Schofield and Wroth, 1968). This theory defines the state of the soil as the combination of deviator stress, mean effective stress and specific volume and considers the shear behaviour as being dependent on the change from an initial state that has to occur in the soil in order for it to reach the ultimate state. These concepts provided coherence to the understanding of the behaviour of reconstituted clays and sands.

Both clays and sands in their natural state possess a "structure" which is absent in reconstituted soils and which derives from the processes taking place during their geological life. The term "structure" was first introduced for clays and identified at a microscopic scale as the combination of fabric and bonding (Burland, 1990). For sands structure was instead mainly associated with the presence of cement between the particles and little emphasis has been given to fabric.

Structural features in the behaviour of natural soils cannot be accounted for by state alone and can be revealed more clearly through comparison with the behaviour of corresponding reconstituted soils (Leroueil and Vaughan, 1990; Burland, 1990). Structure has been widely recognised to influence the stress-strain behaviour of soils prior to and during shearing contributing both to their strength and stiffness. A conceptual understanding of the effects of structure on the behaviour of natural soils is therefore necessary to reduce the degree of subjectivity and uncertainty in engineering judgment and to allow more accurate predictions of the performance of soil structures.

In comparison with natural clays systematic studies of the behaviour of natural sands, either cemented or uncemented, have been rather limited. For uncemented sands one of the reasons lies in the difficulty of retrieving undisturbed samples from the ground. When bonding is present, it is possible to obtain undisturbed samples provided the cement is sufficiently strong to preserve the structure and in particular the fabric of the sand deposit. Another reason which has discouraged studies on naturally cemented sands is their extreme variability in the ground. Therefore much of the research on cemented sands has concentrated on investigating the behaviour of artificial soils in which factors such as grading, initial specific volume and degree of bonding could be controlled (Clough et al., 1981; Coop and Atkinson, 1993; Huang and Airey, 1993). Despite these studies however it has still remained unclear what is the inter-relationship between specific volume and bonding, often because the samples tested all had similar initial specific volumes.

More information is available on the behaviour of cemented sands in isotropic or one-dimensional compression. The shear behaviour has been analysed primarily at relatively large strains with reference to the influence of bonding on the strength of the soil. Studies which have focused on the pre-yield behaviour are rare, mainly because of the limitation of the testing techniques, as the high stiffness of these materials requires the capability of measuring axial strains with higher resolution than those achieved so far in soil laboratories. Moreover the axial strains need to be measured internally to overcome bedding errors. These issues have been widely recognised and Goto et al. (1991) succeeded in obtaining accurate measurements of strains which enabled the determination of stiffness moduli in stiff clays and sandstones. Despite the significant progress represented by these techniques, their study did not address the conceptual understanding of the stress-strain behaviour of the soils tested. A review of research findings relevant to the present work is presented in Chapter 2.

The present study intended to explore the above issues in some detail. The experimental work focused on the investigation of the stress-strain behaviour of two naturally

cemented sands. The materials tested were a calcarenite from the site of the North Rankin platform in Australia, whose study was initiated by Coop and Atkinson (1993), and a silica sandstone from the Lower Greensand series of Kent in England. The calcarenite consisted of a biogenic carbonate sand bonded by calcium carbonate, whereas the silica sandstone consisted of a quartz sand bonded by iron oxide. The two materials represented extreme cases in terms of the soils constituents in that the calcarenite had weak and easily crushable grains bonded by a comparatively strong cement, whereas the silica sandstone had strong grains bonded by a comparatively weak cement.

The behaviour of the two naturally cemented sands was compared to that of compacted reconstituted soils obtained from mechanical breakage of bonding in the intact soils. The investigation of the natural soils was also supported by a study of an artificially cemented sand with controlled characteristics. This soil was prepared by cementing a carbonate sand with gypsum. The work on the artificial soil involved the extension of the previous study performed by Coop and Atkinson (1993) to samples characterized by similar initial specific volumes but a lower degree of cementing. The results from the authors on the artificially cemented sand and on the calcarenite are included in the present work and re-interpreted in the light of the new findings.

The objective of the experimental work was to investigate and contrast the shear behaviour of the two naturally cemented sands from very small to large strains, both in strain-softening and strain-hardening modes of behaviour. The experimental work was also intended to study the variation of the shear modulus from very small strains up to failure and to establish the types of behaviour for each material both before and after yield.

Triaxial compression tests were performed in stress path controlled systems covering a range of confining pressures between 70 and 70000 kPa. The testing programme consisted of drained and undrained shearing and was limited to isotropically compressed samples. The drained tests were performed mainly following constant p' stress paths with

some tests at constant cell pressure. Undrained shearing was performed at constant cell pressure and included series of loading-unloading probes from isotropic states up to deviator stresses which did not cause failure. The influence of bond degradation on the maximum shear modulus and yielding was studied by performing undrained loading and unloading cycles after an initial yield had occurred in the materials.

The study of stiffness and yielding required the development of appropriate laboratory techniques. As the materials tested had values of stiffness that were high and values of strains at yield that were small, the laboratory work concentrated on achieving accurate measurements of axial strains by means of local axial gauges which would not impose any limitation to the axial strains achievable during the tests. The new small strain stiffness measurement techniques were implemented in a high pressure triaxial system. A series of requirements were identified as crucial for the determination of correct and reliable values of stiffness and yield points, leading to the design of various pieces of equipment and the development of new sample preparation and setting up procedures. These requirements and the laboratory techniques developed in the present work are presented in Chapter 3. Also included in this chapter is a detail description of the triaxial systems, of the performance of the instrumentation and of the testing procedures followed.

Chapters 4, 5 and 6 describe the experimental work performed on the artificially cemented sand, the calcarenite and the silica sandstone respectively. For each soil the test results in isotropic compression and shearing from both intact and reconstituted materials are presented and compared and a preliminary analysis and interpretation of the data is performed within Critical State concepts. For the naturally cemented sands the chapters also present the analysis of the stress-strain curves in terms of stiffness and discuss both the pre-yield and post-yield behaviour.

Further interpretation and alternative methods of analysis which led to the conclusions of the work are presented and discussed in Chapter 7. The shear behaviour for the three

types of soils tested is compared and contrasted. The outcome of the analysis is explained in terms of the different material characteristics and for the naturally cemented sands these are related to their different geological origins and histories. The pre-yield and post-yield behaviour of the two naturally cemented soils are compared and the influence of state and structure on the maximum shear modulus discussed. Finally the conclusions from the work are summarised in Chapter 8.

2. LITERATURE REVIEW

2.1 INTRODUCTION

In the last decade research on the fundamental behaviour of soils has drawn specific attention to the study of natural soils in an attempt to provide a unified framework for the understanding of their mechanical properties. Tavenas and Leroueil (1987) reviewed the behaviour of a number of soft clays, showing that the concepts of the limit state and critical state (Roscoe et al, 1958) formulated for reconstituted clays could be applied to natural intact clays. However a clear distinction was made between reconstituted and natural clays. After deposition natural clays undergo a series of geological processes which confer on them a "structure" that influences many aspects of soil behaviour such as strength, stiffness and yielding.

Burland (1990) analysed the influence of structure on the behaviour of natural clays by means of comparisons with reconstituted clays. The latter had properties which were termed "intrinsic" to indicate that these were inherent to the soil. In contrast to reconstituted clays, natural clays had a "structure" which was seen to be the result of fabric and bonding.

The analysis of the influence of structure was extended by Leroueil and Vaughan (1990) to other natural soils such as clay shales, weak mudstones, residual soils, cemented sands and weak rocks in general. These soils were all termed "structured soils" to indicate that they all had common patterns of behaviour which were different from those of reconstituted soils.

In the following review the current knowledge of natural soils will be presented, pointing out aspects of their behaviour which formed the background to the study performed here on naturally cemented sands. Work on artificially bonded soils will also

be considered. One of the sections in this chapter reviews some of the fundamental concepts which explain the shear behaviour of sands and which provided a conceptual basis for the present study.

2.2 THE BEHAVIOUR OF NATURAL CLAYS

2.2.1 One-dimensional compression

Before structure was recognised to influence the behaviour of natural clays, the in situ overconsolidation ratio was considered to be the controlling factor determining the behaviour of clay deposits. For instance the Shansep method proposed by Ladd and Foott (1974) suggested that intact samples be sheared at an overconsolidation ratio equal to that estimated in situ (point C in Figure 2.1), after being one-dimensionally compressed to vertical effective stresses beyond their preconsolidation pressure. The preconsolidation pressure (σ'_{vc}) is the vertical effective stress at which an abrupt change in compressibility occurs in one-dimensional compression. In this case the concern was that of overcoming the effects of sample disturbance but, as observed by Tavenas and Leroueil (1987), the shortcoming of applying stresses in excess of the preconsolidation pressure was that of damaging the structure of the soil so causing irreversible modifications to the soil behaviour. Tavenas and Leroueil pointed out that structural features in natural clays can be observed only if good quality samples are tested. As Figure 2.1 shows, when good quality samples are consolidated to the in situ effective stresses no significant changes of the void ratio from the in situ value would occur and the soil can retain all those physical characteristics derived from its geological history.

In an attempt to quantify the origin of structure in natural soft clays Tavenas and Leroueil (1987) considered the geological processes which are likely to take place during the life of the deposit (Figure 2.2). After primary and secondary consolidation under the overburden pressure (point A), thixotropic hardening, cementation and other processes

producing strengthening of the particle contacts were thought to be those which conferred a structure to a natural clay deposit. Their effect was that of causing an apparent increase of the preconsolidation pressure (point P) beyond the virgin compression line ($\alpha\alpha$). These concepts were re-proposed by Leroueil and Vaughan (1990) who this time emphasised the importance of examining the influence of structure by comparing the behaviour of the intact soil with that of the "destructured" soil obtained through the application of stresses in excess of the preconsolidation pressure.

Figures 2.3 to 2.5a show evidence of structure in three natural clays through comparisons between the one-dimensional compression of intact and reconstituted samples (Mesri et al., 1975; Locat and Lefebvre, 1985; Graham and Li, 1985). The reconstituted samples were generally prepared by reconsolidating a slurry which was obtained from mixing the clay at a water content equal to or greater than the liquid limit. At stresses higher than the preconsolidation pressure all of the graphs showed a rapid convergence of the compression curves of the intact soils towards states defined by the reconstituted soils. However only in the two cases of Figures 2.3 and 2.4 further loading brought the compression curve of the natural soil to coincide with that of the reconstituted soil, whereas the two curves remained parallel in Figure 2.5a. The results for Winnipeg clay shown in Figure 2.5b will be discussed in the following section. As illustrated Figure 2.4 shows a correct comparison between intact and reconstituted soils requires consideration of the pore water chemistry of the natural material. Moreover the application of stresses in excess of the preconsolidation pressure on the intact soil may result in a compression curve which is not coincident with the normal compression line of the reconstituted soil because of differences in fabric which can be eliminated only through further straining.

Burland (1990), recognising the uncertainties related to the definition of "destructured soil", considered reconstituted soils as a reference material to which the behaviour of intact clays could be compared. Fabric was then included as a component of structure

in addition to bonding. Differences in fabric were thought by Coop et al. (1995) to be responsible for the offset and parallelism between the one-dimensional compression lines of intact and reconstituted samples of Boom clay, as shown in Figure 2.6. This conclusion was justified on the basis of results of oedometer tests on artificial samples consisting of separate sand and clay layers for which the normal compression line was found to be parallel to and above that of the equivalent reconstituted samples created by mixing the same proportions of sand and clay. The lower specific volumes of the latter were thought to result from the clay particles infilling the pore spaces between the sand grains. Structure in Boom clay was therefore seen as arising from a fabric at a microscopic scale, giving rise to similar effects to those observed at a macroscopic scale in the artificially layered samples.

Evidence of the presence of structure in natural clays was given by Burland (1990) through the comparison of the in situ states of a large number of normally consolidated clay deposits with the normal compression lines of the same clays when reconstituted. To represent the equilibrium states in one-dimensional compression of the reconstituted clays with a unique normal compression line, the void index (I_v) was plotted against the logarithm of the vertical effective stress (σ'_v) as shown in Figure 2.7. The void index was defined as:

$$I_v = \frac{e - e^*_{100}}{e^*_{100} - e^*_{1000}} = \frac{e - e^*_{100}}{C_c^*} \qquad (2.1)$$

where e^*_{100} and e^*_{1000} indicate the void ratios of the reconstituted soils at values of σ'_v of 100 kPa and 1000 kPa respectively and C_c^* is their compression index. This line was named the intrinsic compression line (ICL), where the attribute intrinsic was used to refer to those properties which were inherent to the soil and independent of its natural state. As shown in Figure 2.8 the in situ states of normally consolidated natural clay deposits when plotted in terms of I_v against the logarithm of σ'_{vo} defined a narrow band which was represented by a single line named the sedimentation compression line (SCL). This line was shown to lie above the ICL and to be approximately parallel to it

for values of σ'_{vo} ranging from 100 to 1000 kPa. The offset between the ICL and the SCL was attributed to the presence of structure in the natural clay deposits. By virtue of their structure the natural clays examined by Burland (1990) were shown to be able to carry a vertical effective stress approximately five times greater than that carried by the reconstituted soils at similar values of I_v. Examples were however given by the author of normally consolidated clays having different in situ states from those represented by the SCL, as shown in Figure 2.9. States above the SCL were associated either with cementing or with a slow deposition which results in an open fabric, easily removable when the soil is one-dimensionally compressed to high stresses. In contrast states lying between the ICL and the SCL were explained as resulting from rapid deposition and an oriented fabric which could not be easily removed by one-dimensional compression at high stresses; in this case no convergence towards the ICL would be observed. Therefore the SCL has to be regarded as representative of the in situ states of clay deposits characterised by similar environments of deposition and similar modes of development of the structure.

For overconsolidated clays the effects of structure and stress history need to be distinguished. In this case the stress at which an abrupt change in compressibility occurs in one-dimensional compression, does not necessarily indicate the maximum pressure or preconsolidation pressure experienced by the soil during its geological history. Burland (1990) suggested that the latter can be estimated from reference to the SCL. However as mentioned above, the SCL is not representative of the in situ states of all normally consolidated clays and a reconstruction of the geological history of the deposit may be helpful in providing an alternative and comparative estimate of the preconsolidation pressure. In addition for overconsolidated clays having low void ratios an abrupt change in compressibility can occur in the vicinity of the ICL so that the effects of structure in one-dimensional compression would be obscured, although these effects would be apparent during shearing (Leroueil and Vaughan, 1990).

2.2.2 Shearing

The shear behaviour of natural soft clays was analysed by Tavenas and Leroueil (1987) using the concepts of Critical State Soil Mechanics (Roscoe et al., 1958; Schofield and Wroth, 1968) developed for reconstituted soils. The initial stress-strain behaviour of natural soft clays was seen to be characterised by small volumetric and shear strains as long as the state of the soil was kept within the state boundary surface or limit state. From a review of data on several clays the authors showed that the location of the state boundary surface of the intact clays was controlled by the preconsolidation pressure (σ'_{vc}) , defined as the effective stress at which an abrupt change in compressibility was observed in one-dimensional compression. In Figure 2.10 σ'_a and σ'_r are the axial and radial effective stresses respectively. It can be seen that the state boundary surfaces of the intact soils can be seen to lie above those of the "destructured soils". Shearing performed on intact samples at confining stresses higher that the preconsolidation pressure produced a reduction in size of the state boundary surface as a consequence of the progressive loss of structure. It was also observed that the different shapes of the state boundary surfaces of intact and destructured clays arose from the increase in strength produced by the presence of structure in the intact soil.

Graham et al. (1983) showed that the concept of normalization developed by Henkel (1960) and Roscoe et al. (1958) for the shear behaviour of reconstituted overconsolidated clays also applies to natural clays. Reconstituted samples unloaded from different preconsolidation pressures on the normal compression line to similar overconsolidation ratios, show similar stress-strain responses when the shear stresses are normalized by the preconsolidation pressure. Graham et al. (1983) tested intact samples of Winnipeg clay taken from the same site and at different depths so that the samples had similar geological histories but different preconsolidation pressures. It should be noted that the preconsolidation pressure of the intact samples was that indicated as σ'_{vc} in Figure 2.5a. It was observed that the stress-strain curves for undrained tests performed on the intact samples at the same overconsolidation ratio were similar if the shear

stresses were normalised with respect to σ'_{vc}. Moreover, as Figure 2.11 shows, normalization of the stress invariants $q = \sigma'_a - \sigma'_r$ (deviator stress) and $p' = (\sigma'_a + 2\sigma'_r)/3$ (mean effective stress) with respect to σ'_{vc} reduced the yield surfaces to a unique curve. The data in this case were obtained from drained and undrained triaxial tests on intact samples which had been one-dimensionally compressed to the in situ state. The yield points were identified examining a variety of stress-strain relationships which were found to be bi-linear.

The outcome of these studies showed that the shear behaviour of natural clays was controlled by their state boundary surfaces. Tavenas and Leroueil (1987) pointed out that the effective stress paths followed in the tests also had an influence on the stress-strain behaviour and strength of natural clays. It should be noted that in the case of undrained tests, the preconsolidation pressure used in the normalization by Graham et al. (1983) can be considered as being comparable to the equivalent pressure. For drained tests the authors probably assumed that volumetric strains before yielding were small so that they could be disregarded; later Graham et al. (1988) suggested that equivalent pressures taken on the locus of either the isotropic yield states or the critical states might have been alternatives to the preconsolidation pressure adopted in the earlier normalisation. As Figure 2.5b shows, these methods in the authors' case were all equivalent simply because the loci of the yield points in isotropic and one-dimensional compression determined from intact samples of different initial specific volumes were parallel in volume-stress space, as was the locus of critical states. It should also be pointed out that for Winnipeg clay the loci of yield states in one-dimensional and isotropic compression did not coincide with the compression curve followed by the soil after yielding, as can be seen in Figures 2.5a and 2.5b.

A different approach was followed by Burland (1990) who suggested that the shear behaviour of natural and reconstituted clays should be compared so that the influence of structure could be highlighted and separated from that due to state. The author proposed to account for the influence of state by normalizing the results of both intact

and reconstituted clays with respect to an equivalent pressure taken on the ICL. An example of such normalization was provided by Rampello et al. (1993) for drained and undrained triaxial compression tests on Vallerica clay, a stiff overconsolidated clay. All of the samples had similar initial specific volumes (v_i) and when isotropically compressed defined a normal compression (NCL) line in semi-logarithmic space which was parallel to and above that obtained for the reconstituted soil. As shown in Figure 2.12b the critical state lines (CSL) of intact and reconstituted soils when plotted in terms of specific volume (v) and mean effective stress, were also found to be parallel to the normal compression lines. The offset between the critical state line and normal compression line of each soil was the same. The differences in the current state of the intact and reconstituted samples at the peak deviator stress were taken into account by normalising the stress invariants q and p' with respect to an equivalent pressure p'_e. Figures 2.12c and 2.12d show the normalized peak states of the intact soil when the equivalent pressure was taken on the normal compression line either of the reconstituted or of the intact natural soils. In the first case (Figure 2.12c) the normalized peak states of the intact soil lay to the right of the critical state defined by the reconstituted samples, reflecting the offset in v : logp' space of the critical state line of the intact soil with respect to that of the reconstituted soil. This effect was accounted for by considering the second type of normalization shown in Figure 2.12d. In this way it was shown that even accounting for differences in the current states relative to the appropriate normal compression lines the behaviour of the natural soil differed from that of the reconstituted soil, resulting in an increase of strength of the former which the authors attributed to the effects of structure.

A similar approach was used by Coop et al. (1995) when analysing the results from undrained triaxial compression and extension tests on intact and reconstituted samples of Boom clay (Figure 2.13). Also in this case normalization for each soil was made with respect to their corresponding normal compression lines defined in isotropic compression which the authors reported to be parallel in v : logp' space. The location of the peak states of the intact soil above those of the reconstituted soil was also in this case

attributed to structure.

2.3 THE SHEAR BEHAVIOUR OF SANDS

The shear strength of sand has been frequently related to the relative density (D_r) (Rowe, 1969; Cornforth, 1973) which is defined as:

$$D_r = \frac{v_{max} - v}{v_{max} - v_{min}} \tag{2.2}$$

where v_{max} and v_{min} are the maximum and minimum specific volumes determined using standard procedures in BS:1377 (British Standards Institution, 1990) and v is the current specific volume. These approaches did not consider the influence on strength of variations in the confining pressure. Casagrande (1936) described the shear behaviour of dense and loose sands. A dense sand after reaching a maximum shear stress which is associated with dilation, undergoes a progressive loss of strength until it finally continues to deform with no further changes in volume and stresses. When a loose sand is sheared the shear stress reaches a maximum value through volumetric compression and further deformation can occur without causing stress and volumetric changes. Casagrande (1936) first introduced the notion of critical void ratio, defined as the state at which shearing occurs without volume changes. Every "cohesionless" soil was seen as having a given critical void ratio. Only later was it recognised that the critical void ratio is stress level dependent. From the notion of critical void ratio the concept of critical state was defined by Schofield and Wroth (1968) as follows: "soil and other granular materials, if continuously distorted until they flow as a frictional fluid, will come onto a well defined critical state determined by the two equations ":

$$q = M\, p' \tag{2.3}$$

$$v = \Gamma - \lambda \ln p' \tag{2.4}$$

where M, Γ and λ are constants for a particular soil. It is therefore possible to combine

the mean effective stress and specific volume of soil "in any state to plot a single point". The loci of the critical states becomes a reference from which to predict the total change from any initial state expected when a soil is uniformly distorted until it flows as a frictional fluid. As pointed out by Schofield and Wroth (1968) the concept of critical state is associated with that of power dissipation as friction and neglects the possible degradation or orientation of particles. Dilation and compression can therefore be explained with reference to the critical state and associated respectively to initial states which are denser (dryer) and looser (wetter) than the critical state.

Although the critical state concept allows the prediction of density changes during shearing, it does not explain the shear mechanism controlling the peak strength of dense soils. This is explained by the stress-dilatancy theories. A simple stress-dilatancy relationship can be derived from a saw-blade model and can be written in the following general form:

$$\phi' = \phi'_c + \nu \qquad (2.5)$$

where ϕ' is the mobilised friction angle, ϕ'_c is the angle of friction along the inclined planes and ν is the angle of friction to the horizontal of the true plane of sliding. The friction angle ϕ'_c can be thought of as being the critical state friction angle (ϕ'_{cs}), constant for a given type of soil, since the condition of zero volumetric changes would imply a ν of zero. According to Equation 2.5 the maximum or peak angle of friction ϕ'_p is mobilised when the angle of friction ν associated with dilation is a maximum (ν_{max}).

The value of ν_{max} is a function of the maximum rate of dilation experienced by the soil. Quantitative relationships between ϕ'_p and ν_{max} are given by various stress-dilatancy theories, some of which consider the soil as a particulate material (Rowe, 1962), others as a continuum (Taylor, 1948).

For shearing in triaxial compression the stress-dilatancy relationship proposed by Rowe (1962) can be written as:

$$\frac{\sigma'_a}{\sigma'_r} = \tan^2 (45^\circ + \frac{\phi'_f}{2}) (1 - \frac{\delta\varepsilon_v^p}{\delta\varepsilon_a^p}) \qquad (2.6)$$

where $\delta\varepsilon_v^p$ and $\delta\varepsilon_a^p$ are the plastic volumetric and plastic axial strain increments respectively and ϕ'_f varies between the inter-particle friction angle ϕ'_μ and the critical state friction angle ϕ'_{cs}. For ϕ'_f equal to ϕ'_c Equation 2.6 can be written in terms of the stress invariants q and p' and of the volumetric and shear plastic strain increments $\delta\varepsilon_v^p$ and $\delta\varepsilon_s^p$ as follows:

$$\frac{\delta\varepsilon_v^p}{\delta\varepsilon_s^p} = \frac{9\ (M - \eta)}{9 + 3M - 2M\eta} \qquad (2.7)$$

where the stress ratio (η) is equal to q/p' and M is the value of η at the critical state.

Following Taylor's (1948) analysis in which the plastic work done by the applied forces on the boundaries is dissipated entirely as friction, the stress-dilatancy relationship for axisymmetric conditions can be written as:

$$\frac{q}{p'} = M - \frac{\delta\varepsilon_v^p}{\delta\varepsilon_s^p} \qquad (2.8)$$

where $\delta\varepsilon_s^p$ is the plastic shear strain increment.

The peak strength in sands is not only influenced by the density of the soil but also by the mean effective stresses which can either encourage the dilation of the soil when these are low or inhibit when they are high. The influence of the confining stress on the peak strength may result in a curved failure envelope so that when this is replaced by a straight line over a certain effective stress range an intercept c' is found which is often called "apparent" cohesion.

The decrease in the peak angle of friction as the mean effective stress at failure increases was shown by Vesic and Clough (1968) and can be seen in Figure 2.14. The dependence of the peak strength and so the maximum rate of dilation on both the specific volume and stress level was investigated by Been and Jefferies (1985). The data in Figure 2.15 from a large number of sands demonstrated that the peak angle of friction was a function of the proximity to the critical state of the initial state of the sand (v_i, p'_i) at the start of shearing to the critical state. This concept was expressed through the definition of the initial state parameter (ψ_i):

$$\psi_i = v_{\lambda i} - \Gamma \tag{2.9}$$

where

$$v_{\lambda i} = v_i + \lambda \ln p'_i \tag{2.10}$$

where λ is the slope of the critical state line as defined by Equation 2.4. Later Jefferies (1993) recognised that although the use of the state parameter ψ_i characterised some features of sand behaviour such as strength, volumetric changes during shearing and maximum rate of dilatancy, the general stress-strain behaviour of sands should be described by reference to the current state. Atkinson and Bransby (1978) suggested the use of v_λ defined as:

$$v_\lambda = v + \lambda \ln p' \tag{2.11}$$

In this way the shear behaviour can be described using the two-dimensional plot q/p' against v_λ which normalizes the stress paths on constant p' sections. Wood (1990) proposed to replace v_λ with the state variable $v - v_{cs}$, where v_{cs} is the specific volume at the critical state for the current mean effective stress. This state variable has the benefit of not requiring the assumption of a straight critical state line in the v : lnp' plane.

Particle breakage in sand has been considered as the major mechanism controlling the plastic volumetric compression (Vesic and Clough, 1968; Coop and Lee, 1993).

Nonetheless data on sands isotropically compressed from both loose and dense states showed that it was possible to identify a unique and straight normal compression line and critical state line in v : lnp' space (Miura and Yamonouchi, 1975; Atkinson and Bransby, 1978; Coop and Lee, 1993). This was justified by Coop and Lee (1993) through a quantification of the amount of particle crushing, defined by the area between the grading curves before and after the test, for three different sands (a carbonate, a quartz and a residual sand). It was observed that two unique relationships existed between the amount of particle breakage and the logarithm of p' which corresponded respectively to the critical state and normal compression lines. Therefore the data from drained shearing of the three different sands could be normalized by the authors considering an equivalent pressure taken on the normal compression line which allowed a state boundary surface to be identified. Figure 2.16 shows an example of the normalization performed on both drained and undrained tests for the carbonate sand from which it can be seen that the state boundary surface has a peak on the wet side of the critical state, a feature that was predicted by Chandler (1985) for soils with crushable grains.

It should be noted that using one of the above representations of the shear behaviour of sands has to be considered as a means of describing only some aspects of their behaviour accounting for the effects of both specific volume and mean effective stress. The shear behaviour of sands is in fact stress path dependent. For the carbonate, quartz and residual sands Coop and Lee (1993) showed that the normalised stress paths of standard drained tests differed from those of drained tests at a constant p' and of undrained tests as the example of the carbonate sand shows in Figure 2.16. In Figure 2.16a the stress paths are mainly from constant p' tests whereas the stress paths labelled as 2 and 5 indicate examples of standard drained tests. The stress paths from undrained tests shown in Figure 2.16b all had a typical "s" shape and for normally consolidated samples they curved inside the state boundary surface identified from the drained tests. Moreover sands can reach a given state both through overconsolidation and through compaction and this was shown by Coop and Lee to result in different stress paths

during undrained shearing as can be seen in Figure 2.17. Overconsolidated samples are those obtained by unloading the soil after being compressed on to the normal compression line, whereas compacted samples are those in which a higher density is achieved under zero stresses. The stiffer behaviour of the overconsolidated sample, which was suggested to be a general feature of sands, was explained as the consequence of less particle crushing experienced in this case by the soil during shearing, since breakage of the grains had already occurred during isotropic compression.

2.4 STRUCTURE IN NATURALLY CEMENTED SANDS

Many examples can be found in nature of sand deposits standing in steep slopes and excavations as reported by Dusseault and Morgenstern (1979), Clough et al. (1981) and Frydman (1982). Such steep gradients can be attributed to three main factors:

- the presence of high suction, usually associated with the presence of clay minerals;
- exceptionally high values of friction angle;
- cohesion due to bonding.

These types of observation have often prompted studies of the behaviour of natural sands.

The term cohesion is often used to indicate the intercept of the failure envelope with the p' equal zero axis. For soils having no tensile strength this intercept can arise when a curved peak failure envelope is replaced by a straight line over a limited range of stresses. In this case the intercept should be more properly referred to as apparent cohesion to distinguish it from the intercept that would be observed for soils with inter-particle bonding. In the present work cohesion, sometimes termed true cohesion, will be

used to refer to the strength that â soil would have at p' equal zero by virtue of the presence of bonding between the particles.

Bonding in sands can be the result of cementation due to the precipitation from aqueous solutions of carbonates, gypsum, aluminum oxides, silicates, iron oxides and hydroxides (Dapples, 1972). However not all of the cement content contributes to cohesion as it may simply infill the pore spaces between the grains, so reducing the porosity of the sediments. Pressure and temperature can be responsible for the solution and redeposition of material at the grain boundaries as cement. The degree of bonding depends on the extent to which the cement coats the grains, its properties of adhesion and the roughness of the grain surfaces. For instance iron oxide present in silica sands provides weak bonding because of its weak adherence to the quartz grains (Dapples, 1972).

Natural sands can also be characterized by a well developed fabric with a high degree of inter-particle contacts. Taylor (1950) studied the processes which cause a reduction in porosity during the diagenesis of a sand deposit. Pore filling by crystallization of cement was not the only cause of porosity reduction but other processes were also recognised which were related to the solution and recrystallization of material at the grain contacts where the stresses are higher. Pressure solution processes were observed for quartz sands and associated with the depth of burial and perhaps also to an increase in geothermal gradient as the solubility of quartz in water increases with increasing pressure and temperature (Maxwell, 1964). Dusseault and Morgenstern (1979) reported that small amounts of solution of silica at the points of grain contact can give rise to a significant increase in density. The authors suggested that this process results in the development of a large amount of grain contacts without necessarily creating a bonded structure. Figure 2.18 shows the types of contact that can arise from pressure solution processes. The term "locked sands" was introduced by Dusseault and Morgenstern to indicate natural sands characterized by this type of fabric and by very high densities. Locked sands when compacted in the laboratory will have maximum densities which are lower than the in situ density and were therefore distinguished by the authors from loose

and dense sands.

A clear distinction can be found in the work by Dusseault and Morgenstern between interlocking and cohesion due to bonding. However other authors have attributed true cohesion to the presence of interlocking. Dobereiner and De Freitas (1986) and Barton (1993) related the degree of interlocking, expressed as the percentage of tangential contacts of all the grain contact types (tangential index TI %) observed in thin sections, to the unconfined compressive strength (Figure 2.19). It should be noted that unless interlocking creates a jigsaw of grain contacts the unconfined compressive strength can only be due to either suction or bonding. Therefore the above relationship should be regarded only as empirical and cannot provide any fundamental explanation of the mechanism governing the shear behaviour of the materials tested. In this respect the contribution of pure interlocking in the absence of bonding to the strength of a locked sand should then be seen as purely frictional and related to the dilation experienced by the soil.

Dusseault and Morgenstern observed that locked sands were characterised by peak frictional strengths higher than those displayed by dense sands and also by unusually high rates of dilation as shown in Figure 2.20. These features were attributed to their interpenetrative fabric. A similar conclusion was drawn by Clough et al. (1981) to explain the high friction angles observed when testing naturally cemented quartz sands. Both works however overlooked the influence of state on the shear behaviour of sands which should have been separated from the effects of fabric. Nevertheless the importance of these works was that they pointed out that natural sands as well as natural clays could have well defined fabric which may be responsible for features of behaviour not accountable for solely in terms of state. In this context therefore the term structure can be introduced also for sands to indicate those physical characteristics which derive not only from bonding but also from fabric.

Although many natural sands are characterised by exceptionally high densities, the

opposite can be also observed. Loose and open types of fabric resulting in high void ratios are found in sands in which the cementing process occurred shortly after deposition, a process which may be termed concurrent bonding. In this case Apthorpe et al. (1988) and Fookes (1988) suggested that the degree of cementing and density were not related to the depth of burial but rather to the environmental conditions during deposition, in particular the water depth, temperature, water current energy and rate of accumulation of the sediments. Therefore, because of the variation of the environmental conditions that can occur during the deposition of sediments, cemented sands from the same site are often extremely variable (Frydman, 1982). This has led many researchers to develop and test artificially cemented sands in which factors such as the degree of bonding, grading and density could be controlled and their effects on the mechanical behaviour separated (Clough et al., 1981; Maccarini, 1987; Huang and Airey, 1991; Coop and Atkinson, 1993).

2.5 THE BEHAVIOUR OF CEMENTED SANDS AND WEAK ROCKS

So far the term bonded sands rather than sandstone has been used, implying that these types of soil had undergone only mild diagenetic processes during their transformation from soils to rocks. These soils also fall in the category of weak rocks which may be defined as those materials with an unconfined compressive strength within the limits established by various classification systems, some of which are reported in Figure 2.21. Studies performed by various researchers on weak rocks such as calcarenite, chalk and volcanic rocks have shown that in these materials structural features are particularly evident. Some of these materials were reviewed by Leroueil and Vaughan (1990) who pointed out the resemblance of many of their patterns of behaviour with those observed for structured soft and stiff clays.

As for clay soils, a better insight into the effects of structure on the behaviour of cemented sands and weak rocks can be obtained by comparing intact and reconstituted

soils. For an artificially cemented sand the corresponding reconstituted soil is represented by the unbonded soil. For a naturally bonded sand the corresponded reconstituted soil should be considered as a soil with the same grading as the intact soil in which bonding and fabric have been destroyed by mechanical action. The properties of the reconstituted soils are again referred to as intrinsic properties.

Figures 2.22 to 2.24 show the results of one-dimensional compression tests from an artificially bonded sand (Maccarini, 1987), a chalk (Leddra, 1990; Petley et al., 1993) and a volcanic rock (Aversa, 1991). Figure 2.22 shows that at a given stress the bonded soil can exist at void ratios which are impossible for the corresponding reconstituted soil. However after yielding as the load is increased the states of the intact soils tend towards those defined by the reconstituted soil. Yielding was associated with the onset of bond degradation. Coop and Atkinson (1993) found similar results for the isotropic compression of an artificially cemented carbonate sand.

The samples of Figure 2.22 each had the same method of creating bonding. The extent of the movement of the states achieved by the bonded soil outside the space permissible for the reconstituted soil was shown to decrease as the initial void ratio decreased. For low values of the initial void ratios yielding occurred very close to the compression line determined for the reconstituted soil. It was also shown that bonding contributed more to the strength of the soil, quantified by the unconfined drained shear strength, as the void ratio decreased. This was explained by Vaughan (1988) as being due to the increase of the bonded inter-particle contacts per unit area. The influence of a variation in the initial void ratio on the one-dimensional compression of the artificially bonded soil from Maccarini (1987) appears to be consistent with the results obtained by Leddra (1990) and Petley et al. (1993) for chalk (Figure 2.23). This is suggested by the fact that the stress paths tend toward that of the "destructured" soil which has a K_o of 1 - $\sin\phi'$ as given by Jaky (1944) for uncemented normally consolidated soils. As can be seen in Figure 2.24 the volcanic tuff tested by Aversa (1991) provided an example of a naturally bonded soil which because of its very high density did not reach states beyond those

permissible to the reconstituted soil in one-dimensional compression. Vaughan (1988) reviewing data from various works showed that the gradient of the post-yield compression curves of bonded soils, as identified in e : log σ_v' space is a function of the initial void ratio corresponding to the in situ void ratio (Figure 2.25).

The shear behaviour of bonded sands and weak rocks in general is governed by the confining pressure. Clough et al. (1981) studied the shear behaviour in drained triaxial compression of naturally cemented sands with various degrees of cementing, in which the cementing agents were mainly silicates and iron oxide. Figures 2.26a and 2.26b show that an increase in the confining pressure produced a transition from brittle to ductile behaviour and that this transition occurred at higher confining stresses for the moderately cemented soil having a greater degree of cementing. These observations were confirmed by the shear behaviour of two artificially cemented sands also studied by the authors, which were prepared at the same density but using two different percentages of Portland cement by weight. This transition from brittle to ductile behaviour was related to the relative contributions of bonding and friction to the mechanisms governing the strength of the soil. For the same degree of bonding both naturally and artificially cemented soils showed a volumetric response which passed from dilation to compression as the confining stresses increased.

Clough et al. (1981) found that peak strength increased with confining stress. As shown in Figure 2.27a the failure envelope of the artificial soils with strong and weak bonding tested at the same initial densities had similar friction angles at peak and increasing cohesion intercepts as the degree of cementing increased. From Figure 2.27b it can be seen that also for the naturally cemented sands the cohesion intercept increased as the degree of cementing increased. The soil with the highest degree of bonding (SLAC-1) was also found to have a higher peak friction angle than that of the more weakly cemented sands (PCA-1 and PCA-2). This was attributed to the higher density of the more strongly cemented sand and to the high degree of interlocking between the particles.

Coop and Atkinson (1993) investigated the behaviour in drained triaxial compression tests of an artificially cemented carbonate soil with gypsum as the cement. A characteristic of carbonate sands is that they have grains which are more susceptible to crushing than other granular soils. The artificially cemented samples had similar initial densities and the same degree of bonding. The stress-strain curves of the cemented samples sheared at low, intermediate and high confining stresses are shown in Figure 2.28 and compared with those of the uncemented soil at similar initial stress-volume states. The mechanisms governing the shear behaviour of the bonded soil were summarised by the authors in the schematic diagram shown in Figure 2.29. At low confining stresses the stress-strain behaviour during shearing was observed to be linear almost up to the peak state (CEM2 in Figure 2.28c). The peak strength was found to be above the frictional failure envelope identified from the reconstituted soil and this was seen as resulting from the cohesive component of strength given by the cement. At high confining stresses, except for CEMF in Figure 2.28a, yield occurred during isotropic compression. The shear strength was then shown to be purely frictional and the stress-strain behaviour of the bonded soil resembled that of the reconstituted soil. At intermediate stresses the bonded soil still exhibited an initial linear stress-strain response during shearing but little or no peak was observed (CEM3 in Figure 2.28b). The yield point at the end of the linear response was associated with the onset of bond degradation and particle crushing as the stresses were transferred to the particles. The shear behaviour of the cemented soil was further analysed by Coop and Atkinson by comparing the normalized stress path of cemented and uncemented sands with respect to an equivalent pressure taken on the critical state line which was found to be unique for both soils. This normalization will be presented and discussed in detail in the following chapters.

Anagnostopoulos et al. (1991) conducted a series of drained triaxial tests on a weak marly rock from the Corinth Canal. At low confining stresses the stress-strain behaviour was brittle and the soil dilated, whereas a ductile response and volumetric compression was observed at higher confining pressures. Yielding was identified as an abrupt change

in the stress-strain curve and was related to the onset of bond degradation. Figure 2.30 shows that also in this case the yield points during shearing were almost coincident with the peak states at low confining stresses, whereas at higher confining stresses they occurred well before failure. An elliptical yield curve centred on the isotropic stress axis was found which was also postulated to be coincident with the surface delineating the stress space of elastic behaviour.

Both the results for the artificially cemented carbonate soil and the marl indicated that at low confining stresses the shear behaviour was characterised by marked strain-softening and by a linear behaviour almost up to the peak state. However no evidence was given for the reversibility of the stress-strain response within the linear range. This aspect was investigated by Elliott and Brown (1985) when studying the shear behaviour in triaxial compression of an air dried oolitic limestone (Bath Stone) tested at various confining pressures up to 30 MPa. Yield was defined as the point at which irrecoverable (plastic) strains started to develop. From the loading-unloading cycles performed during shearing and shown in Figure 2.31 it can be seen that yield occurred at the point where both the deviator stress-axial strain curve and the volumetric strain-axial strain curve ceased to be linear.

Elliott and Brown (1985) reported that at low confining stresses small irrecoverable strains and hysteresis developed between the yield point and the peak state. The authors suggested that in the vicinity of the peak state strain localisation took place resulting in the formation of a macrofracture and in a rapid decrease of the deviator stress. Continued shearing eventually occurred between two substantially intact blocks along the shear discontinuity. At intermediate stress levels shearing was found to occur on multiple shear surfaces. The ductile behaviour at high confining stresses was associated with a progressive pore collapse. A yield curve was determined as can be seen in Figure 2.32, showing the dependence of the deviator stresses at yielding on the confining stresses. At high confining pressures the trend of yield points appears to reach an isotropic state.

A problem often addressed by various authors when examining the strength of bonded sands and weak rocks is that of trying to separate the component of strength due to true cohesion from that due to dilation. Vaughan (1988) analysing the results from Maccarini (1987), observed that the peak state occurred whilst the sample was undergoing volumetric compression and that the maximum rate of dilation took place only subsequently to the attainment of the peak state (Figure 2.33). This observation suggested that the intercept of the failure envelope was due to cohesion arising from bonding rather than dilation. The author also suggested that because of the cohesive nature of the intercept this had to be unrelated to density which seems to contradict the dependence found between density and unconfined drained compressive strength shown in Figure 2.22. A maximum rate of dilation occurring after the peak state was also observed by Aversa et al. (1991) for the volcanic tuff.

The importance of making accurate determinations of stresses at yield for weak rocks was highlighted by Clayton (1989) when reviewing field data on chalk. It was pointed out that although weak rocks are characterized by high values of stiffness, stresses at yield can be small so that settlements of soil structures can become significant when the yield stresses are exceeded.

Laboratory determinations of yield stresses and stiffness of cemented sands and weak rocks in general require the development of appropriate measuring techniques which will be discussed in detail in Chapter 3. Accurate laboratory determinations of stiffness and its variation with strains were obtained for several weak rocks by Goto et al. (1991), Tatsuoka et al. (1993) and Kim et al. (1994) and examples are shown in Figure 2.34. In this figure the Young's modulus (E) was calculated as the secant, tangent and equivalent moduli (E_{sec}, E_{tan} and E_{eq} respectively) and q_{max} is the maximum deviator stress where failure occurs..

Kim et al. (1994) also showed that there was good agreement between the maximum shear modulus determined from drained triaxial compression tests on a weak rock from

the site of Sagamihara and those obtained from field shear wave velocity measurements conducted in situ. Profiles of the maximum Young's modulus (E_{max}) with depth were obtained by Clayton (1989) on chalk at three different sites by means of surface wave velocity measurements as shown in Figure 2.35. The different profiles were attributed to differences in densities and joint characteristics which might have also determined the variation of the modulus with depth. In contrast the field determinations performed by Kim et al. (1994) down to a depth of 100 m showed substantially no variation with depth, leading the authors to conclude that the in situ stresses had substantially no influence on stiffness. The studies of Kim et al. although providing a considerable progress in terms of measuring techniques both in the laboratory and in the field, did not however investigate the factors controlling the stiffness of these soils and in particular the contribution of bonding. In contrast systematic laboratory studies on stiffness have been performed for reconstituted clays and sands. These works established the dependence of stiffness on the current state of the soil (Hardin and Black, 1966; Houlsby and Wroth, 1991; Viggiani and Atkinson, 1995; Rampello et al., 1994) and reference to some of them will be made in the following chapters when relevant to the analysis of the stiffness data obtained in the present work.

3. LABORATORY EQUIPMENT AND PROCEDURES

3.1 INTRODUCTION

The experimental work consisted of triaxial compression tests performed on different types of cemented sands and of a set of similar tests carried out on the corresponding uncemented soils. The testing programme was intended to investigate the behaviour of the cemented soils at both small and large strains, over a large range of mean effective stresses.

In conventional stress path triaxial cells the maximum radial effective stress that can be applied to a sample is well below the isotropic yield of the cemented soils. Since the study was intended to investigate both their strain-softening and strain-hardening behaviour, higher capacity triaxial cells had to be employed. The majority of the experiments were performed in three high pressure stress path triaxial systems having similar facilities as those existing in a conventional triaxial cell. Apparatus developed at City University (Taylor and Coop, 1990) allowed the samples to be tested under maximum confining pressures of 5, 10 and 70 MPa. A stress path controlled Bishop and Wesley (1975) cell was also used for tests at low pressures. Their characteristics and components will be described in the first part of this chapter with details of the accuracy of the data attainable from the measuring devices.

A series of tests was specifically designed to study both yielding and pre-yield behaviour of the cemented samples during shearing and to determine the variation of the shear modulus from very small to relatively large strains. It has been long recognised that conventional triaxial testing methods can only provide reliable stress-strain relationships beyond strains of 0.01 %. For soils characterised by high values of stiffness at small strains and by relatively coarse grain size, as in the case of cemented sands, the limitations identified for the measurement of stiffness of softer soils become more severe

and modifications of apparatus and testing procedures proved necessary. Observations made using external instrumentation in tests on sedimentary soft rocks by Goto et al. (1991) were found to be affected by errors so significant that internal gauges were necessary. As the tests performed in this research needed to determine material stiffness at very small strains, the accuracy normally achieved in the internal measurements of axial stresses and strains had to be improved. On the basis of these considerations one of the high pressure systems was modified and some new components designed.

The first part of the laboratory work was aimed at improving the output signal from the internal instrumentation through modifications to the hardware and software of the system. However, preliminary tests showed that these changes alone were not sufficient to achieve the accuracy of results required and revealed a number of faults in the existing configuration of the apparatus and in the experimental procedures adopted. A non-uniform distribution of stresses and strains throughout the cemented samples as well as an improper functioning of the loading system were found to be problems that had to be addressed in order to attain reliable and accurate determinations of stiffness at small strains. Revisions to the geometry of the apparatus and experimental procedures were undertaken, resulting in the design of new pieces of apparatus and measurement instruments as well as the modification of the sample preparation and setting up techniques. In the second part of the chapter details of these developments are described.

3.2 THE TRIAXIAL SYSTEMS

3.2.1 Low pressure system

The triaxial cell consisted of the original hydraulic cell described by Bishop and Wesley (1975) connected to analogue pressure controllers and instrumented with pressure, force and displacement transducers. An IBM compatible computer fitted with an analogue to digital converter card monitored the stresses and strains.

The cell had three pressure control units: cell pressure, ram pressure and back pressure. Air pressure with a maximum value of 800 kPa was supplied by an air compressor. The air pressure was regulated by analogue electro-pneumatic pressure converters controlled by the computer through the digital to analogue converter on the interface card. Air/water interfaces converted the air pressures to water pressures which were then applied to the cell and in the axial loading cylinder. A 50 cc Imperial College volume gauge acted as the interface for the back pressure supply.

For strain controlled axial loading a Bishop ram (Bishop and Henkel, 1962) was placed between the air/water pressure interface and the axial loading cylinder. A two way valve made it possible to disconnect the air/water interface from the cell to obtain a constant volume system between the Bishop ram and the axial pressure chamber at the bottom of the loading system. In this configuration a stepper motor and a gear box, which were operated by a timed relay, were able to drive the ram at a specified strain rate.

3.2.2 High pressure systems

Three high pressure triaxial cells had been developed at City University (Taylor and Coop, 1990) which were able to reach confining pressures of 5, 10 and 70 MPa respectively. All of them were computer controlled stress path cells.

The cell bodies and motorised loading frames were manufactured by Wykeham Farrance Engineering Ltd. In the 5 and 10 MPa cells the allocation of different pedestals and top platens allowed for the testing of various sample sizes. In the 5 MPa cell it was possible to test 38 and 50 mm diameter samples; in the 10 MPa cell it was possible to test 38, 50, 60 and 83 mm diameter samples. The 70 MPa cell was designed for testing 50 mm diameter samples only.

The original design of the 70 MPa cell by Wykeham Farrance was suitable only for

standard tests carried out in conventional rock mechanics. The cell produced for City University had several modifications. The length of the cell body was increased to give additional space for an internal load cell. The previous design also had a connection between the cell and the upper chamber of the axial ram so that the upward force resulting on the ram from the cell pressure was balanced. In order to allow for stress path capability, with an independent control of axial and radial stresses, the upper chamber was disconnected and provided with a separate control of hydraulic pressure, similar to the Bishop and Wesley cell. The ram stroke was increased from 25 to 50 mm so that large strains could be reached during the shearing stage. Finally, four electrical connections for the local instrumentation were provided through plugs fixed in the base of the cell.

All the cells except for the 10 MPa cell used analogue pressure converters. In the 10 MPa cell the pressure regulators were electro-manostats operated via stepper motors. To achieve both high and low pressures two parallel hydraulic systems existed for the supply of the cell pressure. Figure 3.1 shows a schematic diagram of the initial configuration of the 10 MPa apparatus which was similar to that of the 5 and 70 MPa systems. Up to 700 kPa, the pressure was applied directly through either an air/water or an air/oil interface depending on the liquid used in the cell. For the supply of high pressures a hydraulic pump based on a differential area principle amplified the air pressures delivered by the compressor and controlled by the cell pressure regulator. The high pressure circuit therefore consisted of an air driven liquid pump, a nitrogen gas accumulator which prevented pressure fluctuations and a pressure regulating needle valve. The whole system worked with oil. However since water was used as the cell fluid in the 5 and 10 MPa apparatus, an oil/water interface was placed between the cell pressure control circuit and the cell. The 70 MPa cell was instead filled with oil as the electrical wires used in the internal instrumentation could not be insulated at these pressures. For the same reason when the internal instrumentation was installed in the 10 MPa cell during the present work, the oil/water interface was removed and oil was used as the cell fluid.

Whereas in the 70 MPa cell the axial load was applied to the sample through a hydraulic cylinder located inside the cell body, in the 5 and 10 MPa cells the hydraulic cylinder was placed on the top of the loading frame. A better control and accuracy of the axial pressure was available in the 5 MPa system through the application of a back pressure in the bottom chamber of a double acting cylinder. In these cells the axial load was transferred to a ram passing through the top of the cell and sealed with an 'O'-ring. In the 5 MPa cell the axial force was measured by an internal load cell and in the 10 MPa cell by an external load cell attached to the loading ram. Since the axial force was measured externally, the measured force included the friction between the ram and the 'O'-ring seal at the top of the cell.

The axial pressure delivered to the loading piston was in all cases provided by a second high pressure circuit receiving the air pressure from the axial air pressure regulator as shown in Figure 3.1. The hydraulic circuit worked with oil and was similar to the high pressure circuit described for the cell pressure.

The pump ratios varied from cell to cell. In both the 5 and 10 MPa cells the axial pressure pump ratio was 8:1, while the cell pressure pump ratio was 12:1. In the 70 MPa cell both the cell and axial pump ratios were 110:1. In this case the hydraulic system was provided with different types of valves and accumulators from the other two cells, compatible with the higher pressures produced. In all the systems the pressures delivered by the pumps to the apparatus did not rely on the pump ratios, since a feedback loop controlled the pressures to the required values.

The control of the amplified cell pressure was dependent on a number of factors. In the 10 MPa system the air supply was controlled by electro-manostats which were driven by stepper motors through a set of relays. The control of the air pressure was in this case limited by the change in pressure corresponding to one step of the stepper motor, equal to about ± 0.4 kPa. The operation of the stepper motor required some time between the arrival of the signal from the computer and the actual change in pressure.

Instead the control of the air pressure from the analogue pressure converters mounted on the 5 and 70 MPa systems is both almost immediate and more accurate. The pressure fluctuations generated by the action of the pump were attenuated by setting the gas pressure in the accumulator to be lower than the working pressure for a particular test and by regulating the oil discharge through a needle valve which vented the circuit to the reservoir. The vent was necessary to get a continuous flow of oil through the circuit so that the pressures could be reduced as well as increased. The cell pressure could be controlled within ± 10 kPa in the 10 MPa apparatus, ± 5 kPa in the 5 MPa apparatus and ± 50 kPa in the 70 MPa apparatus.

Figure 3.2 shows a schematic diagram of the axial loading system. From the equilibrium of forces the deviator stress q acting on the sample is given by:

$$q = p_c \frac{A_a}{A_s} - \sigma_r \frac{A_r}{A_s} \tag{3.1}$$

where p_c is the pressure in the cylinder, σ_r is the cell pressure and A_a, A_r and A_s are the areas of the actuator, ram and sample respectively. The accuracy with which q can be controlled depends therefore on the accuracy of the control of p_c and σ_r. The latter has less influence for samples with a larger diameter than the ram diameter which was equal to 49 mm.

In the present work the axial circuit of the 10 MPa system was modified in order to improve the pressure control while maintaining the existing loading cylinder. As shown in Figure 3.3 the apparatus was provided with an air/oil interface so that a low pressure system could be used in parallel with the high pressure one. The use of the low pressure system produced a control of p_c within ± 0.4 kPa as given by the electro-manostat. When high pressure had to be used the control was improved by replacing the existing pump with one having a lower air/liquid pressure ratio (equal to 5:1). The change from the low to the high pressure system could be made accurately by reading the pressure in the line supplying the cylinder using a pressure transducer connected to a digital display. The transducer could be then disconnected from the cylinder and connected to

the high pressure system, ensuring that the pressure from the pump had stabilised at the value currently acting in the cylinder. At this point connection was made between the cylinder and the high pressure system.

Because of the high values of pressures reached in the 70 MPa cell a safety system was present to guard against the possibility of a puncture in the membrane. If this were to happen, the cell pressure would be transferred to the volume gauge, damaging the volume gauge and being potentially hazardous. A microswitch located at the base of the volume gauge would be triggered in such an event which would disconnect the power to the pressure converters. At the same time a safety valve placed between the accumulator and the cell would close, preventing the high pressure still present in the hydraulic system from reaching the cell and consequently the volume gauge. Other safety valves in the system were able to limit the pressure in the volume gauge, venting to the atmosphere if the pressure rose above 1 MPa.

An Imperial College 100 cc capacity volume gauge was connected to both the 5 and 10 MPa cells, while the same volume gauge with a capacity of 50 cc was used in the 70 MPa cell.

In all three systems strain controlled tests were possible using the motorised frames with which the sample could be loaded at different displacement rates, varying from 0.0001 to 5 mm/min.

3.2.3 Instrumentation

The basic instrumentation used for each apparatus consisted of cell and pore pressure transducers, an axial load cell, a volume gauge and an external axial displacement transducer.

In the Bishop and Wesley cell the pore and cell pressures were measured by Druck pressure transducers having a pressure range of 0 - 1000 kPa. The same type of transducer with a higher pressure range equal to 0 - 6 MPa was used to measure the pore pressure in both the 5 and 10 MPa cells and the cell pressure in the 5 MPa cell. A pressure transducer manufactured by Maywood Instruments Ltd with a pressure range of 0 - 10 MPa was used to monitor the cell pressure in the 10 MPa cell. In the 70 MPa cell both cell and pore pressures were measured by Maywood transducers working in the range 0 - 70 MPa. In all cases the pore pressures were measured at the base of the sample.

The axial load was measured by an internal load cell except for the 10 MPa cell, which initially used an external load cell. All of the internal load cells were manufactured by Maywood Instruments Ltd whereas the external load cell was manufactured by RDP Electronics Ltd. The internal load cells were based on an original design by Surrey University and had capacities of 5, 30 and 200 kN respectively for the Bishop and Wesley, 5 MPa and 70 MPa cells. The external load cell on the 10 MPa system had a capacity of 90 kN. In all tests carried out in the 10 MPa cell with the external load cell friction tests were performed before starting the shearing stage, in order to measure the axial load due to the friction on the ram shaft.

Axial displacements were measured externally by means of linear variable differential transformers (LVDTs). In the Bishop and Wesley cell the transducer was attached to the top of the cell and measured the movement of the crosshead of the ram (i.e the pedestal). A transducer with a stroke of 25 mm was used for this purpose. The 70 MPa cell was provided with the same type of transducer, which was attached to the frame and measured the displacement relative to the top of the cell. In the 5 and 10 MPa cells the transducers were fixed to the ram and measured the movement relative to the top of the cell. Since samples with bigger dimensions were tested in these latter two apparatus, transducers with a stroke of 50 mm were used.

Volumetric strains were calculated by the displacements of the internal piston of a volume gauge which was monitored by an LVDT, except for the 5 MPa cell where a resistive displacement transducer was attached. For both the 50 and 100 cc volume gauges the transducers had a stroke of 25 mm.

Axial strains could be measured internally in the Bishop and Wesley cell and the 5 MPa cell by means of Hall effect transducers (Clayton and Kathrush, 1986; Clayton et al., 1987). The linear range of these transducers was 5 to 6 mm and the axial displacements were measured over a central gauge length of 50 mm. Figure 3.4 shows the internal instrumentation mounted on the sample in the 70 MPa system. The instrumentation consisted of two local axial strain transducers and a strain belt. The local axial strain transducers in this case were RDP miniature linear variable differential transformers (LVDTs) type D5/200 with a linear range of 10 mm, fixed to the sample over a central gauge length of 50 mm. To enable these transducers to work under high pressures a non-conductive environment was required so that mineral oil instead of water was used as the cell fluid. A detailed description of the miniature LVDTs will be given in Section 3.3.2. The strain belt mounted on the cell was built by Imperial College and consisted of an opened circular metal strip to which strain gauges were attached to sense its movement. The belt was attached to the sample using two mounts which were glued to the membrane and connected to the belt with small screws. Because of the presence of strain gauges the axial strains reached during the test were limited by the radial strain of the sample which had to be kept within ± 5 %.

3.2.4 Computer and interface system

The apparatus described above were controlled by different types of computers and interfaces. The Bishop and Wesley cell as well as the 5 and 70 MPa cells were each connected to an IBM compatible computer. In the two former cases the interface was internal to the computer and consisted of a PC Super interface card manufactured by

CIL Electronics Ltd. The 70 MPa cell had an external interface system consisting of a Datascan 7200 module manufactured by Measurements System Ltd and connected to the computer via an RS232 cable. The 10 MPa cell was controlled by an Acorn BBC model B computer interfaced to a Spectra Micro MS unit which was manufactured by Intercole System Ltd. The communication in this case occurred via an RS423 serial cable. The BBC system is described by Clinton (1987).

The interface units provided an analogue to digital conversion (A/D) of the signal received from the transducers. The Spectra Micro MS worked with a 12 bit A/D converter over a full scale range of ± 10.24 V. The system autoscaled the voltage input over eleven ranges in order to select the one that best matched the signal. In this way it was possible to achieve a resolution down to 4.88 μV/bit, positioning the transducer as close as possible to the electrical zero. The Datascan 7200 module provided the A/D conversion over a 14 bit basis and autoscaled the signal using four voltage ranges up to ± 10 V, with a smallest resolution of 2.5 μV/bit. In the CIL interface only one gain could be selected for each channel choosing between ± 10 V, ± 1 V and ± 100 mV and the conversion was made on a 16 bit basis. As no autoranging was available the resolution for a given gain was constant unless autoranging facilities were introduced via software. However when an internal interface is used such as the CIL card noise more than resolution is a problem for accurate measurements due to the electrical noise that exists from the other components in the computer.

Another function performed by the interface units was the communication with the pressure regulators. Pressure converters need a digital to analogue (D/A) conversion of the signal sent from the computer in order to work, whereas electro-manostats are controlled by means of relays. The CIL card had a D/A converter which operated pressure converters through analogue outputs. The Spectra Micro MS worked only as a data logger and had an accompanying set of relays controlling the electro-manostats. The Datascan had a D/A converter allowing the use of analogue pressure converters.

With the analogue pressure converters it was potentially possible to control the pressures as accurately as the resolution of the D/A conversion, the only limitation consisting of the accuracy of the pressure measurements. With the electro-manostats the accuracy of the control was determined by the change in pressure that corresponded to one step of the stepper motor which was equal to ± 0.4 kPa.

3.2.5 Accuracy of measurements and calibration of transducers

The accuracy of measurements defines the closeness with which the readings approach the true value. Numerically this is equal to the degree of error in the final result and can be expressed as within plus/minus a percentage of the full scale of the transducer (O'Connor, 1994).

The factors effecting the accuracy are: noise, non-linearity, hysteresis and zero drift. The accuracy is affected by the noise only when this is greater than the resolution of the transducer. Resolution expresses the value of the smallest change in mechanical input which produces a detectable change in the output. It depends on the gain selected for the voltage input from the transducer into the data logger, the number of bits over which the A/D conversion is operated and the calibration constant.

Noise is the electrical disturbance to the signal of the transducers arising for instance from resistance changes in connections, temperature changes, interference from magnetic fields caused by equipment and spikes in the voltage supply. In the BBC system due to the autoranging operated by the data logger on the signal, noise was the major factor affecting measurements at small values of the voltage output. However ,for higher voltage outputs the resolution becomes poorer and noise ceases to be a problem. In this case at the beginning of the shearing stage when small strains had to be resolved the displacement transducers were positioned near the electrical zero. In the IBM system instead the gain of the data-logging card was fixed and the resolution was generally

smaller than the noise. Under these circumstances the autoranging which was operated via software was of no help in increasing the accuracy of the measurements. Resolution or noise can be expressed in the same units as the measurements, using the values of the calibration constants.

During the calibration procedures the errors due to non-linearity, hysteresis and drift can be assessed. At small values of the output voltage usually these errors are negligible when compared to noise. Transducers generally are designed to provide a linear output versus measurand relationship and a linear relationship is considered when they are calibrated. The non-linearity error is the maximum deviation of the output curve from the best fit line obtained by the calibration and is expressed as a percentage of the full scale of the transducer.

The calibration curves of some transducers, in particular for pressures and loads, exhibit hysteresis. This error is measured as the maximum difference between transducer outputs for the same applied measurand for loading and for unloading.

Another source of error is due to zero drift. This represents a variation in the output with time, under constant conditions of load, pressure or displacement. For example the zero drift of the pressure transducers and load cells can be assessed by comparing the variation between the readings corresponding to the zero condition at the start and at the end of the test.

The overall accuracy can be determined by summing up the errors described above. The value obtained represents the worst case since it implies that the contribution of each factor to the total error is in the same direction and has a maximum value. The accuracy and the resolution of each transducer were assessed carefully during the calibration procedures and are summarised in Tables 3.1 and 3.2.

When axial strains are measured externally the compliance of the triaxial cell, porous

stone, filter paper (if used) and of the internal load cell may introduce significant errors. Compliance was measured in compression by running a test on an aluminium dummy sample placed on the porous stone (since sands were tested the filter paper was not used). The compliance test consisted of loading and unloading the dummy sample axially for three different constant cell pressures. The data obtained were interpolated with the best fit curve and corrections introduced into the programs for the calculation of the axial strains.

Since the calibration constant of the volume gauge is affected by the value of the back pressure, the calibration of the volume gauge was performed under the same value of back pressure used during the tests.

All the transducers were calibrated every three to four months. The basic methods for calibrating displacement, pressure and force transducers are described in O'Connor (1994) and details of the standard calibration procedures are given by Lau (1988). Basically they consist of applying either a known value of pressure and load or a known increment of displacement to the measuring device and observing the electrical output. Since LVDT transducers are linear only over a certain range of the output voltage this has to be assessed first in order to calculate the calibration constant. The pressure transducers and the load cells mounted on the high pressure cells were calibrated using a Budenberg dead-weight pressure tester.

3.3 MEASUREMENTS OF SMALL STRAIN STIFFNESS

When soils characterised by high values of stiffness are tested many features of their shear behaviour can be properly investigated only if accurate measurements of small strains are available. In comparison with softer materials the accuracy of stress measurements is less important. Moreover non-uniform strains were found to be one of the main problems to be solved. When uniform strains in the sample cannot be

guaranteed, stiffness and yield stress determinations are unreliable and efforts to measure accurate axial strains become meaningless. This section describes the laboratory developments and modifications aimed at obtaining accurate and reliable determinations of stiffness and yielding. These were carried out in the 10 MPa system which provided a suitable range of confining pressures for most of the tests performed in the experimental work.

3.3.1 Limitations of external axial strain measurements

The errors affecting external measurements of axial strains in triaxial testing have been widely recognised in soil mechanics laboratories and identified as resulting from:

- compliance of the load cell and apparatus;
- misalignment between the apparatus and the sample (referred to as tilting and seating errors by Jardine et al., (1984))
- Irregularities and disturbance of the sample ends (referred to as bedding errors by Jardine et al., (1984)).

Various recommendations can be found in the literature for methods aimed at reducing the magnitude of these errors and extending the range of strains for which reliable external measurements can be taken. Atkinson and Evans (1985) suggested the use of a suction cap to join the load cell and the top platen at the start of the test before any compression or consolidation phases so that errors due to misalignment would be eliminated at the start of shearing. They also observed that a large part of the bedding of the platens into the sample occurred when isotropic stresses were initially applied and that persistence of bedding errors during shearing could be eliminated by performing further isotropic compression. However the use of a suction cap forces alignment between the load cell and the sample and may result in non-uniform stresses and strains in stiffer samples. As pointed out by Jardine et al. (1984) for stiff soils non-uniformity

of strains and bedding errors can still persist at the highest isotropic stresses that can be supplied in ordinary triaxial cells (about 750 kPa). In this case high deviator stresses would be required to overcome these problems making external measurements of axial strains at the start of shearing unreliable.

The above considerations were the outcome of experimental studies on soils, clays and sands, which were softer than the materials investigated in the present work. When dealing with cemented soils other aspects need to be carefully taken into account. For example when testing softer soils external measurements of axial strains, although unsuitable to define the stress-strain behaviour at small strains, are reliable for strain levels at the peak states. For cemented sands the stiff volumetric response during isotropic compression results in the persistence of bedding errors and non-uniformity of strains even when high values of confining pressures are reached. Moreover if shearing is performed at lower values of pressures bedding errors and non-uniformity of strains can still persist up to the peak state which for this type of soils may occur at axial strains lower than 0.1 %.

Figure 3.5 shows compliance, misalignment and bedding errors observed when shearing one of the two naturally cemented sands (D5) at a constant mean effective stress of 5600 kPa. Local LVDTs were used to measure axial strains internally and the samples were attached to an internal load cell at the beginning of the isotropic compression, using a suction cap which had a conical shaped connection which forced axial alignment of the sample and load cell. It can be seen that compliance errors, mainly due to the deflection of the load cell, are of the same magnitude as the internal axial measurements. When corrected for compliance a large difference between external and internal measurements was still observed up to the peak state. This difference includes errors due to bedding and misalignment between the sample and apparatus axis. Therefore in this case due to the high stiffness of the sample, the isotropic loading did not produce sufficient compression to reduce tilting, seating and bedding errors which were still significant even at the peak. These errors reduced in tests performed at higher

values of mean effective stresses. Similar results were found by Kim et al., (1994) when testing soft rocks such as mudstones and sandstones.

From the above observations it follows that the testing techniques suggested in the literature to make external axial measurements more reliable and accurate proved to be ineffective when investigating the stress-strain behaviour of very stiff materials like cemented sands. To overcome bedding and compliance errors local gauges which measure axial strain over the central length of the sample needed to be used. This requirement was essential not only to investigate the shear behaviour at small strains but also in the vicinity of the peak states for the tests performed at lower pressures. Moreover because of the high values of stiffness of the materials considered the determination of the initial stress-strain behaviour during shearing required the improvement of the accuracy of axial strain measurements attainable from the local axial instrumentation. Misalignment errors need to be addressed separately however. Misalignment has the effect of inducing non-uniform deformations in the soil so that the axial strains in the samples cannot be calculated as the average from the two diametrically opposed local transducers. While the literature related to cemented soils has widely recognised the importance of using local axial measurements to overcome bedding errors, it seems not to address in sufficient depth the problems arising from the non-uniformity of strains.

3.3.2 Local axial strain instrumentation and improvement of the output signal

For the reasons discussed above the 10 MPa triaxial cell was provided with internal instrumentation. Local axial gauges were installed and the external load cell was replaced by a submersible one. As discussed by Baldi et al., (1988) the measurements from an external load cell are affected by the friction between the loading ram and sealing system which becomes significant at small deviator stresses and when a moment

is applied to the ram due to the incorrect alignment between the apparatus and the sample.

A number of requirements were identified as being essential in the choice of sensor to use for the measurement of local axial strains. These were :

- adequate accuracy below the strain levels at which yielding occurs during shearing;
- capability of working under high pressures;
- a working range sufficient to cover both isotropic compression and shearing up to the peak state;
- ability to undergo large strains at the end of shearing without being damaged;
- light weight to enable the correct positioning on the sample before the application of the cell pressure.

A wide variety of local axial transducers have been proposed so far which were considered for the choice of sensor to install. LVDTs were used by Costa Filho (1985) and Brown and Snaith (1974) and electrolevels were first employed by Burland and Symes (1982). Other devices available are Hall effect transducers (Clayton et al., 1987), proximity transducers (Hird and Yung, 1987) and X-ray optical methods (Balassubramanian, 1976; Arthur and Philips, 1975). With these gauges axial strains as low as 0.001 % can be resolved, so that they would not have suited the requirements of the experiments. More recent work on the soil behaviour at small strains has been based on more accurate devices. These were represented by the pendulum inclinometers for which Ackerly et al., (1987) reported an accuracy of ± 0.0005 % and by the local deformation transducers (LDTs) developed by Goto et al., (1991) which were successfully used to determine the stress-strain relationship of stiff soils resolving strains as low as 0.0001 %. However in spite of the good resolution of the LDTs their design, which was based on the bending of a thin strain gauged bronze strip, imposes restrictions to the strain levels reached at the end of the test .

RDP miniature LVDTs type D5/200 had proved to fulfil most of the conditions required since they had been employed at City University in the 70 MPa system (Section 3.2.3). However their existing configuration did not give the level of accuracy required and needed to be altered in order to improve the accuracy of the output signal.

The functioning of LVDT transducers are described in detail by O'Connor (1994). Basically the transducers consist of a primary and two secondary coils which is inside the body of the transducers. A metal rod forms the armature which is able to move freely within the coils. The armature movement creates a magnetic flux and a variation in the electrical output signal.

The LVDTs which are designed to function under high pressures have a hole drilled into the casing allowing the cell fluid to enter the transducer body, so relieving the high differential pressures that otherwise would act between the inside and the outside of the transducer body. Because of the presence of this hole a non-conductive environment was required to prevent short circuits. Therefore the cell fluid in the 10 MPa apparatus was changed to oil and the oil/water interface was removed. Having oil as a cell fluid allowed the use of the very light flexible copper wire for the electrical connections which did not need to be insulated. With these electrical connections the transducers could be easily positioned on the sample without any tendency to tilt. It should be noted that the water submersible model of these transducers has instead a stiff insulated cable which makes positioning on the sample difficult. These transducers could not in any case be used as they can only withstand pressures up to 2 MPa. An additional advantage of having such small and light weight transducers was that they could be mounted on the sample by simply gluing the transducer holders to the membrane. This avoided the use of pins which presented the following difficulties. Firstly passing pins through a membrane creates a potential for leakage to occur, despite the use of sealants. Secondly pins are ineffective when used with granular soils as when penetrating the soil this is disturbed resulting in the pins becoming loose. In addition pins were not necessary since when using glue to attach the transducer holders to the sample it is unlikely that relative

movements can occur between the sample and the membrane because of the high differential pressures applied during testing. Moreover there is evidence in the literature that the relative movements between the membrane and the sample become significant only at large strains (Jardine et al., 1984).

The set up of the internal LVDTs on the sample is illustrated in Figure 3.6. The LVDTs were fixed to the sample over a central gauge length of 50 mm using shaped aluminium holders. The body of the transducer was fixed to the sample using the upper holder. The armature of the transducer rests on a shaped aluminium piece which does not impose any restraint to the movement of the armature. The verticality of the transducers as set up on the sample depended entirely on the correct position of the upper holder given the small size and weight of the gauge and the flexibility of the electrical connections. Large strains could be achieved during the test without the transducers imposing any physical restraint. This was because of the presence of a hole drilled in the top of the transducer body and the removal of the threads from the non-sensitive end of the armature so that it could pass freely through the LVDT.

The major cause of poor accuracy in the readings at low strains obtained from the LVDTs in their previous configuration was found to be the noise in the output signal. Reduction of noise was achieved through alterations to the hardware components as well as to the software controlling the system. The noise arising from the input voltage to the transducers (10 V) was reduced by replacing the power supply with one having a more stable output. The AC output signal from the LVDT transducers was rectified to provide a DC input for the data logger by an amplifier (RDP S7AC) external to the data logger. The amplified signal gave ± 3 V over a working range of 6 mm. The increase of the amplification factor both increased the resolution of the measurements and was found to reduce the electrical noise.

The data logger operating in the 10 MPa system was a Spectra Micro MS, which autoscaled the signal from the transducers. In this way displacements of 5 x 10^{-6} mm

could be resolved over a range of ± 0.01 mm around the position of the armature corresponding to the electrical zero. At the maximum output signal the resolution was 0.001 mm. The electrical zero could be set not only by altering the armature position but also by varying the zero potentiometer in the amplifier, allowing the best resolution to be achieved at any position of the armature. The calibration constants of the transducers were found to remain unaltered when changing the zero setting in the amplifier and the transducer amplifiers were therefore set near the electrical zero at the start of the shearing stages.

The modification to the software involved the evaluation of the optimum signal integration period over which the data logger averaged the signals. The integration period needed to be sufficiently long to reduce the noise but also sufficiently short to allow sufficiently fast logging at the strain rates used during the shearing stage of the test. It was found that during shearing the strain rates had to be as high as was possible given the logging interval to avoid temperature drift of the readings of the transducers. The permeability of the soils tested did not limit the strain rates adopted. Using an integration period of 0.5 seconds, the noise of both transducers was monitored over a period of 15 minutes and was found to result in a variation of the readings of $\pm 5 \times 10^{-5}$ mm (Figure 3.7a).

Similar criteria were applied to improve the output signal from the internal load cell. The device installed in the apparatus was manufactured by Maywood Instruments Ltd and was based on a Surrey University design. The load cell had a capacity of 80 kN and a full scale output voltage of 34 mV. Because of the low output an amplifier external to the data logger was again used. Half of the full working range was used in the experiments and the gain of the amplifier was chosen to give an output between 0 and 3 V corresponding respectively to 0 and 32 kN. The resolution provided by the data logger near the electrical zero was then equal to 0.02 kPa for a 50 mm diameter sample and remained as such over a range of 40 kPa. Figure 3.7b shows readings from the load cell over a period of about 40 minutes at constant load. The noise varies between

± 1 kPa and a drift of 5 kPa can be seen.

The accuracy of the load cell and local axial strain readings were compatible for the values of stiffness of the cemented soils tested. For values of $\delta q/3\delta\varepsilon_{al}$ equal to 3000 MPa which was the highest value determined in the experimental work, a value of the deviator stress of 9 kPa would correspond to a strain of 0.0001 %. The drift detected in the load cell over 35 minutes would cause a negligible error in the deviator stresses since a complete cycle of loading and unloading up to a deviator stress of 400 kPa (the smallest cycle applied during shearing) was completed over a similar period of time.

3.3.3 Limitations of the apparatus

As shown by some preliminary tests, high resolution and accuracy of stress and strain readings, although necessary to define the initial part of the stress-strain curve of stiff materials, were not sufficient on their own to guarantee accurate and reliable determinations of stiffness at small strains. The sources of errors and uncertainties in the evaluation of stiffness were given by:

- non-uniformity of stresses and strains throughout the sample;
- inadequate functioning of the loading system (dependent on the ratio between the apparatus stiffness and the sample stiffness).

For a homogenous sample non-uniform strains are often induced by incorrect alignment and non-centrality of the longitudinal axis of the apparatus and the sample and by non-perpendicularity of the horizontal surfaces to the axis. In cemented soils the tolerances for the end finishes of the samples have to be small to guarantee the uniform strains on which the reliability of small strain stiffness measurements are highly dependent. The tolerances that had been applied to check the conformity of the apparatus and sample

axes were also found to be inadequate. Figure 3.8 shows the stress-strain data from the two LVDTs for a constant p' test performed in the 10 MPa apparatus at a mean effective stress of 5600 kPa. This test was performed after improvements to the accuracy of the LVDTs and load cell had been made but prior to modifying the setting up and testing procedures. It can be seen that when non-uniformity occurred, the stress-strain curves from the two local axial transducers gave different values of stiffness. In this condition it was not correct simply to average the strain readings from the two transducers to calculate stiffness. As it will be shown later the stiffness obtained from the stress-strain curve when strains in the sample were uniform was different from that which would have been obtained from the average of the two local axial strains in Figure 3.8.

Provided isotropic compression is performed to sufficiently high stresses, misalignment errors at the start of shearing may be reduced if the connection of the sample to the loading system is made at the early stages of the test before isotropic loading. This however should not be considered as a procedure to rely upon during testing and every effort should be made to guarantee the best setting of the sample in the apparatus. The accurate setting up of the sample in the apparatus becomes critical for those samples sheared at relatively low mean effective stresses which are normally the stresses of interest in engineering practice.

As shown in Figure 3.8 reliable determination of the high stiffness of cemented sands at small strains, even with very accurate internal instrumentation, would have required careful verification of the apparatus geometry within tolerances far smaller than normally considered. Improvements in sample preparation and setting up procedures and highly accurate checks of the geometry of the system once the sample had been installed in the cell proved to be necessary. The techniques developed to achieve such conditions are described later in this chapter.

The improvement of the loading system for the evaluation of stiffness involved both alterations to the testing procedures and to the way in which the deviatoric load was

transferred to the sample. For stiff materials, in order to be able to monitor a small variation of the deviator stress it is necessary to run tests using very low external strain rates but this leads to a number of disadvantages. In stress controlled tests it is possible to achieve a low rate of loading but when the test includes loading-unloading cycles the reversal of loading becomes impractical because of the large change of pressure necessary to overcome the friction of the piston in the hydraulic loading cylinder which results in delays in the reversal of loading. When low strain controlled rate is used the readings from the transducers are more susceptible to temperature drift which can be significant at these very small strains and creep can occur during any delay in the reversal of load. Strain controlled tests proved to be more suitable for tests involving cycles, but not without other difficulties. When unloading, the load reversal takes place only after the slack between the gears of the motor is overcome introducing a delay and at low displacement speeds this requires a long time, with a consequent drift of readings due to temperature changes or creep. These problems would be overcome by the use of higher strain rates. However when the load is transferred to the sample through a stiff connection, the use of higher strain rates can produce too quick an increase of the deviatoric load and the logging interval maybe not sufficient to detect the initial part of the stress-strain curve. A rigid loading system is also very sensitive to any slight imperfection of the geometry of the sample and apparatus.

In order to be able to use higher strain rates of the motorised frame whilst maintaining low rate of loading on the sample so that small variations of strains and stresses could be monitored, a new connection (top cap) between the sample and the internal load cell was designed. This device was also designed to be able to minimise the effects on the sample due to minor eccentricities of load and tilting of the surfaces in contact.

3.3.4 Design of the sample-load cell connection

Various types of connections between the samples and an internal load cell have been suggested for triaxial testing (Figure 3.9) and some of them are described by Baldi et al. (1988). Connections that use a steel ball and cone seating in the top cap and ram force the sample into alignment with the loading system, creating uncertainties of the external axial strains at the start of testing, non-uniformity of strains and disturbance of the sample ends. The connection that uses a flat-ended ram and halved steel ball in a cone seating on the top cap allows a better definition of the initial external strains but non-uniformity of strains would be caused by the eccentricity of the load and tilting of the sample ends. This connection was used in the present work for some of the tests carried out on carbonate cemented soils where the mechanical behaviour was studied at larger strains using external measurements. In these tests care was taken in the trimming and setting up of the sample in order to reduce misalignment problems. The advantage of the half steel ball and flat ram connection was that it did not force alignment which would have caused disturbance of the sample ends. In one of the early tests on the sandstone, for which accurate internal instrumentation was fitted, a top cap with a male to female cone connection and a suction cap was used (Figure 3.10). This type of connection was chosen because by forcing alignment at the start of the test, it was hoped that any consequent non-uniformity would have been overcome at high values of confining pressures. This proved not to be the case so that the procedures described in the following sections had to be developed.

In order to be able to determine stiffness at small strains a new top cap was designed which solved the problems previously encountered. The design of the top cap is illustrated in Figure 3.11. This consisted of a stainless steel platen with a cone seating containing a steel ball. A flat stainless steel adapter was screwed to the centre of the load cell. The device could also be used with a suction cap which could be vented to the atmosphere. The top cap was also designed for 50 mm diameter samples which was the sample size used for the tests in which stiffness determinations were carried out.

In the design of the top cap the cone seating and ball were chosen to avoid forcing the sample into alignment with the loading system, thus transferring a bending moment to the sample. When connecting the sample to the load cell it was inevitable that an abrupt and significant change in the deviator stress would be caused. This occurrence was overcome by introducing a flat rubber cushion between the platen and load cell adapter. This cushion was thick enough to avoid contact between the steel bodies at low deviator stresses. The function of the cushion was also to absorb small differential deformations due to any eccentricity of load, preventing the transferral of non-uniform stresses to the sample. The deformation of the rubber at the start of shearing also meant that low loading rates could be applied to the sample whilst maintaining a reasonable rate of displacement in the motorised frame.

At the base of the cone a precision made brass disk was located. This transferred the load to the sample after the rubber cushion had deformed sufficiently for the ball to make contact with the top platen and before the ball made contact with the cone seating. The disk provided a more flexible connection when the deviator stress was still quite low, attenuating the abrupt change in loading rate which would occur if the ball made direct contact with the cone.

Figure 3.12a shows the results of a loading test on a dummy sample carried out to verify the efficiency of the design and to optimise the thickness of the rubber cushion and brass disk. The initial test (Figure 3.12a) was performed using a brass disk with a thickness of 2.5 mm. Although a smooth variation of the loading rate had been achieved, jumps in the deviator stress were observed. In the final test the thickness of the brass disk was increased to 3.5 mm. The results in Figure 3.12b show the optimised design in which the jumps in the previous configuration were eliminated.

3.4 EXPERIMENTAL PROCEDURES AND MODIFICATIONS

The experimental procedures for sample preparation, setting up techniques and testing methods varied according to objectives of the tests. New procedures were developed for those tests aimed at investigating the mechanical properties at small strains. These will be presented separately from the standard techniques adopted. The methods used to prepare and set up natural and reconstituted samples are also described.

3.4.1 Preparation of intact samples

Intact samples were obtained either from blocks in the case of the silica sandstone or for the calcarenite from cores 83 mm in diameter. The core samples of calcarenite tested in the 10 MPa cell were cut to a length of 160 mm and an 83 mm pedestal was mounted in the cell. The core samples were trimmed to a diameter of 50 mm and a length of 100 mm when tested in the 5 or 70 MPa cells and also for tests in the 10 MPa cell to determine stiffness. All the silica sandstone samples obtained from blocks were trimmed to a 50 mm diameter and cut to a 100 mm length. The samples were cut to the final diameter by hand in a soil lathe using a file. In order to ensure proper placement of the sample in the lathe, the ends were flattened by rubbing them against a regular horizontal surface covered in sand paper. By placing the samples in a cradle the end surfaces could be cut parallel to each other within 0.03 mm.

For tests where small strain stiffness had to be determined such tolerances would have not been acceptable and would have resulted in non-uniform strains during testing even at relatively high pressures. The method used for the preparation of the samples was therefore improved. By ensuring that the steel cutting tool used during the trimming process in the lathe had a perfectly straight edge it was possible to obtain an uniform diameter throughout the length of the sample to within 0.02 mm. The ends of the sample were prepared in a specially built split mould as shown in Figure 3.13. The sample was

placed in the mould and the ends were first approximately trimmed with a file. An aluminium disk was then screwed into the base of the mould so that the sample protruded by 1 mm at the other end for more accurate trimming. A second aluminium disk of 3 mm thickness was inserted into the base of the mould after the sample was removed. Finally the sample was rotated through 180° so that the other end could be trimmed. This procedure ensured the parallelism between the end surfaces with a variation in the sample height strictly within 0.01 mm which corresponded to half the value suggested by the International Society of Rock Mechanics specification (ISRM, 1981).

3.4.2 Preparation of reconstituted samples

Reconstituted samples were prepared using two methods: pluviation and freezing. The soils tested consisted of poorly graded sand so that during sedimentation in water, the particles did not tend to segregate and homogeneous samples could be obtained. The sand samples were generally prepared in the loosest state possible in order to be able define the normal compression line over a large range of mean effective stresses. The freezing method allowed lower densities to be produced than those obtained by pluviation.

(i) Pluviation

The conventional method is described by Bishop and Henkel (1962). A split mould was placed on the base pedestal of the cell and a latex membrane stretched against the inner face of the mould by applying vacuum to the tube attached to the mould. Silicon grease on the perimeter of the pedestal and 'O'-rings were used to ensure a tight seal and to prevent the penetration of particles between the pedestal and the membrane. The mould was partly filled with distilled de-aired water and a pre-weighed oven dried sand was

then poured uniformly into the mould trying to keep the pouring speed constant. The sand was poured from 5 cm above the water surface to ensure a constant height which would determine the density throughout the sample. The sedimentation of particles was almost immediate and no segregation was observed. Once the surface of the sample was approximately 1 cm below the top of the mould the excess water was removed with a syringe. The top cap, with its sides covered with silicon grease, was located on the sample and the membrane around the mould was then lifted onto the top cap to seal the sample temporarily whilst the vacuum was released. Following this a small suction was applied to the sample using a burette which was attached to the drainage system of the triaxial cell. The mould was then removed and 'O'-rings were placed to seal the membrane to the pedestal and top cap.

The remaining dry sand was weighed and the dimensions of the sample were measured with a calliper in a number of positions. The average dimensions of the sample were calculated accounting for the thickness of the membrane. The specific volume of the sample was then calculated using the specific gravity of the soil. When the samples were tested at confining pressures higher than 500 kPa a second membrane was placed after the sample had been prepared to avoid punctures.

(ii) Freezing

A split mould was placed on a steel base and sealed using silicon grease. The inner surfaces were lubricated with a thin layer of silicon oil to facilitate the sample removal after freezing. Pre-weighed oven-dried sand was poured into the water filled mould, following the same procedures described for pluviation. The mould was then placed in the freezer for 24 h. Due to the expansion of water when freezing, the top surface of the frozen sample was slightly convex and was flattened by carefully melting the protruding ice. The porous stone and the top cap were also placed in the freezer to prevent the ends of the sample from melting when it was set up. The dimensions of the samples were

taken after removal of the mould and the sample was then replaced in the freezer. A burette was attached to the drainage system of the triaxial cell and de-aired water was flushed from the burette through the drainage lead. The sample was then placed on the pre-cooled pedestal and the membrane put in place and sealed to the pedestal and top cap. The burette was placed on the floor imposing a suction of about 10 kPa at the base of the sample while it melted. The average dimensions of the samples were calculated accounting for the thickness of the membrane. A second membrane was used for tests reaching confining pressures up to 10 MPa and a third membrane for tests up to 70 MPa. The specific volumes were calculated both from sets of dimensions taken when the sample was still frozen and after the sample had melted, considering the specific gravity and the dry weight of the sand. The two specific volumes usually agreed to within ± 0.02.

3.4.3 Sample saturation and standard setting up procedures

The methods described in this section refer to the high pressure system. Descriptions of the setting up procedures in the Bishop and Wesley cell are similar and are described in detail by Lau (1988) and Ho (1988). Before installing the samples in the cell the drainage leads connected with the pore pressure transducer and the volume gauge were flushed with de-aired water and the readings from the pore and cell pressure transducers were set to zero at atmospheric pressure. A de-aired porous stone was used but a filter paper at the base was not necessary given the grain size of the soils tested.

Intact samples were saturated by placing the samples submerged in the pore fluid in an air-tight container on which a valve allowed a gentle incremental reduction of pressure. For the carbonate samples a collapse of the fine particles on the sides of the sample had been observed when applying the vacuum suddenly. This did not occur when the application of the vacuum was gradual. Due to the relatively high permeability of the samples saturation was complete after 3 to 4 hours. Saturation of the intact samples was

repeated once these had been mounted on the pedestal and after the membranes were placed. This was achieved using the specially designed perspex container shown in Figure 3.14. The cylinder was placed onto the top of the sample and the membrane was sealed onto it by means of 'O'-rings. Then the cylinder was partially filled with water and the vacuum was gradually applied for 15 minutes to eliminate air bubbles trapped between the pedestal, porous stone, sample and membrane.

In the apparatus using oil as the cell fluid a neoprene outer membrane was used since latex deteriorated in the presence of mineral oil. When natural carbonate samples were tested in the high pressure cells the membranes were more likely to puncture. To prevent this a total membrane thickness of 1.2 mm was required. For the other intact samples a latex membrane of 0.3 mm and a neoprene membrane of 0.6 mm were sufficient to avoid punctures during the tests.

The local axial instrumentation was mounted on opposite sides of the sample over a central gauge length of 50 mm. The transducer holders were glued to the membrane and each transducer carefully positioned along the longitudinal axis of the sample. The transducer armature was positioned at the initial position and the amplifiers were set near the zero voltage.

After placing and sealing the top cap, the triaxial cylinder was fitted and the centre of the top cap was checked for centrality within the cell with a ruler placed against the inner surface of the cylinder. The top part of the cell and axial loading system was positioned and the cell was filled until the internal load cell was immersed. At this point the axial and cell pressure readings were set to zero. The top part of the cell was fixed in position with the tie bars whilst checking with a calliper that the distance between the top and base of the cell was kept to within ± 0.01 mm all around the cell. This procedure ensured the perpendicularity and centrality of the ram and load cell axis to the horizontal surfaces of the cell.

The samples were saturated by the application of back pressure whilst maintaining the mean effective stress in the sample at a constant value of 60 kPa. A high degree of saturation could be achieved in the high pressure systems, since the back pressure could be increased to values of 600 kPa. In the high pressure apparatus the low cell pressure circuit could supply pressures up to 700 kPa which covered the whole saturation stage. Due to the high stiffness of the materials tested water could not be considered as an incompressible fluid and full saturation would therefore correspond to B values (Skempton, 1954) less than 1 as will be shown in Section 6.7.4. Changes of B values were monitored during the saturation stage as the back pressure increased and full saturation was considered to be achieved when B reached a constant value. This usually occurred for back pressures of about 450 kPa.

3.4.4 Modifications of the setting up procedures

Although in the standard procedures care had been taken to ensure centrality and alignment of the sample and apparatus longitudinal axes as well as flatness of the horizontal surfaces, the tolerances applied proved to be unsatisfactory for accurate determination of the small strain stiffness of the cemented soils. The methods adopted in the sample installation and in the checks of the system geometry were therefore reconsidered. This objective was pursued for the tests in the 10 MPa cell by modifying some parts of the setting up procedures and by designing two new devices. These devices allowed the checking of the geometry of the system with high accuracy after the installation of the sample.

The two devices are illustrated in Figures 3.15 and 3.16. The device shown in Figure 3.15 was used to establish and check the centrality of the sample at two different heights, therefore verifying the uniformity of the diameter of the sample, its centrality in the cell and the perpendicularity of the longitudinal axis of the sample to the base of the cell. Two guide pins mounted in the base block of the tool enabled its rotation

around the groove at the base of the cell. The two steel rods were locked in place ensuring the same protrusion from the vertical steel bar of the tool while touching the lateral surface of the sample.

Figure 3.16 shows the device that was designed to verify the perpendicularity of the horizontal surfaces of the pedestal, sample ends and top cap to the longitudinal axis of the system. The steel bar was placed on the horizontal and circular surface along its diameter and was provided with a central pointer which enabled the centrality of its position to be checked by reference to a target cross drawn at the centre of the horizontal surface. The surface of the cell base was accurately machined and was therefore taken as a reference. The two steel bars were locked in position when they touched this surface. By rotating the instrument through 180° it was possible to see if the horizontal surface to be checked was parallel to the reference. The ratio of the bar length to the diameter of the horizontal surfaces (50 mm) amplified any variation in the height measured. The gap between the rod tip and the cell base was measured with feeler gauges and checked that it was within 0.01 mm. The checks were repeated during the assembly of the sample and top cap in the cell. In order to avoid using rods that were too long or flexible when measuring the higher surfaces, two accurately machined blocks were located on the reference surface from which the checks were performed.

The procedures for the installation of the sample were modified so that the position of the sample could be first temporarily fixed to allow preliminary checks and then permanently fixed after final adjustment. To fix the position of the sample, the pedestal and the base of the top cap were provided with a brass ring. This had a diameter 2 mm larger than that of the sample and protruded 4 mm over the lateral surface of the sample at each end. The space between the ring and the sample was filled with gypsum cement as shown in Figure 3.17. As the cement set (this took 15 minutes) it was possible to make any minor adjustments. The use of the cement at the top and bottom of the sample proved to be very effective in preventing puncturing of the membranes during the tests, since these were the more susceptible points.

Some of the tests aimed at determining the stiffness of the soil were performed undrained so that the sealing of the system was crucial. Care was taken to clean the surfaces where the 'O'-rings were placed. No silicon grease was used as this tended to trap particles of soil and dirt and the 'O'-rings were placed around the sample according to the scheme in Figure 3.18. Figure 3.19 shows the stress-strain data obtained from the system after the setting up and testing procedures had been modified where it can be seen that strains were uniform and the results from the two local axial transducers overlap.

4. EXPERIMENTAL WORK ON THE ARTIFICIAL SOIL

4.1 REVIEW OF PREVIOUS WORK

The investigation of the artificial soil extended the work carried out by Coop and Atkinson (1993) on the mechanics of cemented carbonate sands. Their work was prompted by the problems encountered in the installation of piles in calcareous soils for the construction of the North Rankin gas platform off North West Australia. Because of the variable nature of the calcarenite from Rankin, the authors considered it necessary to initiate the study with an investigation on the mechanical properties of an artificially cemented carbonate soil. The model material provided a means to control variables such as grading, specific volume and degree of cementing and so to understand their separate influences on the mechanical behaviour of the soil.

The experimental work was performed by the authors both on the artificially cemented soil and on the uncemented soil used to create the model material. Some of the effects of bonding could be highlighted by comparing the mechanical behaviour of the cemented soil with that of the uncemented soil (see Section 2.5). A limitation of the work was that the samples tested were all characterised by similar initial specific volumes and the cemented samples were all prepared with the same degree of cementing.

The artificially cemented samples were prepared by cementing a carbonate sand with gypsum. The soil used was collected from Dog's Bay in Ireland and, as shown in Figure 4.1a, consisted of a poorly graded medium sand. The soil particles were of biogenic origin and were plate like and angular as can be seen in the thin sections of Figure 4.1b. The sand was found to have a calcium carbonate content of 88-94 % (Houlsby et al., 1988), with particles consisting mainly of mollusc shells and foraminifera. References to the mechanical behaviour of this sand can be found in

Evans (1987), Houlsby et al. (1988), Golightly and Hyde (1988) and Coop (1990).

Coop and Atkinson (1993) produced the artificially bonded soil by mixing the following percentages by weight: 54.6 % of dry sand, 16.4 % of dry gypsum and 28.9 % of distilled water. During the preparation of the samples the grading curve of the sand (Figure 4.1a) was carefully reproduced for each sample by controlling the proportions used of each soil fraction. The gypsum plaster passed the 63 μm sieve and its addition resulted in an increase of the fines content of the sand from 1 % to 24 %. After mixing the sand, cement and water thoroughly, the mixture was placed in a cylindrical mould with lubricated faces. During placement each layer was lightly tamped. The mixture was left to set for 24 h at atmospheric pressure and at 20 ° C. After removal from the mould, the sample was left to cure, weighing at intervals until a constant weight was achieved. The samples obtained had all similar initial specific volumes. Gypsum plaster is an unhydrated calcium sulphate and has the property that its strength degrades in water. In order to ensure that the bond strength achieved in the dry sample after the curing period was not altered by the presence of the pore fluid, the authors used silicon oil rather than water as the pore fluid to test the samples. The type of silicon oil used had similar viscosity to water. Before installation in the triaxial cell the cemented samples were immersed in a bath of silicon oil and saturated under vacuum. In the following sections these samples will be referred as strongly cemented.

Thin sections from the untested samples are shown in Figure 4.2. These, as also the thin sections of the other materials tested in the present work, were prepared at the Geology Department of University College, London. It can be seen that the cement is present at the particles contacts and partly infills the voids. The preparation method adopted by Coop and Atkinson (1993) was aimed at approximating the natural process of bonding for those soils such as the calcarenite form Rankin, in which the precipitation of cement takes place at low confining pressures as it is almost coincident with sedimentation (see Section 5.1). Therefore during the preparation of the artificially cemented samples the mixture was only lightly tamped and left to cure at atmospheric pressure. Huang and

Airey (1991) also prepared an artificial soil where a carbonate sand from the North West Shelf of Australia was cemented with gypsum plaster. The artificial material was used to simulate the behaviour of the calcarenite from Rankin in the belief that the extreme variability of density and degree of cementing made the natural soil unsuitable for an investigation of its fundamental behaviour. Samples with different degrees of cementing were prepared and variation in densities were obtained by one-dimensionally compressing the soil-cement mixture. This method of preparation may cause breakage of the weak sand particles during the one-dimensional compression so that it would be difficult to control the grading of the soil and would be more suitable to simulate the case of soils in which cementation occurs together with the burial of the sediments.

Coop and Atkinson (1993) had shown that the variation in grading induced by the addition of the cement fines to the soil effects its intrinsic behaviour. Following the concept given by Burland (1990), the "intrinsic" behaviour is defined as the behaviour of the reconstituted or uncemented soil (Section 2.1). This observation implied that for a correct comparison between cemented and uncemented soils it was necessary to ensure that the two soils had the same grading. The uncemented samples considered by the authors were therefore obtained by mixing the sand with the same amount of gypsun plaster as used in the cemented soil. In order to avoid that the water in the pores reacted with the gypsum plaster, the uncemented samples were prepared by pluviation through silicon oil which was also used as the pore fluid during testing. Since the control of grading proved to be essential for correct comparisons between cemented samples with different degrees of bonding and between cemented and uncemented sands, the results presented by Huang and Airey (1991) and later by Huang and Airey (1993) on their artificially cemented carbonate sand could not provide a reference for the present work as the grading for each of the materials tested was different. Coop and Atkinson (1994) presented a discussion of this point emerging from the study from Huang and Airey (1991).

4.2 PREPARATION OF THE WEAKLY CEMENTED SAMPLES

In the present work the testing programme on the artificially cemented soil was aimed at investigating the influence of the degree of bonding on the mechanical response of the soil. Artificially cemented samples with similar specific volume but a smaller degree of bonding than considered by Coop and Atkinson (1993) were prepared and tested in triaxial compression both at low and high confining pressures. In the following the samples with weaker bonds will be referred to as weakly cemented to distinguish them from the bonded samples investigated in the previous research, which will be referred to as strongly cemented.

To achieve samples with weaker bonds two different methods were tried. In the first method (A), the cemented samples were prepared using the same mixture as used for the strongly cemented samples and the reduction in the bond strength was achieved by using water as the pore fluid. Although this method proved to be successful in reducing the strength of the bonds, it presented the disadvantage of not being able to control the way in which water acted in weakening the bonds.

Because of these considerations a second method (B) was employed. In this case a lower bond strength was obtained by reducing the amount of cement and silicon oil was used as the pore fluid. The ratio of gypsum to sand was decreased from 1:3.33 to 1:10. The grading of the soil was left unvaried by replacing the amount of gypsum subtracted from the mixture with an equal amount of calcium carbonate fines, consisting of the sand particles passing the 63 μm sieve. Coop and Atkinson (1993) tested uncemented samples in which the gypsum fines were completely replaced by calcium carbonate fines and found that no significant change could be detected in the mechanical response of the soil, showing that the precise mineralogy of the fines was unimportant. The control of the grading in the preparation of the weakly cemented samples allows reference to the same intrinsic properties as the strongly cemented samples. The weakly cemented samples were prepared following the same procedures described in Section 4.1 for the

strongly cemented samples. The weakly cemented samples had similar initial specific volumes to the uncemented and strongly cemented samples.

4.3 TESTING PROGRAMME

Four artificially cemented samples were prepared according to method A and four samples according to method B. The triaxial compression tests were conducted in the Bishop and Wesley cell and in the 5 and 10 MPa apparatus. At the time when these tests were performed, the 10 MPa apparatus had only external instrumentation for the axial strain and deviatoric force.

All of the samples were isotropically compressed and sheared at a constant axial strain rate under drained conditions over a wide range of mean effective stresses (50 to 6400 kPa). Constant p' stress paths were followed in the tests reaching higher mean effective stresses, while constant σ'_r stress paths were generally followed at lower stresses. Details of the tests are given in Tables 4.1 and 4.2.

4.4 PRELIMINARY CALCULATIONS

The specific volume at the start of the tests (v_i) was calculated from the dry weight and the dimensions of the sample before its installation using:

$$v_i = G_s \frac{\gamma_w}{\gamma_{di}} \tag{4.1}$$

where the G_s is the specific gravity, γ_w is the unit weight of water and γ_{di} is the dry unit weight of the sample at the start of testing.

The specific gravity G_s was taken equal to 2.54 and 2.65 for the samples prepared with methods A and B respectively. The values of G_s were determined from a knowledge of

the specific gravities of the carbonate sand and gypsum plaster, equal to 2.71 and 2.13 respectively, and considering the ratios by dry weight of gypsum to sand used for each method. The specific gravities were determined according to the method described in the British Standard BS:1377 (British Standards Institution, 1990) for fine, medium and coarse grained soils.

For the samples prepared with method A (tested using water as the pore fluid), the specific volume at the beginning of the test was also back calculated from a knowledge of the water content of the sample at the end of the test (w_f) and of the overall volumetric strain experienced by the sample during testing (ε_{vf}), according to the formula:

$$v_i = \frac{1 + G_s w_f}{1 - \frac{\varepsilon_{vf}}{100}} \qquad (4.2)$$

For the samples tested with silicon oil the initial specific volume was obtained only from Equation 4.1. The average between the values calculated with Equations 4.1 and 4.2 was taken as the initial specific volume of the samples tested with water as the pore fluid. In the latter case the values from the two equations agreed within ± 0.005.

For the tests performed in the 10 MPa cell the axial force for these tests was measured only by an external load cell which included both the friction between the ram and the 'O'-ring seal at the top of the cell and the force acting on the cross sectional area of the ram due to the cell pressure.

The second contribution was accounted for by the control program which subtracted the axial force on the ram due to the cell pressure from the force measured by the load cell. "Friction tests" were performed at the start of the shearing stage by raising the cell at constant speed whilst the ram was connected to the load cell and before applying the axial load to the sample. The average deviatoric force monitored during the friction test

was subtracted from the deviatoric load calculated by the control program.

The axial stress was calculated by the controlling software of the triaxial system taking into account the variation of the cross sectional area of the sample during the test (A_c) which was derived under the assumption that the sample deformed as a right cylinder:

$$A_c = A_i \frac{100 - \varepsilon_v}{100 - \varepsilon_a} \tag{4.3}$$

where A_i is the initial area of the sample, A_c the current area and ε_v and ε_a are respectively the current volumetric and axial strains in percentage.

The errors in the axial and radial stresses due to the effects of membrane restraint (La Rochelle et al, 1988) were considered negligible both because of the high strength and stiffness of the samples and because of the high confining pressures applied.

The results from the tests have been analyzed in the following sections in terms of specific volume (v), mean effective stress (p'), deviator stress (q), axial strain (ε_a) and volumetric strain (ε_v). The external axial strains considered are those measured externally but are corrected for the apparatus compliance.

4.5 ISOTROPIC COMPRESSION

The results from the isotropic compression of the artificially cemented samples which were loaded to the highest mean effective stresses are shown in v : lnp' space in Figure 4.3. In the same figure the isotropic compression curves of the uncemented samples tested by Coop and Atkinson (1993) to the highest isotropic mean effective stresses are superimposed.

The compression curves from the uncemented soil show an indistinct yield with which is associated a progressive increase of compressibility. At higher stresses the gradient

of the curves becomes constant and a straight Normal compression line (NCL) can be defined:

$$v = N - \lambda \ln p' \tag{4.4}$$

where N = 3.420 and λ = 0.189.

The weakly cemented sample prepared by method B and isotropically loaded to the highest pressure (Figure 4.3a) yielded abruptly at around 500 kPa. After yielding the soil became more compressible and approached the normal compression line as the mean effective stress increased.

The indistinct isotropic yield observed in sands both prepared in a loose state and compacted has been attributed by various authors to the occurrence of particle breakage (Section 2.3). By means of thin sections and the grading analysis of the untested and isotropically compressed samples, Coop (1990) found that the high compressibility of Dog's Bay sand was the result of particle breakage. In the cemented soil the presence of cement prevents particle degradation, which is likely to develop only after yielding. Before yielding it would be expected that the load is distributed between the cement and the soil particles proportionally to their stiffness. In this hypothesis the overall stiffer behaviour observed for the cemented soil when compared to the uncemented soil would suggest that before yielding the isotropic load is mainly carried by the cement. At yielding the load carried by the cement is shed onto the particles and this is reflected in the abrupt change of compressibility shown by the cemented soil.

The two samples prepared by method A and isotropically compressed to high stresses (Figure 4.3b) also showed an initially stiff response with an abrupt yield point. However the post-yield compression curves of the type A samples is located below that of type B but has similar gradient to the NCL defined by the uncemented samples. A tentative intrinsic compression line (ICL) was traced in Figure 4.3b which is parallel to the NCL of the uncemented samples and has a coefficient N of 3.24. Here the ICL is referred to

as the line approached by the cemented samples at large volumetric strains.

If the response of the weakly cemented samples prepared by method B is compared with that of the strongly cemented samples (Figure 4.4), it can be seen that by virtue of the stronger bonds the latter reached states outside the domain of the weakly cemented and uncemented samples. The stronger bonds determine much higher isotropic yield points and a more compressible post-yield behaviour. As for the type B samples the post-yield compression of the strongly cemented samples tends to converge with the NCL at large volumetric strains as the mean effective stresses increase.

The above results seem to suggest that the location of the ICL for the type A samples below the NCL defined by the uncemented soil resulted from using water rather than silicon oil as the pore fluid during the tests. It should be noted that the strongly cemented samples, the weakly cemented samples of the type B and the uncemented samples were all tested using silicon oil as the pore fluid and the NCL of the uncemented soil defined the line approached by the cemented soils at large strains irrespective of their degree of bonding. Therefore when the behaviour of the weakly cemented soil is compared with that of the strongly cemented and uncemented soils reference will be made only to the samples which were prepared according to method B.

4.6 SHEARING

Following isotropic compression, all the samples were sheared in triaxial compression under drained conditions. Strain-controlled tests were performed in order to follow the stress-strain curves during strain-softening.

The samples prepared with the smaller quantity of cement (type B) were all sheared at constant values of σ'_r (equal to 100, 300 and 600 kPa), except for one sample which was

isotropically compressed to a high mean effective stress (6400 kPa) and then sheared at a constant value of p'. Typical stress-strain curves are presented in Figure 4.5 where the volumetric strains are also shown. The stress-strain curve of sample DCSG reaches a peak, followed by a progressive decrease of the deviator stress (Figure 4.5a). The tested sample showed discrete zones of failure which were likely to have formed near the peak when localization of strains took place. The $\varepsilon_v : \varepsilon_a$ curve shows compression followed by a change to dilation corresponding with the major drop in the deviator stress. Because of the localisation of strains the volumetric strain measured beyond the peak is not representative of the volumetric response of the soil within the failure zones. Moreover the volumetric strain measured at the beginning of the shearing stage is also affected by errors due to bedding, which are higher at low confining pressures as discussed in Section 3.3.1. Figure 4.5b shows the stress-strain curve of sample DCSD which had yielded during isotropic compression. The stress-strain curve shows no peak and approaches a constant deviator stress. The volumetric response is compressive with a progressive decrease of gradient which tends to zero as the axial strain increases.

Of the four samples tested with water as the pore fluid (type A), three were sheared at constant values of p' (equal to 250, 300 and 4400 kPa) and one at a constant σ'_r of 50 kPa since a constant p' stress path at this value would have led to a negative radial effective stress being required during shearing. Typical stress-strain curves are shown in Figure 4.6. Sample DCOG2, which was sheared under a mean effective stress lower than the isotropic yield, experienced a brittle failure (Figure 4.6a). The volumetric strains were negligible up to peak and compression followed at large axial strains. Sample DCOF, which yielded under isotropic loading, showed a strain-hardening behaviour which converged towards a constant deviator stress at the ultimate state (Figure 4.6b). The sample compressed and tended to approach constant volume at high strains.

The values of the deviator stress reached by the weakly cemented samples (types A and B) at the end of the tests are shown against the corresponding mean effective stresses in Figure 4.7. This figure also shows the results obtained by Coop and

Atkinson (1993) for the uncemented and strongly cemented samples. The authors defined two different critical state lines for the uncemented and strongly cemented soils, with values of M equal to 1.65 (ϕ'_{cs} of 40°) and 1.5 (ϕ'_{cs} of 37°) respectively. The lower gradient was found to be close to the value obtained for two samples made only from cemented gypsum plaster. Since the presence of gypsum fines in the uncemented soil was found not to affect the M value, the authors concluded that while in the uncemented soil the mechanism of failure was governed by the larger particles, in the cemented soil after yielding gypsum probably coated the particles so that it controlled the friction angle at failure. For the weakly cemented samples which reached an ultimate value of the deviator stress the value of the coefficient M agreed with that defined by the strongly cemented samples.

Figures 4.8 and 4.9 show the stress-strain curves in terms of stress ratio η against ε_a for all the tests performed on the weakly cemented soil. Figure 4.8 shows that the type B samples tended to reach similar stress ratios at large strains, except for sample DCSG which showed a brittle failure. The two samples which yielded during isotropic compression both strain-hardened. The data from the two samples which did not yield in isotropic compression initially show a stiff and linear stress-strain response followed by a peak in the stress ratio. The yield point during shearing was identified as the point where the behaviour ceased to be linear. The linear portion was identified from external measurements of strains disregarding the initial part of the stress-strain curve since this was affected by bedding errors. The same consideration was applied when considering the volumetric response. Similar patterns of behaviour to those observed for the type B samples are shown by the results for the type A samples in Figure 4.9.

The specific volumes reached at the end of the tests by the weakly cemented samples are plotted against the final values of the mean effective stresses in Figure 4.10. This figure also shows the states at the end of the test for the strongly cemented and uncemented samples. The majority of the samples were characterised by a strain-hardening behaviour and reached an almost constant volumetric strain. For the samples

undergoing strain-softening shear bands formed in the proximity of the peak state so that the specific volumes at the end of tests cannot be considered as representative of that at the critical state. In this case the end of test states were labelled with an arrow indicating the direction towards which the correct critical state would be expected to be located. The state points for the weakly (type B), strongly cemented and uncemented samples lie all within a narrow band. For the purposes of the analyses a unique critical state line (CSL) was considered, which was also assumed to be parallel to the NCL and having the equation:

$$v = \Gamma - \lambda \ln p' \tag{4.5}$$

where $\Gamma = 3.165$ and $\lambda = 0.189$.

The weakly cemented samples prepared with method A reached states which consistently lay below those defined by the other samples. These points are aligned on a straight line parallel to and below the CSL defined by Equation 4.5 with a value of Γ of 3.040. The use of water as the pore fluid rather than silicon oil in the type A samples seems to have an effect on the location of the CSL similar to that seen on the NCL in Section 4.5.

Figures 4.11 and 4.12 show a comparison between the shear behaviour of strongly cemented, weakly cemented and uncemented soils sheared at intermediate and high confining pressures. In these figures η / M is plotted against ε_a reducing the differences between cemented and uncemented soil behaviour due to the variation in the value of M. In order to compare the behaviour of the cemented and uncemented soils, samples which had similar initial values of p'/p'_{cs} at the start of shearing $(p'/p'_{cs})_i$ and which were subjected to the same stress paths were considered, with p'_{cs} indicating an equivalent pressure taken on the CSL as defined in the following section. Since the samples were characterised by similar initial specific volumes before testing and by high stiffness, the similarity of the initial value of p'/p'_{cs} would reflect also similarity in the specific volumes at the start of the shearing stage. The approach followed during the comparison will be that any difference between the cemented and uncemented soil

behaviour can be attributed to the contribution of bonding.

The state of sample UNCA was located on the NCL at the start of shearing which was performed at a constant value of p'. The cemented samples (DCSD and CEMC) approached the NCL at high mean effective stresses and were then sheared at constant values of p'. The curves from the weakly and strongly cemented samples are almost coincident with that from the uncemented sample. The mechanism of failure of the two cemented samples appears therefore to be entirely frictional as for of the uncemented soil.

At intermediate stresses sample UNC6 was the one that had the closest initial value of p'/p'_{cs} to the cemented samples DCS1 and CEM4. In all cases drained shearing was performed at constant cell pressure. The two cemented samples did not yield during isotropic compression. The graphs in Figures 4.11 and 4.12 show that the cemented soils were much stiffer than the uncemented one. The strongly cemented sample yielded at a slightly higher stress ratio than the weakly cemented sample. Both samples in this case yielded at a value of η lower than M and approached the ultimate state after reaching a small peak. The influence of cement on the initial shearing response of the cemented soils is evident and the small peak stress ratio suggests that its influence was still present after yielding.

Figure 4.13 shows η/M plotted against ε_a for the strongly, weakly and uncemented samples which were sheared at low confining stresses. Again all three were sheared under drained condition at constant cell pressure from similar initial values of p'/p'_{cs}. Both cemented samples reached higher peak states than that reached by the uncemented sample. For the strongly cemented sample the stronger bonds resulted in a higher peak stress ratio than that reached by the weakly cemented sample. The initial shearing response of the cemented samples was stiffer than that of the uncemented sample and both CEM2 and DCSG yielded in the vicinity of the peak state. From the observations above it follows that at low confining stresses not only the cement contributed to the

stiffness of the soil but also enhanced the strength of the soil. The higher peak states reached by the cemented samples can be attributed to the cohesive component of strength due to the interparticle bonding. This component has to be distinguished from the component given to the peak strength of uncemented granular soils by dilation.

4.7 NORMALIZED STRESS PATHS

In order to display information about states of stress (q, p') and specific volume (v) in a two-dimensional plot, the stress paths of the weakly cemented samples were normalized with respect to an equivalent pressure. The equivalent pressure was taken on the CSL as suggested by Coop and Atkinson (1993) and allows comparison with the normalized stress paths from the strongly cemented and uncemented soils presented by the authors.

Figure 4.14 shows the normalized stress paths for the weakly cemented samples prepared with method B, in which q and p' are divided by the equivalent pressure (p'_{cs}) calculated as:

$$p'_{cs} = \exp \frac{(\Gamma - v)}{\lambda} \qquad (4.6)$$

where $\Gamma = 3.165$ and $\lambda = 0.189$.

Some tests from Coop and Atkinson (1993) on the uncemented samples are replotted and superimposed in the same figure. To facilitate the comparison between cemented and uncemented soils the deviator stress was normalized with respect to M. Also for those samples which reached the NCL but had initial states which did not lie on it because of errors in the water content measurements, the specific volumes were adjusted to bring the initial state of the soils onto the NCL.

The stress path labelled as UNCA can be considered as a state boundary surface (SBS)

for the uncemented soil which limits the possible states that this soil can achieve (Coop and Atkinson, 1993). The stress path followed by the weakly cemented sample which in isotropic compression yielded and reached the NCL (sample DCSD), overlaps with the SBS of the uncemented soil. In the graph the attribute intrinsic was given to this SBS (ISBS) to indicate that this surface is a boundary to which the cemented soil tends as degradation of bonding occurs. It can be observed that the critical state (CS) does not lie at the apex of the ISBS, a feature that Chandler (1985) predicted for soils with crushable grains and had been observed for uncemented granular soils by Coop and Lee (1993).

The stress path of the weakly cemented sample DCSF, which was sheared soon after yielding in isotropic compression, shows no peak in terms of the stress ratio η. This sample was sheared under a constant effective radial stress and the initial linear part of the stress path indicates negligible volumetric strains probably due to some remaining influence of bonding which was still able to prevent the occurrence of larger volumetric strains. As degradation of bonding took place, the stress path of sample DCSF tends to resemble the stress path followed by the nearby uncemented sample UNC6.

The results from the two samples which did not yield during isotropic compression (DCS1 and DCSG) show a peak in the stress ratio. The stress paths reach states beyond the ISBS which is later approached when the soil strain-softens. A comparison between the stress paths of the uncemented sample UNC8 and the cemented one DCSG, both sheared from similar states relative to the CSL and at constant cell pressure, shows the higher peak stress ratio and the more rapid strain-softening of the cemented sample. The stress path of sample DCSG is linear up to yield which is almost coincident with the peak state. Also for sample DCS1 the stress path is linear up to yield but in this case yield occurs at a value of η less than M and the stress ratio at the peak state is only slightly higher than M. In contrast to this pattern of behaviour, the uncemented sample located on the wet side of critical (UNC6) and in the vicinity of DCS1 showed no peak.

The normalized stress paths of the strongly cemented samples (Coop and Atkinson, 1993) are shown in Figure 4.15. In contrast with the weakly cemented soil the strongly cemented samples which yielded in isotropic compression have stress paths that lie outside the ISBS which is approached only at the critical state. It can also be seen that the stress paths of the strongly cemented samples which yielded during shearing reach states far outside the ISBS by comparison with the weakly cemented soil. For current values of p'/p'_{cs} on the wet side of critical the weakly cemented soil showed substantially no peak and its behaviour became close to that of the uncemented soil. In contrast at states on the wet side of critical the influence of bonding on the behaviour of the strongly cemented samples was still significant and allowed the attainment of peak states. Moreover in Figure 4.15 it is not possible to identify a trend for the yield points. These results together with those from the weakly cemented soil will be analysed according to a different approach in Section 7.1.

Finally the normalized stress paths followed by the weakly cemented samples prepared with method A are plotted in Figure 4.16. The values of p'_{cs} were calculated using Equation 4.6 with values of Γ and λ of 3.040 and 0.189 respectively.

The stress paths show patterns of behaviour consistent with those observed for the weakly cemented samples prepared with method B (Figure 4.14). The initial state for the stress paths of the samples which where isotropically yielded and compressed to high stresses are located at lower values of p'/p'_{cs} than seen for samples DCSD and UNCA. This reflects the smaller distance that there was between the CSL and ICL for the samples tested with water as the pore fluid when compared to the samples tested with silicon oil. As for the samples with strong and weak cement of type B, the samples of type A which were sheared at lower confining pressures showed a peak in the stress ratio, with the higher values corresponding to the lower current values of p'/p'_{cs}. The peak stress ratios of the type A samples are intermediate between those of the strongly cemented samples and weakly cemented samples of type B. These results were presented only for completeness and will not be considered in the analysis which will be

performed in Chapter 7 where the shear behaviour of the strongly cemented, weakly cemented and uncemented soils will be compared.

5. EXPERIMENTAL WORK ON THE CALCARENITE

5.1 SOIL DESCRIPTION

The naturally cemented carbonate sand tested as part of this research was a calcarenite retrieved from two boreholes drilled at the site of the offshore gas platform North Rankin "A", located on the North West Shelf off the coast of Western Australia. The samples were obtained using rotary core drilling and had a diameter of 83 mm. The majority of the samples were taken from a borehole (borehole B2-6) drilled at one corner of the platform, at a depth between 127 and 142 m below the sea bed. Two additional samples were taken from another borehole (borehole FSS-W), from a depth of 97 m below the sea bed. The distance between the two boreholes was about 200 m.

The sequence of sediments in the first 200 m below the sea bed belongs to the upper part of a carbonate formation called the Delambre Formation (Price, 1988), which has been deposited since the Pleistocene period. The sediments of this formation are mainly bioclastic carbonate soils having different degrees of cementing (from uncemented to strongly cemented) and grain sizes which vary from silts to sands to fine gravels.

Apthorpe et al. (1988) divided the sequence of sediments into three units on the basis of the grain composition, grain size and degree of cementing. This allowed the interpretation of the environment of deposition such as the water depth and water energy. The two upper units (Units 2 and 3) of the depositional sequence described by Apthorpe et al. (1988), extended to a maximum depth of 100 m and consisted of uncemented to weakly cemented sediments (fine calcarenites and calcisiltites) which were deposited in relatively deep water typical of a middle and outer shelf environment. The lower unit (Unit 1), from which the cores were retrieved, lay below a depth of about 100 m and was penetrated up to a depth of 180 m. This consisted of coarser and more strongly cemented sediments (calcarenites) which were interpreted as being

deposited in shallow water. The same authors suggested that Unit 1 was mainly formed during the final stage of a marine regression which occurred in the Early Pleistocene period. Following this regression the weakly cemented and uncemented sediments accumulated as the sea level rose. This sequence includes currently accumulating sediments and is believed by the authors to be at present under the maximum stresses it has experienced.

In the geological investigation Apthorpe et al. (1988) found that the distribution of degree of cementing could not be related to the depth of burial but rather to the type of environment at the time of deposition, so that the shallower the water depth the stronger the degree of cementing. Variations in the types of grains and their grading were also believed to be controlled by the environmental conditions at deposition. The cementing process for sediments deposited in shallow water was attributed to the precipitation of calcium carbonate from the saturated sea water which took place during or soon after deposition (McClelland, 1988; Fookes, 1988).

All the samples tested were retrieved from the sediments belonging to Unit 1 and, as such, they were all part of the more strongly cemented medium sand. Thin sections of the samples were prepared by the Geology Department of University College London and examined with the optical microscope. These can be seen in the two thin sections shown in Figure 5.1 where the black areas represent the voids. The thin sections of Figures 5.1a and 5.1b were taken from two samples retrieved from borehole B2–6 at a depth of 132.5 m and 139.2 m below the sea bed. The soil consisted of a cemented fairly uniform carbonate sand with small amounts of silt and fine gravel. The samples chosen for testing were among those that had the most similar grading. The particles were found to be predominantly the skeletal remains of marine organisms such as mollusc and foraminifera shells. The cement consisted of calcite crystals growing outward from the carbonate grain surfaces. In Figure 5.1 the cement appears as a thin fringe around the particles and often forms bridges between the grains. The voids are partly infilled by the cement so that an increase in the amount of cement would

correspond with a decrease of the void spaces and of the specific volume. These structural features have a reasonable resemblance with those shown by the thin sections of the artificially cemented sand in Figure 4.2.

The samples tested covered a range of specific volumes between 1.68 and 2.03. As shown in Table 5.1 there is no relationship between specific volumes and depth of burial of the samples. Only a set of four samples which were retrieved within between 133.7 m and 135.5 m below the sea bed had similar specific volumes (ranging between 1.850 and 1.871). This feature is consistent with the geological interpretation which attributed the fabric and bonding of the calcarenite to depositional environment rather than to a lithification process occurring through burial.

5.2 TESTING PROGRAMME

In the present work the calcarenite from Rankin was extensively studied by conducting triaxial compression tests over a large range of mean effective stresses (between 400 kPa and 30 MPa). Some preliminary tests had been conducted by Coop and Atkinson (1993), where only intact samples at similar initial specific volumes were considered. Their tests which were performed under varying confining pressures were aimed at a comparison with the results obtained for the artificially cemented sand with strong bonds which were also at a fixed specific volume.

The present work intended to investigate the influence of density as well as bonding on the behaviour of the calcarenite so that samples with a large variation of the initial specific volume were considered. Moreover reconstituted samples were prepared from the calcarenite and were tested following a similar approach to that of the artificially cemented sand. The present experimental work therefore included triaxial compression tests on reconstituted samples at low and high mean effective stresses, which provided a comparative framework for the patterns of behaviour observed in the intact soil. The

reconstituted samples of calcarenite were prepared using some of the intact samples with the weakest bonds which could be easily broken when the soil was submerged in water and crumbled between the fingers. The procedure followed limited damage to the particles which would have caused a variation in grading. Figure 5.2 shows the grading curve determined from the reconstituted soil, which corresponds to that of a uniform sand with a d_{50} of about 0.2 mm. The reconstituted samples were prepared in a loose state, either by freezing (samples R1 and RF) or by pluviation (samples R2 and RF2) according to the procedures described in Section 3.4.2.

The testing programme consisted of a series of eight tests performed on the intact samples and five tests performed on reconstituted samples. The samples were all isotropically compressed and then sheared at a constant axial strain rate, generally following drained constant p' stress paths except for sample C1 which was sheared undrained at a constant cell pressure. Details of the tests are summarised in Tables 5.2 and 5.3. In all the constant p' tests performed in the 10 MPa cell the axial strain and deviatoric force were measured using external instrumentation, whereas for test C1 internal instrumentation was used. Two of the tests, one on an intact sample (C3) and one on a reconstituted sample (C2), were performed to investigate the stiffness of the soil at small and larger strains. These tests were carried out in the 10 MPa cell after having modified the apparatus to allow measurements of small strain stiffness (Section 3.3). For samples C3 (intact) and C2 (reconstituted) cycles of loading and unloading were performed during undrained shearing at a constant cell pressure. The cycles were repeated for various initial mean effective stresses (p'_i) to which the samples were brought in isotropic compression. The final stage of the test performed on sample C3 consisted of isotropic unloading and subsequent shearing under drained conditions at a constant effective radial stress. A detailed description of the testing procedures followed for tests C3 and C2 is given in Section 5.6 and the various stages are summarised in Tables 5.4 and 5.5. For these tests the stiffness was computed for each loading path in terms of shear moduli.

Both intact and reconstituted samples had various diameters but a constant ratio of height to diameter of 2. Since the calcarenite cores had a diameter of 83 mm, a 83 mm pedestal was manufactured for the 10 MPa cell. The majority of the intact samples tested in the 10 MPa cell were therefore prepared by simply trimming the cores to a height of 166 m. As one of the cores (No. 80) was damaged at the ends the sample had to be prepared in the lathe with a 60 mm diameter and trimmed to a 120 mm height following the procedures described in Section 3.4.1. The 10 MPa cell in this case was provided with a 60 mm diameter pedestal. The same preparation procedures described in Section 3.4.1 were adopted for the samples tested in the 5 and 70 MPa cells which had 50 mm diameter pedestals and for samples C1 and C3 which were tested in the 10 MPa when this was modified and provided with a 50 mm diameter pedestal.

The angularity of the soil grains required the use of four latex membranes. Where mineral oil was used as the cell fluid the outermost membrane was neoprene, as latex membranes were found to deteriorate in oil.

The results from a preliminary series of five tests carried out by Coop and Atkinson (1993) on intact samples of calcarenite have been included in the figures which follow for comparison and if necessary reanalysed to maintain consistency with the analyses performed in the present work. The samples tested by Coop and Atkinson (1993) were all isotropically compressed to mean effective stresses between 450 and 7200 kPa and then sheared following constant p' stress paths under drained conditions with constant axial strain rate. Details of these tests are given in Table 5.6 and when included in the figures the tests will be labelled accordingly.

5.3 PRELIMINARY CALCULATIONS

The specific gravity G_s of the calcarenite was determined using the method described in BS:1377 (British Standards Institution, 1990) for determinations for fine, medium and

coarse grained soils and was found to be equal to 2.71.

The specific volumes of the intact samples at the start of testing (v_i) were calculated as the average of the following determinations:

a) The ends of the cores remaining after trimming the samples were saturated under vacuum and their water contents (w_i) were determined. The specific volume was then calculated as:

$$v_i = 1 + G_s w_i \tag{5.1}$$

b) After saturation in the vacuum the intact samples were weighed and their dimensions determined. The specific volume was then obtained from knowledge of the total unit weight at the start of testing (γ_{ti}):

$$v_i = \gamma_w \frac{G_s - 1}{\gamma_{ti} - \gamma_w} \tag{5.2}$$

where γ_w is the unit weight of water.

c) The specific volume was back calculated from knowledge of the water content of the sample at the end of the test (w_f) and of the volumetric strain experienced by the sample during testing (ε_{vf}), using Equation 4.2.

d) At the end of the test the dry weight of the sample (W_s) was determined and the specific volume was calculated from a knowledge of the initial volume of the sample (V_i) as follows:

$$v_i = G_s \frac{V_i}{W_s} \gamma_w = G_s \frac{\gamma_w}{\gamma_{di}} \tag{5.3}$$

where γ_{di} is the initial unit weight of dry soil.

Of the above determinations those varying by more than ± 0.01 from the others were disregarded when calculating the average.

For the reconstituted samples the initial specific volume was calculated from the weight of the dry soil used and the dimensions of the sample using Equation 5.3. An average was taken between this value and that back-calculated from the water content and overall volumetric strain at the end of the test.

For the tests performed in the 10 MPa cell before the modifications were carried out (all tests except for C1, C2 and C3) the axial force was corrected to account for the friction between the ram and the 'O'-ring seal at the top of the cell and for the force induced by the cell pressure on the ram area as described in Section 4.4. For all of the samples the axial stress was calculated considering the current area with the assumption that the sample deformed as right cylinder and errors due to membrane restraint were not considered (Section 4.4). Local axial strains (ε_{al}) were measured only for tests C1, C2 and C3 so that for these tests the calculations of the current area of the sample was performed by replacing the external axial strains with local axial strains in Equation 4.3. The external axial strains (ε_a) were corrected for the apparatus compliance. The analysis of the results presented in this chapter has been performed in terms of v, p', q, q, ε_v, ε_a and ε_{al}.

5.4 ISOTROPIC COMPRESSION

The results from the isotropic compression of the intact and reconstituted samples are shown in Figure 5.3 where v is plotted against lnp'. For clarity the data from the samples isotropically compressed to the lowest mean effective stresses (R1, R2 and C1) and those from the isotropic stages of tests C2 and C3 are omitted. Included are the three tests conducted by Coop and Atkinson (1993) at the highest mean effective stresses, namely RAN1, RAN3 and RAN4.

As shown in Table 5.1 the initial specific volumes had no relationship with the depth from which the samples were retrieved and as a consequence with the in situ effective stresses. It follows that factors such as particle packing and amount of cement, which determine the specific volumes, do not correlate with the depth of burial. These features are consistent with the geological observations that the fabric and degree of bonding of the calcarenite were controlled by the environmental conditions at the time of deposition rather than by the depth of burial.

The isotropic behaviour of the intact soil was initially stiff and presented an abrupt change of compressibility. The point at which a dramatic change of compressibility occurred will be referred as the gross yield and the compression curve followed subsequently will be referred as the post-yield compression line. Examination of the initial part of the isotropic compression curves in terms of v and p' revealed that the stiff response of the soil was initially linear but became slightly non-linear just before reaching the gross yield. Although the yield point should identify the onset of plastic strains, in the absence of loading-unloading probes the yield point will be referred in the following as the state of the soil at the end of the linear range and will be distinguished from the gross yield. As shown in Figure 5.3 the mean effective stress at the gross yield increases as the specific volume decreases. Therefore in the same way in which the specific volume is not related to the in situ effective stresses, so the points of gross yield had no relationship with the effective overburden pressure.

One of the particular features of the isotropic compression response of the calcarenite was that the intact samples before reaching the normal compression line (NCL) generally followed post-yield compression curves which lay on a unique line, irrespective of their initial specific volumes. Therefore it is possible to refer to a unique post-yield compression line which in the following will be indicated as the PYCL. The PYCL represents therefore a portion of the state boundary limiting the domain of possible states for the intact soil in isotropic compression before the NCL was approached. This

feature which was observed for the calcarenite from Rankin, differs from what was reported by Vaughan (1988) who showed that the gradient of the post-yield compression curves of bonded soils in one-dimensional compression is a function of the initial void ratio (Figure 2.25, Section 2.5).

The sample brought to the highest pressures (30 MPa), which on Figure 5.3 has an initial specific volume of 1.77, followed initially the same post-yield compression line defined by the looser samples. At high mean effective stresses however, the compressibility of the soil decreased so that the post-yield compression line bent defining a straight line with a smaller gradient. This was also the normal compression line to which the isotropic compression of the reconstituted samples taken to high pressures converged. The NCL can be represented by the equation:

$$v = N - \lambda \ln p' \tag{5.4}$$

where $N = 2.697$ and $\lambda = 0.132$.

Both the yield and gross yield points of the intact samples corresponded to states which lie above and to the right of the NCL. If the NCL is extrapolated to pressures lower than those where data exist, it can be seen that the intact samples are able to support higher mean effective stresses than those defined by the NCL. As the initial specific volume of the intact soil decreases the extent of the movement of the state boundary outside the NCL decreases up to the point at which the state boundary of the intact sample would coincide with that of the reconstituted soil. The presence of cement had therefore the effect of enhancing the volumetric stiffness of the soil and of moving the yield points to higher mean effective stresses than those reached by the reconstituted soil.

In contrast the reconstituted soil showed a softer and non-linear volumetric response which resulted in an indistinct yield. This feature is similar to that observed for the uncemented artificial soil and can be attributed to the fragile nature of the carbonate particles which undergo progressive crushing from the early stages of the compression

(Section 4.5). The presence of cement bonding in the intact samples initially prevents the occurrence of particle breakage and the isotropic load is carried by the cement since this is considerably stiffer and stronger than the soil particles. The end of the linear and stiff volumetric response of the intact soil is likely to correspond to the yield of the cement which is reflected by the consequent abrupt increase of compressibility when the isotropic load is transferred onto the breakable particles. However since all samples systematically followed the same and well defined post-yield compression line, this would indicate that the soil structure is able to support the applied stress without undergoing an instantaneous collapse and the yield point is the point at which bond degradation is initiated. This process of degradation continues progressively along a line whose gradient is a function of the relative contribution of the soil particles and the cement in supporting the applied stresses. At a particular stress level the complete degradation of bonding is achieved and the soil converges towards the equilibrium state of the uncemented soil.

As the intact samples each had a similar grading, their variation in specific volume can be thought mainly to be the result of a variation in the packing and arrangement of the particles and/or a variation in the amount of cement infilling the void spaces. From the results it can also be inferred that the influence of bonding on isotropic compression decreases as the specific volume decreases, up to a point in which density more than bonding will be the major factor controlling the isotropic yielding of the soil. Intact samples having a specific volume lower than that corresponding to the point of convergence of the PYCL with the NCL would be expected to yield on the NCL. For such a sample the high density of the soil tends to hide the effects of bonding in isotropic compression which would instead be apparent only during shearing at mean effective stresses which do not exceed the isotropic yield. For structured soils and in particular clays, isotropic states outside the NCL have also been attributed by various authors to differences in fabric as reported in Section 2.2.1. In the case of the calcarenite from Rankin differences in fabric would be expected between intact samples and reconstituted samples prepared at the same density as the intact ones. However such

differences are likely to be easily erased during the progressive degradation of bonding given the fragility of the particles as shown by the convergence between the behaviour of the intact soil with that of the reconstituted soil.

As shown in Figure 5.3 two samples, RAN3 and RAN4, showed intermediate behaviour between the reconstituted soil and the other intact samples of calcarenite, reaching states which passed the NCL but which were below the state boundary defined by the rest of the intact samples. These two samples belonged to the set of four samples which, as discussed in Section 5.1, had both a similar depth of retrieval and similar initial specific volumes. As seen for the artificially cemented soil, at a given specific volume, a lower degree of bonding results in a reduction of the mean effective stresses at yielding. It is possible that different depositional environments might have existed for this group of samples, resulting in a lower degree of bonding than the rest of the samples tested. Samples RAN3 and RAN4 will therefore be referred in the following sections as weakly cemented to distinguish them from the rest of the calcarenite samples which showed higher yield points and so a higher influence of bonding at similar specific volumes.

5.5 SHEARING

Typical stress-strain curves of the intact samples during shearing at low, intermediate and high confining pressures are shown in Figures 5.4 to 5.9. These figures also show the volumetric or pore pressure response o f the samples. The results are from constant p' stress path tests except for sample C1 which was sheared undrained at a constant cell pressure. Among the tests presented in this section, test C1 was the only one for which axial strains were measured locally as well as externally. For the other tests, despite the fact that the axial strain measurements were only made externally the end of the linear stress-strain behaviour could be determined and the yield point defined.

At low pressures (Figures 5.4 and 5.5) the samples reached marked peaks in the deviator

stress which are likely to correspond to the formation of localised zones of shearing. The stress-strain relationship is linear almost up to peak. During this phase for sample RAN6 which was sheared at a constant p', the volumetric strains were negligible. If volumetric strains were not coupled with the deviator stresses, then the increase in the pore pressure shown by the undrained test (C1) up to the yield point is probably entirely related to the increase in the mean effective stress. However the increase in the pore pressure was less than $\Delta q/3$ and, as will be shown in Section 6.7.4 for the silica sandstone, this results from the fact that the compressibility of the pore water cannot be considered negligible in comparison with the stiffness of the soil. For both samples C1 and RAN6 the peak states were followed by a rapid strain-softening. Sample RAN6 however regained strength before converging towards a constant deviator stress. The post-peak phase of sample RAN6 was accompanied by volumetric compression which tended towards a constant volume at large strains allowing the identification of a critical state. Similar features of behaviour are shown by sample C1 with the sample rapidly strain-softening towards an ultimate state.

At intermediate stresses (Figures 5.6 and 5.7) the stress-strain curves from constant p' tests show little or no peak, but in both cases the effects of cement are still reflected by the initially stiff and linear response. Sample RAN5 (Figure 5.6) strain-hardened up to the critical state at which also the volumetric strain stabilized. Yield in this case occurred at a lower deviator stress than that at the critical state. In Figure 5.7a it can be seen that sample N3 reached a constant deviator stress through a gentle strain-softening, although at large strains the sample was still compressing. Figure 5.7b shows that peak is preceded by a progressive decrease of stiffness.

At high confining pressures (Figures 5.8 and 5.9) the stress-strain curves show a typical ductile compression. At the start of shearing sample N2 had a state which lay on the isotropic state boundary of the intact samples but had not reached the NCL, whereas the state of sample N7 lay on the NCL. At large stains both samples reached a critical state as shown by the constant values of the deviator stress and the volumetric strains.

The patterns of shear behaviour illustrated for the intact samples at different pressures can be compared with those observed from testing the reconstituted soil. Figures 5.10 and 5.11 show the stress-strain curves and the volumetric response of two reconstituted samples which were sheared at constant p' at low and high pressures respectively. At the start of shearing the state of sample R2 was on the dry side of the critical state. The peak state was only slightly above the ultimate state and occurred at much higher axial strains than those observed for the intact samples tested at low confining stresses. The stress-strain behaviour was almost entirely non-linear, in contrast with what was observed for the intact samples. Shearing was accompanied by an initial compression followed by dilation until a constant volumetric strain was achieved at the ultimate state. At high confining pressures the reconstituted soils strain-hardened and reached practically a constant deviator stress, as shown in Figure 5.11 by sample RF which reached a constant volume by the end of the test. The shear behaviour resembles that seen for the intact samples sheared at high confining stresses, after isotropic yield.

The deviator stresses at the ultimate states for the intact and reconstituted soils are plotted against the corresponding mean effective stresses in Figure 5.12. Figure 5.13 shows the peak states of both soils which are labelled with numbers indicating the current specific volumes (v) at the peak states. Since at the highest mean effective stress M is only slightly lower than the values observed at lower pressures, a unique value of M of 1.46 was chosen to represent the critical state line over the whole range of mean effective stresses. This value corresponds to a friction angle ϕ'_{cs} of 36°. The peak data in Figure 5.13 are insufficient to identify peak failure envelopes. However it can be seen that the peak states defined by the intact soil lie well above those defined by the reconstituted soil and their trend seems to suggest that there is an influence of the mean effective stress on the peak strength of the intact soil. A much lower peak strength than those of the other two intact samples is shown by sample RAN6 which however still has a higher peak strength than that of the reconstituted soil despite its lower density. The reduction of strength of sample RAN6 is significant compared to the strengths of samples C1 and N3, but it seems unlikely that this is due to the lower mean effective

stress and it is more probable that it resulted from a lower degree of bonding. As can be seen in Table 5.1 this sample was retrieved from a similar depth as samples RAN3 and RAN4 which, as seen from the isotropic compression results, did not reach the state boundary defined by the rest of the intact samples. These three samples had in common not only the depth of retrieval but also their initial specific volumes (see Table 5.1). These considerations suggest that the lower peak strength of sample RAN6 was the result of the lower strength of the bonds which was reflected by a peak strength which was intermediate between those of the reconstituted and more strongly bonded samples.

In Figure 5.14 the specific volumes at the end of the tests are plotted against lnp'. For the samples which did not reach a constant volume at the end of shearing or for which localisation prevented the correct determination of the specific volume at the ultimate state, the end of test states are labelled with an arrow. The critical states of the reconstituted samples and of the intact samples with weaker and stronger bonding, all defined a unique critical state line which is parallel to the NCL and can be expressed as:

$$v = \Gamma - \lambda \ln p' \qquad (5.5)$$

where $\Gamma = 2.545$ and $\lambda = 0.132$.

As discussed earlier the sample tested at the highest pressure (N7) at the end of shearing reached both a constant deviator stress and volume. Therefore the location of the critical state point in v : lnp' space for this test suggests that the critical state line curves as it approaches the minimum specific volume of unity, but the lack of data does not permit the full definition of this part of the CSL.

In Figures 5.15 and 5.16 the shear behaviour of the intact samples is compared where possible with that of the reconstituted samples, by plotting the stress ratio η against the axial strain. The comparison at low pressures is made between samples RAN6 and R2 which both followed constant p' stress paths and were sheared at similar initial values

of p'/p'_{cs}, where p'_{cs} is the equivalent pressure taken on the CSL. The expression used to calculate the equivalent pressure will be given later in Section 5.7 The intact sample showed initially a much stiffer behaviour than the reconstituted one and in contrast with the latter had linear stress-strain curve almost up to a peak which is well above that reached by the reconstituted soil. Although sample RAN6 as discussed earlier was likely to belong to the group of more weakly bonded samples, its shear behaviour at small and relatively large strains clearly displays the influence of cementing. At large strains the intact sample tended to reach a similar stress ratio to the reconstituted one. The same type of comparison is made in Figure 5.16 for the constant p' tests conducted at mean effective stresses higher than the isotropic yield locus. The curves have all similar shapes showing the similarity in behaviour between the intact and reconstituted soils, once the intact samples had been yielded during isotropic compression.

5.6 STIFFNESS

5.6.1 Introduction

In Section 5.5 it was shown that during the initial stage of shearing the calcarenite exhibited a linear stress-strain behaviour for mean effective stresses below the isotropic yielding. In the absence of internal measurements of the stress-strain curves the yield point during shearing was identified as the end of the linear range. Since the intact samples were all subjected to a monotonic increase of the deviator stress there was no evidence for the reversibility or otherwise of the shear behaviour within the linear range and for this reason the attribute elastic was avoided.

In order to verify whether within the linear range the stress-strain behaviour was reversible, the intact soil (sample C3) was subjected to a number of stress reversals. The purpose of loading and unloading the cemented samples was also to assess whether their stiff response was affected and in particular deteriorated by the number of cycles

applied. The testing programme therefore as well as studying the stiffness of the calcarenite during shearing also investigated the effects of bond degradation on stiffness and yielding.

Studies conducted on the stiffness of clays have established the dependence of this parameter on the current state of the soil (Houlsby and Wroth, 1991; Viggiani and Atkinson, 1995). Within the framework of Critical State Soil Mechanics the mean effective stress and specific volume also account for differences in the overconsolidation ratios of reconstituted clays. As discussed in Section 2.3 for sands a distinction needs to be made between compacted and overconsolidated samples, since they may exhibit different stiffness even when fixing mean effective stress and specific volume at the same values. Less evidence exists in the literature about the factors controlling the stiffness of bonded soils in general and of cemented sands in particular. The reason lies in the fact that it is only recently that systematic studies have been carried out on these types of material with the consequence that appropriate laboratory techniques for measuring the high stiffness characterising the response of these soils are still being developed. Kim et al. (1994) investigated the variation of stiffness with confining stress for a mudstone in standard undrained and drained compression triaxial tests using highly accurate internal axial strain measurements. The authors found a slight increase in the Young's modulus of approximately 15% when the radial effective stresses were increased up to the in situ overburden pressure and no variation at higher stresses. For a sandstone Tatsuoka et al. (1993) suggested a higher dependence of the Young's modulus on the confining stresses even for stresses which were higher than the overburden effective stress, but no data were presented in support of their observations.

In the present work the variation of stiffness with mean effective stress was investigated by means of undrained shearing cycles performed on the same sample of calcarenite at different initial mean effective stresses p'_i (Table 5.4). Since only a few samples remained at this stage of the project the testing programme was designed to maximise the information from a single test. The advantage of considering stiffness determinations

at different values of p'_i on the same sample (C3) was that of ensuring that, at least at stresses below the isotropic yield, the corresponding specific volumes remained reasonably constant. At mean effective stresses higher than the isotropic yield the variations of the mean effective stress as well as of the specific volume will both influence stiffness. The sample was brought to the required initial value of mean effective stress by means of isotropic compression and was then subjected to three cycles. At the end of each cycle in order to reestablish the same initial value of mean effective stress as in the previous cycle, any excess pore pressure which had built up was fully dissipated by opening the drainage tap. The values of the maximum deviator stress (q_{max}) for the cycles were chosen such that the volumetric strain associated with the dissipation of the excess pore pressure at the end of each cycle was kept small and caused negligible variation in the specific volume. In this way for each set of probes the initial specific volume was kept substantially constant and is therefore indicated as v in the relevant figures and tables. The state of the sample in terms of p'_i and v for each series of loading-unloading probes is reported in Table 5.4 together with the values of q_{max} reached in cycle.

In Section 5.5 it was shown that intact samples sheared at intermediate mean effective stresses and before isotropic yielding (Figure 5.6), had yielding during shearing at values of stress ratio η less than M and strain-hardened to the critical state. Due to the strain-hardening it is likely that the transition towards the frictional behaviour was accompanied by a progressive degradation of bonding taking place throughout the whole sample. The effects of this bond degradation on stiffness and yielding were investigated through a number of cycles which were extended beyond the linear range, when bond degradation was likely to develop within the sample.

Undrained loading and unloading shearing cycles were also carried out on a reconstituted sample (C2) obtained from the same core as the intact sample C3 and the stiffnesses from the two samples have been compared. The shearing cycles were performed at similar initial effective stresses for both samples. Again for the

reconstituted soil the loading paths were limited to deviator stresses which produced small variations of the specific volume when the excess pore pressure was dissipated at the end of each cycle. Table 5.5 shows the values of p'_i, q_{max} and v for each undrained loading-unloading series of probes.

For both the intact and reconstituted soils the stiffness was determined in terms of tangent shear modulus G as $\delta q/3\delta\varepsilon_{al}$, where ε_{al} was calculated by averaging the measurements from the two local axial transducers. A linear regression was used over a set of five data points, each data point corresponding to an increment in the local axial strain of about 0.00005 %. In the following two sections, which discuss the stiffness of the intact and reconstituted samples, the shear moduli calculated over the loading path of cycles performed at the same values of p_i' and v are superimposed in the same diagram and plotted against the deviator stress and/or the local axial strains ε_{al} using a semi-logarithmic scale.

5.6.2 Intact soil

Figure 5.17 shows the deviator stress against the local axial strains obtained from a serious of three cycles performed on the intact sample C3 at a value of p_i' of 800 kPa which was smaller than the isotropic yield stress. It can be seen that the stress-strain relationship is linear and that the axial strains at the end of the unloading paths are recoverable with only a minor hysteresis. The tangent shear moduli G from this set of data and from a set of cycles performed at a p_i' of 250 kPa are plotted against the logarithm of the local axial strains ε_{al} in Figures 5.18a and 5.18b. The values of the moduli show a scatter of about ± 5 % around the average which therefore represents the accuracy of the stiffness determinations. As expected from the linearity of the stress-strain relationship the shear modulus remains constant. In both graphs the variation of the average shear modulus from the first to the third cycle is only about 100 kPa which corresponds to a reduction of 9 %. The effect of cycling on stiffness can therefore be

considered as being small since the variation of the average shear modulus is only slightly larger than the scatter of the stiffness determinations. This scatter can obviously be reduced by extending the regression analysis to more data points. However when the regression is made over a larger number of data points abrupt breaks in the stiffness curves are smoothed preventing the exact determination of the yield points. Figures 5.18a and 5.18b also show essentially no variation of the shear modulus with mean effective stress.

Figure 5.19a shows the stress-strain curves of cycles performed at a value of p_i' of 1550 kPa which was close to but still smaller than the isotropic yield stress. The variation of the tangent shear moduli with the logarithm of the deviator stress during the loading paths is shown in Figure 5.19b. This type of representation for the variation of G is preferred to that which considers variations with strains since it allows determinations of the deviator stresses at yielding. In the first loading the tangent shear modulus remains initially constant and has a maximum value (G_{max}) and yielding is marked by a rapid decrease of stiffness. After yielding plastic strains developed as shown by the irreversibility of the stress-strain curves in Figure 5.19a. The interesting feature shown by the intact soil at this pressure is that on reloading the value of G_{max} does not vary but a smaller range of linearity can be observed with the yield point moving back to a lower deviator stress. As further reloading takes place the value of G_{max} and the yield point remain substantially the same as in the previous cycles but a more gentle decrease of stiffness can be observed soon after yielding.

A number of probes were performed at a slightly higher value of p_i' of 2000 kPa. The variation of the tangent shear modulus with logq for each loading probe is shown in Figure 5.20. The values of G_{max} in the first probe show a slight increase from the values observed at a p_i' of 1550 kPa indicating some influence of the change in state (p' and v) on stiffness. Yielding occurs at a lower deviator stress compared with the first probe performed at a p'_i of 1550 kPa. The second probe causes now a significant decrease in the value of G_{max} indicating that a substantial deterioration of bonding took place at this

stage, which no longer effects only the yield point but also the value of stiffness.

The tangent shear moduli for the three loading paths performed at a p_i' of 8400 kPa are plotted against the logq in Figure 5.21. In this case the state of the soil at the start of each probe was located along the isotropic post-yield compression line (PYCL). It can be seen that in the first loading the value of G_{max} (1050 kPa) is higher than those in the last two shearing paths performed at a p_i' of 2000 kPa. After an initial linear stress-strain response the tangent shear modulus decreases with development of plastic strains. Again in this case the length of the loading path was limited to deviator stresses such that the volumetric changes occurring after dissipation of the excess pore pressures at the end of each cycle were small. In the second and third loading the value of G_{max} remained substantially constant but the linear range extended to high deviator stresses showing the strain-hardening characteristics now acquired by the soil.. The type of behaviour shown when probes were performed from a state located on the PYCL contrasted with the type of behaviour seen for the probes performed from states located before the PYCL. In the latter case when the soil was reloaded after an initial yield a reduction of the range of linear stress-strain behaviour was observed.

The response in terms of pore pressures is illustrated in Figures 5.22a to 5.22c where the effective stress path is plotted as q against p' for the three sets of probes performed at p_i' values equal to 800 kPa, 1550 kPa and 2000 kPa respectively. At the lowest initial mean effective stress the stress-strain behaviour during the probes was shown to be linear and reversible. Linearity and reversibility can be observed in Figure 5.22a in terms of pore pressure response in the second and third cycles whereas during the first cycle the effective stress path shows a departure from an initial linear response and irrecoverabilty on unloading. In contrast the stress-strain behaviour detected in the first cycle from the local axial gauges was linear over the whole cycle and irreversible so that the observed pore pressure response is likely to be the result of bedding errors. On subsequent cycles the effects of bedding errors disappear and the real behaviour in terms of pore pressures can be observed. An interesting feature shown by the effective stress

path is that the ratio of $\delta q/\delta p'$ is different from the vertical paths expected for undrained tests on isotropic elastic materials. The path is inclined to the right, indicating that the pore pressures generated during shearing were smaller than those expected for an isotropic elastic soil. This particular feature was also observed in undrained shearing of the silica sandstone as will be discussed in Sections 6.7.3 and 6.7.4. It will be also shown that the observed pore pressures for the silica sandstone agree with the values expected for isotropic and elastic materials if the compressibility of water is accounted for. This seems to exclude inherent anisotropy of the material as a possible cause for the inclined effective stress path.

In Figures 5.22b and 5.22c the pore pressure response for every probe is irreversible and corresponds to irreversible stress-strain behaviour. However it can be seen that for the probes performed at a p_i' equal to 1550 kPa the initial linear stress-strain behaviour is reflected also in the linearity of the effective stress path which also in this case is inclined to the right. However the initial part of the effective stress path tends to become vertical in the second and third probes performed at a p_i' equal to 2000 kPa when also the value of stiffness decreased. This feature might be explained as the result of the increased compressibility of the soil skeleton after degradation of bonding so that the compressibility of the pore water becomes less important. This type of consideration should be taken into account for very stiff materials before inferring anisotropy, unless tests specifically aimed at studying anisotropy are performed.

5.6.3 Reconstituted soil

Figures 5.23a to 5.23d show the shear modulus against the logq for the loading paths of cycles performed on a reconstituted sample at different values of p_i'. Compared to the intact soil the stiffness plateau during the first loading at each mean effective stress extends only over a small range of deviator stresses, so that there is a substantially non-linear and plastic response. Successive probes have the effect of reducing the non-

linearity of the soil and increasing the values of the deviator stress and axial strain at yielding. This typical strain-hardening response contrasts with the decrease of the deviator stress at yielding produced in the intact soil by the degradation of bonding and observed in Figure 5.19b when the intact soil was reloaded after having yielded for the first time. A similar strain-hardening response to that of the reconstituted soil was instead observed for the intact soil only for those probes performed at the highest confining stress once bonding had been degraded (Figure 5.21).

Comparison between the shear moduli of the intact and reconstituted samples at similar values of p_i' (Figures 5.18, 5.20, 5.21 and 5.23) shows that, although the reconstituted soil was denser than the intact one it had lower values of G_{max} and a much smaller elastic range. This observation shows that the presence of cement in the intact sample has the effect of increasing both the value of the stiffness and the range in which the soil behaves elastically.

For the reconstituted soil the value of G_{max} remained substantially the same in the first and second cycles at all values of p_i', showing that rotation of the stress path does not influence the value of G_{max}. The results also show that the maximum shear modulus increases as the initial mean effective stress and density increase. In contrast for the intact soil it was shown that an increase of the maximum shear modulus with mean effective stress and density took place only after there had been a major deterioration of the bonding and stiffness of the sample. The comparison between the stiffnesses of intact and reconstituted samples will be described further in Section 7.4.

5.7 NORMALIZED STRESS PATHS

The shear behaviour of the calcarenite can be represented in a unified picture both in terms of stresses and volume by normalizing both the deviator stress and the mean effective stress with respect to an equivalent pressure. A tentative critical state line was defined by Coop and Atkinson (1993) in logv : logp' space from their results on intact samples of calcarenite, providing a reference line for the normalization. The tests performed by the authors considered only intact samples which had been deliberately chosen among those having similar initial specific volumes. The extension of the present experimental work to intact samples with a large variation of specific volumes as well as to the reconstituted soil, necessarily required the use of a method of normalization of the results in an attempt to give them significance and coherence. In Section 5.5 it was shown that the intact soil, irrespective of the initial specific volume and degree of bonding, defined a unique CSL in v : lnp' space which also represented the critical states of the reconstituted soil. This line, which was redefined on the basis of both the previous and new results, was therefore in the first instance considered as a convenient reference for normalization, giving an equivalent pressure as follows:

$$p'_{cs} = \exp \frac{\Gamma - v}{\lambda} \qquad (5.6)$$

where $\Gamma = 2.545$ and $\lambda = 0.132$.

Figure 5.24a shows the normalized stress paths of the reconstituted samples. From them a state boundary surface can be defined which will be referred to as the intrinsic state boundary surface (ISBS). This surface is similar in shape to that of the uncemented artificial soil (Figure 4.14) determined by Coop and Atkinson (1993), with the critical state (CS) located below and to the left of the apex of the surface.

Figure 5.24b shows the normalized stress paths of the intact samples which yielded during isotropic compression and the comparison with the ISBS. With the exception of tests RAN3 and RAN4, at the start of shearing the states of the intact samples lay along

the same post-yield isotropic compression line (PYCL), which at high pressures coincided with the NCL defined by the reconstituted soil. Samples sheared from states located on the initial portion of the PYCL have initial values of p'/p'_{cs} which are higher than the intersection of the ISBS with the isotropic axis, since the PYCL was located to the right of the NCL. Moreover as the CSL and the PYCL are not parallel in v : lnp' space, the initial points of the normalized stress paths have increasingly lower values of p'/p'_{cs} as the initial state of the soil moves towards the NCL.

The stress paths shown in Figure 5.24b have all the typical shape expected for soils undergoing ductile compression. All of the paths reach states which are outside those permitted for the reconstituted samples and only at large strains do the states of the intact soil tend to converge towards the critical state which is unique for both reconstituted and intact soils. The stress path which reaches the furthest states outside the ISBS corresponds to the sample which travelled the least distance down the PYCL. The way in which the normalized stress paths shrink towards the ISBS seems to reflect the convergence of the behaviour of the intact soil towards the intrinsic as also seen in isotropic compression. This type of behaviour was envisaged by Coop and Atkinson (1993) when normalizing the stress paths of samples RAN1, RAN3 and RAN4 but further considerations are needed and will be discussed in Section 7.1.1. The most rapid convergence towards the ISBS is from sample N5 which in isotropic compression reached a state which was very close to the point of convergence of the PYCL with the NCL. Sample N7 was isotropically compressed to very high stresses and reached the NCL. The initial normalized state in this case coincides with the intersection of the ISBS with the isotropic axis. The normalized stress path would have been expected to follow closely the ISBS. The divergence that in contrast can be observed in Figure 5.24b is likely to be the result of having considered the locus of critical states in v : lnp' as a straight line even at such high pressures. If instead the normalization had been done with respect to a curved critical state line in this interval of mean effective stresses, as suggested from the critical state of N7 in v : lnp' space, the values of p'_{cs} would have increased so producing a stress path closer and probably coincident with the ISBS.

Samples RAN4 and RAN3 also show stress paths which have the typical shape expected for soils which compress and strain-harden. Again in this case the two samples reach states during shearing which are beyond those defined by the ISBS. However the smaller influence of cementing displayed by their lower yield points in isotropic compression, locates their normalized stress paths below those defined by samples N2 and N4, even though the latter two samples had been compressed further beyond their isotropic yield. The last portion of the stress path of sample RAN3 rapidly converges towards the ISBS and crosses that of sample RAN4. Analyses of the test data revealed that the break in shape shown by the stress path corresponded to an increase in the strain rate.

The normalized stress paths of samples which had been isotropically compressed to mean effective stresses below the isotropic yield prior to shearing are shown in Figure 5.24c. These stress paths are superimposed over some of the ones shown in Figure 5.24b. All of the samples sheared before isotropic yielding reached states which are above the ISBS. The yield points indicate the end of the linear stress-strain range and for the constant p' drained tests also the range in which the volumetric strains due to shearing were zero. For the samples sheared at the lowest initial values of p'/p'_{cs} (RAN6 and C1) yielding is well above the ISBS and very close to the peak points of the stress paths, which occur at values of η greater than M. After having reached the peak stress ratio, the stress paths bend backwards towards the ISBS.

The effects of bonding on the shear behaviour of the intact soil can be highlighted and separated from the frictional effects by comparing the normalized stress paths of intact and reconstituted samples at similar initial values of p'/p'_{cs} (to account for differences in the initial values of p' and v) and for similar stress paths. If for instance the constant p' stress path of sample RAN6 (Figure 5.24c) is compared with the nearby constant p' stress path of sample R1 (Figure 5.24a), two main features resulting from bonding can be highlighted. One of these is the initial verticality of the stress path of the intact sample in contrast with that of the reconstituted sample, which shows that because of bonding volumetric strains due to shearing are prevented. The other feature is that the

presence of bonding brings the peak state of the intact soil well above that of the reconstituted sample. Moreover for the reconstituted sample the peak state is accompanied by dilation, whereas no volumetric change occurs for the intact sample before failure.

The undrained normalized stress path (C1) can be seen to differ from those corresponding to drained constant p' tests. For the artificially cemented carbonate soil it was shown that up to yield standard drained and constant p' tests, when normalized, were also different (Section 4.7) from each other. This can be explained as being due to the absence of volumetric strains as long as the cement is intact, so that the effect of the normalization below yielding is simply to scale the stress path in terms of q and p' by a constant factor given by the initial value of p'_{cs}. In a similar way the undrained stress path is scaled by a constant factor resulting in a normalized stress path which has the same inclination as the q : p' stress path. This one as shown in the previous section is inclined to the right prior to yielding.

At intermediate values of p'/p'_{cs} (samples N3 and RAN5) the contribution of bonding to the shear behaviour of the intact soil is still evident up to yield, with a normalized stress path which rises vertically up to this point. Yield in this case occurs at values of η less than M and the shear behaviour becomes progressively frictional as there is bond degradation, particle breakage and volumetric compression until the soil reaches a critical state. Although the intact soil is still able to reach states beyond the ISBS, the stress ratio does not greatly exceed M. The stress path for sample NF1 is omitted from Figure 5.24c because of its particularly high specific volume which would have required the extrapolation of the CSL far beyond its range of definition.

Sample C3 was sheared under a constant cell pressure after being isotropically compressed up to the PYCL and then isotropically unloaded to a state on the dry side of critical. It can be seen that the normalized stress path resembles those of the reconstituted soils sheared on the dry side of the critical state. The previous stress

history experienced by the sample in this case caused the degradation of bonding so that shearing states achieved by the soil are contained within the ISBS.

This normalization of the shear behaviour has highlighted a number of limitations which will be discussed and overcome in Section 7.1. In particular this type of representation is not able to describe yielding and boundary of the intact soil although it provides a useful means to compare features of the shear behaviour of intact and reconstituted soils so highlighting the influence of bonding as opposed to friction.

6. EXPERIMENTAL WORK ON THE SILICA SANDSTONE

6.1 GEOLOGICAL STUDY FOR THE SELECTION OF THE SILICA SANDSTONE

The results presented in Chapters 4 and 5 showed that many features of the behaviour of the artificially cemented soil with strong bonds could also be observed for the naturally cemented soil from Rankin. It was also shown how these features were modified by a variation in the bond strength by testing the artificial soil with weaker bonds. These observations led the research towards investigating a second naturally cemented soil which by comparison with the calcarenite from Rankin could be considered as weakly cemented. Since both the natural and artificial carbonate soils had the common feature of having easily crushable grains, the choice of the third soil was directed towards a material in which a weak cement bonded together strong particles.

In order to identify such type of soil a geological investigation was carried out aimed at locating possible deposits available within the United Kingdom that met the required characteristics. The geological investigation started from a desk study in which several sources of information were examined. These sources included reviews of the geological literature, consultations with geologists, a study of the Solid and Drift editions of geological maps and memoirs published by the British Geological Survey and an examination of the rock sample library at City University.

Samples of oolitic limestone from the rock sample library were found to be weakly cemented and suggested this as a material to be examined further. This rock belongs to the Middle Jurassic period, outcropping in Gloucestershire. At the same time a review of the geological literature on the Cretaceous sediments of Southern England (Casey, 1961; Gallois, 1965; Kirkaldy, 1975) indicated the Lower Greensand as a potential source for the required material. The sediments of the Lower Greensand

comprise arenaceous deposits with a varying degree of cementing and can be found in extensive areas of the Isle of Wight and the Weald (Kent, Surrey and Sussex). In these areas, known as the Southern Basin, the deposition of the Lower Greensand marked the beginning of an important cycle of marine sedimentation which took place in Britain during the Aptian and Lower Albian stages of the Lower Cretaceous (Casey, 1961). In discussions with geologists (Fookes, 1993) the Isle of Wight was indicated as the best area for a preliminary site study. On the island the Lower Greensand reaches a maximum thickness of 240 m and the whole succession of strata can be found exposed in the cliffs.

During the site visits the deposits identified in the desk study were examined and evaluated for their possible use in the laboratory testing program. One of the most notable outcrops of the oolitic limestone was found to the south of Cheltenham in the Birdlip anticline. The exposed strata belonged to the Inferior Oolite and formed during the Middle Jurassic period in a shallow sea where deposition was interrupted at frequent intervals by earth movements, which caused slight warping and folding of the sea floor. Although the sample seen in the rock library had a weak cement that could be broken under finger pressure, the corresponding outcrop revealed that the rock was very hard and could only be marked by means of a hammer blow. Weaker rocks were looked for unsuccessfully at other outcrops in the area so that the site investigation was redirected towards the younger deposits of the Lower Greensand on the Isle of Wight.

A complete exposure 800 feet (244 m) thick of the Lower Greensand was visible on a south facing beach at Redcliff in the northern part of Sandown Bay, on the Isle of Wight. The strata dipped at an angle of approximately 15° to the northeast so that all of the different layers were accessible as the beach was traversed. By identifying the distinct pale blue Atherfield clay at the base of the Lower Greensand it was possible to trace the sequence of strata as described by Osborne Wight (1921) in the Geological Memoirs and to identify in particular the sandy layers. The section examined is shown schematically in Figure 6.1. By using simple testing techniques it was then possible to

assess the presence of bonding in the samples examined and eliminate those that were uncemented or too weakly cemented and those that were too strong. Those samples which resisted crushing under finger pressure were immersed in a bucket of water to check that the observed strength was not due to suction. Strata that resisted hammer blows were excluded as being too strongly cemented. On the basis of these techniques the strata identified as potential material to study were part of the so called Ferruginous Sands.

Although fulfilling the requirements, the material found at Redcliff was excluded as a suitable soil for the experimental work for two main reasons. Firstly the strata in the cliff were weathered and it was not clear how far into the cliff the weathering process had penetrated. Secondly the dip of the strata and the presence of a fault which could be seen within 15 m of the location examined suggested that this area had been subjected to complex stresses during its geological history which were likely to influence the behaviour of the soil.

The search was then widened to identify materials similar to the Ferruginous Sands of Redcliff in other locations of Southern England which had not been subjected to weathering and where the strata were horizontal. Consultation of the geological literature indicated the presence of Ferruginous Sand deposits in the Weald as part of the Folkestone Beds, the youngest sediments of the Lower Greensand series. The outcrop of the Lower Greensand of the Weald area extends in the east-west direction from Folkestone to Petersfield and in the north-south direction from Sevenoaks to Eastbourne. In Kent the outcrop thickens at Maidstone where the Folkestone Beds mainly consist of Ferruginous Sands. Their current-bedding indicated that their deposition occurred in a shallow water marine environment (Casey, 1961). A particular feature of the Folkestone Beds is the alternation of fine to medium quartz sand bands with varying degrees of cementing from uncemented sands to sandstones or sandy limestones, as was also observed at Redcliff in the Isle of Wight. From the literature review undertaken (Casey, 1961; Gallois, 1965) it appears that the mechanisms by which these alternations

developed has never been adequately understood. The cement in the sediments consists of iron oxide as was also confirmed later by the analysis of thin sections. As pointed out by Warren (1995) the iron oxide cement content can be found in larger quantities as the grain size increases and this suggests that its origin was from the action of the ground water which found in the coarser sediments preferential routes of flowing. This would indicate that the cementing process was unlikely to have occurred in the early stages of the diagenesis of the sediments but was related to the presence of environmental conditions which favoured the precipitation of the cement from the ground water flowing in the sediments.

On the geological history of the deposits the only information found was a reconstruction of the paleogeography of the Weald by Kirkaldy (1975) who suggested that the ground level at the time at which the overlying Gault and the overlain Weald Clay were deposited must have been at least 300 ft higher than present. Therefore in order to receive an approximate indication of the depth of burial of the Lower Greensand in the Weald area, the sections from the Solid and Drift maps of the surrounding areas were considered. From this examination it would appear that the Folkestone Beds were overconsolidated to different degrees according to the amount of overburden deposited in the various areas and subsequently removed by the erosion which followed tectonic movements. The Weald of Kent, Sussex and Surrey is in the form of a plunging anticline towards the east, dying out in the neighbourhood of Peterfield in Hampshire. In the area of Maidstone it would appear that the overburden removed from the Folkestone Beds, from which the samples tested were retrieved, was of the order of about 440 m. This estimate was based from an examination of the Solid and Drift map of Maidstone (Sheet 288) and the Drift maps of Sevenoaks and Dartford (Sheet 287 and 271 respectively). The overburden estimated did not take into account unconformities but included the removal of the Lower London Tertiaries and overlying drift deposits. On this basis therefore the maximum past total overburden pressure experienced by the deposit under discussion would be approximately equal to 8.8 MPa.

6.2 SOIL SAMPLING AND THIN SECTIONS

Ferruginous Sands were found exposed in a quarry near Maidstone owned by Ready Mixed Concrete. This quarry supplies aggregates that were used primarily for highway construction in the surrounding area. One of the recently excavated faces of the quarry displayed deposits of weakly cemented medium sands of yellow-orange colour exposed in sub-horizontal strata. The presence of cohesion in the sediments allowed the undercutting and removal of an intact block of approximately 80 x 50 x 60 cm by means of an excavator. Prior to sampling the horizontal and vertical directions of the sample in the ground were marked. The depth of retrieval was about 5 m below the current ground level.

In the laboratory the block was shaped into smaller blocks of 60 x 60 x 120 mm using a circular saw, ensuring that the sample was orientated as in the ground. Cylindrical samples of 50 mm diameter and 100 mm height were trimmed from the shaped blocks according to the procedures described in Section 3.4.1.

Reconstituted samples could be easily obtained by the immersion of the intact soil in water and desegregation using a rubber pestle. Because of the strong nature of the soil grains the mechanical action used was unlikely to cause any particle damage. The grain size distribution determined from the reconstituted soil is shown in Figure 6.2. It can be seen that the grain size distribution of the silica sandstone was that of a uniform sand with a d_{50} of 0.2 mm.

The microfabric of the silica sandstone was studied by examination of thin sections which were prepared by the Geology Department of University College London. Impregnating the samples with epoxy resin prevented disturbance of the microfabric. In some cases a blue dye was also used to highlight the pore spaces. Figures 6.3 and 6.4 show optical micrographs of thin sections from the intact material with different degrees of magnification and under white and plain polarized light. The micrographs were taken

by Geomaterials Research Services Ltd, Basildon. It can be seen that the soil consists of a poorly graded medium sand. All the grains consist of quartz of sub-rounded and sub-angular shape and sometimes almost blade like. A red-brown fine rim of iron oxide surrounds each quartz grain.

The fabric and bonding of the intact soil are displayed more clearly in the scanning electron micrographs in Figure 6.5 which were performed at Queen Mary and Westfield College, London. The electron micrographs of Figures 6.5a and 6.5c were performed on a sample of intact soil with unpolished surfaces so that the texture of the soil could be examined whereas Figure 6.5b refers to a polished thin section. The chemical analysis performed with the scanning electron microscope revealed a 97 % silica content, 1.5 % of iron and traces of other elements such as aluminium. In Figure 6.5 the iron oxide appears white and adjacent grains are only in a few cases in contact through the cement. Through magnification of the scanning electron micrograph the average thickness of the cement coating was found to be 5 μm, such that for grains in contact the coating would be likely to weld the grains together. Because of the low cement content and the absence of matrix material, the low specific volumes of about 1.45 found for the silica sandstone was entirely the result of the dense packing of the grains. Both the optical and electron micrographs display a high incidence of particle contacts. These types of contacts can be defined as straight and concavo-convex (see Section 2.4 and Figure 2.18). Other features shown by the scanning electron micrographs in Figures 6.5a and 6.5c are the roughness of the grain surface and solution cavities which resemble the features described by Dusseault and Morgenstern (1979) for "locked sands" (Section 2.4).

6.3 TESTING PROGRAMME

The testing programme summarised in Tables 6.1 and 6.2 for the silica sandstone consisted of triaxial compression tests conducted on intact and reconstituted samples over a large range of mean effective stresses (900 kPa - 70 MPa). The samples were

isotropically compressed and sheared at a constant axial strain rate. Drained constant p' shearing was performed on seven intact samples and eight reconstituted samples. The tests were performed in the 10 and 70 MPa cells and all included accurate measurements of local axial strains. For these tests the 10 MPa cell had been modified to allow accurate determination of small strain stiffness and new sample preparation and setting up procedures were followed (see Section 3.4). Both the reconstituted and intact samples had a diameter of 50 mm and a height of 100 mm. The intact samples were cut from block samples recovered from the quarry face and trimmed in a lathe to the required cylindrical shape.

For each drained shearing test performed on the intact samples the variation of the stiffness from very small strains to failure was determined. Since all of the intact samples had similar densities and were characterised by a high degree of uniformity, the series of drained tests enabled the variation of the small strain stiffness of the soil with mean effective stress to be determined. As well as drained tests undrained compression tests were performed where several strain-controlled loading-unloading cycles were followed at an initial mean effective stress (p'_i) equal to 1760 kPa. The maximum deviator stress (q_{max}) reached in the cycles was progressively increased but kept below the failure stress. At each value of the deviator stress three to five cycles were performed as shown in Table 6.3. During each loading path the stiffness was computed in terms of tangent shear modulus (G).

The reconstituted soil was prepared by first submerging the intact soil in water and then breaking the soil into grains with a rubber pestle. Because of the strong nature of the soil grains, breakage of particles was not a concern during this process. The samples were then prepared in a loose state by pluviation (Section 3.4.2).

To be able to compare the stiffness during shearing of the intact and reconstituted samples similar initial states for the two soils in terms of specific volume and mean effective stress were necessary. Several methods were attempted to prepare the

reconstituted samples at an initial density which was as close as possible to that of the intact soil. The densest sample was obtained from pouring dry sand through a coarse sieve located at a known height above the mould. This method produced a specific volume equal to 1.65 which was not sufficiently close to the specific volume of 1.44 for the intact soil. A slightly higher specific volume of 1.665 was obtained by tamping the sand layers during pluviation (sample R10). The reasons for which it was not possible to obtain a specific volume similar to that of the intact soil will be explained later in Section 7.2.3.

One of the reconstituted samples (R9) prepared by pluviation did achieve a similar density to the intact soil by means of overconsolidation. The sample was isotropically compressed until the maximum value of p' of 70 MPa was achieved in the triaxial apparatus and was then unloaded to a p' of 14 MPa. The variation of stiffness during shearing from the reconstituted sample with the highest densities (R9) was investigated in constant p' tests and compared with the stiffness obtained from the intact soil.

6.4 PRELIMINARY CALCULATIONS

The specific gravity of the sandstone was determined using the method described in BS:1377 (British Standards Institution, 1990) and was found to be equal to 2.66.

The initial specific volumes for the intact and reconstituted samples were determined in the same way as described for the calcarenite in Section 5.3.

6.5 ISOTROPIC COMPRESSION

Figure 6.6a shows the isotropic compression curve from the intact sample which was taken to the highest mean effective stress (60 MPa). This curve is representative of the

isotropic compression results obtained from the other intact samples which had very similar specific volumes, varying from 1.435 to 1.445. In the same graph are shown the results from the isotropic compression of two of the reconstituted samples which reached the highest mean effective stresses (R10 and R9). Sample R9 was prepared in a loose state so that it was possible to identify the normal compression line (NCL) over a wide range of mean effective stresses. This sample was also subjected to a number of isotropic unloading- reloading paths which can be compared with those of the intact soil.

The isotropic compression of samples R9 and R10 to high mean effective stresses allowed the identification of the NCL for the reconstituted soil which was defined as:

$$v = N - \lambda \ln p' \qquad (6.1)$$

where $N = 3.233$ and $\lambda = 0.161$.

Because of the low specific volumes of the intact soil the maximum confining pressure of 70 MPa in the triaxial apparatus was not sufficient to bring the state of the soil to the above NCL. In these conditions it was not possible to verify whether the NCL was also the intrinsic compression line to which the intact soil converged at large volumetric strains.

The isotropic response of the intact soil was stiffer than that of the reconstituted soil during both the first loading and the unloading-reloading paths. In Figure 6.6b the isotropic compression curves of two of the intact samples brought to the highest values of p' are shown in more detail and compared with the closest unloading-reloading path performed on the reconstituted soil. It can be seen that the intact soil initially exhibits a linear response in v : lnp' space up to a value of p' of 11000 kPa. This becomes subsequently non-linear as the curve of the intact soil approaches the NCL. The small unloading-reloading cycles performed on the intact sample A1 in the non-linear part of the isotropic compression curve also show the irreversible response of the soil at these values of p'. As for the calcarenite, the end of the linear response in v : lnp' space was

interpreted as the isotropic yield point of the intact soil. A clearer identification of the yield point was obtained from the variation of the bulk modulus (K) with the logarithm of p' shown later in Section 6.7.4. The occurrence of the isotropic yield to the left of the NCL resembles the isotropic compression response of the artificially cemented carbonate soil with weak bonding (Section 4.5).

The reconstituted soil shows a non-linear and softer isotropic response through the first loading as well as through the unloading-reloading paths (Figures 6.6a and 6.6b) with no distinct yield as was already observed for the reconstituted carbonate soils (Sections 4.5 and 5.4). The mechanism governing the change of compressibility in both the silica and carbonate reconstituted soils can be explained as the result of particle breakage as observed by Coop and Lee (1993). The linear response of the intact soil probably results from the presence of cementing and the yield point is likely to correspond to the yield of the cement with a consequent transferral of the isotropic load onto the particles. When comparing the isotropic compression of the intact soil with the unloading-reloading path of the reconstituted soil it can be seen that before yield the intact soil displays a much stiffer volumetric response than the reconstituted soil. After yielding the volumetric response of the intact soil resembles that of the reconstituted soil within the same range of pressures.

6.6 SHEARING

Figures 6.7 and 6.8 show typical stress-strain curves of the intact samples which were sheared following constant p' stress-paths at values of p' equal to 900, 3460, 14400 and 60000 kPa respectively. In the same graphs the volumetric response of the samples during shearing is also shown. At small strains the values of axial strains are those from the internal measurements whereas at relatively large strains the external measurements were considered.

As shown in Figures 6.7 and 6.8a, even at relatively high values of mean effective stress the intact samples defined clear peak deviator stresses followed by a rapid loss of strength. Shearing after peak took place within localised shear zones which probably formed near the peak state, although the occurrence of the shear zones could not be observed because of the steel cell chamber. The localization was reflected by an abrupt change in the rate of dilation as shown by the volumetric response during the strain-softening phase. Because of this localisation of strains the measured volumetric strains are not representative of the volumetric changes within the shearing zones, which would be expected to be larger than those measured. Before the peak states the stress-strain curves showed a very stiff response. The peak and post-peak responses were accompanied by dilation. The volumetric response will be discussed in detail in Section 7.2.3.

At the highest mean effective stresses (Figure 6.8b) the stress-strain curve shows no peak and converges towards an ultimate value of the deviator stress. The sample underwent ductile compression but a significant rate of change in the volumetric strain was still observed when the sample reached a constant deviator stress. The test ended at an axial strain of about 9 % due to limitations imposed by the radial strain belt mounted on the sample.

Figures 6.9a and 6.9b show the stress-strain behaviour of two reconstituted samples sheared following constant p' stress paths at the lowest and highest values of p' considered in the testing programme (900 and 36750 kPa). At low pressures the stress-strain behaviour was characterised by a smooth peak. The volumetric strains tended towards a constant value after gentle dilation. The volumetric response of the reconstituted soils will be described further in Section 7.2.3 and compared with that from the intact soil. At high pressure the stress-strain curve shows no peak and the deviator stress tends directly towards an ultimate state. Shearing is accompanied by volumetric compression and a condition of constant volume is approached at large strains.

The ultimate states in terms of q and p' for the intact and reconstituted soils are shown in Figure 6.10. For values of p' up to about 20 MPa both soils defined the same strength envelope which is well fitted by a straight line through the origin having a stress-ratio M of 1.29 and a friction angle ϕ'_{cs} of 32.1°. At higher values of p' an arrow is shown next to the state of the reconstituted sample to indicate that this test was not complete as shown in Figure 6.9b, whereas the question mark next to the ultimate state of the intact sample indicates that this is uncertain due to the premature ending of the test (see Figure 6.8b). The peak and ultimate states for the intact and reconstituted soils are plotted in Figure 6.11. Since the intact samples had a relatively small range of variation of specific volume at peak (between 2.425 and 1.445), the trend of the data points in Figure 6.11 predominantly shows the influence of mean effective stress on peak strength. A straight line closely fits the peak data except for the peak state corresponding to the p' of 14.4 MPa which seems to indicate a curved peak failure envelope and a convergence towards the critical state envelope at higher values of p'. Despite the localised shearing of the intact samples after peak, the end of test states were aligned along the critical state line defined by the reconstituted soil. Figure 6.11 also shows the peak states of the reconstituted samples. A correct comparison between the peak states of the reconstituted and intact samples is not possible in this case since for a given value of p' the two soils had very different specific volumes. These differences will be accounted for in Sections 7.2 and 7.3 by means of normalisation of the data with respect to an equivalent pressure.

Figure 6.12 shows the states at the end of shearing in v : lnp' space for both intact and reconstituted soils. Four of the reconstituted samples reached a constant volume and for those samples which did not reach a condition of constant volume at the end of the test an arrow is drawn to indicate the direction of the stress-volume path at large strains. The

critical states of the reconstituted soil are fitted with a straight line which is also parallel to the NCL having the equation:

$$v = \Gamma - \lambda \ln p' \tag{6.2}$$

with $\Gamma = 2.986$ and $\lambda = 0.161$.

The end of test points of the majority of the intact samples lie well to the left of the CSL defined by the reconstituted soil. As previously shown the shear behaviour of the intact soil was characterised by a marked strain-softening over a large range of mean effective stresses and at the peak state shearing was accompanied by localisation of strains. Therefore for these samples it was not possible to identify the critical state volume. Among the samples which strain-softened, the one which was sheared at the highest value of p' (equal to 14.4 MPa) reached a constant volume and the end of test point happened to lie on the CSL of the reconstituted soil. For this sample however the post-peak rate of dilation abruptly became zero, probably being the result of localisation rather than an indication of the attainment of a critical state. For this reason a question mark has been shown on the graph. When considering the intact sample sheared in ductile compression a constant volume condition was not reached at the end of the test. In conclusion for the intact samples the locus of the critical states in the stress-volume space could not be defined and, unlike the artificially cemented sand and the calcarenite, for the silica sandstone it was not possible therefore to verify whether the critical state line of the intact and reconstituted soils were coincident. This aspect will be reconsidered in the next chapter through the analysis of the stress-dilatancy relationships for the intact and reconstituted soils. Until then the critical state line of the reconstituted soil will be taken as a reference for normalisation when comparing the shear behaviour of intact and reconstituted samples.

Figures 6.13a and 6.13b show the comparison between the shear behaviour in terms of stress ratio η against the axial strains for two pairs of intact and reconstituted samples which had similar initial values of p'/p'_{cs}. The equivalent pressure p'_{cs} was in both cases

taken on the critical state line defined by the reconstituted soil. The peaks of the intact samples are higher than those of the reconstituted samples. It is worth noting that the peak shown by sample A2 in Figure 6.13b, which was sheared from an initial state beyond isotropic yield, was not observed with the cemented carbonate soils when shearing was performed beyond isotropic yielding (Figure 5.16). For the silica sandstone the peak state was accompanied by a marked dilation and an analysis of the stress-dilatancy relationship of the intact and reconstituted samples will be carried out in the next chapter in order to assess whether the higher peak strength observed for the intact soil can be explained in terms of dilation.

6.7 STIFFNESS

6.7.1 Introduction

The silica sandstone showed marked strain-softening behaviour over an extended range of mean effective stresses. Peak states were observed at values of p' as high as 14.4 MPa although isotropic yielding occurred at a p' of 11 MPa. High pressures were therefore essential to characterise the overall mechanics of this soil and the tests were all performed in the 10 and 70 MPa capacity cells. Both apparatus had internal instrumentation for the measurement of axial strains and deviatoric forces.

When the intact soil was sheared in the 10 MPa apparatus before further modifications were carried out, non-uniform local axial strains were observed. Even if high mean effective stresses were reached non-uniform strains could not be avoided by attaching the ram to the sample at an early stage of the isotropic compression because of the stiff volumetric response of the soil below the isotropic yield (see Section 3.3.3). Under these circumstances the stress-strain curve and the stiffness of the material could not be determined correctly irrespective of the accuracy of the internal instrumentation so that it was necessary to develop new techniques for the verification of the coincidence of the

sample and apparatus axes (Section 3.4.4). Moreover when using a rigid connection between the sample and the ram a rapid increase in the deviator stress was observed at the start of shearing even at low strain rates, preventing the determination of the initial part of the stress-strain curve. The new type of connection described in Section 3.3.4 was designed to reduce the rate of loading whilst maintaining a relatively high external displacement rate of 0.03 mm/min. The use of higher axial displacement rates had the advantage of minimizing the temperature effects on the measurements. The new techniques developed for the measurement of small strain stiffness were all applied to the samples tested in the 10 MPa apparatus, since in this case mean effective stresses were below the isotropic yield.

The non-uniformity of deformations at the start of shearing was found to be less serious for the samples compressed beyond the isotropic yield which were tested in the 70 MPa cell. The main limitation encountered for this apparatus resulted from the type of connection used to attach the sample to the internal load cell. The connection was based on a ball and socket joint. The lower part of the connection resting on the sample consisted of a half sphere with the same diameter as the sample and the upper part had a complementary socket. Because of the high stiffness of the material and the rigid connection, a rapid increase in the deviator stress (150 - 200 kPa) was observed at the start of shearing as the load cell was brought into contact with the sample. Consequently for these tests the stress-strain response could be measured only at deviator stresses higher than 200 kPa as the results will show later. An external displacement rate of 0.03 mm/ min was again used to minimise the temperature effects on the readings from the internal instrumentation.

In the drained constant p' tests the samples were monotonically loaded to failure under a constant external displacement rate. The general patterns of behaviour observed during shearing and the strength characteristics of the soil were described in Section 6.6. In the next sections the pre-failure behaviour of the intact soil is presented and the stress-strain results are analysed in terms of tangent stiffness.

A total of seven constant p' tests were carried out of which five tests were performed in the 10 MPa cell and two in the 70 MPa. Uniformity among the samples was ensured because the samples were prepared from the same block retrieved from the quarry face. This enabled comparisons to be made of the stiffness as obtained from each test at different values of p' to assess the influence of a variation of p' both on the maximum shear modulus (G_{max}) and on yielding.

The pre-failure behaviour of the silica sandstone was also investigated in the 10 MPa cell during undrained strain-controlled shearing performed with a constant cell pressure and again with nominal displacement rates of 0.03 mm/min. As for the calcarenite the aim was that of assessing the reversibility of the stress-strain response before yield and to study the mechanism of bond degradation and its effects on stiffness and yielding. The loading-unloading probes on the silica sandstone were performed from the same isotropic state at a p'_i of 1760 kPa and to various values of the deviator stress as shown in Table 6.3. For each maximum value of the deviator stress (q_{max}) the cycles were repeated from 3 to 5 times. At the end of each cycle any excess pore pressure was allowed to dissipate fully in order to re-establish the same value of p' in the isotropic state. The dissipation of pore pressure resulted in negligible volumetric strains so that the specific volume of the soil was kept reasonably constant as can be seen in Table 6.3.

6.7.2 Stiffness of the intact soil in drained shearing

The tangent stiffness during constant p' drained shearing was determined as $\delta q/3\delta\varepsilon_s$ and plotted against the logarithm of either q or ε_s. Since the strains were small the values

of $\delta\varepsilon_s$ could be calculated as:

$$\delta\varepsilon_s = \delta\varepsilon_{al} - \frac{\delta\varepsilon_v}{3} \tag{6.3}$$

where $\delta\varepsilon_{al}$ is the average value of the two local axial strain measurements and $\delta\varepsilon_v$ is the volumetric strain measured by the volume gauge, both of which are linear strains. At a strain level of 0.1 %, which is close to the peak state, the difference between linear and natural shear strains is about $5x10^{-5}$ % which was considered negligible. At the start of shearing the volumetric strain measurements were affected by bedding errors and could not be used to calculate the shear strains. The accuracy of the volumetric strains of ± 0.001 % was about an order of magnitude lower than that of the local axial strains, but there would have been no point in trying to improve it through the use of the volume gauge because of the presence of bedding errors. Due to these limitations it was therefore assumed that the soil had isotropic properties and that volumetric strains were zero during the linear part of the stress-strain response for shearing at a constant value of p'. Shear strains were calculated from the measurements of volumetric strains only when the bedding errors, could be considered negligible as indicated by a comparison between local and external axial strain measurements.

The tangent stiffness was determined using a linear regression of the $q : \varepsilon_s$ curves over a set of five data points, each data point corresponding to an increment in the local axial strain of 0.00005 %. If the soil had isotropic properties then the values of stiffness for constant p' shearing calculated as described above would represent the shear modulus G.

For soils having transversely isotropic properties the elastic relationship between stress and strain increment tensors can be expressed as:

$$\begin{bmatrix} \delta p' \\ \delta q \end{bmatrix} = \begin{bmatrix} K & J \\ J & 3G \end{bmatrix} \begin{bmatrix} \delta\varepsilon_v \\ \delta\varepsilon_s \end{bmatrix} \tag{6.4}$$

where K is the bulk modulus, G is the shear modulus and J is the cross anisotropic

modulus (Graham and Houlsby, 1983).

Equation 6.4 can be inverted and expressed in terms of the compliance matrix:

$$\begin{bmatrix} \delta\varepsilon_v \\ \delta\varepsilon_s \end{bmatrix} = \begin{bmatrix} C_1 & C_2 \\ C_2 & C_3 \end{bmatrix} \begin{bmatrix} \delta p' \\ \delta q \end{bmatrix} \tag{6.5}$$

where $C_1 = 3G/det$, $C_2 = - J/det$, $C_3 = K/det$ and $det = (3KG - J^2)$.

For constant p' tests the relationship between $\delta\varepsilon_s$ and δq is then given by:

$$\delta\varepsilon_s = C_3 \, \delta q \tag{6.6}$$

from which

$$\frac{\delta q}{3\delta\varepsilon_s} = \frac{1}{3C_3} = \frac{3KG - J^2}{3K} \tag{6.7}$$

From Equations 6.4 and 6.7 it can be seen that for a transversely anisotropic soil a stiffness calculated as $\delta q/3\delta\varepsilon_s$ from constant p' and undrained tests would be different and only the latter would give the shear modulus G. For isotropic soils instead G can be calculated as $\delta q/3\delta\varepsilon_s$ irrespective of the stress path followed since no coupling would exist between $\delta p'$ and $\delta\varepsilon_s$ or between δq and $\delta\varepsilon_v$. As mentioned above the silica sandstone was assumed to be isotropic and the values of $\delta q/3\delta\varepsilon_s$ determined from constant p' tests will be referred to as the shear modulus. The validity of this assumption will be demonstrated in Section 6.7.5 through comparisons between the results obtained from constant p' and undrained tests.

Figures 6.14a and 6.15 show the shear modulus G plotted against the logarithm of q from two of the constant p' tests (D2 and D5) conducted in the 10 MPa cell at values of p' of 1800 and 5600 kPa respectively. The shear modulus from test D2 is also shown in Figure 6.14b plotted against the logarithm of the shear strain. In the following discussion the representation of G : logq is preferred since the variation of the shear

modulus with the deviator stress was used to identify the yield point.

It can be observed that the shear modulus forms a well defined plateau which extends to relatively high values of the deviator stress. The constant modulus has an average value of 3050 MPa and a scatter of ± 6%. Comparison between Figures 6.14a and 6.15 shows that within the scatter of data there is no variation of the modulus with p'. The end of the linear stress-strain behaviour is well defined and is followed by a rapid decrease of stiffness as failure is approached. For each constant p' test the yield point was determined and identified as the point at which the behaviour ceased to be linear. The values of the shear modulus and of the yield points could be accepted with confidence only because the local axial strains were uniform.

Figures 6.16 and 6.17 show the variation of the tangent shear modulus with the logarithm of q for the samples (A2 and A1) sheared in the 70 MPa cell at mean effective stresses beyond the isotropic yield point. As anticipated stiffnesses could be obtained from these tests only for deviator stresses higher than 200 kPa. From these stress levels onwards the graphs show a progressive decrease of the shear modulus with the deviator stress. Although for these tests a plateau in stiffness was not identified, in both cases it can be seen that extrapolation of the results to small deviator stresses indicates a higher shear modulus than those determined for the samples sheared before isotropic yielding. Moreover at any fixed value of q the shear modulus of sample A1 is higher than that of sample A2 which was sheared at lower values of p'. It appears therefore that after isotropic yielding p' influences the values of stiffness. However the specific volume also has to be considered as an additional influencing factor. At the start of shearing sample A1 had a smaller specific volume than sample A2 and subsequently the difference in specific volume increased as sample A1 compressed and sample A2 dilated.

6.7.3 Stiffness and effective stress paths of the intact soil in undrained shearing

The tangent stiffness for the undrained shearing was calculated during each loading path by means of a linear regression of the $q : \epsilon_{al}$ curve, where axial strains were obtained from averaging the readings from the two local axial transducers. In the regression five data points were considered, each corresponding to an increment of axial strains of about 0.00005 %. The undrained loading probes allowed the calculation of the tangential shear modulus G as $\delta q/3\delta\epsilon_{al}$.

Figure 6.18 shows the deviator stress against the average local axial strain from three of the loading probes (series B probes) performed in an undrained test from an isotropic state at a p'_i of 1760 kPa and up to a deviator stress of 900 kPa. The stress-strain relationship is shown to be linear and substantially reversible. The shear moduli determined on the corresponding loading paths are plotted against the local axial strains and the deviator stress in semi-logarithmic scales in Figures 6.19a and 6.19b respectively. The results all lie within a band of ± 150 MPa which corresponds to a scatter of ± 6 % of the average value of 2750 MPa. The graphs therefore show that within the accuracy of the determinations the shear modulus in each loading path was constant and independent of the number of cycles applied.

The shear moduli obtained from three of the loading probes performed up to a deviator stress of 2000 kPa (series C probes) are shown in Figure 6.20. This stage of the test was preceded by a total of ten cycles of which five reached a deviator stress of 400 kPa and the other five reached a deviator stress of 900 kPa. The value of shear modulus was the same as that determined in the previous loading paths and was again constant with the deviator stress. Also in this case the stress-strain behaviour was found to be substantially reversible.

A subsequent set of three probes was performed up to a deviator stress of 4500 kPa (series D probes). The stress-strain curves are shown in Figure 6.21 and the tangent

shear moduli calculated from the loading paths are plotted against the logarithm of q in Figure 6.22. In this case the stress-strain curve shows hysteresis and irreversible strains at the end of each cycle. During the first probe the shear modulus is initially constant and has a maximum value (G_{max}). It then decreases abruptly at a value of q of 2200 kPa, which is slightly greater than the maximum deviator stress reached in the previous sets of probes (series C probes). On reloading G_{max} remains the same as in the previous cycle but yielding occurs at a lower deviator stress and the range of linearity decreases. On a second reloading (cycle 3) G_{max} and the yield point remained almost unchanged but a smoother decrease of the shear modulus can be observed after yielding.

The last set of probes (series E probes) was performed up to a deviator stress of 6000 kPa. The shear moduli are plotted against the logarithm of q in Figure 6.23. During the first loading path the variation of the shear modulus is similar to that observed in the previous probe (cycle 3 of the series D probes) and so is the location of the yield point. However the higher values of deviator stress reached during this stage caused a reduction of the deviator stress at yield to a value of about 60 kPa on subsequent loading as shown by the data for cycle 2. After this point the non-linear behaviour was associated with larger plastic strains than those developed during the series D probes so that when the sample was subsequently reloaded for the third cycle a reduction of almost 30 % in G_{max} was observed. In this case the soil had regained its linear properties over an extended range of stresses and yield occurred at a deviator stress of about 2200 kPa. The patterns observed for the shear modulus during the probes of the series D and E are similar to those observed for the calcarenite in Figure 5.19b and 5.20 (Section 5.6.2).

The pore pressure responses observed during the probes of the series C, D and E are shown in Figures 6.24a to 6.24c. For the probes which extended within the elastic range (Figure 6.24a) the direction of the effective stress paths ($\delta q/\delta p'$) is inclined to the right and not vertical as it would be expected for isotropic elastic soils sheared under undrained conditions. In the first cycle the effective stress path during loading is linear

up to the maximum deviator stress of 900 kPa which was reached in the previous set of probes but then it bends to the left. On unloading the pore pressure response is irreversible in contrast to the stress-strain behaviour which was found to be substantially reversible. This feature was also observed for the undrained probes performed on the calcarenite and, as in that case, can be attributed to bedding errors which disappeared when the sample was reloaded over the same range of deviator stress. In the following cycles the effective stress paths are linear and reversible over the whole range of stresses.

The effective stress paths from the probes of the series D are shown in Figure 6.24b. In this case yielding took place as can be seen in Figure 6.22, but the stress-strain behaviour was characterised only by a minor hysteresis and small plastic strains at the end of each cycle (Figure 6.21). Similarly the pore pressure shows no significant irreversibility in the second and third cycles. A more evident irreversible response can be seen in the first cycle as was observed in the first cycle of the probes of series C, but this does not reflect the true response of the soil.

In the final series of probes (series E), which reached the highest value of deviator stress, the effective stress paths become clearly non-linear as shown in Figure 6.24c. In this case for clarity the effective stress path from the second cycle was omitted. The stiffness graph of Figure 6.23 showed that in the second cycle of this set of probes yielding occurred at a low deviator stress and on subsequent loading the value of G_{max} decreased. Although not very evident it appears in this case that as for the calcarenite (Section 5.6.2) this resulted in a direction of the effective stress path closer to the vertical.

6.7.4 Pore pressure response of the intact soil

The inclination to the right of the effective stress paths observed in the elastic range indicated that the excess pore pressures generated during undrained shearing were smaller than those expected for an isotropic elastic soil. If the soil is isotropic and the pore water is incompressible in comparison with the soil skeleton, the effective stress path during undrained shearing in the elastic range should be vertical. The observed inclination of the effective stress path may be considered as an indication that one or both of the above assumptions are not satisfied for the silica sandstone. In the following discussion the theoretical pore pressures generated in the elastic range during the undrained test will be calculated assuming that the soil is isotropic and the contribution of various factors influencing the pore pressure response will be considered.

For an isotropic elastic soil in which the particles are assumed incompressible, Bishop and Eldin (1950) derived the following expression relating changes in pore pressures (Δu) to total changes in isotropic stresses ($\Delta\sigma$):

$$\Delta u = \Delta\sigma \frac{1}{1 + n \frac{C_w}{C}} \tag{6.8}$$

where:

C	is the compressibility of the soil skeleton
C_w	is the compressibility of the pore water
n	is the porosity of the soil.

For very stiff soils Wissa (1969) found that, depending on the system used, the influence on the pore pressures due to the compressibility of the pore pressure measuring system may be comparable to that of the soil skeleton and water. Later Bishop (1976)

generalised the expression proposed by Wissa to include also the influence of the compressibility of the soil particles and obtained:

$$\Delta u = \Delta\sigma \frac{1}{1 + n\frac{C_W - C_S}{C - C_S} + \frac{V_L}{V}\frac{C_W}{C - C_S} + \frac{C_L + C_M}{V(C - C_S)}} \qquad (6.9)$$

where:

C_S is the compressibility of the soil particles

C_I is the compressibility of the pore water drainage lines

C_M is the compressibility of the pore water measuring device

V_L, V are the volumes of water in the pore water drainage lines and the volume of the sample respectively.

For granular materials the penetration of the rubber membrane into the lateral surface of the sample may also influence significantly the pore pressures under undrained changes of total stresses. The contribution of membrane penetration together with that of the soil skeleton and water compressibility was taken into account by Baldi and Nova (1984) who derived the following expression for the excess pore pressure:

$$\Delta u = \Delta\sigma \frac{1 + \frac{f_m}{VC}}{1 + \frac{f_m}{VC} + n\frac{C_W}{C}} \qquad (6.10)$$

in which f_m is the membrane flexibility defined as the volume change caused by the penetration of the membrane per unit change in the effective radial stress.

For the axisymmetric stress conditions existing during shearing in triaxial tests and for an elastic material the excess pore pressure can be calculated substituting the mean total

stress into Equations 6.8 and 6.9:

$$\Delta p = \Delta\sigma_r + \frac{1}{3}(\Delta\sigma_a - \Delta\sigma_r) \qquad (6.11)$$

which for standard undrained shearing, where $\Delta\sigma_r = 0$, simplifies to:

$$\Delta p = \frac{1}{3}\Delta\sigma_a = \frac{1}{3}\Delta q \qquad (6.12)$$

In Equations 6.11 and 6.12 σ_a and σ_r are the total axial and total radial stresses respectively. The compressibility C of the soil skeleton is the bulk compressibility measured in drained conditions at a constant pore pressure and represents the increment of volumetric strain per unit increment in mean effective stress. Figure 6.25 shows the volumetric strains typically observed in isotropic compression both when measured externally by the volume gauge and when calculated as three times the average of the local axial strains. At low pressures both graphs show a high compressibility and non-linear response, whereas for p' values higher than approximately 1000 kPa the volumetric response becomes approximately linear and very stiff. The large initial compression observed can be attributed mainly to membrane penetration. During the initial stages of isotropic loading the readings from the internal transducers are also affected, since at low pressures the movement of the membrane was followed by the transducer holders which were glued to the membrane. At intermediate pressures (between 1000 and 5000 kPa) the effects of membrane penetration appear to become negligible but bedding errors were still present as shown by the higher compressibility of the curve for the volume gauge compared to that from the internal instrumentation. At high pressures these errors tend to disappear and the two curves become parallel as would be expected for an isotropic material. It should be emphasised that the effects of the above errors have to be considered before interpreting a ratio of the volumetric to axial strain which is not equal to three as an indication of anisotropy.

The effects of bedding errors on the volumetric strain readings from the volume gauge were considered in the calculation of the specific volumes of the samples at the start of

testing when these were back-calculated from the final water contents and from the overall volumetric strains at the end of the test. The volumetric strains during isotropic compression were corrected at low pressures by extrapolating the linear part of the stress-volumetric strain curve. When isotropic compression was not extended to high stresses the volumetric strains were then calculated from the measured bulk modulus of the soil. The initial specific volumes were back-calculated using the total volumetric strains corrected in this way.

The variation of the bulk modulus with p' is shown with a semi-logarithmic scale in Figure 6.26. The values of K were obtained from a linear regression of the stress-volumetric strain curve in isotropic compression, in which the volumetric strains were calculated as three times the average of the internal axial strain readings. A clear yield point can be identified in isotropic compression at the end of the linear behaviour which corresponds to the mean effective stress at yield of 11000 kPa discussed in Section 6.5. The maximum value of the bulk modulus is shown to be equal to 5800 MPa, corresponding to a value of C equal to 1.7×10^{-5} cm^2/Kg_f. Since the compressibility of water C_w is equal to 4.8×10^{-5} cm^2/Kg_f it follows that for the silica sandstone the hypothesis of an incompressible pore fluid is not valid when calculating values of excess pore pressures due to undrained changes in total stresses.

In order to calculate the excess pore pressure generated during the undrained shearing the more general Equation 6.9 will be first considered and the relative importance of the various terms assessed. It should be pointed out that shearing was performed from an initial p' of 1760 kPa, at which level the effects of the membrane penetration became negligible. Values of the compressibility of soil particles can be found in the literature and for a silica sandstone Zisman (1933) estimated a C_s of 0.27×10^{5} cm^2/Kg_f. In both the 10 MPa cell where the test was performed and also in the other high pressure systems, the pore pressure transducer was connected directly to the side of the cell base so that the drainage lines are drilled through solid metal and can be considered incompressible (i.e. $C_L = 0$). The influence of the compressibility of the electrical

transducer (C_M) can be evaluated using a value of 9.05×10^{9} $cm^3/Kg_f/cm^2$ supplied by Druck Ltd (1995) for the type of transducer used. For an estimated V_L of 1.4 cm^3 and a V of 196 cm^3 the influence of the compressibility of the pore pressure measuring system is found to be negligible, as it gives rise to an error of less than 1 % of the change in pore pressure, which is within typical errors accepted during testing. Considering that the value of the porosity n was equal to 0.31, if the compressibility of the soil particles is accounted for then Equation 6.9 gives:

$$\frac{\Delta u}{\Delta p} = 0.50 \qquad (6.13)$$

whereas the simplified expression from Equation 6.8 which assumes incompressible particles gives:

$$\frac{\Delta u}{\Delta p} = 0.53 \qquad (6.14)$$

The value given by Equation 6.13 is 10 % higher than that observed experimentally. It appears therefore that within this error the direction of the effective stress path can be justified assuming that the soil is isotropic and elastic.

The reliability of the pore pressures observed during shearing was ensured by careful saturation of the sample and drainage system as described in Section 3.4.3. Full saturation for such stiff material can then be assessed in two ways. One method is to check that the pore pressure coefficient B (Skempton, 1954) observed experimentally is equal to the value theoretically calculated, considering carefully all the factors which significantly influence the calculations. The samples were all saturated using a maximum back pressure of 600 kPa and a mean effective stress of 60 kPa. Before starting the isotropic compression stage values of B of 0.99 and 0.995 were measured. In order to obtain a reliable theoretical determination of B at low mean effective stresses it is necessary to consider the effect of the membrane flexibility as well as the effects of the compressibility of the soil skeleton, soil particles and water. The membrane compressibility was determined as the gradient at low stresses of the stress-strain curve

of Figure 6.25 considering the volumetric strains measured by the volume gauge. This gradient would correspond to the ratio f_m/V in Equation 6.10 and was found to be equal to $1.7x10^{-3}$ cm^2/Kg_f. The value of B calculated from Equation 6.10 would then be equal to 0.99 which is in agreement with the value observed experimentally. Baldi and Nova (1984) derived a semi-empirical expression to evaluate the membrane compressibility in which the most uncertain coefficient is the Young's modulus of the membrane material. If this is considered equal to the value suggested by the authors the compressibility of the membrane would be equal to $3.8x10^{-4}$ cm^2/Kg_f and the value of B for full saturation would be 0.97. In this case, since the value observed experimentally was higher than the latter, this discrepancy may be due to either the approximations inherent in the formula used to calculate the membrane compressibility or to an incorrect value assumed for the Young's modulus of the membrane.

An alternative method to check for complete saturation was to verify that the B value remained constant as the back pressure was increased and the effective stress was maintained constant. This method was suggested by Wissa (1969) and when membrane penetration is present can be still considered valid, provided the effective stresses at each back pressure increment are kept constant. This approach is useful in absence of reliable determinations of the coefficients necessary to calculate the expected theoretical value of B in very stiff soils and was adopted for the saturation of both the silica sandstone and the carbonate cemented soils. Generally the B value was first found to increase with increasing back pressure becoming constant from a value of back pressure of about 450 kPa onwards.

6.7.5 Comparison between G_{max} determined from drained and undrained tests

In the following discussion some of the considerations presented in Section 6.7.4 will be used to compare the values of the maximum shear modulus (G_{max}) determined in drained constant p' tests and undrained tests, which will be denoted as $G^{p'}_{max}$ and G^{u}_{max}

respectively. For the samples sheared from initial stresses below isotropic yield, the ratio of $G^{p'}_{max}$ to G^{u}_{max} was found to be equal to 1.1, whereas the two moduli would be expected to be the same in the case of an isotropic elastic material. In shearing at constant p' and for the assumption of an isotropic material the elastic volumetric strain increment ($\delta\varepsilon^e_v$) would be zero and $G^{p'}_{max}$ would be defined as $\delta q/3\delta\varepsilon^e_a$ (see Equation 6.7 for J equal to zero). This definition of the shear modulus was considered for convenience when determining the maximum value of the shear modulus in the constant p' tests before isotropic yielding, since the volumetric strains had both a poor accuracy compared to the local axial strains and also included bedding errors. In undrained tests, if the compressibility of water and of the soil grains are considered, volumetric changes of the sample can occur and $\delta\varepsilon^e_v$ is not zero. Therefore the shear strain is not equal to the axial strain and the shear modulus can be corrected (G^u_{cor}) to include the contribution of the elastic volumetric strains which occur as follows:

$$G^{u}_{cor} = \frac{\delta q}{3\delta\varepsilon^e_s} = \frac{\delta q}{3\delta\varepsilon^e_a\left(1 - \dfrac{\delta\varepsilon^e_v}{3\delta\varepsilon^e_a}\right)} = \frac{G^{u}_{max}}{1 - \dfrac{\delta\varepsilon^e_v}{3\delta\varepsilon^e_a}} \qquad (6.15)$$

The volumetric strain increment considering the compressibility of the grains can be expressed according to Bishop (1973) as:

$$\delta\varepsilon^e_v = n\,C_w\,\delta u + (1-n)\,C_s\,\delta u + C_s\,\delta p' \qquad (6.16)$$

and the ratio of the volumetric strain to the axial strain increment then becomes equal to:

$$\frac{\delta\varepsilon^e_v}{\delta\varepsilon^e_a} = \frac{n\,C_w\,\delta u + (1-n)\,C_s\,\delta u + C_s\,\delta p'}{\delta q\,/\,3G^{u}_{max}} \qquad (6.17)$$

If the theoretical value of $3\delta u/\delta q$ equal to 0.5 as given by Equation 6.13 is used, which was closer to the value determined experimentally, a value of $\delta\varepsilon^e_v/\delta\varepsilon^e_a$ equal to 0.267 is

obtained from Equation 6.17. The value of $\delta\varepsilon_v^e/\delta\varepsilon_a^e$ can then be substituted in Equation 6.15 to give:

$$G_{cor}^{u} = 1.1\ G_{max}^{u} \tag{6.18}$$

so that G_{cor}^{u} is equal to $G_{max}^{p'}$. This confirms that the difference between the values of the maximum shear moduli $G_{max}^{p'}$ and G_{max}^{u} determined in the drained and undrained tests respectively arose from the high stiffness of the soil skeleton which had a compressibility comparable to that of the pore fluid. In this case the difference between the two maximum shear moduli determined experimentally seems not to arise from anisotropy and can be justified considering the material to be isotropic and elastic.

6.7.6 Stiffness of the reconstituted soil

In order to obtain values of the shear modulus of reconstituted samples which can be compared with those from the intact samples it is necessary to consider the soils at similar initial densities and mean effective stresses. This condition however is not sufficient to guarantee a correct comparison since the stiffness of sands is likely to be influenced by the overall stress history experienced by the soil. Whereas for reconstituted clays the influence of the overall stress history is accounted for once the values v and p' are fixed as the overconsolidation ratio is dependent on v and p', sand samples can reach a given state either through compaction or by means of overconsolidation. This was seen by Coop and Lee (1993) to affect the stress path in undrained shearing of uncemented granular soils (Section 2.3) and would be expected to affect the value of stiffness.

For the silica sandstone when considering the comparison between the stiffness of the intact and reconstituted soils two problems had to be considered. The first one was that compacted reconstituted samples could not be prepared at densities as high as those of the intact samples. The maximum density obtained for the reconstituted soil

corresponded to a specific volume of 1.65. Higher densities could therefore be obtained only through compression of samples to very high pressures and unloading to the required value of mean effective stress. However even when overconsolidating the reconstituted samples the 70 MPa capacity of the high pressure apparatus limited the maximum densities achievable. The reasons for the high density of the silica sandstone will be discussed further in Section 7.2, but it is unlikely that the high density of the intact soil results from overconsolidation, since this would have implied a very much higher overburden than the maximum overburden estimated for the soil from a geological reconstruction (see Section 6.1). Even if similar states to the intact soil were achieved for the reconstituted soil by overconsolidation, this would not necessarily guarantee a similarity in grading, in particle arrangement and contacts which are factors that can also have an influence on stiffness.

Figure 6.6b shows the state at the start of shearing achieved for sample R9 which was isotropically compressed to a p' of 70 MPa and then unloaded to a p' of 19900 kPa. It can be seen that the state of the reconstituted sample was reasonably close to that of the intact sample A2 so that the shear moduli from these two tests will be compared. Sample R9 was sheared in a strain-controlled test performed at a constant value of p'. The shear modulus was determined as $\delta q/3\delta\varepsilon_s$ and is plotted against the shear strains in a semi-logarithmic scale in Figure 6.27. Values of the shear modulus could not be calculated for shear strains lower than 0.006 % because of the poorer resolution of the local axial transducers (equal to 0.001 %) in the 70 MPa apparatus and also because of the increase in the deviator stress at the start of shearing caused by the type of connection used in this apparatus as discussed in Section 6.7.1. The results show that the stiffness modulus decreases smoothly as shearing progressed and the behaviour of the reconstituted soil is non-linear. From the trend of the data it is apparent that at low strains the shear modulus is much lower than that obtained for sample A2. The differences between the shear moduli of the reconstituted and intact soils can be attributed to various reasons. Firstly, as discussed above, it is likely that the two soils had a different grading because of the particle crushing experienced by the reconstituted

soil during the isotropic compression. Secondly despite the fact that sample A2 was sheared after having passed the isotropic yield the high values of the shear modulus compared with the reconstituted sample may be an indication that the influence of cement or more likely of the soil fabric were still present as will discussed in Section 7.4. Much higher mean effective stresses would be required to strain the intact soil sufficiently to erase its in situ structure.

7. DISCUSSION

7.1 THE SHEAR BEHAVIOUR OF THE CEMENTED CARBONATE SANDS

7.1.1 Introduction

In Section 5.4 a boundary was identified in v : lnp' space for all the possible states of the calcarenite in isotropic compression (Figure 5.3). Irrespective of the specific volume of the intact soil at start of testing, both gross yield and post-yield compression states were located along this boundary. At higher specific volumes the isotropic state boundary of the intact soil, indicated as the PYCL, was located to the right of the normal compression line (NCL) representing the isotropic state boundary of the reconstituted soil. As the specific volume decreased the offset between these two boundaries reduced until they became substantially coincident. Therefore at the lowest specific volumes the boundary of the intact soil was given by the NCL. Following Burland (1990), for the calcarenite the NCL also defined the intrinsic compression line (ICL) as it represented the loci of states reached by the intact soil once sufficient strain caused its behaviour to coincide with that of the reconstituted soil. In the present work it was preferred to address the isotropic compression line of the reconstituted soil simply as the NCL. The reason for this was to maintain consistency with soils such as the silica sandstone for which it was not conclusive whether the NCL was also the line approached by the intact soil at large strains (ICL) as discussed in Section 6.5.

For the calcarenite the initially stiff and linear response of the intact samples was marked by an abrupt change in compressibility (gross yield) which was attributed to the onset of bond degradation. The following gradual convergence between the post-yield compression curve and the NCL indicated that as bonding degraded the characteristics of the intact soil evolved towards those of the reconstituted soil.

The response of the calcarenite during shearing was presented in Section 5.5 and compared with that of the reconstituted soil. In an attempt to unify the shear behaviour of both soils in a single plot the effective stress paths were normalized considering an equivalent pressure which was taken on the critical state line (CSL) defined in v : lnp' space. From data at the ultimate states, the CSL was interpreted as being unique for both intact and reconstituted soils (Figure 5.14), thus providing a common reference for the normalization. Intact samples sheared from initial states beyond isotropic yielding showed a contraction of the normalized stress paths towards the intrinsic state boundary surface (ISBS) defined by the reconstituted soil. The reducing size of the normalized stress paths (Figure 5.24b) of the intact samples corresponded to decreasing values of the initial normalized state p'/p'_{cs} until the latter approached the value corresponding to the NCL. Such a decrease of the initial normalized state corresponded to intact samples sheared from states which moved along the isotropic boundary and towards the NCL and resulted from the non-parallelism between the initial portion of the isotropic boundary of the intact soil and the CSL to which the normalization was referred. In a similar way if intact and reconstituted soils had the same shear behaviour the above non-parallelism would have resulted in normalized stress paths of the intact soil moving towards the ISBS. Therefore the observed convergence of the normalized stress path did not necessarily indicate that the shear behaviour of intact and reconstituted soils were initially different and then progressively more similar, but may have artificially resulted from the method of normalization adopted.

For the intact samples sheared from states which were below the isotropic boundary, no trend was produced in terms of yield points when these were normalized with respect to the CSL (Figure 5.24c). This was attributed to the following two reasons. Firstly the mentioned lack of parallelism between the initial portion of the isotropic boundary of the intact soil and the CSL not only spread the normalized stress paths of the samples sheared after isotropic yielding, but also the normalized stress paths and yield points for the samples sheared before isotropic yielding. Secondly there was no reason to believe that stresses at yielding which resulted from cohesion, should have been controlled by

the location of the state of the intact soil relative to a line, the CSL, which is a reference state for frictional behaviour. Since a relationship between yielding and specific volume in isotropic compression existed so a relationship between yield points corresponding to different specific volumes might also be expected during shearing.

Similar considerations were also applied to the artificially cemented carbonate soil. For example in Figure 4.15 it can be seen that when the CSL was considered as a reference for the normalization of results from the artificial soil with strong bonds (Coop and Atkinson, 1993) neither a yield surface nor a state boundary surface were defined. The above considerations led to a re-examination of the reference line to be used for the normalization of the shear behaviour of the cemented carbonate sands.

7.1.2 New method of normalization

The alternative line of reference for the normalization of the shear behaviour of the cemented carbonate sands was identified as the isotropic boundary of the intact soil, since this was the line controlling yielding in isotropic compression. In this way it was also possible to obtain a unique point representing all the initial states of samples sheared after isotropic yielding.

The complete isotropic boundary of the calcarenite in v : lnp' space will be referred in the following as the intact isotropic boundary (intact IB). This could be represented by either a power function or by two straight lines one coincident with the PYCL and convergent to the NCL, the other coincident with the NCL. The latter option was chosen so that the analysis performed at states for which the NCL represented the isotropic boundary, remained consistent with Critical State Soil Mechanics with a CSL parallel to the NCL in v : lnp' space. The two straight lines identifying the complete isotropic

boundary of the intact soil are shown in Figure 7.1. The equivalent pressures were therefore determined as:

$$p'_{IB} = \exp \frac{(3.658 - v)}{0.235} \qquad \text{for} \quad v > 1.465 \tag{7.1}$$

and

$$p'_{IB} = \exp \frac{(2.695 - v)}{0.132} \qquad \text{for} \quad v < 1.465 \tag{7.2}$$

where v = 1.465 represents the value of the specific volume at which the two straight lines join. Equation 7.2 also provided the values of the equivalent pressure used to normalize the results from the reconstituted soil for all values of specific volumes. In general for those samples having states at the start of shearing close to but not coincident with the relevant reference line, the initial specific volume was adjusted to obtain a normalized value of p'/p'_{IB} of unity so that the inaccuracy of the water content measurements was accounted for. No correction was considered when initial states were located below the isotropic boundary if it was evident that this resulted from creep occurring between the end of the isotropic compression and the start of shearing. It should be pointed out that in this type of normalization the critical state is identified by a single point only for values of the specific volume smaller than 1.465. Critical states reached at higher specific volumes are located along the line represented by a value of the stress ratio η equal to M and by values of p'/p'_{IB} less than 0.34.

For the artificial soil the results from the strongly cemented samples obtained by Coop and Atkinson (1993) were reanalysed considering the isotropic boundary of the intact soil (intact IB) shown in Figure 7.2 as the reference for the normalization. The isotropic boundary of the intact soil was represented by two straight lines, one convergent to the NCL of the reconstituted soil and the other coincident with the NCL. Following the new type of normalization the effective stress paths and yield points of the artificial soil with weak bonds were normalized using the boundary limiting the states achieved by the intact soil in v : lnp' space when isotropically compressed (intact IB). Before the

convergence to the NCL of the reconstituted soil, the isotropic boundary of the weakly cemented soil was interpreted as being coincident with the isotropic compression line between the states at yielding and those lying on the NCL as shown in Figure 7.3. The equivalent pressures of the artificial soil with strong and weak bonds were respectively given by:

$$p'_{IB} = \exp \frac{(3.910 - v)}{0.242} \qquad \text{for} \quad v > 1.659 \tag{7.3}$$

and

$$p'_{IB} = \exp \frac{(3.035 - v)}{0.142} \qquad \text{for} \quad v > 1.881 \tag{7.4}$$

For both of the soils, when the specific volumes were lower than the limits given in the above equations, the equivalent pressure was taken on the NCL and calculated as:

$$p'_{IB} = \exp \frac{(3.417 - v)}{0.189} \tag{7.5}$$

The equivalent pressure given by Equation 7.5 also corresponded to that used to normalize the effective stress paths of the reconstituted soil for all specific volumes. Also for the artificial soil where discrepancies were believed to result from errors in the water content measurements, the specific volume of samples sheared after isotropic yielding were adjusted to give states lying on the isotropic boundary. Differences in states which resulted from creep were not adjusted.

7.1.3 Yielding of the cemented carbonate sands during shearing

In this section the artificial soil will be examined first. Figure 7.4 shows the yield points of the strongly and weakly artificially cemented samples, normalized with respect to the equivalent pressures given by Equations 7.3 and 7.4 respectively. The yield points during shearing were identified as the end of the linear stress-strain response and for the

strongly cemented soil were re-interpreted from the original data of Coop and Atkinson (1993). It should be noted that the isotropic boundary given by Equation 7.3 was chosen to average the isotropic post-yield compression curves of the strongly cemented samples which had some scatter as can be seen in Figure 7.2. This scatter was as large as the difference between yield and gross yield so that for the isotropic compression of the artificially cemented soil there would have been no scope for distinguishing these two states. Therefore the intact state boundary in Figure 7.2 was also assumed to represent the line on which the stress-strain behaviour of the strongly cemented soil ceased to be linear in isotropic compression. In this way the isotropic yield point in Figure 7.4 would correspond to a value of p'/p'_{IB} of unity. Although for the weakly cemented sand shown in Figure 7.3 less data are available, similar considerations to those mentioned above for the strongly cemented sand can be applied.

Allowing for some scatter of data, a clear trend can be observed in Figure 7.4 for the normalized yield points during shearing and a yield surface common to both the strongly and weakly cemented soils can be identified. Firstly a comparison between the yield points of the strongly cemented soil normalized with respect to the isotopic boundary with those plotted by Coop and Atkinson in q : p' space in Figure 7.5 shows that specific volume has an influence on yielding. Secondly a comparison of the yield points of the strongly cemented soil in Figure 7.4 with those normalized with respect to the CSL in Figure 4.15 shows that the influence of the specific volume can be accounted for correctly, only when referring the current state of the intact soil to its isotropic boundary rather than to the CSL. Finally although only two data points were available from the weakly cemented soil, Figure 7.4 seems to suggest that the influence on yielding of different degrees of bonding can be accounted for by referring the states of the weakly and strongly cemented soils to the appropriate isotropic boundary. It can also be seen that the stress ratio at yielding decreases as the state of the soil becomes closer to the isotropic boundary. For a given degree of bonding the decrease of stress ratio at yielding can be interpreted as a decrease of the influence of bonding on the shear behaviour as the state of the soil moves towards the isotropic boundary, that is to say

as the specific volume and/or mean effective stress increase. Although the stress ratio at yielding does not necessarily provide a measurement of the absolute strength of the bonds, in the following discussion for simplicity higher bond strengths will be associated with a higher influence of bonding on the behaviour of the cemented soils and therefore with a higher value of the stress ratio at yield during shearing.

The possibility for the artificial soil of unifying on the same curve yield points of samples having different degrees of bonding proved relevant for the analysis of the yielding of the calcarenite. In fact some of the calcarenite samples (RAN3 to RAN6) tested by Coop and Atkinson were shown to have a smaller degree of bonding than that of the rest of the intact soil. In particular samples RAN3 and RAN4 had isotropic yield points at states which were located below the isotropic boundary of the rest of the intact samples and sample RAN6 had a lower peak stress ratio that seemed not to be justifiable in terms of state (Section 5.5). Moreover it was observed that the above three samples together with sample RAN5, had very similar densities and were obtained from successive cores in the borehole (see Table 5.1). It was therefore probable that this group of samples represented a material which formed in a similar depositional environment which conferred on them a smaller degree of bonding compared to the other calcarenite samples tested. With this assumption and consistent with the analysis performed for the artificially cemented soil, the stresses at yielding of samples RAN5 and RAN6 were normalized with reference to a tentative line which was located between the NCL and the isotropic boundary defined by the rest of the calcarenite samples as shown in Figure 7.6. As from samples RAN3 and RAN4 only the isotropic yield points were known but no information was available on their post-yield compression, the reference line for the normalization of the more weakly cemented samples had to be assumed. As shown in Figure 7.6 the intact isotropic boundary for the samples with weaker bonding was assumed to converge to the NCL at a value of v of 1.465, this value being the specific volume at which the isotropic boundary of the more strongly cemented sample intersected the NCL. The intact isotropic boundary assumed for the

more weakly cemented samples of calcarenite provided an equivalent pressure given by:

$$p'_{IB} = \exp \frac{(3.069 - v)}{0.172} \qquad \text{for} \quad v > 1.465 \qquad (7.6)$$

Figure 7.7 shows the yield points from all of the calcarenite samples normalized with respect to the appropriate equivalent pressures. All the yield points identified states at the end of the linear range. Unlike the artificially cemented sand for the calcarenite the yield and gross yield points could be distinguished. In isotropic compression the yield points identified at the end of the linear response were located to the left of the isotropic boundary on which the abrupt change in compressibility (gross yield) occurred. Therefore the state at the end of the linear stress-strain behaviour in isotropic compression when normalized resulted in a value of p'/p'_{IB} less than 1 as shown in Figure 7.7. For the isotropic yield points no correlation was found between the values of p'/p'_{IB} and the specific volumes so that the band defined by the data in Figure 7.7 is likely to represent simply a scatter of results. Included in Figure 7.7 are the yield points labelled as C1 and D1 obtained from the stiffness graphs in Figures 5.19b and 5.20. The yield points C1 and D1 refer to the first loading paths of the undrained probes performed on one of the intact samples from values of p'_i of 1550 (series C probes) and 2000 kPa (series D probes) respectively.

A yield surface was identified through interpolation of the data points in Figure 7.7, where a dashed line indicates the portion of curve were no experimental results were available. The yield point at the lowest value of p'/p'_{IB} is from an undrained test and it can be seen that this is in agreement with the rest of the points which instead refer to constant p' drained shearing. Moreover there is a close resemblance between the yield curves defined for the calcarenite and for the artificially cemented carbonate soil (Figure 7.4). As was seen for the artificially cemented soil, the yield points for the more weakly cemented samples of calcarenite are consistent with the trend defined by the yield points of the more strongly cemented samples. Finally normalization proved to be crucial for the calcarenite as it was possible to account for the large variability of the

specific volumes of the samples tested and its influence on yielding. As will be shown in Section 7.3 the identification of yielding proved to be essential for the understanding and description of the mechanisms governing the shear behaviour of the calcarenite as well as of the artificially cemented carbonate sand.

7.1.4 The shear behaviour of the cemented carbonate sands after yielding

Figure 7.8a shows the normalized stress paths of the intact samples of calcarenite with stronger bonding and of the reconstituted samples, all sheared along a constant p' stress path starting from an initial state after isotropic yielding. It can be seen that for the intact samples sheared from states located on the portion of the isotropic boundary convergent with the NCL the stress paths lie above the intrinsic state boundary surface (ISBS) defined by the reconstituted soil. At stress ratios η equal to M the states of the intact soil converge towards the critical state reached by the reconstituted soil ($p'_{cs}/p'_{IB} = 0.34$). As shown by sample N5, as the state of the intact soil prior to shearing approaches the NCL the stress path becomes coincident with the ISBS. From the results available however it is not possible to assess whether the state paths of the intact samples progressively reduce in size to reach the ISBS, as the state of the soil prior to shearing moves towards the NCL. An alternative possibility, although unlikely, could be the existence of two different boundaries, an upper one for samples which yielded on the portion of the isotropic boundary convergent towards the NCL and a lower one coincident with the ISBS for samples which yielded close to or on the NCL. In any case the space of permissible states of the intact soil can be better delineated if normalization is referred to the isotropic boundary rather than to the CSL.

Figure 7.8b shows the normalized stress paths for the samples with weaker bonding (RAN3 and RAN4), for which the dashed line replaces data affected by poor control of the stress path. Superimposed are the ISBS and the state paths from the samples with stronger bonding shown in Figure 7.8a. The samples with weaker bonding were both

sheared soon after isotropic yielding and it can be seen that during shearing they reached states which are above the ISBS but within the space limited by the stress paths of the more strongly cemented samples.

In Figure 7.9 the stress paths of the calcarenite samples sheared before isotropic yielding and the yield surface are superimposed on the ISBS. Also shown is the outer stress path defined in Figure 7.8 by the intact samples sheared after isotropic yielding. In Figure 7.9 the outer stress path has been indicated as the outer intact state boundary surface (outer intact SBS).

In Figure 7.10a are shown the normalised stress paths for the strongly and weakly cemented samples of the artificial soil which were sheared after isotropic yielding. Except for the outer stress path which corresponds to an undrained test, all the other stress paths are from tests performed at a constant p'. As seen in Section 4.7 the normalized stress path for the weakly cemented sample sheared at the highest confining pressures coincided with the ISBS. The latter is shown in Figure 7.10a where also indicated is the outer state boundary surface for the intact soil.

In Figure 7.10b the normalized stress paths of the artificially cemented samples sheared before isotropic yielding and the yield surface are superimposed on the ISBS. Also shown is the outer boundary surface defined in Figure 7.10b by the intact samples sheared after isotropic yielding. The discussion and description of the results shown in Figures 7.9 and 7.10b will follow in Section 7.3 where comparisons will be made with the shear behaviour of the silica sandstone.

7.2 THE SHEAR BEHAVIOUR OF THE CEMENTED SILICA SAND

7.2.1 Introduction

One of the features that distinguished the silica sandstone was its low specific volume which was approximately equal to 1.44. This specific volume could not be obtained in the laboratory when compacting reconstituted samples to their maximum density. Only one reconstituted sample that was isotropically compressed to 70 MPa had an unloading-reloading isotropic curve which was located in the vicinity of the isotropic compression curve of the intact soil (Figure 6.6). Because of the strong nature of the particles high confining pressures had to be reached to define the NCL of the reconstituted soil and at the values of density of the intact samples the apparatus was not capable of bringing their states onto the NCL. However the range of pressures covered in the experimental work was sufficient to take the intact soil beyond its isotropic yield point and to observe part of its post-yield behaviour. The trend of the post-yield compression curve seemed to indicate a convergence towards the NCL of the reconstituted soil (Figure 6.6b). The occurrence of the isotropic yield point to the left of the NCL resembles the behaviour of the artificially weakly cemented soil in isotropic compression. Despite this similarity shown by the silica sandstone to the artificially cemented soil arising from the fact that they were both weakly bonded soils, the two materials were very different. Whereas for the silica sandstone the weak bonding was associated with a high density, for the artificial soil the weak bonding was associated with a low density. For this reason in the isotropic compression of the silica sandstone, once yielding occurred the behaviour and the states achieved by the soil were largely controlled by its density. On the basis of these considerations the NCL was then interpreted as the isotropic boundary of the silica sandstone, in contrast with the weakly cemented artificial soil for which the latter was represented by the post-yield compression line. More discussion on this point will follow in the next section.

7.2.2 Normalized stress paths

The shear behaviour of the silica sandstone was shown to be characterised by a marked strain-softening over an extended range of pressures up to a p' of about 15 MPa, whereas strain-hardening was observed only for the sample sheared at a p' of 60 MPa. Because of the localization of strains following the peak state of the soil during shearing, the loci of critical states in v : lnp' space could not be identified. Instead the critical states of the reconstituted samples could be represented by a line which was parallel to the NCL.

In the following the shear behaviour of the silica sandstone is analysed and compared with the shear behaviour of the reconstituted soil. As for the reconstituted soil the data from the intact soil were normalized with respect to an equivalent pressure taken on the NCL, since this was assumed to represent the isotropic boundary of the intact soil. Consistent with the carbonate soils, the equivalent pressure will be indicated as p'_{IB}. In addition the choice of considering the NCL as the intact isotropic boundary as well as having a conceptual justification also represented a necessity for the normalization. Unlike the case of the artificial soil with weak bonds, the post-yield compression curve of the silica sandstone could not provide a reference for the normalization, since this was not defined in the range of specific volumes reached by the samples during shearing which except for one all dilated. The equivalent pressure for both intact and reconstituted soils was calculated as:

$$p'_{IB} = \exp \frac{(3.233 - v)}{0.161} \qquad (7.7)$$

The normalized stress paths of the reconstituted and intact soils are compared in Figure 7.11. The stress paths of the reconstituted soil define a boundary for all the possible states that this soil could achieve. The portion of this boundary defined on the dry side of the critical state of the reconstituted soil can be interpreted as the Hvorslev surface. On the wet side of the critical state the portion of the boundary can be interpreted as the Roscoe surface. From the stress paths of the intact soil it is also

possible to define a portion of the boundary surface which limits the possible states achieved by the soil during shearing. The boundary of the intact soil on the dry side of the critical state can be interpreted as the Hvorslev surface for this soil. The Hvorslev surface of the intact soil can be seen to lie above that of the reconstituted soil.
The test on the wet side of the critical state suggests that also in this case the state boundary surface of the intact soil is above the Roscoe surface of the reconstituted soil.

The states of the intact soil at yield are superimposed on an enlargement of the above graph in Figure 7.12. The yield points were identified from the stiffness graphs presented in Section 6.7 as the point at which the stress-strain behaviour ceased to be linear and are therefore the "true" yield points. A yield surface was identified through the yield points. It can be seen that the yield surface encloses only a small portion of the states contained within the boundary surface of the intact soil with states at yielding which do not lie in the proximity of the peak states as was the case for the cemented carbonate soils.

7.2.3 Stress-dilatancy

In order to study the post-yield behaviour of the intact soil during shearing and understand the nature of the peak strength, the stress-dilatancy relationship was analysed. The rate of dilation (dilatancy) d can be defined as:

$$d = -\frac{\delta \varepsilon_v^p}{\delta \varepsilon_s^p} \tag{7.8}$$

The stress-dilatancy graphs have been plotted only from values of the stress ratio at which the elastic component of the strains became negligible and the plastic and total strain increments could be considered substantially coincident. Also for lower stress ratios the dilatancy d could not be correctly determined because of the presence of bedding errors which affected the volumetric strain measurements.

Figure 7.13 shows the stress-dilatancy relationship of one the intact samples (D5) which was sheared at a constant value of p' equal to 5600 kPa, prior to isotropic yielding. An initial volumetric compression was followed by dilation. At the peak stress ratio the sample reached the maximum rate of dilation. The same graph shows the stress-dilatancy relationship for a reconstituted sample also sheared at constant p'. To allow comparison between the stress-dilatancy of the reconstituted and intact soils, the two samples considered were chosen among those having initial shearing states a similar distance from the CSL. Also for the reconstituted sample the peak stress ratio was achieved at the maximum dilatancy. The lower value of the peak stress ratio that the reconstituted sample shows when compared to the intact sample also corresponded to a lower rate of dilation. Figure 7.14 shows the stress-dilatancy from one of the samples (D3) sheared at a lower p' of 3460 kPa. An initial compression was again followed by dilation. However after reaching the peak stress ratio the rate of dilation increased with no further increase in the stress ratio until an abrupt change in the volumetric strain occurred which probably corresponded to localization of strains taking place in the sample. In this case it was not possible to associate uniquely the peak stress ratio and the maximum dilatancy.

Figure 7.15 shows the values of the peak stress ratios (η_p) plotted against the corresponding maximum dilatancy (d_{max}) for both reconstituted and intact samples. Data for which a unique rate of dilation at the peak stress ratio could not be defined as in Figure 7.14 were omitted. The data from the reconstituted and intact samples appear to be aligned and define the same relationship between peak stress ratio and maximum dilatancy. The straight line at the intersection of d = 0 axis has a value of η equal to 1.29 which corresponds to the value of M found from the critical states of both reconstituted and intact samples (Section 6.6). The stress-dilatancy relationship at the peak state can be expressed as:

$$\eta_p = M + \alpha\ d_{max} \tag{7.9}$$

where M = 1.29 and α = 0.53.

This relationship has the same form as the flow rule used by the original Cam Clay (Roscoe and Schofield, 1963) in which the coefficient α is equal to 1 and is in agreement with the expression reported by Nova and Wood (1979) for sands sheared in triaxial compression. The relationship from Equation 7.9 is compared with that from the original Cam Clay in Figure 7.15. Also represented in the same figure is the stress-dilatancy relationship proposed by Rowe (1962) which when expressed in terms of the stress invariants q and p' rather than σ'_a and σ'_r can be written as:

$$d = \frac{9\ (\eta\ - M)}{9\ + 3M\ - 2M\eta} \tag{7.10}$$

It can be seen that the predictions from both models overestimate the peak stress ratios, particularly in the range of values of d_{max} defined by the intact soil.

In any case in the range of d_{max} for which Equation 7.9 was defined the stress-dilatancy analyses shows that the peak strength of the silica sandstone can be regarded as purely frictional since it is related to the maximum dilation experienced by the soil.

The higher peak strength of the intact soil when compared to the reconstituted soil seems to be explained by its higher dilatancy. The higher rates of dilation of the intact soil were compared to those of the reconstituted soil to assess whether they resulted from differences in state relative to the CSL. Therefore in Figure 7.16 values of p'/p'_{cs} at the peak stress ratio, indicated as $(p'/p'_{cs})_p$, were plotted against d_{max} for both soils. For each soil a relationship exists between d_{max} and $(p'/p'_{cs})_p$ and their comparison shows that for the same normalized state the dilatancy at peak of the intact soil is higher than that of the reconstituted soil. The graph also shows that for the intact soil $(p'/p'_{cs})_p$ at a value of d_{max} of zero is greater than 1, indicating for the intact soil a CSL in v : lnp' space located to the right of the CSL found experimentally for the reconstituted soil. As discussed in Section 6.6 ultimate states in terms of specific volumes could not be defined for the intact soil because of the localization of strains taking place after peak. For a carbonate sand Coop (1990) showed that the NCL depends on the initial grading of the soil prior to testing. The NCL of carbonate sand samples was found to be steeper

and to the right of the NCL of samples whose grading was changed by crushing the original carbonate sand. The influence of the initial grading on the NCL for a carbonate sand was later confirmed by Coop and Atkinson (1993) when the grading of the sand was changed by the addition of fines rather than by crushing the particles. Particle crushing may have occurred in the silica sandstone before being cemented as a result of the overburden pressure experienced during its geological history, which was estimated to have reached a maximum value of 8.8 MPa (Section 6.1). Therefore the reconstituted soil obtained from the silica sandstone was likely to have a different grading from the original grading that the intact soil had during deposition. It is possible that differences in the initial grading between the intact and reconstituted soil may have had an effect on the location of the CSL in v : lnp' space similar to the effect that Coop (1990) and Coop and Atkinson (1993) observed on the NCL. This would cause the states of the intact soil to be located at a greater distance from the offset critical state line and would therefore justify, at least in part, the higher rates of dilation observed.

In Figure 7.17 the states of the intact soil are normalized accounting for the offset found from Figure 7.16 and assuming that the critical state line of the intact soil is parallel to the CSL of the reconstituted soil. The expressions for the equivalent pressures used here are given later in Section 7.3. The comparison with the data of the reconstituted samples using a normalization referring each soil to its own CSL, shows that even accounting for a possible offset of the two CSLs the intact soil still shows higher rates of dilation and therefore higher peak strengths.

From the above analyses it follows that the location of the Hvorslev surface of the intact soil above that of the reconstituted soil cannot be explained simply in terms of states and other factors have to be investigated. It is interesting to note that for the reconstituted soil the data of Figure 7.17 indicate a dilatancy of about 0.3 at the lowest value of $(p'/p'_{cs})_p$ and that a maximum value of dilatancy of 0.75 was reported by Rowe (1969) for sands with the densest possible packing. In contrast the rates of dilation observed for the intact soil all exceeded a value of 0.9.

Unusually high rates of dilation were observed by Dusseault and Morgenstern (1979) in shear box tests performed on three natural quartz sands which each had an age older

than Quaternary (see Figure 2.20, Section 2.4). The authors report that these sands were not cemented as they disintegrated in water. Their maximum rates of dilation at the peak state were found to be much higher than those of Ottawa sand, which they considered as an example of typical sand behaviour. The higher rates of dilatation of the geologically old sands were attributed to an interpenetrative fabric characterized by a high incidence of well developed grain contacts which formed during the diagenesis of the sand deposit. Dusseault and Morgenstern defined this type of materials as "locked sands" to distinguish them from loose or dense sands. Although in their study the authors overlooked the influence of state on the behaviour of sands, it should be noted that the rates of dilation of the locked sands were in any case higher than the values generally observed for sands having states far to the left of the critical state. The dilatancy at the peak states of the locked sands were similar to those found for the silica sandstone. Moreover the silica sandstone had all the characteristics which the authors used to identify locked sands: quartz composition, a high degree of interparticle contacts and a rough grain surface texture. These features were observed from examination of the thin sections of the silica sandstone in the optical and scanning electron microscopes shown in Figures 6.3 to 6.5 and were described in Section 6.2. Concavo-convex and straight contacts between the quartz grains were present in the silica sandstone which resulted in a well defined fabric characterised by a large contact area. In addition Dusseault and Morgenstern pointed out that locked sands can present some true cohesion but this is generally small as has been found for the silica sandstone where iron oxide was present in small amounts around the particles. Dapples (1972) also reported that iron oxide has a weak adherence to the quartz grains so that when present in silica sands the bonds are weak (Section 2.4).

Other common features between the silica sandstone and the locked sands were their age being older than Quaternary, and their densities being higher than the maximum density attainable when the same soil was reconstituted and compacted. For a carbonate sand Coop (1990) found that the maximum densities obtained upon reconstituting for samples which had previously been isotropically compressed and sheared were lower than those that had been reached during the triaxial tests. As was also observed by Dusseault and Morgenstern for undisturbed samples, Coop attributed the high densities achieved during the triaxial tests to the presence of interparticle contacts which, once disrupted, could not be reproduced by simple compaction of the same soil. Although both studies viewed

the large contact area between the grains as responsible for the high densities of the soils, different mechanisms caused the development of the particle contacts. For the carbonate sand this was due to the crushing of the soil particles under the stresses applied in the triaxial tests. For the natural old sands instead the high degree of particle contacts was seen as the result of pressure solution and recrystallization of quartz at the grain surfaces. Maxwell (1964) and Dusseault and Morgenstern (1979) both suggested that quartz solution processes are caused, among other factors, by contact stresses which can be significantly higher than the stresses due to the overburden and that even a small amount of solution of quartz can significantly increase the density of the sediments.

The studies on the old silica sands from Dusseault and Morgenstern seem therefore to provide a possible explanation for the high densities of the silica sandstone since these values could not be justified in terms of maximum past total overburden pressure experienced by the soil (8.8 MPa) during its geological history.

On the basis of the above discussion it is suggested that the high rates of dilation and thus the high peak stress ratios of the silica sandstone, which cannot be justified only in terms of state, are likely to be the result of the high degree of particle contacts that distinguished the fabric of the intact soil from that of the reconstituted soil. The larger contact areas in the intact soil reduces the contact stresses so that the soil element can support higher stress ratios at peak.

However fabric is not the only factor likely to influence the shear behaviour of the silica sandstone. Additional considerations for the dilatancy of the intact soil are apparent comparing the stress-dilatancy relationships from three intact samples sheared at different mean effective stresses with the relationship found for the reconstituted soil as shown in Figure 7.18. All the reconstituted soils had stress-dilatancy relationships during shearing which followed the flow rule given by Equation 7.9. In Figure 7.18 it can be seen that although at peak the stress ratios and dilatancy values for the intact soil satisfy Equation 7.9, prior to peak the stress-dilatancy relationships lie above that of the reconstituted soil. Moreover as the mean effective stress increases the stress-dilatancy relationship of the intact soil tends to approach that of the reconstituted soil. In particular the stress-dilatancy of the intact soil which is closest to that of the reconstituted soil corresponds to the sample which was sheared at stresses just past the

isotropic yield point. From the general trend shown by the results in Figure 7.18 it can be seen that at a given stress ratio prior to peak, the dilatancy of the intact soil is smaller than that which would be seen for the reconstituted soil. This means that the dilation of the intact soil was delayed when compared to the reconstituted soil and that the delay increased as the mean effective stresses decreased.

The delayed dilation observed for the intact soil can be qualitatively interpreted in terms of energy balance as follows. After yielding the total work done by the stresses at the boundary of the soil element (ΔW) can be thought as partly dissipated in friction (ΔW_{fric}) and partly spent in disrupting the bonding between the soil particles (ΔW_{bon}) so that:

$$\Delta W = \Delta W_{fric} + \Delta W_{bon} \tag{7.11}$$

If referred to triaxial test conditions and to a unit volume Equation 7.11 can be also written as:

$$q\ \delta\varepsilon_s^p + p'\ \delta\varepsilon_v^p = M\ p'\ \delta\varepsilon_s^p + \Delta w_{bon} \tag{7.12}$$

where Δw_{bon} indicates the work spent in disrupting the bonding per unit volume. By rearranging, Equation 7.12 gives:

$$\frac{q}{p'} = M - \frac{\delta\varepsilon_v^p}{\delta\varepsilon_s^p} + \frac{\Delta w_{bon}}{p'\ \delta\varepsilon_s^p} \tag{7.13}$$

The development of a mathematical expression for Δw_{bon} in Equation 7.13 was beyond the scope of the present work so the following discussion will be limited only to a qualitative interpretation. To maintain a balance in Equation 7.13 for a given stress ratio, since M is a constant, an increase in the work spent in disrupting the bonds has to correspond to a decrease in the rate of dilation. A comparison of the stress-dilatancy relationships shows that at a given stress ratio the higher dilatancy would correspond to the reconstituted soil whereas the lowest dilatancy would correspond to the intact sample which was sheared at the lowest mean effective stresses. More work had to be spent to degrade the bonds at the lowest mean effective stresses where the stress ratio at yield was higher (as p' decreases the stress ratio at yield increases) so that at a given stress ratio a larger amount of bond degradation had still to occur.

This qualitative interpretation seems therefore to suggest that the dilatancy of the intact soil is likely to be controlled by bond degradation and that this subsequently effects the strength of the intact soil. Unlike the reconstituted soil the intact soil in the early stages of shearing and up to the yield point has linear behaviour (Section 6.7.2) and dilation is prevented by the presence of bonding. After yielding the gradual degradation of bonding is accompanied by an increasing rate of dilation. However for a given stress ratio the higher the influence of bonding (higher stress ratio at yield) the lower the rate of dilation. The greater the delay of dilation the greater the rate of dilation that the intact soil subsequently experiences during shearing to recuperate this delay which then results in higher frictional peak strengths associated with the rate of dilation when this reaches a maximum. However the dilatancy of the intact soil is also likely to result from the interpenetrative fabric of the intact soil which, together with the process of bond degradation, may inhibit (but not prevent) and delay the dilation of the soil which is later recuperated through greater maximum rates of dilation and higher peak strengths. Although for the intact soil its is not possible to separate the two effects of bond degradation and fabric, the possible influence of fabric on the dilation and peak strength of the silica sandstone is supported by the study of Dusseault and Morgenstern (1979) who observed similar high rates of dilation and high peak strengths for silica sands with no bonding.

7.3 COMPARISONS BETWEEN THE SHEAR BEHAVIOUR OF THE CEMENTED CARBONATE AND SILICA SANDS

The review of some of the fundamental works on sands in Section 2.3 showed that their behaviour can be described within the framework of Critical State Soil Mechanics and the stress-dilatancy theories. The shear behaviour of sands is controlled by the change from the initial state that the soil has to experience in order to reach a critical state and dilation and compression are associated with strain-softening and strain-hardening respectively. When these concepts are combined with the stress-dilatancy theories the mechanism governing the strength of soils can be understood. The maximum angle of friction is mobilized when the soil reaches the maximum rate of dilation. These concepts proved to be the basis for a unified picture for the behaviour of sands and clays.

For cemented sands the influence of bonding and fabric as well that of state (q, p', v) on the shear behaviour need to be considered. Differences in states were accounted for by using the normalization presented in the previous sections of this chapter which referred the states of the soil to its own isotropic boundary determined in v : lnp' space. In the following discussion it is postulated that yielding coincides with the onset of bond degradation so that pre-yield behaviour will be considered entirely cohesive. The stress ratios at yielding can be considered as a measure of the influence of bonding. Higher stress ratios at yielding therefore will be regarded as a decreased susceptibility of the bonds to break and in this respect will be viewed as an increase in the strength of the bonds.

Figure 7.9 shows the yield curve of the calcarenite, together with the outer state boundary surface identified from those samples which had yielded in isotropic compression and the ISBS determined from the reconstituted soil. A consistent trend for the yield points was obtained from undrained tests performed at constant cell pressure and form drained tests performed at constant mean effective stress (Figure 7.7, Section 7.1.3). This would suggest that yielding is a function of the state of the soil and not of the stress path followed.

From Figure 7.9 it can be seen that the yield curve of the calcarenite occupies a large portion of the domain of possible states for the intact soil and is not all contained within the ISBS. For states located within the yield surface the shear behaviour is controlled by bonding and can therefore be considered as cohesive. For states outside the yield surface the shear behaviour is influenced by a progressive degradation of bonding, also resulting in the development of a frictional response. In this case particle breakage occurs because of the fragile nature of the calcarenite grains. The transition between these two types of shear behaviour is well defined by the value of p'/p'_{IB} of 0.42 on the yield surface where the latter meets the line of gradient M.

When the normalized states are such that the stress ratio at yield η_y is greater than M, the peak strength is cohesive and brittle failure occurs. When the normalized states are such that η_y is less than M, the strength of the soil is frictional and failure is reached through strain-hardening to an ultimate state. The ultimate strength of the intact soil then also corresponds to the strength of reconstituted samples sheared on the wet side of

critical. However whereas the behaviour of the reconstituted soil would be non-linear from the initial stages of shearing, the initial shear behaviour of the intact soil is influenced by bonding and results in linear stress-strain behaviour and in higher values of stiffness as will be shown in the next section. As the soil reaches initial states which are closer to the isotropic boundary the maximum stiffness remains substantially unchanged as will be discussed in Section 7.4, but the range of stress-strain linearity decreases (η_y decreases). This decrease of the linear range continues until, for states which cause yielding in isotropic compression, the behaviour is non-linear from the initial stages of shearing and the soil strain-hardens to the critical state. At this point the behaviour of the intact soil resembles that of an uncemented soil.

The decrease of the stress ratio at yielding with increasing values of p'/p'_{IB} can be interpreted as a decrease of the strength of the bonds as the current state of the soil moves towards the isotropic boundary. For a given specific volume an increase in the mean effective stresses would therefore correspond to a smaller influence of bonding, whereas for a given value of p' a lower specific volume would correspond to a higher influence of bonding. In the interpretation of tests from Maccarini (1987), Aversa (1991) attributed the decreasing offset between the isotropic yield point of the intact soil and the NCL with decreasing specific volume as a decrease in the effect of bonding (see Figure 2.22). On the basis of the above discussion it should be noted that Aversa's interpretation would be correct only if the relationship between bond strength and specific volume is referred to states having similar location with respect to the NCL and CSL. Vaughan (1988) when reviewing the same results from Maccarini (1987) observed that a decrease in the specific volume corresponded instead to an increase in the strength of the bonds as measured by the unconfined drained shear strength (Section 2.5). This observation is consistent with the framework found for the calcarenite, since the relationship between bond strength and specific volume from Vaughan would correspond to samples at the same value of the confining stresses which in that case was equal to zero.

The general framework developed for the calcarenite agrees well also with the behaviour of the artificially cemented carbonate soil. Figure 7.10b shows the yield curve identified for the artificially cemented sand, together with the outer state boundary surface identified from those samples which had yielded in isotropic compression and the ISBS

determined from the reconstituted soil. There is a close similarity between the unified graphs of the artificial and natural carbonate soils. It should be noted that in isotropic compression yield and gross yield for the artificial soil were not distinguished since their difference lay within the scatter of the post-yield compression curves on the basis of which the isotropic boundary was chosen. Therefore in the normalization the yield surface of the cemented carbonate sands intercepts the isotropic axis at a p'/p'_{IB} of 1. In contrast for the isotropic compression of the calcarenite a minor non-linearity followed yielding and preceded the isotropic boundary where gross yield occurred. The isotropic yield points were scattered and one single average point was identified for the isotropic yield on the normalized graph for the calcarenite (Section 7.1.3).

Figures 7.9 and 7.10b show that both the calcarenite and the artificially cemented sand sheared before isotropic yielding reached states which are located between the ISBSs and the outer stress paths followed by the intact samples sheared after isotropic yielding. In Figures 7.9 and 7.10b the outer stress paths are denoted as the outer intact state boundary surfaces (outer SBS) to indicate that these are upper limits for the states reached by the intact soil during shearing. At present the relationship between the outer intact SBS and the post-yield stress paths of the intact samples which did not yield in isotropic compression is not clear. A proper analysis and interpretation of this aspect would require an insight into the mechanisms governing the particle breakage occurring after yielding which controls the frictional response of the carbonate sands, but this was beyond the scope of the present work.

The shear behaviour of the two carbonate cemented soils can be compared and contrasted with that of the silica sandstone. In Figure 7.12 the effective stress paths and the yield points of the silica sandstone where normalized with respect to the NCL of the reconstituted soil and compared to the ISBS. Similar graphs are shown in Figures 7.19 and 7.20. In Figure 7.19 the intact and reconstituted states were in both cases referred to the CSL of the reconstituted soil using the following equivalent pressure p'_{cs}:

$$p'_{cs} = \exp \frac{(2.986 - v)}{0.161} \qquad (7.14)$$

In Figure 7.20 instead the states of the intact soil were referred to a different critical

state line from that of the reconstituted soil as indicated by the results in Figure 7.16. The critical state line of the intact soil was assumed to be parallel to that of the reconstituted soil so that the value of Γ of 2.986 in Equation 7.14 was replaced with a value of 3.061. In contrast with the carbonate cemented soils, in both Figure 7.19 and Figure 7.20 it can be seen that the yield surface of the silica sandstone occupies only a small portion of the state boundary of the intact soil and is all contained within the ISBS.

The enlargements of Figures 7.19 and 7.20 at low stress levels show that for all tests the stress ratios at yielding were equal to or lower than M. When extrapolating the yield surface and Hvorslev surface of the intact soil to lower normalized states an intercept with the p'/p'_{cs} equal to zero axis can be identified, indicating that a truly cohesive peak strength can be achieved only at very small mean effective stresses. Otherwise the peak strengths of the silica sandstone were frictional as was discussed in Section 7.2.3 and not cohesive as observed for the cemented carbonate soils. In the carbonate soils the strength of the cement was such to bring the states of the soil above the Hvorslev surface of the reconstituted soil. For states at which the bond strength had reduced so that the stress ratio at yield was lower than M, the transferral of load onto the particles resulted in particle breakage, which at this point was the principal mechanism governing the shear behaviour of the soil rather than dilation. In contrast for the silica sandstone the weak bonding resulted in stress ratios at yield equal to or lower than M and because of the strong particles when the load after yielding was transferred to the grains, the main mechanism governing the shear behaviour was dilation which then resulted in the attainment of the peak strength. However also for the silica sandstone the failure envelope at peak was above that of the reconstituted soil and this was attributed to possible effects of bond degradation and interpenetrative fabric on the rate of dilation. These two components were both likely to have an influence on the shear behaviour of the silica sandstone after yielding, although it is not clear what their relative importance was.

Whereas in the carbonate soil bonding was the principal factor influencing the shear behaviour, for the silica sandstone this seems to be influenced by fabric and bonding. In this respect the behaviour of the calcarenite and silica sandstone reflected their different geological origins and histories. In the calcarenite the precipitation of cement

at the early stages of deposition prevented the development of a pronounced fabric. In this case when the bonds were disrupted and the soil was reconstituted it was possible to obtain similar densities as those of the intact soil. Moreover for the calcarenite the early deposition of cement and the relatively low stresses experienced in the ground were likely to prevent the occurrence of particle breakage so that reconstituting did not result in a different NCL and CSL from those of the intact soil after disruption of bonding. Conversely in the silica sandstone, the cement formed in the latter stages in the diagenesis of the sediments once the uncemented soil had possibly already undergone some particle breakage and a substantial reduction of its porosity under the weight of the overburden. According to this interpretation for the silica sandstone substantial diagenetic processes occurred before the cement had precipitated, which allowed the soil to develop a well defined fabric characterised by a large grain contact area. When the cement was disrupted and the soil reconstituted only lower densities could be obtained as it was not possible to reproduce through compaction the same particle arrangement and contacts which characterise the intact soil. Unlike the calcarenite it is also probable that the NCL and CSL of the reconstituted soil did not coincide with that of the intact soil since the latter was likely to have a different initial grading at the time of deposition which was later changed by the particle breakage caused by relatively high stresses experienced in the ground.

For the calcarenite the large portion of domain of possible states occupied by the yield surface and the transition to frictional behaviour being controlled by particle crushing can be seen as the result of the soil having strong bonds and comparatively weak grains. For the silica sandstone instead the weak cement and the comparatively strong grains resulted in a yield surface occupying only a small portion of the domain of possible states and in a transition to frictional behaviour which, for states on the dry side of the critical state, was controlled by dilation. In this case particle crushing would occur but probably only when the soil is sheared at high mean effective stresses and on the wet side of the critical state. The small influence of bonding observed for the silica sandstone resulted in features of shear behaviour following the general concepts of Critical State Soil Mechanics. These concepts fail to predict the behaviour of the calcarenite since bonding rather than friction was shown to be the main mechanism governing its shear behaviour.

7.4 STIFFNESS OF THE CALCARENITE AND SILICA SANDSTONE

As has emerged from the above discussion, determinations of yield curves proved to be essential in the understanding of the mechanisms governing the shear behaviour of these cemented soils. Together with yielding, the variation of stiffness during shearing was investigated for the calcarenite and silica sandstone using local axial strain measurements. Because of their high rigidity accurate strain measurements were more critical than deviatoric stress measurements for the determination of stiffness and yielding. For these to be reliable and correct, uniform deformations within the sample had to be guaranteed. The development of testing techniques were therefore aimed at fulfilling these requirements as described in Section 3.3.

For the silica sandstone stiffness determinations from very small to relatively large strains were performed in drained (constant p') and undrained tests, the latter including a series of loading-unloading shearing probes from the same initial values of p' and at similar values of specific volume (Section 6.7). For the calcarenite the majority of the available samples were tested before and during the development of the stiffness measurement techniques, leaving only few samples for an accurate investigation of stiffness later in the project. A series of undrained loading-unloading probes at different mean effective stresses was therefore designed to maximise the amount of information obtainable from a single sample (Section 5.6).

For the silica sandstone because of the uniformity of the samples and the similarity of their specific volumes, the values of G_{max} from the drained tests could be compared to investigate their variation with mean effective stresses as discussed in Section 6.7.2. It was found that before isotropic yielding the mean effective stress had substantially no influence on G_{max} as shown in Figures 6.14 and 6.15. This result was also obtained from bender element measurements of G_{max} performed in the present work in a Bishop and Wesley cell at lower isotropic stresses from 50 to 600 kPa. The test was intended to investigate the suitability for very stiff soils of improved bender element techniques (Jovicic, 1995). Figure 7.21 shows a typical trace from the oscilloscope obtained in the range of pressures investigated and data for the calculation of G_{max} are given. It should be noted that the value of G_{max} of 2500 MPa obtained from the bender element test is dependent on the interpretation of the time of the first arrival of the shear wave and the

specific volume of the sample. In any case in terms of absolute value, G_{max} from the bender elements was of the same order of magnitude as the value of 3050 MPa obtained from the local axial strain transducers. Both measuring techniques showed no substantial variation of the shear modulus with mean effective stress.

For the drained shearing performed in the 70 MPa apparatus after isotropic yielding it was not possible to determine values of G_{max} at very small strains since in this apparatus the developments carried out in the 10 MPa cell were not performed. However Figures 6.16 and 6.17 show that from relatively small deviator stresses to failure the values of shear moduli are higher for the test performed at the highest mean effective stresses. It should be noted that in Figure 6.17 the higher values of the shear modulus corresponded not only to higher values of p' but also to lower specific volumes which arose from the volumetric compression experienced by the soil prior to and during shearing. From an extrapolation of the stiffness graphs to very small deviator stresses it appears that after isotropic yielding an increase in the mean effective stress would cause an increase in the maximum shear modulus of the silica sandstone.

For the calcarenite the dependence of G_{max} on p' was investigated through undrained probes performed from different initial values of p'. In Figures 7.22a and 7.22b the values of G_{max} corresponding to the data points labelled as A1, B1 and C1 were determined from the first loading probes of the A, B and C series performed on the intact sample (Figures 5.18a, 5.18b and 5.19b). In all cases the soil had not experienced yielding either in isotropic compression or shearing and the specific volume was essentially constant as shown in Figure 7.22b. As was seen for the silica sandstone the value of G_{max} prior to yielding did not vary with changes in mean effective stresses.

The first loading path of series C probes caused yielding which was also associated with a progressive degradation of bonding. Figure 5.19b showed that from this point onwards when the soil was brought back to the previous isotropic state and then reloaded, the value of G_{max} did not vary but yielding occurred at progressively lower deviator stresses. As discussed in Section 6.7.3 a similar result was obtained from the undrained loading-unloading probes performed on the silica sandstone from an initial value of p' lower than the isotropic yielding and up to deviator stresses which caused yielding during shearing (see Figure 6.22). For both the calcarenite and the silica sandstone the reduction in the

deviator stress at yield as the soil is cycled can be explained in terms of bond degradation which was likely to be a process which developed progressively within the sample. The occurrence of bond degradation after first yield can be thought as a process that took place initially only in some parts of the sample reducing the remaining stiffer and elastic portion where the cement was still intact and where the load would be expected to concentrate. Therefore on subsequent loading higher local stresses were likely to act and cause yielding in this stiffer part of the sample when a smaller deviator stress than that corresponding to the previous yield point was applied at the boundary of the soil element.

If cycles are continued the same mechanism repeats and yielding occurs progressively at smaller and smaller deviator stresses until eventually also the value of G_{max} decreases. The reduction of G_{max} eventually caused by the cycles was observed in the undrained probes performed on both the calcarenite and the silica sandstone as shown in Figures 5.20 and 6.23. From the results and from the above interpretation it appears therefore that the mechanism of bond degradation is associated with a reduction of the stresses at yield and eventually with a decrease in the maximum shear modulus.

The factors controlling the maximum shear modulus before and after the occurrence of yield for bonded soils can be analysed comparing intact and reconstituted samples. In the following discussion the comparison is made for the calcarenite. In Figures 7.22a and 7.22b the data point D1 refers to the stiffness value of the calcarenite after yielding but before the deterioration in stiffness, instead D3 shows the reduced value of G_{max} observed in the third loading path of the same set of probes (Figure 5.20). From this point onwards changes in states would be expected to cause changes in the shear modulus as for uncemented soils, although not necessarily according to the same relationship. As shown in Figures 7.22a and 7.22b the value of G_{max} corresponding to the first loading probe of the E series (point E1) performed after the deterioration of stiffness (see Figure 5.21), is higher than that corresponding to point D3. This increase in the shear modulus corresponds to a variation in state and in particular to an increase of mean effective stress and to a decrease in specific volume.

In Figures 7.22a and 7.22b the values of G_{max} from the first loading of a series of undrained probes performed on a reconstituted sample at various values of p'

(Figures 5.23a to 5.23d) are plotted against p' and v respectively. It can be seen that G_{max} increases with increasing p' and decreasing v. The variation of G_{max} of the intact soil with state, shown by the data points D3 and E1, was compared with that of the reconstituted soil by plotting G_{max} against the normalized variable p'/p'_{IB} in Figure 7.23 which identifies the state of the intact and reconstituted soils with respect to their own isotropic boundaries; the intact IB and NCL respectively. The results from the reconstituted soil show that in the first isotropic compression up to the NCL the values of G_{max} increased linearly with the normalized state variable according to the following relationship:

$$\frac{G_{max}}{p_r} = 990 \frac{p'}{p'_{IB}} - 282 \qquad (7.15)$$

where p_r is a reference pressure equal to 1 MPa, used to make Equation 7.15 non-dimensional.

At comparable states the maximum shear modulus of the intact soil is always higher than that of the reconstituted soil, but the variation with state shown by the data points D3 and E1 is parallel to that of the reconstituted soil. This observation suggests that the reduction of stiffness from D1 to D3 was the consequence of the degradation of bonding developing through the whole sample so that in the subsequent stages of the test state became the predominant factor governing the response of the soil as in uncemented sands.

In Figure 7.24 the values of G_{max} of both the reconstituted and intact soils were normalized with respect to the equivalent pressure p'_{IB}. This normalization has been derived from a reinterpretation of the relationship proposed by Rampello et al. (1994) between maximum shear modulus and state for clays. The shear modulus was expressed by Rampello et al. as a function of p'/p'_e and of $G^{(nc)}_{max}$, where p'_e is the equivalent pressure taken on the normal compression line and $G^{(nc)}_{max}$ is the maximum shear modulus for normally consolidated states and is solely a function of either the specific volume or the mean effective stress. In Figure 7.24 $G^{(nc)}_{max}$ was replaced by the variable p'_{IB}, which is also solely a function of v, and G_{max}/p'_{IB} was then plotted against p'/p'_{IB}. The graph shows that as the state of the intact soil approaches its isotropic boundary, the response in terms of stiffness tends towards that of the reconstituted soil. Higher stresses could not be

reached because of the limitation of the confining stress in the apparatus but it is possible that even when the states of the intact soil reach the NCL of the reconstituted, some differences may continue to exist between the stiffness of the two soils in the initial stages of shearing.

The above analysis was not performed for the silica sandstone. Because of the high density and overall stress history of the intact soil a correct comparison with the reconstituted soil in terms of stiffness would have required reference not only to compacted reconstituted samples as for the calcarenite but also to overconsolidated samples. As discussed in Section 6.7.6, the variation of the maximum shear modulus for reconstituted sands would be expected to be a function both of the state of the soil in terms of p' and v and of the way in which this state was achieved, whether through compaction or overconsolidation. These aspects added complexity to the comparison and would have required a preliminary study of the factors controlling the stiffness of reconstituted sands which was beyond the scope of the present work.

8. CONCLUSIONS

8.1 INTRODUCTION

The behaviour of two naturally cemented sands was studied and compared with that of corresponding compacted reconstituted soils. The materials considered were a calcarenite from the site of the North Rankin Platform in Australia and a silica sandstone from the Lower Greensand series of Kent in England. The calcarenite consisted of a biogenic carbonate sand bonded by calcium carbonate. The silica sandstone consisted of a quartz sand bonded by iron oxide. The two materials were deliberately chosen to compare and contrast the behaviour of two naturally cemented sands having different geological histories and representing extremes in terms of soil constituents. The calcarenite represented a material with weak grains bonded by a comparatively strong cement. Conversely the silica sandstone represented a material with strong grains bonded by a comparatively weak cement. In terms of geological history the calcarenite had a younger age (Pleistocene) and in situ was currently under its maximum overburden pressure. The silica sandstone was older (Cretaceous) and in its geologically history had been subjected to higher stresses than at present.

The study of the naturally cemented sands was supported by that of an artificially cemented carbonate sand. The work on the artificial soil involved reinterpretation of the results obtained from Coop and Atkinson (1993) for the case of strong inter-particle bonds and extension of test results to the case of weak bonds. The artificial material consisted of a biogenic carbonate sand cemented with gypsum plaster. The nature of the constituents and the methods of preparation provided a model material with similar characteristics to the calcarenite.

The experimental work consisted of triaxial tests performed in stress path controlled systems covering a range of confining pressures between 70 and 70000 kPa. Laboratory techniques were developed to determine stiffness variations from very small strains to failure by means of local axial gauges. The testing programme consisted of drained and undrained shearing of isotropically compressed samples. Constant p' stress paths were generally followed in the drained tests. Undrained shearing was performed at constant

cell pressure and included a series of loading-unloading probes from isotropic states up to deviator stresses which did not cause failure.

8.2 GENERAL FEATURES OF BEHAVIOUR

8.2.1 Isotropic compression

The large variation of initial densities of the calcarenite samples offered the opportunity to study the influence of specific volume as well as mean effective stresses on the material behaviour. When isotropically compressed the calcarenite reached states which were impossible for the reconstituted soil. A clear relationship existed between the specific volumes and mean effective stresses at yield which resulted in the identification of an isotropic yield locus. This was found to be substantially coincident with the post-yield compression curves and thus defined the boundary for the possible states attainable in isotropic compression. The offset between the isotropic boundaries of the intact and reconstituted soils decreased as the specific volume decreased until the two boundaries became coincident (Figure 7.1).

The silica sandstone samples all had similar initial densities. For this material isotropic yielding occurred inside the permissible space of the reconstituted soil (Figure 6.6b). Unlike the calcarenite the isotropic boundary of the silica sandstone appeared to coincide with the boundary of the original uncemented soil as this was deposited in the ground. The latter was likely to have a different initial grading from that of the reconstituted soil considered for comparisons because of the particle breakage that the original uncemented soil may have experienced in the ground under the high overburden pressure which acted before the intact soil became cemented. As shown by Coop (1990) and Coop and Atkinson (1993) for carbonate sands, the normal compression line is controlled by the initial grading. In the present work the convergence towards a different normal compression line from that found for the reconstituted soil could not be confirmed by test results because of the limitation of the confining stress in the apparatus.

Results from samples of the artificially cemented sand, which all had similar initial specific volumes, showed that the attainment of states outside or within the isotropic

boundary of the reconstituted soil depended on whether the soil was strongly or weakly cemented (Figures 7.2 and 7.3). As for the artificially weakly cemented sand, the weak bonds of the silica sandstone resulted in a yield point which took place within the permissible space of the reconstituted soil (Figure 6.6b).

8.2.2 Shearing

When sheared the calcarenite was found to reach the same critical states as the reconstituted soil both in terms of stress ratio M and in terms of specific volumes, irrespective of the initial densities of the intact samples (Figures 5.12 and 5.14). The critical state line in v : lnp' space was also found to be parallel to the normal compression line of the reconstituted soil. The artificial sand with weak bonds had loci of critical states in v : lnp' and q : p' spaces which were coincident with those identified by Coop and Atkinson (1993) for the artificial sand with strong bonds (Figures 4.7 and 4.10). This confirmed that critical states were not dependent on the strength of the bonds. The silica sandstone reached similar stress ratios at the ultimate states to the reconstituted soil (Figure 6.10) but localised failure of the intact soil prevented the identification of critical states in v : lnp' space (Figure 6.12). For the reconstituted soil the specific volumes at the critical states when plotted against lnp' defined a line parallel to the normal compression line.

Shearing of both naturally and artificially cemented sands showed that increases in confining pressures transformed the behaviour from strain-softening to strain-hardening. The results from the artificially cemented sand also showed that for similar specific volumes a decrease in the degree of cementing required smaller confining stresses to cause the transition from strain-softening to strain-hardening but the general features of behaviour remained similar. When the artificially cemented sand and the calcarenite strain-softened, a linear stress-strain behaviour was observed almost up to the peak state and this was accompanied by no substantial volumetric changes (Figures 4.5a and 5.7). Conversely the silica sandstone had linear stress-strain behaviour only in the initial stages of shearing and the peak states were preceded and accompanied by dilation (Figure 6.7).

In all cases yielding was defined as the end of the linear stress-strain behaviour and was associated with the onset of bond degradation. For the calcarenite and the artificially cemented sand the near coincidence of peak states and yielding clearly indicated the cohesive nature of the peak strength of the soils.

From stress-dilatancy analyses the peak states of the silica sandstone were found to occur when the rate of dilation was at its maximum (Figure 7.13) so that the peak strength was frictional. Intact and reconstituted soils followed the same stress-dilatancy relationship at the peak states but the intact soil was found to have unusually high values of dilatancy (Figure 7.15). Even after accounting for differences in states the intact soil still had a peak strength which was higher than that of the reconstituted soil and associated with higher rates of dilation (Figure 7.16). The latter were seen to be the result of the intact soil having to recover from a much smaller dilation experienced in reaching the same stress ratio as the reconstituted soil. Qualitative considerations of the energy balance suggested that the delayed dilation of the intact soil was likely to be caused by work that had to be spent in degrading the bonds. The smaller initial dilation was also seen as a possible consequence of smaller interparticle contact stresses that the intact soil had with respect to the reconstituted soil, because of the large grain contact areas of the former as revealed by the thin sections. Therefore for the silica sandstone it was possible that dilation was influenced not only by bond degradation mechanisms but also by the fabric of the soil. These factors together resulted in a higher peak strength of the intact soil, in contrast to the cemented carbonate soils for which the higher peak strengths resulted purely from cohesion.

8.3 STIFFNESS AND YIELDING OF NATURALLY CEMENTED SANDS

8.3.1 Developments of laboratory techniques

Determination of stiffness from stress-strain curves in cemented sands could only be obtained if axial strains were measured internally because of the presence of significant bedding errors in the external readings (Figure 3.5). Moreover the study of yielding over an extended range of pressures was found to be essential to the understanding of the behaviour of these materials. Since yielding during shearing occurred at small strains

and because of the high stiffness of the cemented sands laboratory techniques were developed in the high pressure triaxial system which enabled accurate and reliable determinations of both stiffness and yield points. To satisfy these requirements it was found that local axial strains had to be measured to an accuracy of 0.00005 % and uniform strains had to be guaranteed within the sample. LVDTs were chosen since it was possible to use them under high pressures and the tests could be extended to large axial strains with no damage to the gauges. The local transducers were installed in the 10 MPa stress path controlled triaxial system and the required accuracy was obtained by reducing the noise affecting the output signal of the transducers. Uniformity of strains was achieved by designing a new connection of the sample to the axial loading system and by modifying sample preparation and setting up procedures to reduce the eccentricity of the axial load on the sample (Sections 3.3 and 34) . On the basis of these developments maximum shear moduli and yield stresses could be determined with accuracies of ± 6 % and ± 10 kPa respectively.

8.3.2 Test results

When sheared at mean effective stresses below isotropic yielding both the calcarenite and the silica sandstone had maximum shear moduli which were found to be independent of the mean effective stresses. However changes in the mean effective stresses resulted in a variation of the deviator stresses and strains at yielding.

Undrained loading-unloading probes showed that the pre-yield stress-strain behaviour for the two natural cemented sands as well as being linear was also reversible (elastic) within the accuracy of the measurements (Figures 5.17 and 6.18). Loading beyond yield resulted in abrupt changes to the shear modulus and the development of plastic strains.

The mechanism with which bond degradation developed in the cemented samples was investigated by performing series of undrained loading-unloading probes. These probes were performed from either the same initial isotropic state as for the silica sandstone or from isotropic states which, although different, did not affect the stiffness as for the calcarenite. For both naturally cemented sands it was found that loading beyond the first yield point caused a decrease of the deviator stress at yield on subsequent reloading but

no variation in the maximum shear modulus. The yield stress continued to decrease with the number of cycles performed until, after a sufficient number of probes, also the value of the maximum shear modulus decreased (Figures 5.19b, 5.20, 6.22 and 6.23).

For the calcarenite it was also found that the reduced value of stiffness was still higher than that of the reconstituted soil at equivalent states. However the maximum shear modulus of the intact soil tended to converge towards that of the reconstituted soil as the state of the intact soil travelled along the isotropic boundary and approached the normal compression line of the reconstituted soil (Figure 7.24).

8.4 INFLUENCE OF v, p' AND BOND STRENGTH ON THE SHEAR BEHAVIOUR OF THE CEMENTED SANDS

For each cemented sand the shear behaviour was unified in a two-dimensional representation which described yielding, strength and the state boundary surface. Identification of the yield surface allowed the definition of the domain of states in which the shear behaviour was cohesive and governed by bonding. States beyond the yield surface and within the boundary surface were associated with bond degradation and frictional behaviour.

In Critical State Soil Mechanics one of the ways of unifying the shear behaviour of uncemented soils in a two-dimensional representation is that of normalizing q and p' by an equivalent pressure. When the critical state line defined in v : lnp' space and the normal compression line are parallel, the equivalent pressure can be taken on either of them. This type of normalization was applied to the results for the reconstituted soils.

Normalization with respect to the critical state line for the artificially cemented sand and the calcarenite did not produce unique yield and state boundary surfaces (Figures 4.15 and 5.24). It was shown however that these surfaces could be identified by taking an equivalent pressure p'_{IB} on the isotropic boundary of the intact soil (Figures 7.9 and 7.10b). When the yield and state boundary surfaces were superimposed, the value of the state variable p'/p'_{IB} at yielding could be used to distinguish modes of shear behaviour of the intact soil. For the silica sandstone yield and state boundary surfaces were

identified by taking an equivalent pressure on the critical state line (Figure 7.20). The two types of normalization used for the silica sandstone and the cemented carbonate sands can be regarded to be consistent. Because of the high initial density of the silica sandstone and the weak bonding its behaviour in isotropic compression could be considered similar to that of an uncemented sand for which the critical state line and the isotropic boundary are parallel.

By means of the above method of normalization it was found that the yield surface of the calcarenite occupied a large portion of the permissible space of the intact soil indicating the large influence that bonding and thus cohesion had on the shear behaviour of the soil. When states between the yield surface and the state boundary surface were reached the shear behaviour was compressive and controlled by bond degradation and particle crushing. Peak strengths for the calcarenite could only be cohesive as stress ratios higher than M only occurred on the yield surface. Otherwise when the stress ratio at yielding was lower than M the strength was frictional and coincident with the critical state. However in this case, provided the soil had not been yielded in isotropic compression, bonding still influenced the shear behaviour by enhancing the stiffness and increasing the range of the linear stress-strain response. Similar features were observed for the artificially cemented sand.

Unlike the cemented carbonate sands the yield surface of the silica sandstone was found to occupy only a small portion of the permissible space demonstrating that the shear behaviour was mainly frictional. States between the yield and state boundary surfaces were associated with bond degradation and dilation if on the dry side of the critical state, or compression and possible particle crushing if on the wet side of the critical state. A peak strength resulting from cohesion was observed only at the lowest pressures. Otherwise the peak strength was frictional but in any case higher than that of the reconstituted soil. The additional peak strength of the intact soil was thought to be related to the influence of fabric and bond degradation. The ultimate strength with no peak state was obtained when failure occurred on the wet side of the critical state.

8.5 CORRELATION BETWEEN SHEAR BEHAVIOUR AND MATERIAL PROPERTIES

The shear behaviour of the two naturally cemented sands, once the influence of density had been accounted for, was interpreted in the light of the differences in the nature of the material constituents and of the geological histories they experienced. Sands with a strong cement and comparatively weak grains such as the calcarenite are likely to have a cohesive shear behaviour largely controlled by the bonds and when these are degraded would show a frictional behaviour mainly controlled by particle crushing. Sands with weak cement and comparatively strong grains such as the silica sandstone are likely to behave as frictional materials with shear mechanisms dominated by dilation, whereas particle crushing would only be restricted to the highest stresses.

For sands in which bonding formed concurrently with deposition as for the calcarenite, fabric is not likely to be an important feature of the material behaviour. The results from the calcarenite demonstrated that density had an important influence on the behaviour of the soil which cannot be accounted for by referring to the general concepts of Critical State Soil Mechanics. In particular it was found that the influence of bonding on the shear behaviour became greater as the density of the soil increased and the mean effective stresses decreased (Section 7.3).

The silica sandstone represented the case of a geologically aged sand in which bonding formed in the later stages of the diagenesis. This allowed the development of fabric features characterized by well developed interparticle contacts. The high density of the material derived from the close contacts between the grains which, once disrupted, could not be recreated through compaction, resulting in much lower densities when preparing the reconstituted soil. The large particle contact area and consequent high density had been observed by other authors in other aged silica sands and attributed to the pressure solution of the quartz constituting the grains (Section 7.2.3). These processes, although related to the depth of burial, can cause increases in density which could not be achieved solely through compression under the overburden pressure experienced by the soil. As shown by the silica sandstone, in these cases the peak strength is likely to be affected not only by the presence of bonding in the initial stages of shearing but also by the fabric of the soil. Despite the influence of fabric and because of the weakness of

bonding the shear behaviour of the intact soil remained largely consistent with the concepts of Critical State Soil Mechanics.

8.6 IMPLICATIONS OF THE RESEARCH

It has been shown that different mechanisms controlled the peak strength of naturally cemented sands, depending on the strength of the bonds relative to the strength of the particles. Cemented sands similar to the calcarenite (where the cement is strong and the particles are weak) are likely to display a peak strength due to cohesion, brittle stress-strain behaviour and yielding substantially coincident with the peak state. Conversely when the cement is weak compared to the particles as in the silica sandstone, the peak strength was seen to be frictional, except at low confining stresses.

In the former case if shear stresses and mean effective stresses in the ground were uniform, safe conditions would be guaranteed when their values do not exceed those corresponding to yielding. However the strength of the cemented soil can be significantly modified by the presence of discontinuities. The main danger for brittle materials arises from concentration of stresses, since the dramatic strain-softening of a small zone would cause failure to propagate into neighbouring zones causing a premature collapse of the structure. In these conditions reference to a strength higher than that at the critical state may be unsafe. In materials such as the silica sandstone the peak strength is achieved through dilation and strain-softening is less dramatic, with the strength achieved by the soil after peak being reasonably close to the critical state strength. Design criteria for these types of soil could follow those applied to "dense" sands and the choice of the critical state strength can be considered as conservative. In addition it was observed that natural quartz sands can have in situ specific volumes which are lower than those achievable when compacting reconstituted soils to their maximum densities in the laboratory. In these cases the determination of the peak strength from reconstituted soils is likely to underestimate the peak strength of the soil in the ground, not only as the result of differences in densities but also as a result of differences in fabric. With respect to the design of structures, more accurate prediction of their performance and more economic design could be achieved by considering a strength higher than that at the critical state, given the additional contribution to peak

strength that geologically aged quartz sands can offer in the ground compared to reconstituted soils at similar states.

The work has also shown that strain-softening and strain-hardening types of behaviour depend on the state of the soils as given by the combination of mean effective stress and specific volume. When the cementing is weak compared to the particle strength reference to the location of the current state of soil with respect to the critical state line in v : lnp' space can be used to predict the transition from one type of behaviour to the other. When the cementing is strong compared to the particle strength reference to states on the "dry" or "wet" side of the critical state become meaningless unless the soil undergoes volumetric strains prior to shearing sufficiently large to degrade the bonds. The example of the calcarenite suggests however that the transition from brittle to ductile behaviour can be predicted in terms of state provided the states of reference are chosen appropriately. For both the calcarenite and the artificially cemented carbonate sand these were found to be the isotropic boundaries. In any case when the soil state produces strain-hardening behaviour the strength of the soil is that at the critical state and coincides with the strength of the reconstituted soil.

Soils like the silica sandstone where their state is generally such that it produces dilation during shearing, will offer high bearing capacities under confinement such as around the shaft of a driven pile due to the increase of the horizontal stresses during driving. Soils like the calcarenite can exist at specific volumes higher than those of the reconstituted soils at similar mean effective stresses as the result of bonding. If sheared in these conditions compression can be large and would cause a decrease of the horizontal stresses if confined, with a subsequent reduction of the shaft frictional capacity.

Since in cemented sands strains before yield are small a knowledge of the stresses at yielding is important if prediction of settlements are to be made. It was also shown that when sands are cemented, irrespective of whether the cement is strong or weak when compared to the grains, the stresses at yield decrease as the soil is subjected to stress cycles which go beyond first yielding. This behaviour eventually also effects the stiffness of the soil. The comparison between the maximum shear moduli of the intact and reconstituted soils of calcarenite showed that the contribution of bonding to stiffness after first yield was a function of state and reduced as the states of the intact soil

approached the isotropic boundary.

8.7 RECOMMENDATIONS FOR FUTURE WORK

The investigation of the shear behaviour of naturally cemented sands in triaxial compression was limited to samples which were isotropically compressed and which followed mainly constant p' stress paths during shearing. Further investigation should consider the behaviour in one-dimensional compression and its influence on the response of the soil during shearing. A variety of stress paths should be followed during shearing to verify their influence on the state boundary and yield surfaces.

Experimental work should be performed on other types of cemented sands according to the methodology followed in the present work. These investigations would be useful to assess the more general validity of the conclusions from the present work .

Laboratory techniques able to provide measurements of volumetric strains which are not affected by bedding errors should be developed. The accuracy currently achieved in volumetric measurements also needs to be improved. This would allow complete identification of the relationship between stress and strain increment tensors.

For the silica sandstone from the Lower Greensand it would be of interest to extend the experimental work to other depths of the deposit having the same soil constituents but a different degree of cementing and possibly different initial specific volumes.

The maximum shear moduli determined for the naturally cemented sands by means of direct measurements of stresses and strains can be compared with values obtained using alternative techniques. Dynamic measurements of the maximum shear moduli performed in situ and in the laboratory could be compared with the set of data provided by the present work.

Finally the present work provides a conceptual basis and useful sets of data for the development of constitutive models able to describe the features observed for the behaviour of naturally cemented sands.

REFERENCES

Ackerly, S. K., Hellings, J. E., Jardine and R. J. (1987). Discussion on: A new device for measuring local axial strain on triaxial specimens by Clayton, C. R. I. and Khatrush, S. A. Géotechnique, Vol. 37, No. 4, pp. 414-415.

Anagnostopoulos, A. G., Kalteziotis, N. and Tsiambaos, G. K. (1991). Geotechnical properties of the Corinth Canal marls. Geotech. and Geol. Engng, Vol. 9, pp. 1-26.

Apthorpe, M., Garstone, J. and Turner, G. J. (1988). Depositional setting and regional geology of North Rankin A foundation sediments. Proc. Int. Conf. Calcareous Sediments, Perth, Vol. 2, pp. 357-366.

Arthur, J. R. F. and Philips, A. B. (1975). Homogeneous and layered sand in triaxial compression. Géotechnique, Vol. 25, No. 4, pp. 799-815.

Atkinson, J. H. and Bransby, P. L. (1978). The mechanics of soils. An introduction to critical state soil mechanics. McGraw-Hill, Maidenhead.

Atkinson, J. H. and Evans, J. S. (1985). Discussion on: The measurement of soil stiffness in the triaxial apparatus by Jardine, R. J., Symes, N. J. and Burland, J. B. Géotechnique, Vol. 35, No. 3, pp. 378-382.

Aversa, S. (1991). Mechanical behaviour of soft rocks: some remarks. Workshop on Experimental Characterization and Modelling of Soils and Soft Rocks, Naples, pp. 191–223.

Aversa, S., Evangelista, A. and Ramondini, M. (1991). Snervamento e resistenza a rottura di *un tufo a grana fine. Proc. of 2nd Meeting of G.N.C.S.I.G., Ravello, Vol. 1*, pp. 3-22.

Aversa, S., & Evangelista, A. Leroueil, S. and Picarelli, L. (1993). Some aspects of the mechanical behaviour of structured soils and soft rocks. Proc. Int. Symp. Geotech. Engng of Hard Soils - Soft Rocks, Athens, Vol. 1, pp. 359–366. Balkema, Rotterdam.

Balassubramanian, A. S. (1976). Local strains and displacement patterns in triaxial specimens of a saturated clay. Soils and Foundations, Vol. 16, No. 1, pp. 101-114.

Baldi, G., Hight, D. W. and Thomas, G. E. (1988). A reevaluation of conventional triaxial test methods. Advanced Triaxial Testing of Soil and Rock, Am. Soc. Test. Mat., STP 977, pp. 219-263.

Baldi, G. and Nova, R. (1984). Membrane penetration effects in triaxial testing. J. Geotech. Engng, Am. Soc. Civ. Engrs, Vol. 110, No. 3, pp. 403-420.

Barton, M. E. (1993). Cohesive sands: the natural transition from sands to sandstones. Proc. Int. Symp. Geotech. Engng of Hard Soils - Soft Rocks, Athens, Vol. 1,pp. 367–374. Balkema, Rotterdam.

Been, K. and Jefferies, M. G. (1985). A state parameter for sands. Géotechnique, Vol. 35, No. 2, pp. 99-112.

Bishop, A. W. (1973). The influence of an undrained change in stress on the pore pressure in porous media of low compressibility. Géotechnique, Vol. 23, No. 3, pp. 435-441.

Bishop, A. W. (1976). The influence of system compressibility on the observed pore-pressure response to an undrained change in stress in saturated rock. Géotechnique, Vol. 26, pp. 371-375.

Bishop, A. W. and Eldin, A. K. G. (1950). Undrained triaxial tests on saturated sands and their significance in the general theory of shear strength. Géotechnique, Vol. 2, No. 1, pp. 13-32.

Bishop, A. W. and Henkel, D. J. (1962). The measurement of soil properties in the triaxial test. Edward Arnold (2nd edition), London.

Bishop, A. W. and Wesley, L. D. (1975). A hydraulic triaxial apparatus for controlled stress path testing. Géotechnique, Vol. 25, No. 4, pp. 657-670.

Bjerrum, L., Kringstad, S. and Kummenje, O. (1961). The shear strength of a fine sand. Proc. 5th Int. Conf. Soil Mech. Fdn Engng, Paris, Vol. 1, No. 5, pp. 29-37.

British Standards Institution (1990). Methods of tests for soils for civil engineering purposes. BS 1377. BSI, London.

Brousseau, P. (1983). Généralisation des états limites et de la destructuration des argiles naturelles. MSc thesis, Laval University, Québec.

Brown, S. F. and Snaith, M. S. (1974). The measurement of recoverable and irrecoverable deformation in the repeated load triaxial test. Géotechnique, Vol. 24, No. 2, pp. 255-259.

Burland, J. B. (1990). On the compressibility and shear strength of natural clays. 30th Rankine Lecture, Géotechnique, Vol. 40, No. 3, pp. 329-378.

Burland, J. B. and Symes, M. (1982). A simple axial displacement gauge for use in the triaxial apparatus. Géotechnique, Vol. 32, No. 1, pp. 62-65.

Casagrande, A. (1936). Characteristics of cohesionless soils affecting the stability of earth fills. J. Boston Soc. Civ. Engrs, January. Contribution to Soil Mechanics 1925–1940, October 1940, Boston, Soc. Civ. Engrs.

Casey, R. (1961). The stratigraphical palaeontology of the Lower Greensand. Palaeontology, Vol. 3, Part 4, pp. 487-621.

Castro, G. (1969). Liquefaction of sand. PhD thesis, Div. Engng and Appl. Phys., Harvard University, Boston.

Chandler, H. W. (1985). A plasticity theory without Drucker's postulate suitable for granular materials. J. Mech. Phys. Solids, Vol. 33, pp. 215-226.

Clayton, C. R. I. (1989). The mechanical properties of the Chalk. Keynote address. Proc. Int. Chalk Symp., Brighton, pp. 213-232. Thomas Telford, London.

Clayton, C. R. I. and Khatrush, S. A. (1986). A new device for measuring local axial strains on triaxial specimens. Géotechnique, Vol. 36, No. 4, pp. 593-597.

Clayton, C. R. I., Khatrush, S. A., Bica, A. V. D. and Siddique, A. (1987). The use of hall effect semiconductors in geotechnical instrumentation. Geotech. Test. J., GTJODJ, Vol. 12, No. 1, pp. 69-76.

Clinton, D. B. (1987). The determination of soil parameters from stress path tests. PhD thesis, City University, London.

Clough, G. W., Sitar, N. and Bachus, R. C. (1981). Cemented sands under static loading. J. Geotech. Engng Div., Am. Soc. Civ. Engrs, Vol. 107, GT6, pp. 799-818.

Coop, M. R. (1990). The mechanics of uncemented carbonate sands. Géotechnique, Vol. 40, No. 4, pp. 607-626.

Coop, M. R. and Atkinson, J. H. (1993). The mechanics of cemented carbonate sands. Géotechnique, Vol. 43, No. 1, pp. 53-67.

Coop, M. R. and Atkinson, J. H. (1994). Discussion on: The mechanics of cemented carbonate sands by Huang, J. T. and Airey, D. W. Géotechnique, Vol. 44, No. 3, pp. 533-537.

Coop, M. R., Atkinson, J. H. and Taylor, R. N. (1995). Strength and stiffness of structured and unstructured soils. Proc. XI Eur. Conf. on Soil Mech. and Found. Engng, Copenhagen, Vol. 1/10.

Coop, M. R. and Lee, J. K. (1993). The behaviour of granular soils at elevated stresses. Proc. Wroth Memorial Symp., pp. 186-198. Thomas Telford, London.

Cornforth, D. H. (1973). Prediction of drained strength of sands from relative density measurements. Am. Soc. Test. Mat., Special Tech. Publ., No. 523, pp. 281-303.

Costa Filho, L. M. (1985). Measurement of axial strains in triaxial tests on London Clay. Geotechnical Testing Journal, Am. Soc. Test. Mat., Vol. 8, No. 1, pp. 3-13.

Dapples, E. C. (1972). Some concepts of cementation and lithification of sandstones. Bulletin Am. Ass. of Petroleum Geologists, Vol. 56, No. 1, pp. 3-25.

Dobereiner, L. and De Freitas, M. H. (1986). Geotechnical properties of weak sandstones. Géotechnique, Vol. 36, No. 1, pp. 79-94.

Druck Ltd (1995). Personal communication.

Dusseault, M. B. and Morgenstern, N. R. (1979). Locked sands. J. Engng Geology, Vol. 12, pp. 117-131.

Elliott, G. M. and Brown, E. T. (1985). Yield of a soft, high porosity rock. Géotechnique, Vol. 35, No. 4, pp. 413-423.

Evans, K. M. (1987). A model study of the end bearing capacity of piles in layered carbonate soils. DPhil thesis, Oxford University.

Fookes, P. G. (1988). The geology of carbonate soils and rocks and their engineering characterisation and description. Proc. Int. Conf. Calcareous Sediments, Perth, Vol. 2, pp. 787-806.

Fookes, P. G. (1993). Personal Communication

Frydman, S. (1982). Calcareous sands of the Israeli Coastal Plain. Proc. Symp. Geotech. Properties, Behaviour and Performance of Calcareous Soils. Am. Soc. Test. Mat., STP 777, pp. 226-251.

Gallois, R. W. (1965). The Wealden District. British Regional Geology Guide Survey and Museum, pp. 1-101. H.M. S.O., London.

Geological Society (1990). The logging of rock cores for engineering purposes. Q. J. Engng Geol. Vol. 3, No. 1, pp. 1-24.

Golightly, C. R. and Hyde, A. F. L. (1988). Some fundamental properties of carbonate soils. Proc. Int. Conf. Calcareous Sediments, Perth, Vol. 1, pp. 69-78.

Goto, S., Tatsuoka, F., Shibuya, S. Kim, Y. -S. and Sato, T. (1991). A simple gauge for local small strain measurements in laboratory. *Soils and Foundations, Vol. 31, No. 1,* pp. 169-180.

Graham, J., Crooks, J. H. A. and Lau, S. L. K. (1988). Yield envelopes: identification and geometric properties. Géotechnique, Vol. 38, No. 1, pp. 125-134.

Graham, J. and Houlsby, G. T. (1983). Anisotropic elasticity of a natural clay. Géotechnique, Vol. 33, No. 2, pp. 165-180.

Graham, J. and Li, E.C.C. (1985). Comparison of natural and remoulded plastic clay. J. Geotech. Engng Div., Am. Soc. Civ. Engrs, Vol. 111, GT7, pp. 865-881.

Graham, J., Noonan, M. L. and Lew, K. V. (1983). Yield states and stress-strain relationships in a natural plastic clay. Can. Geotech. J., Vol. 20, No. 3, pp. 502-516.

Hardin, B. O. and Black, W. L. (1966). Sand stiffness under various triaxial stresses. J. Soil Mech. Fnd. Div., Am. Soc. Civ. Engrs, Vol. 92, SM2, pp. 27-42.

Henkel, D. J. (1960). The shear strength of saturated remoulded clays. Proc. Am. Soc. Civ. Engrs Research Conf. on Shear Strength of Cohesive Soils, Boulder, pp. 533-554.

Hird, C. C. and Yung, P. (1987). Discussion on: Clayton, C. R. I. and Kathrush, S. A. (1986). A new device for measuring local axial strains on triaxial specimens. Géotechnique, Vol. 37, No. 3, pp. 413-414.

Ho, E. W. L. (1988). Geotechnical properties of deep ocean sediments: a critical state approach. PhD thesis, City University, London.

Horseman, S. T., Winter, M. G. and Entwistle, D. C. (1987). Geotechnical characteristics of Boom clay in relation to the disposal of radioactive waste. CEC Report EUR 10987.

Houlsby, G. T., Evans, K. M. and Sweeney, M. (1988). End bearing capacity of model piles in layered carbonate soils. DPhil thesis, Oxford University.

Houlsby, G. T. and Wroth, C. P. (1991). The variation of the shear modulus of a clay with pressure and overconsolidation ratio. Soils and Foundations, Vol. 31, No. 3, pp. 138-143.

Huang, J. T. and Airey, D. W. (1991). The manufacture of cemented carbonate soils. Research Report R 631, School of Civil and Mining Engineering, The University of Sidney.

Huang, J. T. and Airey, D. W. (1993). The effects of cement and density on an artificially cemented sand. Proc. Int. Symp. Geotech. Engng of Hard Soils - Soft Rocks, Athens, Vol. 1, pp. 553-560. Balkema, Rotterdam.

International Society of Rock Mechanics (1978). Suggested methods for the quantitative descriptions of discontinuities in rock masses. Int. J. Rock Mech. Min. Sci., Vol. 15, No. 6, pp. 319-368.

International Society of Rock Mechanics (1981). Rock Characterization testing and monitoring. ISRM suggested methods. Editor Brown, E .T. Pergamon Press, Oxford.

Jaky, J. (1944). The coefficient of earth pressure at rest. J. Soc. Hungarian Archit. Engrs, Vol. 22, pp. 355-358.

Jardine, R. J., Symes, M. J. and Burland, J. B. (1984). The measurement of soil stiffness in the triaxial apparatus. Géotechnique, Vol. 34, No. 3, pp. 323-340.

Jefferies, M. G. (1993). Nor-Sand: a simple critical state model for sand. Géotechnique, Vol. 43, No. 1, pp. 91-103.

Jovicic, V. (1995). Small strain shear modulus of soils and soft rocks. 1st year research report, City University, London.

Kim, Y. -S., Tatsuoka, F. and Ochi, K. (1994). Deformation characteristics at small strains of sedimentary soft rocks by triaxial compression tests. Géotechnique, Vol. 44, No. 3, pp. 461-478.

Kirkaldy, J. F. (1975). William Topley and the geology of the Weald. Proc. Geol. Ass., Vol. 86, No. 4, 373-388.

Ladd, C. C. and Foott, R. (1974). New design procedure for the stability of soft clays. J. Geotech. Engng Div., Am. Soc. Civ. Engrs, Vol. 100, GT7, pp. 763-786.

Lade, P. V. (1972). The stress-strain and strength characteristics of cohesionless soils. PhD thesis, University of California at Berkeley.

La Rochelle, P., Leroueil, S., Trak, B., Blais-Leroux, L. and Tavenas, F. (1988). Observational approach to membrane and area corrections in triaxial testing. Advanced Triaxial Testing of Soil and Rock, Am. Soc. Test. Mat., STP 977, pp. 715-731.

Lau, W. H. W. (1988). The behaviour of clay in simple shear and triaxial tests. PhD thesis, City University, London.

Leddra, M. J. (1990). Deformation of chalk through compaction and flow. PhD thesis, University of London.

Leroueil, S., Tavenas, F., Brucy, F., La Rochelle, P. and Roy, M. (1979). Behaviour of destructured natural clays. J. Geotech. Engng Div., Am. Soc. Civ. Engrs, Vol. 105, GT6, pp. 759-778.

Leroueil, S. and Vaughan, P. R. (1990). The general and congruent effects of structure in natural soils and weak rocks. Géotechnique, Vol. 40, No. 3, pp. 467-488.

Locat, J. and Lefebvre, G. (1985). The compressibility and sensitivity of an artificially sedimented clay soil: the Grande-Baleine marine clay, Québec. Marine Geotechnol., Vol. 6, No. 1, pp. 1-27.

Maccarini, M. (1987). Laboratory studies of a weakly bonded artificial soil. PhD thesis, Imperial College of Science and Technology, London.

Magnan, J. P., Shahanguian, S. and Josseaume, H. (1982). Etude en laboratoire des états limites Dúne argile molle organique. Revue Française de Géotechnique, No. 20, pp. 13–19.

Maxwell, J. C. (1964). Influence of depth, temperature and geologic age on porosity of quartzose sandstone. Bulletin Am. Ass. of Petroleum Geologists, Vol. 48. No. 5, pp. 697-709.

McClelland, B. (1988). Calcareous sediments: an engineering enigma. Proc. Int. Conf. Calcareous Sediments, Perth, Vol. 2, pp. 777-784.

Mesri, G., Rokhsar, A. and Bohor, B. F. (1975). Composition and compressibility of typical samples of Mexico City clay. Géotechnique, Vol. 25, No. 3, pp. 527-554.

Miura, N. and Yamonouchi, T. (1975). Effect of water on the behaviour of a quartz-rich sand under high stresses. Soils and Foundations, Vol. 15, No. 4, pp. 23-34.

Morgenstern, N. R. and Eigenbrod, K. (1974). Classification of argillaceous soils and rocks. J. Geotech. Engng Div., Am. Soc. Civ. Engrs, Vol. 100, GT10, pp. 1137-1156.

Nova, R. and Wood, D. M. (1979). A constitutive model for sand in triaxial compression. Int. J. for Numerical and Analytical Methods in Geomechanics, Vol. 3, pp. 255-278.

O'Connor, K. (1994). Swelling behaviour of unsaturated fine grained soils. PhD thesis, City University, London.

Osborne Wight, H. J. (1921). A short account of the geology of the Isle of Wight. District Memoir of the Geological Survey of Great Britain (England & Wales). HMSO, London

Paré, J. (1983). Etat limite et destructuration de trois argiles naturelles. MSc thesis, Laval University, Québec.

Petley, D., Jones, M., Fan, C., Stafford, C., Leddra, M. and Kageson-Loe. (1993). Deformation and fabric changes in weak fine-grained rocks during high pressure consolidation and shearing. Proc. Int. Symp. Geotech. Engng of Hard Soils - Soft Rocks, Athens, Vol. 1, pp. 737-751. Balkema, Rotterdam.

Price, G. P. (1988). Fabric of calcareous sediments at North Rankin "A", North West Shelf. Proc. Int. Conf. Calcareous Sediments, Perth, Vol. 2, pp. 367-376.

Rampello, S., Silvestri, F. and Viggiani, G. (1994). The dependence of small strain stiffness on stress state and history for fine grained soils: the example of Vallerica clay. Proc. Int. Symp. on Pre-Failure Deformation Characteristics of Geomaterials, IS-Hokkaido, Vol. 1, pp. 273-278. Sapporo, Japan.

Rampello, S., Viggiani, G. and Georgiannou, V. N. (1993). Strength and dilatancy of natural and reconstituted Vallerica clay. Proc. Int. Symp. Geotech. Engng of Hard Soils - Soft Rocks, Athens, Vol. 1, pp. 761-778. Balkema, Rotterdam.

Roscoe, K. H. and Schofield, A. N. (1963). Mechanical behaviour of an idealised "wet" clay. Proc. European Conf. Soil Mech. and Fdn Engng, Wiesbaden, Vol. 1, pp. 47-54.

Roscoe, K. H., Schofield, A. N. and Wroth, C. P. (1958). On the yielding of soils. Géotechnique, Vol. 8, No. 1, pp. 22-53.

Rowe, P. W. (1962). The stress-dilatancy relation for static equilibrium of an assembly of particles in contact. Proc. Roy. Soc. London, A269, pp. 500-527.

Rowe, P. W. (1969). The relation between the shear strength of sands in triaxial compression, plane strain and direct shear. Géotechnique, Vol. 19, No. 1, pp. 75-86.

Schofield, A. N. and Wroth, C. P. (1968). Critical state soil mechanics. McGraw-Hill, London.

Skempton, A. W. (1954). The pore-pressure coefficients A and B. Géotechnique, Vol. 4, pp. 143-147.

Tatsuoka, F., Kohata, Y., Mizumoto, K., Kim, Y. -S., Ochi, K. and Shi, D. (1993). Measuring small strain stiffness of soft rocks. Proc. Int. Symp. Geotech. Engng of Hard Soils - Soft Rocks, Athens, Vol. 1, pp. 809-816. Balkema, Rotterdam.

Tavenas, F. and Leroueil, S. (1987). Laboratory and in situ stress-strain-time behaviour of soft clays: a state-of-the-art. Int. Symp. on Geotech. Engng of Soft Soils, Mexico City, pp. 1-46.

Taylor, D. W. (1948). Fundamentals of soil mechanics. John Wiley, New York..

Taylor, J. M. (1950). Pore-space reduction in sandstones. Bulletin Am. Ass. of Petroleum Geologists, Vol. 34, No. 4, pp. 701-716.

Taylor, R. N. and Coop, M. R. (1990). Stress path testing of Boom Clay from Mol, Belgium. Proc. Conf. on The Engng Geology of Weak Rock, University of Leeds, pp. 89-98.

Vaughan, P. R. (1988). Characterising the mechanical properties of in-situ residual soils. Keynote paper. Proc. 2nd Int. Conf. on Geomechanics in Tropical Soils, Singapore, pp. 469-487.

Vesic, A. S. and Clough, G. W. (1968). Behaviour of granular materials under high stresses. J. Soil Mech. Fdn Div., Am. Soc. Civ. Engrs, Vol. 94, SM3, pp. 661-688.

Viggiani, G. and Atkinson, J. H. (1995). Stiffness of fine-grained soil at very small strains. Géotechnique, Vol. 45, No. 2, pp. 249-265.

Warren C. (1995). Sir William Halcrow and Partners. Personal Communication.

Wissa, A. E. Z. (1969). Pore pressure measurement in saturated stiff soils. J. Soil Mech. Fdn Div., Am. Soc. Civ. Engrs, Vol. 95, SM4, pp. 1063-1073.

Wood, D. M. (1990). Soil behaviour and critical state soil mechanics. Cambridge University Press.

Zisman, W. A. (1933). Compressibility and anisotropy of rocks at and near the earth's surface. Proc. Natn. Acad. USA, Vol. 19, pp. 666-679.

Transducer	Working Range	Output Voltage	Cell	Typical Calibration Constant	Resolution	Noise	Typical error due to: non linearity, drift, hysteresis
Wykeham Farrance Load Cells	5 kN	20 mV	B&W[d]	0.65 V/kN[e]	0.05 N	± 1 N	± 5 N
	30 kN		5MPa 10MPa[a]	60 mV/kN	0.5 N	± 2 N	± 20 N
	90 kN	25 mV	10MPa[b]	0.27 mV/kN	18 to 35 N	± 18 N	——
	200 kN	20 mV	70MPa	110 mV/MN	23 N	less than resolution	± 50 N
Druck Pressure Transducers	1000 kPa	100 mV	see note c	9.7×10^{-2} mV/kPa	0.03 kPa	± 0.2 kPa	± 2 kPa
	6 MPa		5 MPa	1.5×10^{-2} mV/kPa	0.2 kPa	± 0.4 kPa	± 12 kPa
					0.3 to 2 kPa		
Maywood Pressure Transducers	10 MPa		10MPa	1.2×10^{-2} mV/kPa	0.3 to 2 kPa	± 0.8 kPa	± 20 kPa
	70 MPa	210 mV	70MPa	0.3×10^{-2} mV/kPa	0.8 to 53 kPa	less than resolution	± 140 kPa

Notes: a After modification
b Before modification
c Device installed in B&W, 5 and 10 MPa systems
d Bishop and Wesley cell
e After amplification

Table 3.1 Characteristics of the load cells and pore pressure transducers.

Transducer	Working Range	Output Voltage	Cell	Typical Calibration Constant	Resolution	Noise	Typical error due to: non linearity, drift, hysteresis
External LVDTs	25 mm	± 2 V	B&W[d]	180 mV/mm	1.5×10^{-3} mm	± 0.0015 mm	± 0.1 mm
	50 mm		70MPa		from 1.4×10^{-5} to 7.0×10^{-3} mm		± 0.2 mm
			5MPa	145 mV/mm	2.0×10^{-3} mm		
			10MPa	90 mV/mm	from 5.4×10^{-5} to 1.4×10^{-2} mm		
Volume Gauge	35 cm^3		B&W	97×10^{-3} V/cm^3	3.1×10^{-3} cm^3	± 0.001 cm^3	± 0.15 cm^3
			70MPa		from 2.6×10^{-5} to 2.9×10^{-3} cm^3		
	80 cm^3		10MPa	45×10^{-3} V/cm^3	from 1×10^{-4} to 3×10^{-2} cm^3		± 0.2 cm^3
	100 cm^3	±100mV	5MPa	65×10^{-3} V/cm^3	5×10^{-3} cm^3	± 0.005 cm^3	
Local LVDTs	6 mm	± 3 V	10MPa	1000 mV/mm[e]	from 5×10^{-6} to 1.7×10^{-3} mm	± 5×10^{-5} mm	± 5×10^{-3} mm
	10 mm		70MPa	600 mV/mm[e]	from 4.2×10^{-6} to 2.6×10^{-4} mm	± 5×10^{-4} mm	± 7×10^{-3} mm
Hall effect	5 mm	± 1 V	B&W 5MPa	0.26 V/mm	1.2×10^{-4} mm	± 1×10^{-3} mm	± 5×10^{-2} mm

Notes: d Bishop and Wesley cell
e After amplification

Table 3.2 Characteristics of the displacement transducers and volume gauges.

Test	Cell	Sample diameter (mm)	v_i	Stress path	Shearing		
					p_i' (kPa)	$\bar{v}_i$	v_f
DCSG	B & W	38	2.102	$\delta\sigma_r = 0$	100	2.090	2.131
DCS1	B & W	38	2.098	$\delta\sigma_r = 0$	300	2.070	1.917
DCSF	B & W	38	2.202	$\delta\sigma_r = 0$	600	2.102	1.858
DCSD	10 MPa	60	2.158	$\delta p' = 0$	6400	1.759	1.540

Table 4.1 Testing programme for the artificially cemented samples prepared using method B.

Test	Cell	Sample diameter (mm)	v_i	Stress path	Shearing		
					p_i' (kPa)	$\bar{v}_i$	v_f
DCOGN	B & W	38	2.109	$\delta\sigma_r = 0$	50	2.106	2.101
DCOG2	B & W	38	2.034	$\delta p' = 0$	250	2.015	2.030
DCOFN	5 MPA	50	2.161	$\delta p' = 0$	3000	1.742	1.500
DCOF	5 MPa	50	2.100	$\delta p' = 0$	4400	1.650	1.480

Table 4.2 Testing programme for the artificially cemented samples prepared using method A.

Sample No. in present work	Borehole No.	Core No. from BP(**)	Depth below the sea bed (m)	v
N3	FSS-W(*)	111	96.6	1.779
N2	FSS-W(*)	112	96.8	1.840
C1	B2-6	29	127.4	1.738
N7	B2-6	52	128.3	1.770
C3	B2-6	54	129.9	1.850
RAN6	B2-6	67	133.7	1.854
RAN4	B2-6	68	134.5	1.850
RAN3	B2-6	69	134.8	1.863
RAN5	B2-6	70	135.5	1.871
RAN1	B2-6	74	137.1	1.914
NF1	B2-6	75	137.6	2.030
N5	B2-6	80	141.4	1.675
N4	B2-6	81	141.7	1.980

* Borehole within 200 m of the main borehole B2-6

** Reference number given to the rotary cores by British Petroleum Ltd

Table 5.1 Depth of retrieval of calcarenite samples and initial specific volumes.

Test	Cell	Sample diameter (mm)	isotropic compression	Strress path	Shearing		
			v_i		p_i' (kPa)	$\bar{v}_i$	v_f
C1	10 MPa	50	1.738	undrained	255	1.738	1.738
C3*	10 MPa	50	1.850	$\delta\sigma_r = 0$	325	1.541	1.569
NF1	5 MPa	50	2.030	$\delta p' = 0$	900	2.000	1.727
N3	10 MPa	83	1.779	$\delta p' = 0$	1400	1.751	1.650
N4	10 MPa	83	1.980	$\delta p' = 0$	4900	1.660	1.462
N2	10 MPa	83	1.840	$\delta p' = 0$	4910	1.659	1.440
N5	10 MPa	60	1.675	$\delta p' = 0$	8400	1.520	1.343
N7	70 MPa	50	1.770	$\delta p' = 0$	30000	1.325	1.236

* see Table 5.5 for loading-unloading probes

Table 5.2 Testing programme for intact samples of calcarenite.

Test	Cell	Sample diameter (mm)	isotropic compression	Stress path	Shearing		
			v_i		p_i' (kPa)	$\bar{v}_i$	v_f
R2	B & W	38	1.813	$\delta p' = 0$	400	1.759	1.726
R1	B & W	38	1.890	$\delta p' = 0$	500	1.770	1.722
RF2	5 MPA	50	1.762	$\delta p' = 0$	5000	1.567	1.398
RF	10 MPa	60	1.920	$\delta p' = 0$	5200	1.560	1.393
C2*	10 MPa	50	-	-	-	-	-

* see Table 5.6 for loading-unloading probes

Table 5.3 Testing programme for reconstituted samples of calcarenite.

Series	No. of cycles	p_i' (kPa)	q_{max} (kPa)	v
A	3	250	1000	1.850
B	3	800	1000	1.840
C	3	1550	680-920	1.835
D	3	2000	600-780	1.825
E	3	8400	1000	1.540

* Within a given series of probes the specific volume at the start and end of each cycle remained substantially constant.

Table 5.4 Testing programme for the undrained loading-unloading probes performed on an intact sample of calcarenite.

Series	No. of cycles	p_i' (kPa)	q_{max} (kPa)	v
A	3	300	180	1.805
B	2	800	300-750	1.715
C	3	2000	1500	1.635
D	3	8400	2000	1.505

* Within a given series of probes the specific volume at the start and end of each cycle remained substantially constant.

Table 5.5 Testing programme for the undrained loading-unloading probes performed on a reconstituted sample of calcarenite.

Test	Sample diameter (mm)	Stress path	Shearing		
			p_i' (kPa)	$\overline{v}_i$	v_f
RAN6	38	$\delta p' = 0$	450	1.806	1.776
RAN5	83	$\delta p' = 0$	1000	1.832	1.647
RAN4	83	$\delta p' = 0$	2215	1.735	1.54
RAN3	83	$\delta p' = 0$	2300	1.738	1.528
RAN1	83	$\delta p' = 0$	7210	1.550	1.390

Table 5.6 Testing programme performed by Coop and Atkinson (1993) on intact samples of calcarenite.

Test	Cell	Sample diameter (mm)	isotropic compression	Stress path	Shearing		
			v_i		p_i' (kPa)	$\overline{v}_i$	v_f
D1	10 MPa	50	1.443	$\delta p' = 0$	900	1.443	1.585
D2	10 MPa	50	1.432	$\delta p' = 0$	1800	1.432	1.568
D3	10 MPa	50	1.428	$\delta p' = 0$	3460	1.427	1.545
D5	10 MPa	50	1.436	$\delta p' = 0$	5600	1.435	1.525
D4	10 MPa	50	1.432	$\delta p' = 0$	8600	1.430	1.482
A2	70 MPa	50	1.450	$\delta p' = 0$	14400	1.425	1.442
A1	70 MPa	50	1.448	$\delta p' = 0$	60000	1.405	1.360

Table 6.1 Testing programme for intact samples of silica sandstone.

Test	Cell	Sample diameter (mm)	isotropic compression	Stress path	Shearing		
			v_i		p_i' (kPa)	$\bar{v}_i$	v_f
R4	10 MPa	50	1.760	$\delta p' = 0$	900	1.727	1.784
R3	10 MPa	50	1.718	$\delta p' = 0$	1800	1.688	1.740
R8	10 MPa	50	1.780	$\delta p' = 0$	2400	1.730	1.729
R2	10 MPa	50	1.737	$\delta p' = 0$	3470	1.666	1.668
R7	10 MPa	50	1.777	$\delta p' = 0$	5500	1.706	1.647
R1	10 MPa	50	1.754	$\delta p' = 0$	8600	1.672	1.570
R9	70 MPa	50	1.766	$\delta p' = 0$	19100	1.451	1.390
R10	70 MPa	50	1.666	$\delta p' = 0$	36750	1.536	1.367

Table 6.2 Testing programme for reconstituted samples of silica sandstone.

Series	No. of cycles	p'_i (kPa)	q_{max} (kPa)	$v^{(*)}$
A	5	1760	450	1.445
B	5	1760	800	1.445
C	5	1760	2100	1.445
D	3	1760	4200	1.444
E	3	1760	6000	1.443

* Within a given series of probes the specific volume at the start and end of each cycle remained substantially constant.

Table 6.3 Testing programme for the undrained loading-unloading probes performed on an intact sample of silica sandstone.

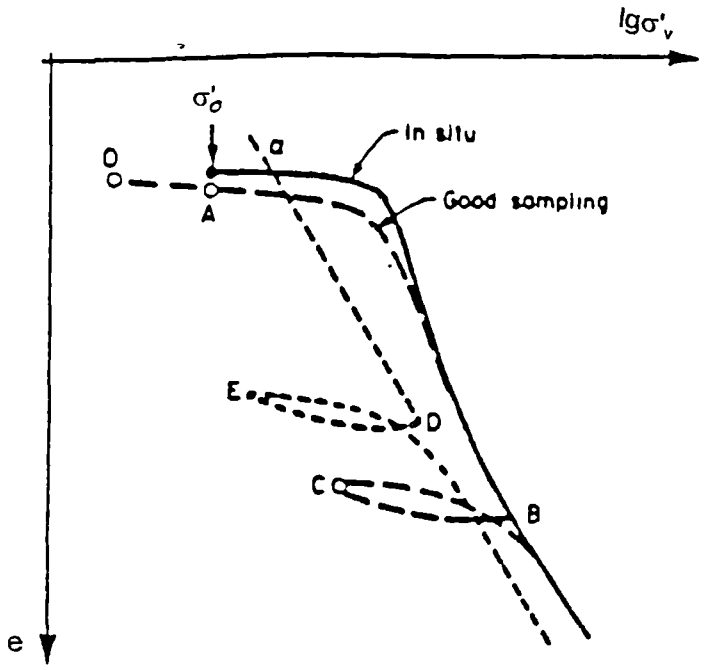

Figure 2.1 One-dimensional compression for a reconstituted sample, a good quality undisturbed sample and a natural clay in situ. (after Tavenas and Leroueil, 1987).

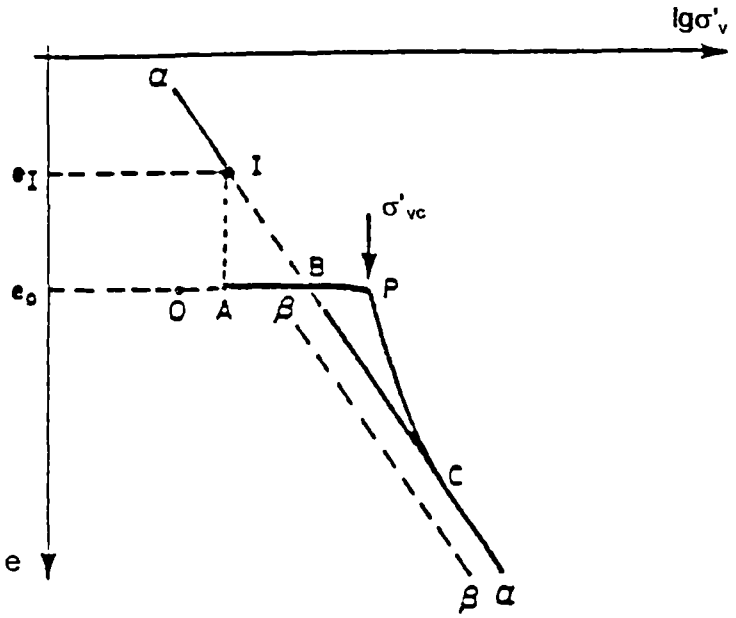

Figure 2.2 Schematic description of the consolidation of a natural clay deposit (after Tavenas and Leroueil, 1987).

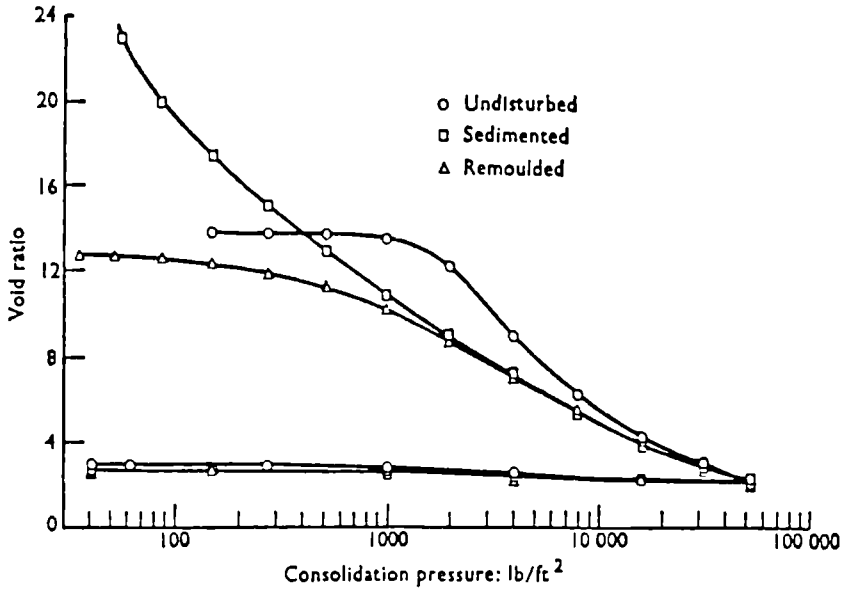

Figure 2.3 One-dimensional compression of Mexico City clay (after Mesri et al., 1975).

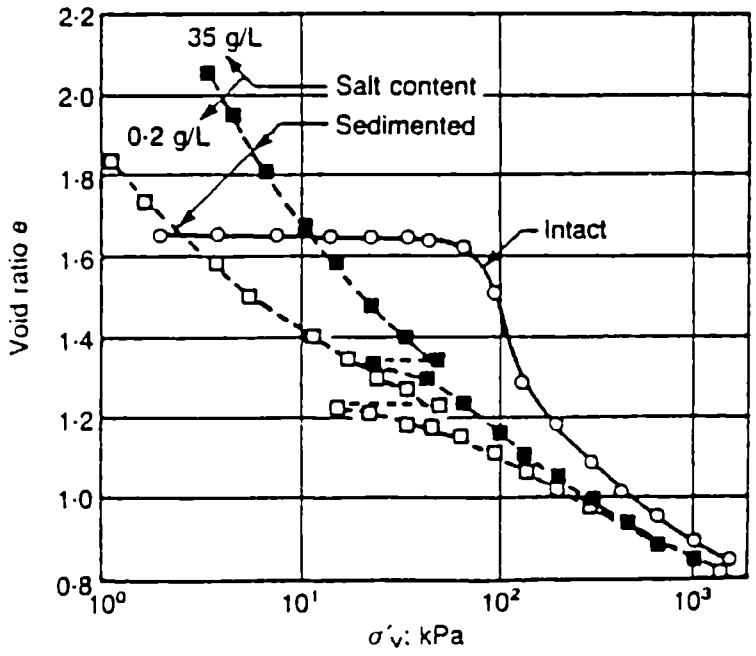

Figure 2.4 One-dimensional compression of the Grande Baleine clay (after Locat and Lefebvre, 1985).

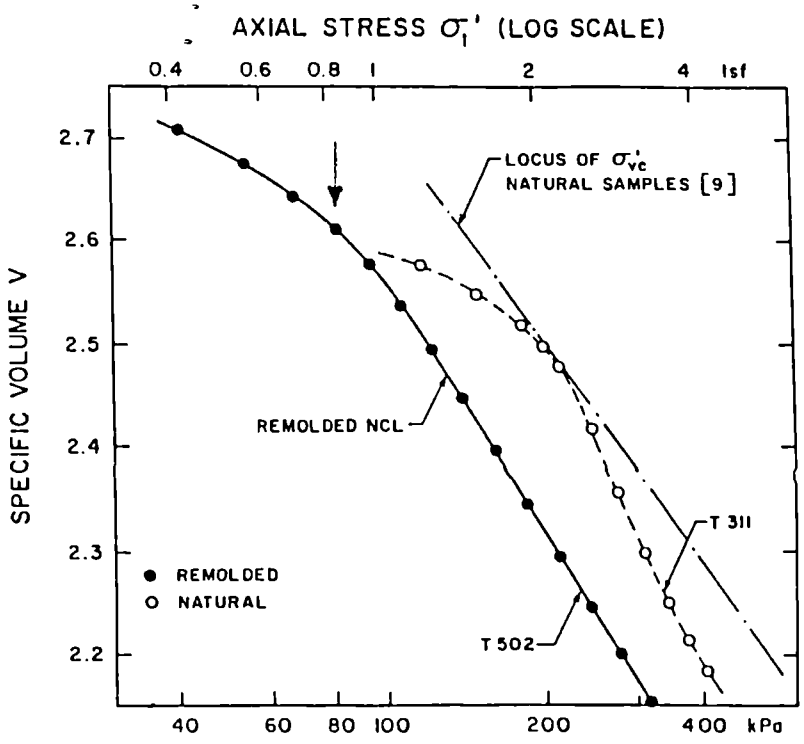

Figure 2.5a One-dimensional compression of Winnipeg clay (after Graham and Li, 1985).

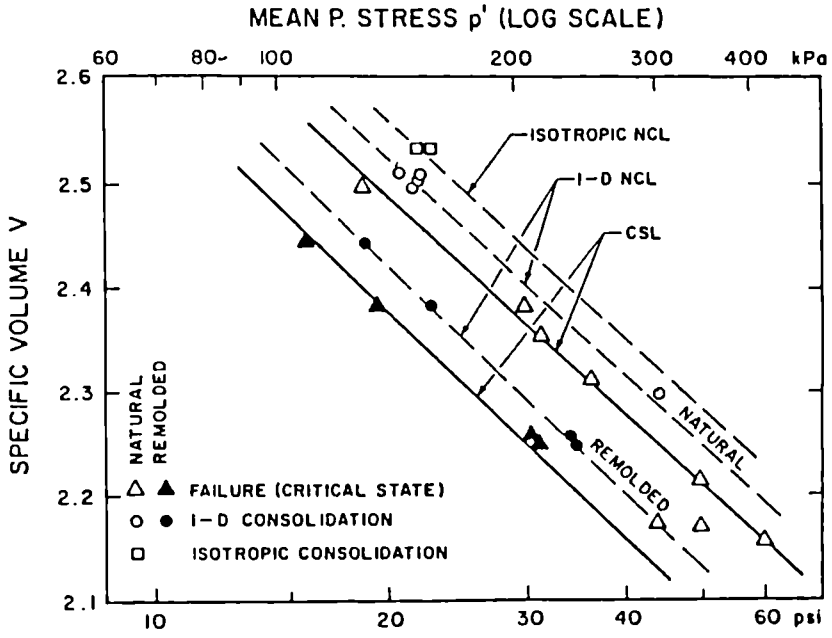

Figure 2.5b Loci of isotropic and one-dimensional preconsolidation pressures (σ'_{vc} in Figure 2.5a) and critical states for Winnipeg clay (after Graham and Li, 1985).

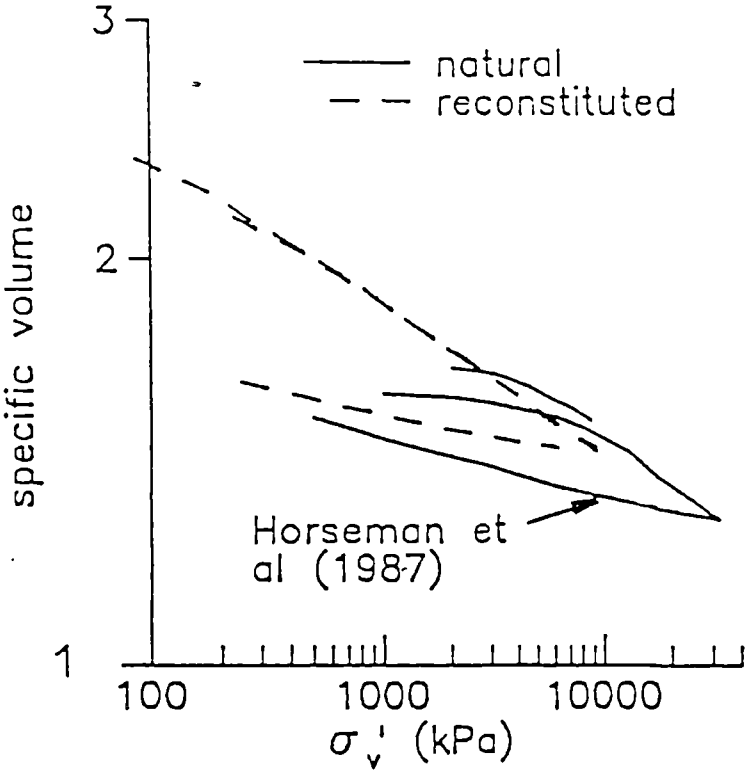

Figure 2.6 One-dimensional compression of Boom clay (after Coop et al., 1995).

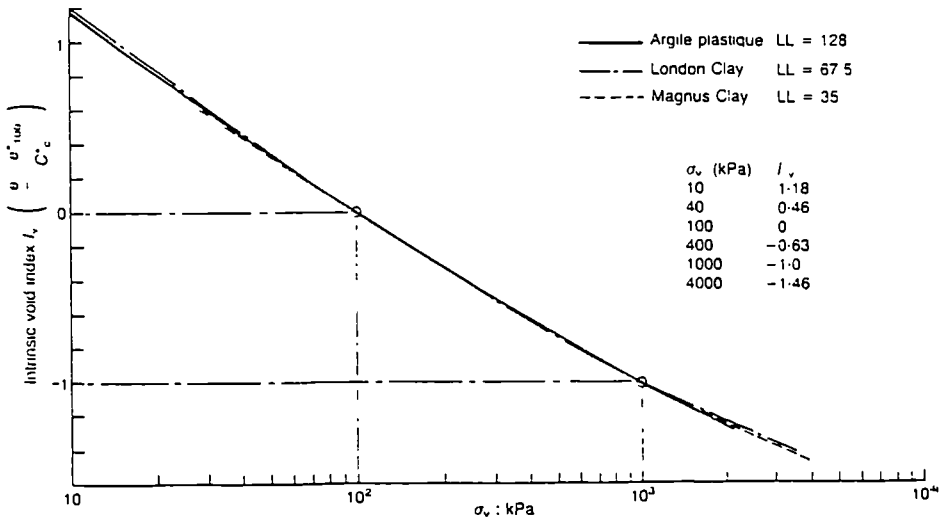

Figure 2.7 Normalized one-dimensional compression curves of reconstituted clays (after Burland, 1990).

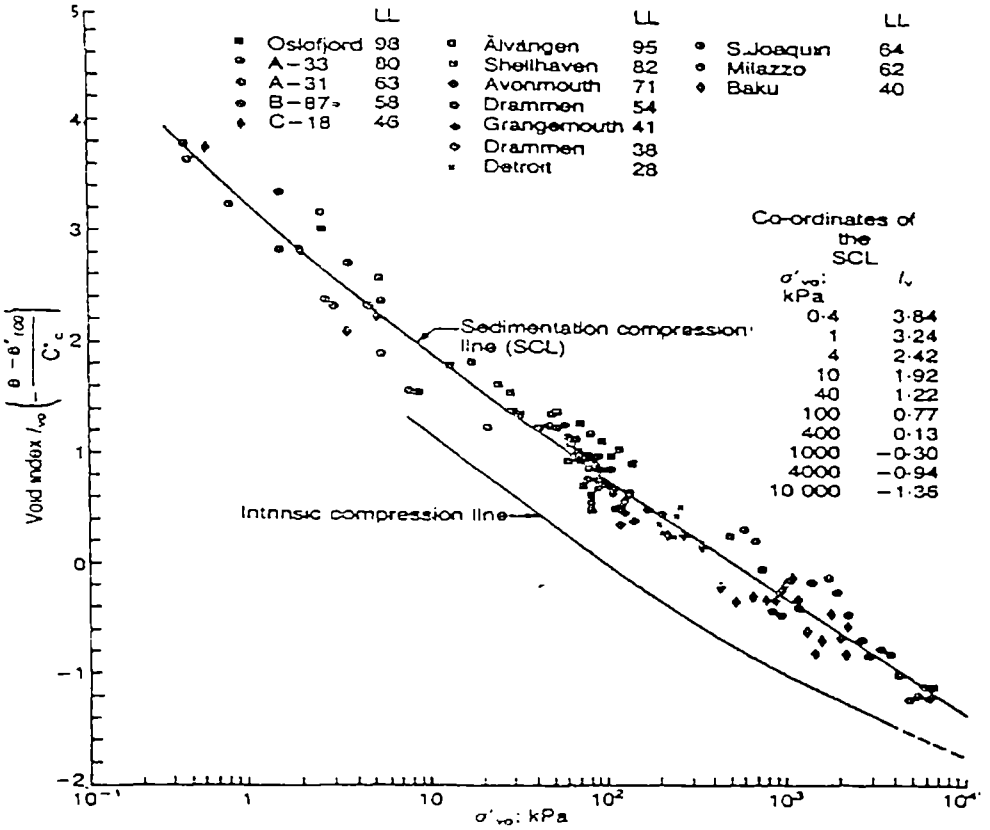

Figure 2.8 Sedimentation and intrinsic compression lines for normally consolidated clays (after Burland, 1990).

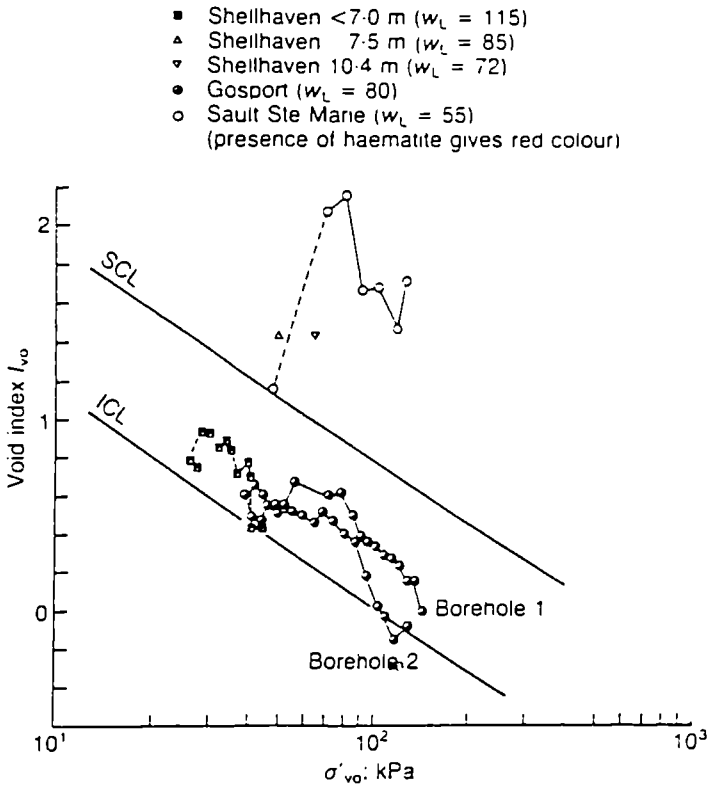

Figure 2.9 Examples of clays having in situ states which are above and below the sedimentation compression line (after Burland, 1990).

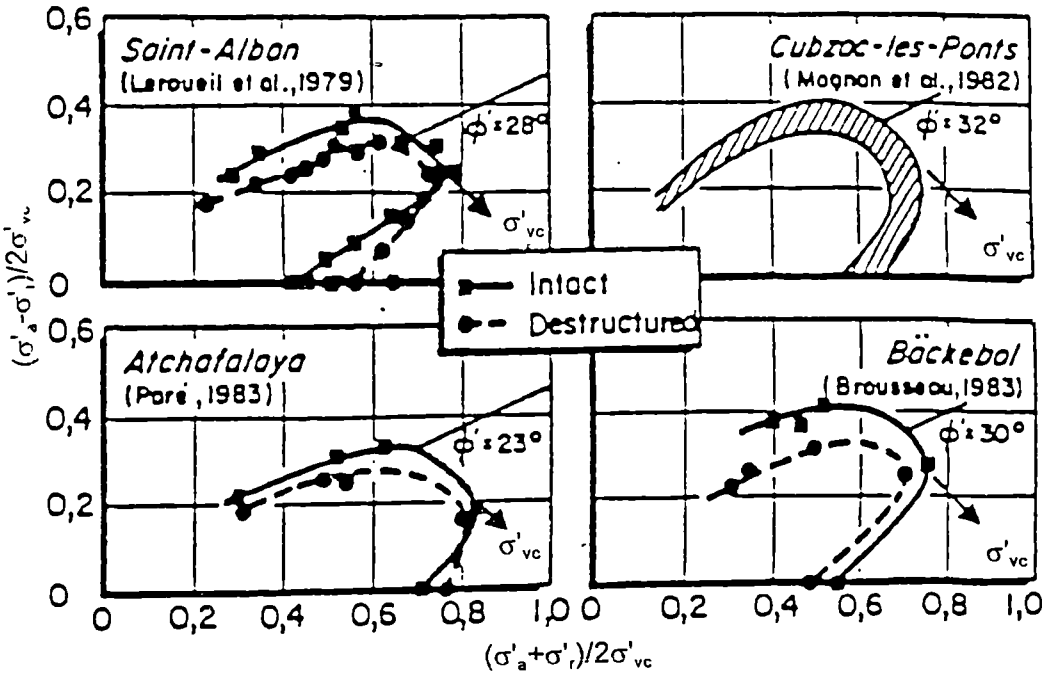

Figure 2.10 State boundary surfaces for intact and destructured clays (after Tavenas and Leroueil, 1987).

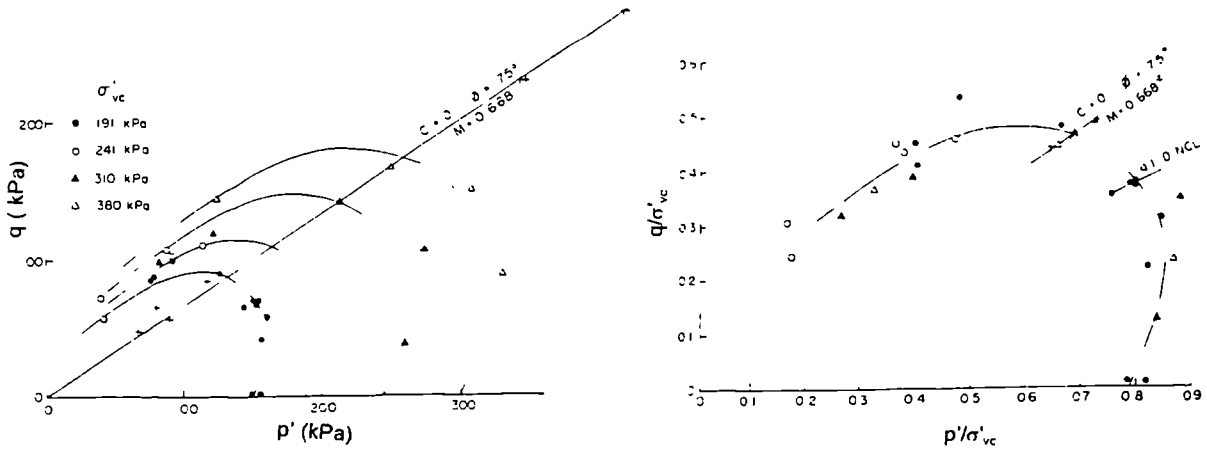

(a) (b)

Figure 2.11 Yield states from drained and undrained triaxial tests on Winnipeg clay in: (a) stress space; (b) normalized stress space (after Graham et al., 1983).

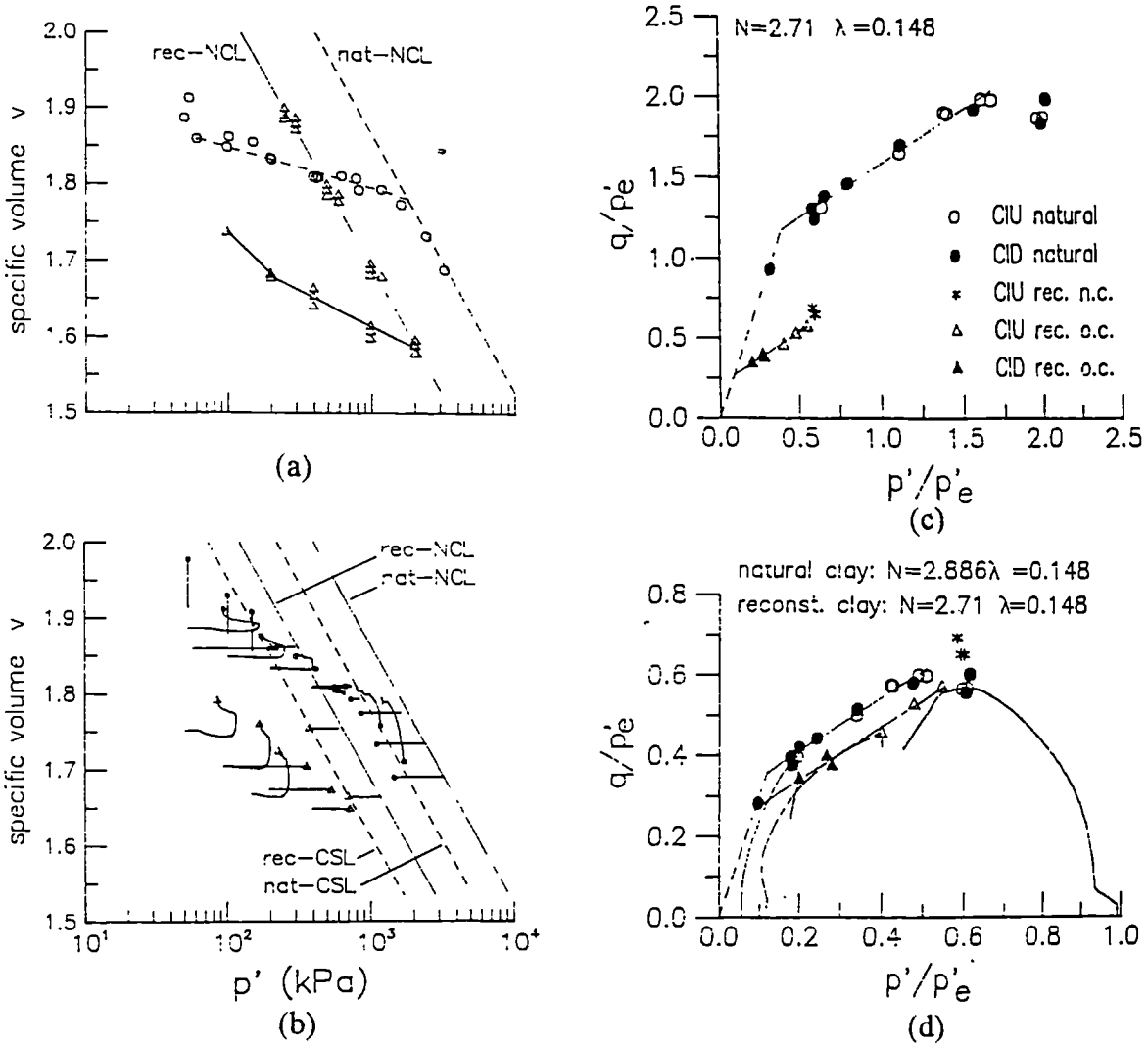

Figure 2.12 Comparison between natural and reconstituted Vallerica clay: (a) isotropic compression; (b) stress-volume paths during shearing ; (c) peak states normalized by a p_e' taken on the reconstituted NCL; (d) peak states normalized by a p_e' taken on the appropriate NCL (after Rampello et al., 1993).

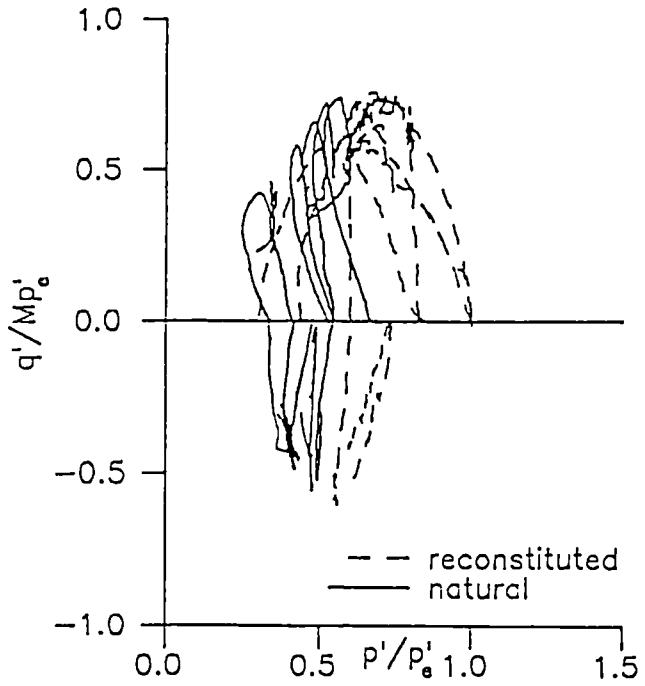

Figure 2.13 Normalized stress paths for Boom clay in undrained triaxial compression and extension tests (after Coop et al., 1995).

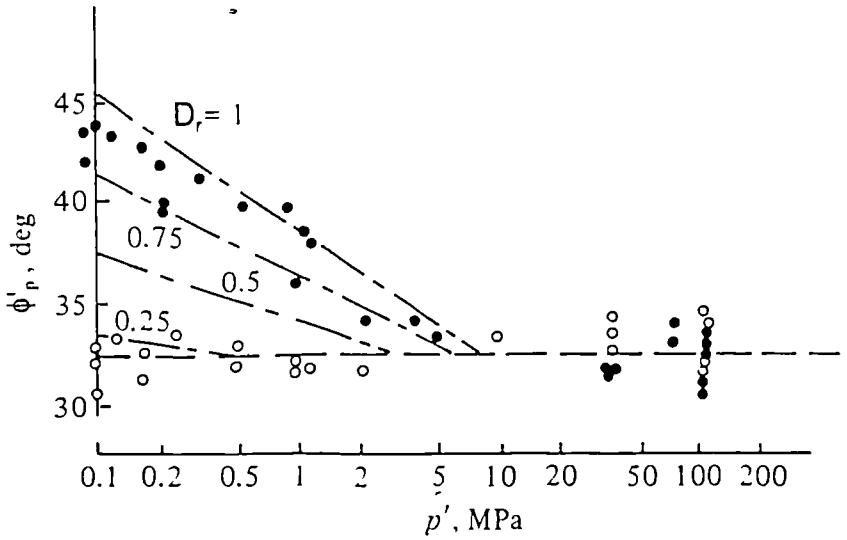

Figure 2.14 Variation of the peak angle of friction with mean effective stress and relative density D_r for initially loose (○) and dense (●) samples of Chattahoochee River sand (after Vesic and Clough, 1968).

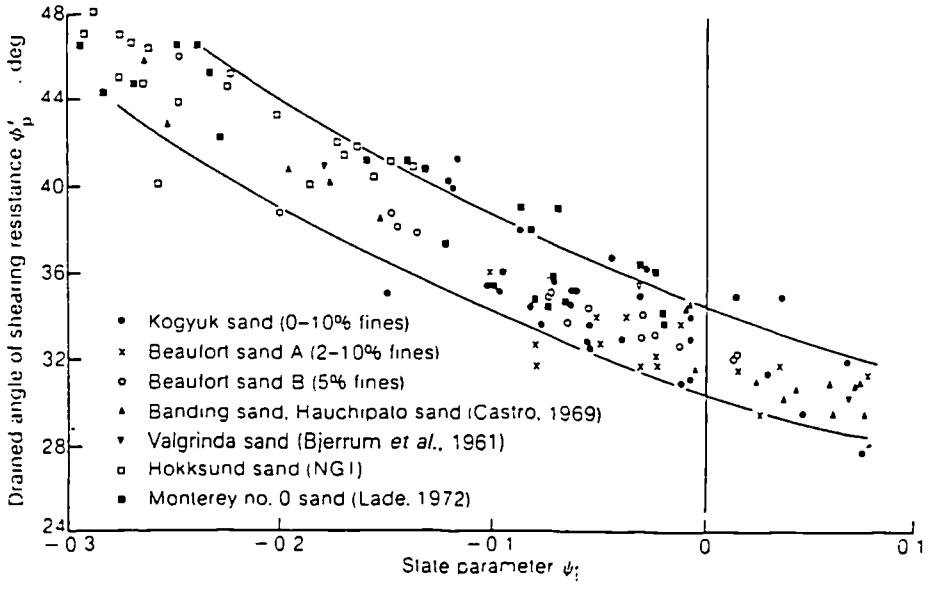

Figure 2.15 Variation of the peak angle of friction of sands with the state parameter ψ_i (after Been and Jefferies, 1985).

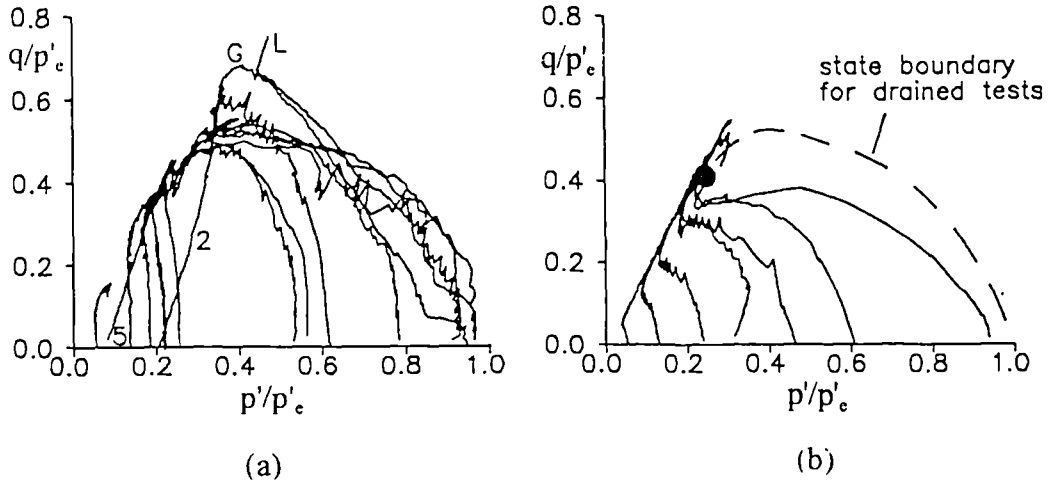

Figure 2.16 Normalized stress paths for Dog's Bay sand: (a) drained tests; (b) undrained tests (after Coop and Lee, 1993).

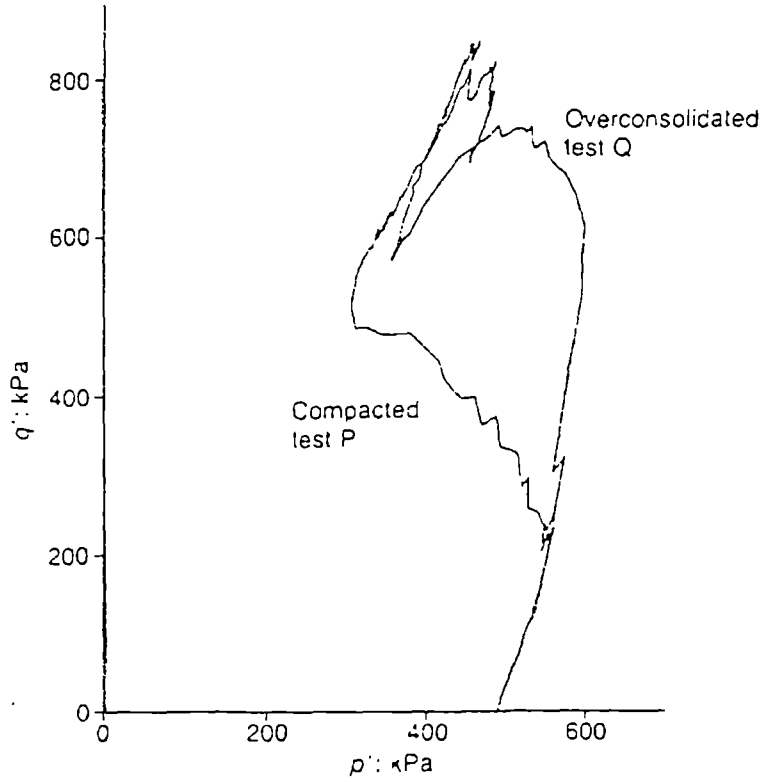

Figure 2.17 Stress paths for compacted and overconsolidated samples of a carbonate sand in undrained triaxial tests (after Coop and Lee, 1993).

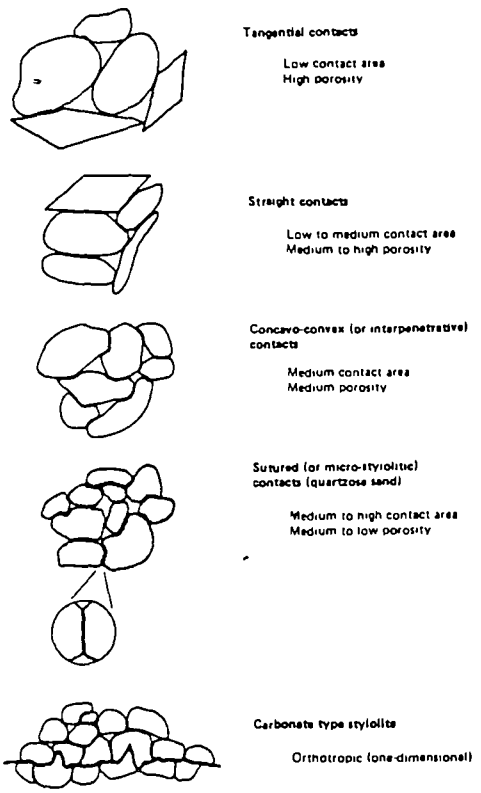

Figure 2.18 Intergranular fabric classification (after Dusseault and Morgenstern, 1979).

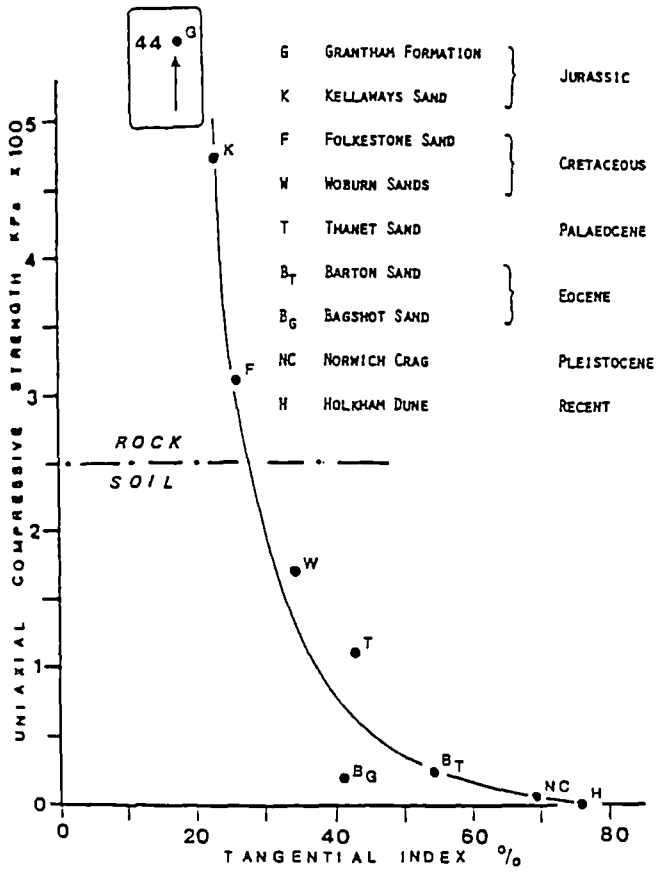

Figure 2.19 Unconfined compressive strength as a function of the tangential index (TI %) for a group of locked sands from the U.K. (after Dobereiner and De Freitas, 1986).

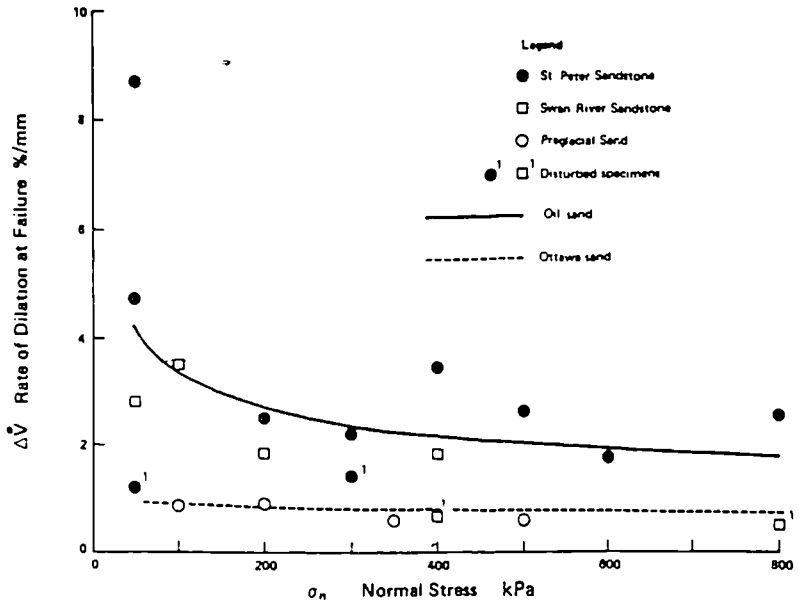

Figure 2.20 A comparison between the rate of dilation at failure for shear box tests on locked sands (oil sands) and Ottawa sand (after Dusseault and Morgenstern, 1979).

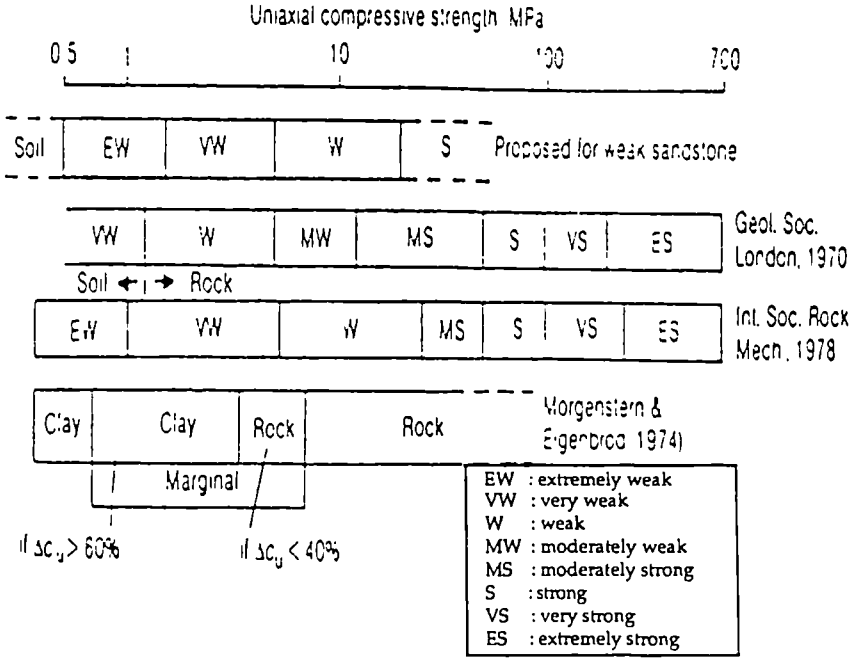

Figure 2.21 Some classification systems of soils and rocks (after Dobereiner and De Freitas, 1986).

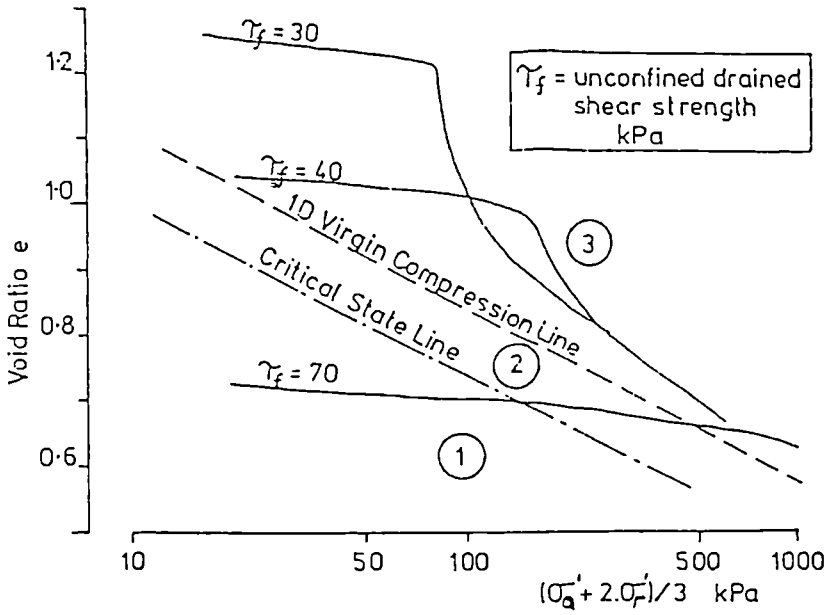

Figure 2.22 One-dimensional compression for three samples of an artificially cemented soil with the same grading and degree of bonding but different initial void ratios (after Maccarini, 1987).

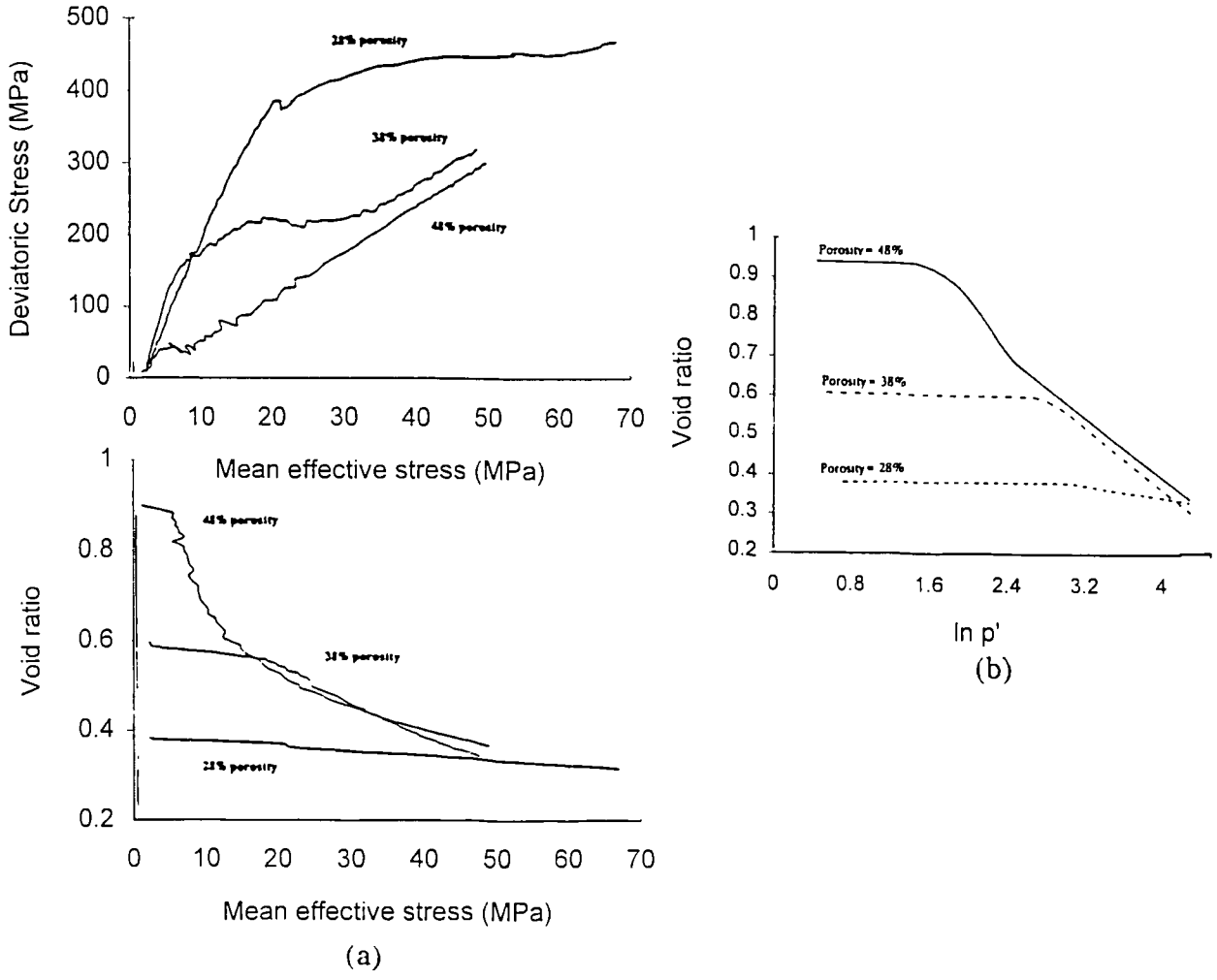

Figure 2.23 One-dimensional compression for samples of chalk with different initial void ratios: (a) after Leddra, 1990; (b) after Petley et al., 1993.

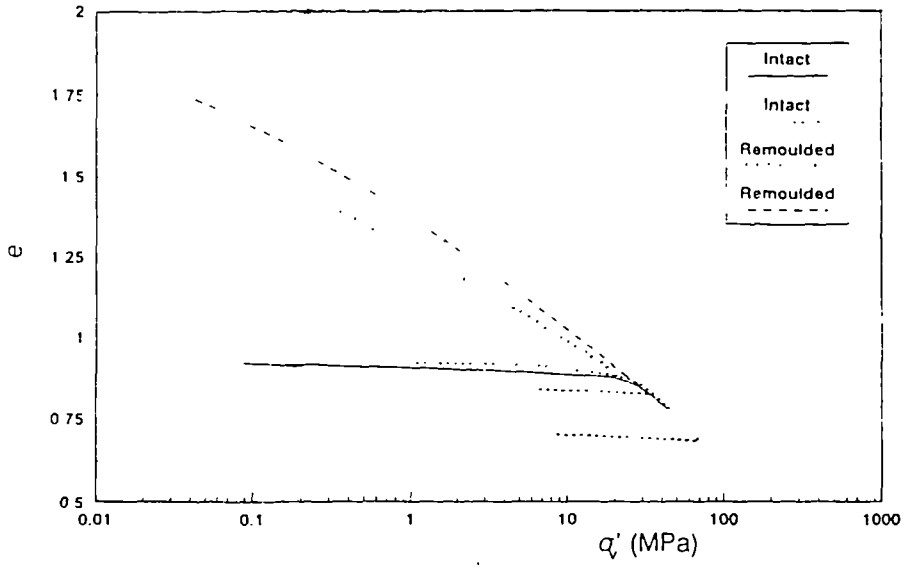

Figure 2.24 One-dimensional compression for intact and reconstituted samples of a fine grained tuff (after Aversa, 1991).

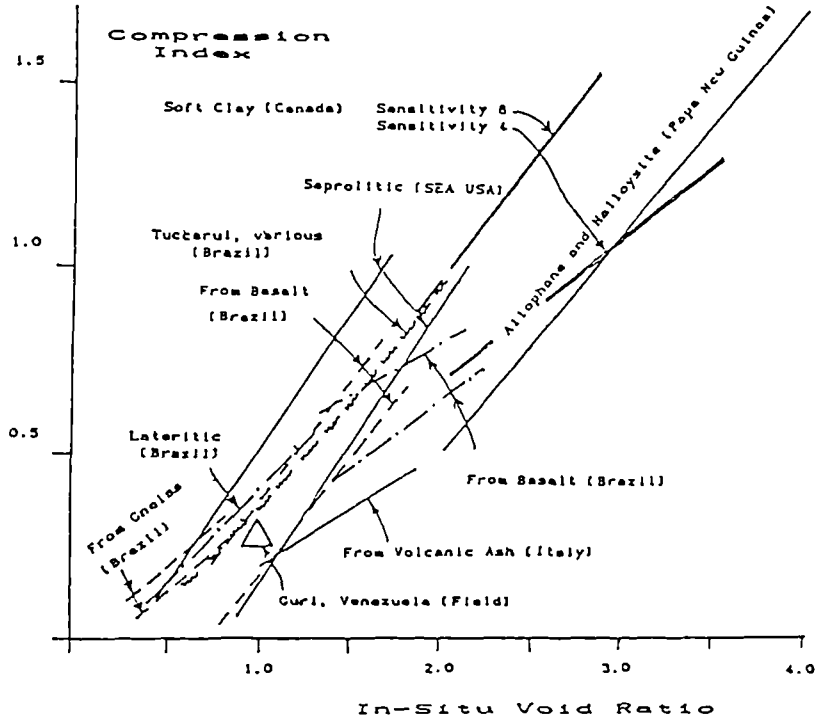

Figure 2.25 Relationship between compression index and initial void ratio in one-dimensional compression (after Vaughan, 1988).

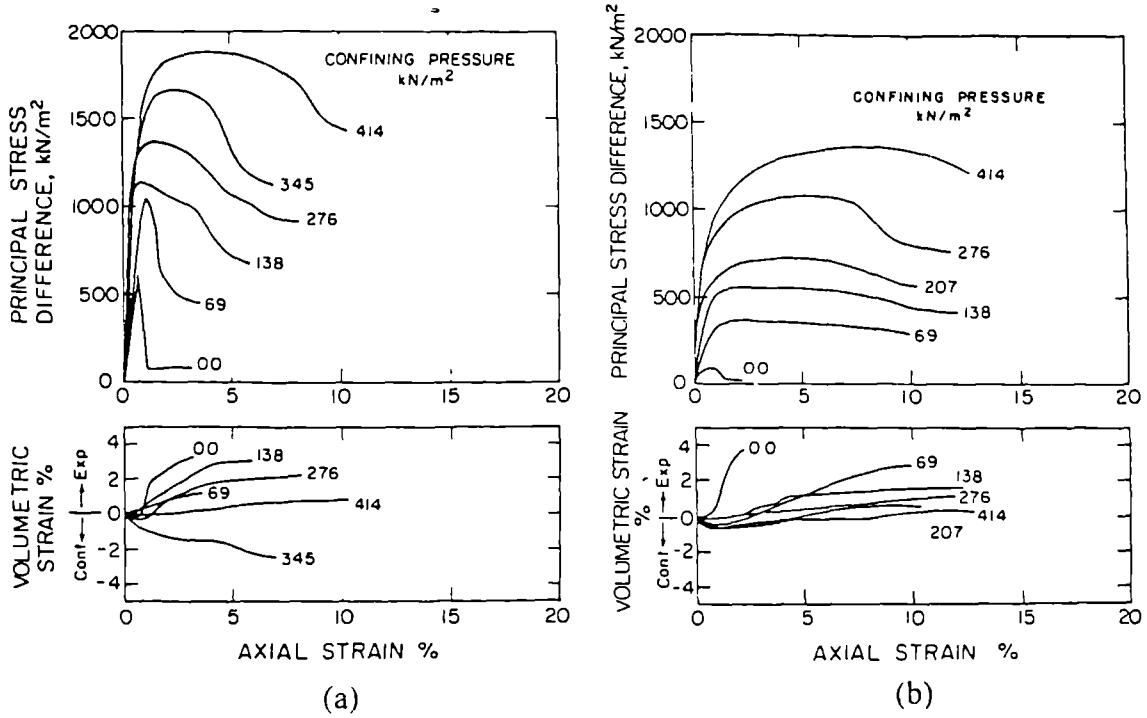

Figure 2.26 Shear behaviour in drained triaxial compression for a naturally cemented sand: (a) moderately cemented; (b) weakly cemented (after Clough et al., 1981).

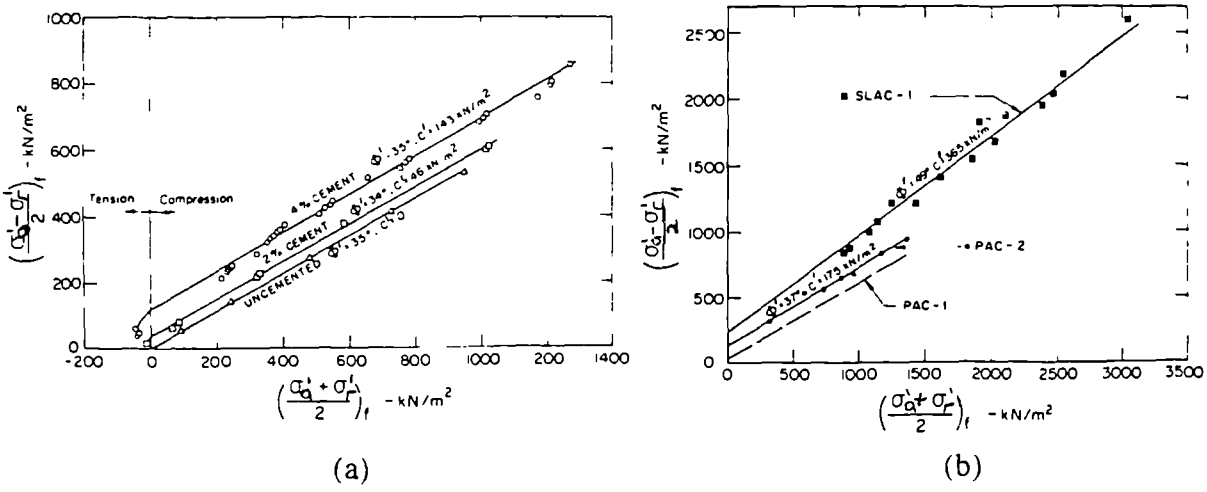

Figure 2.27 Peak strength envelopes (after Clough et al., 1981): (a) artificially cemented sand; (b) naturally cemented sand with stronger bonding (SLAC-1) and weaker bonding (PCA-1 and PCA-2).

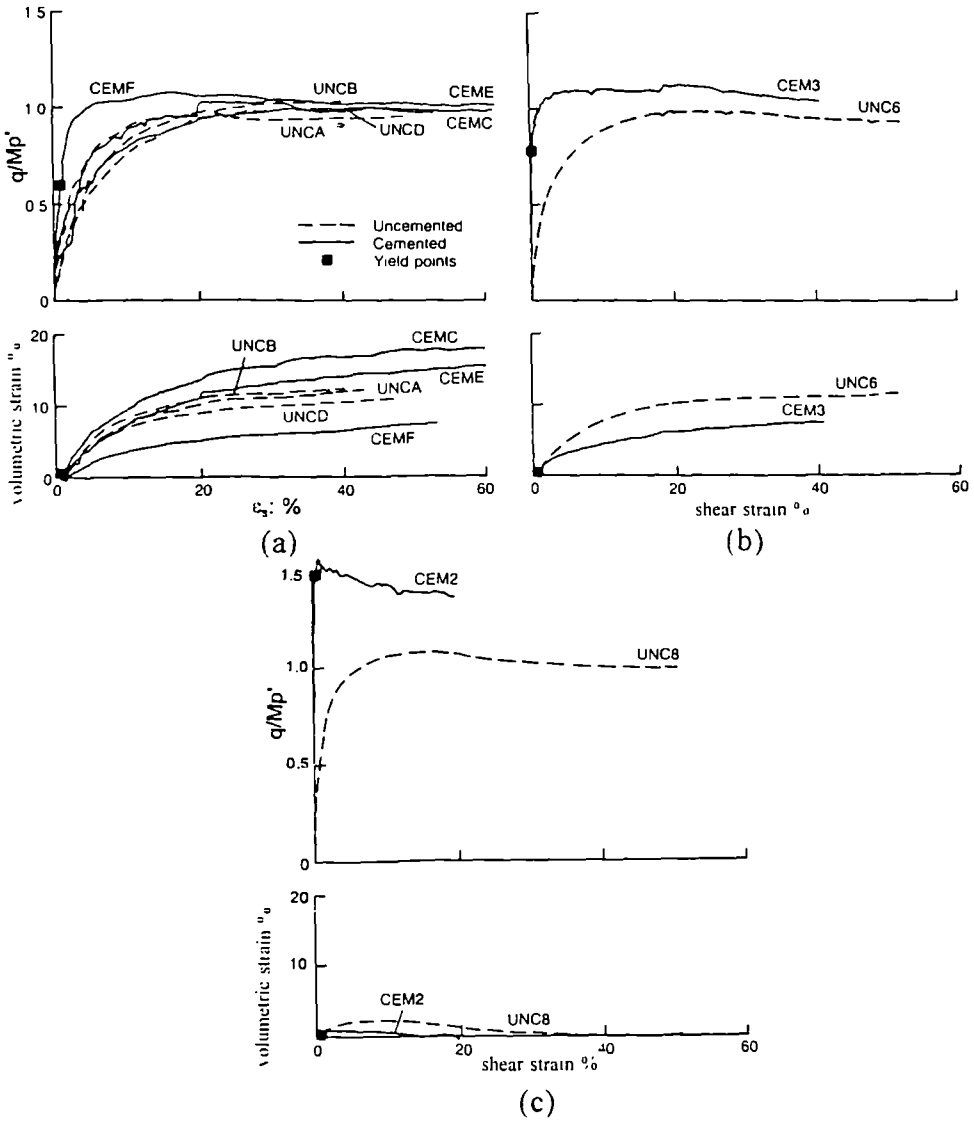

Figure 2.28 Comparison between the shear behaviour of an artificially cemented and an uncemented carbonate sand: (a) at high confining pressures; (b) at intermediate confining pressures; (c) at low confining pressures (after Coop and Atkinson, 1993).

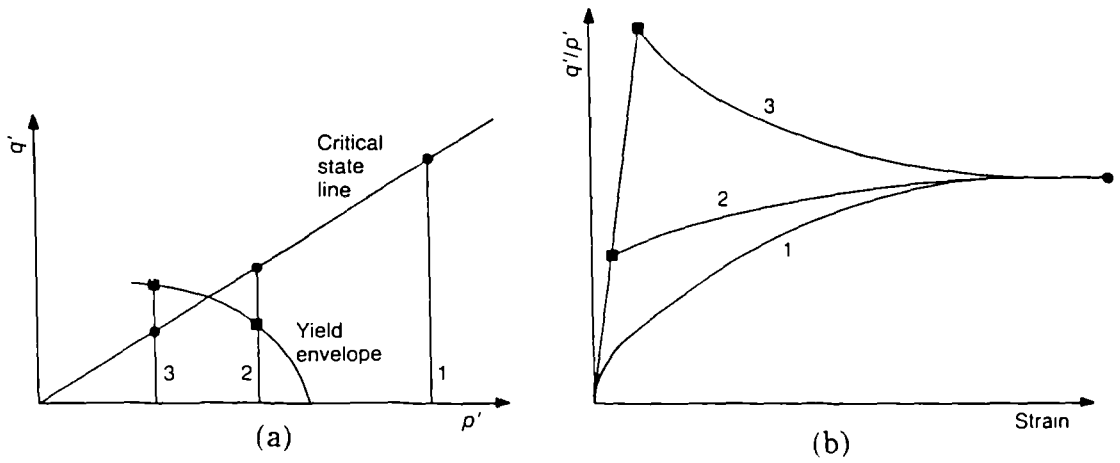

Figure 2.29 Idealized shear behaviour of cemented soils: (a) stress paths: (b) stress-strain behaviour (after Coop and Atkinson, 1993).

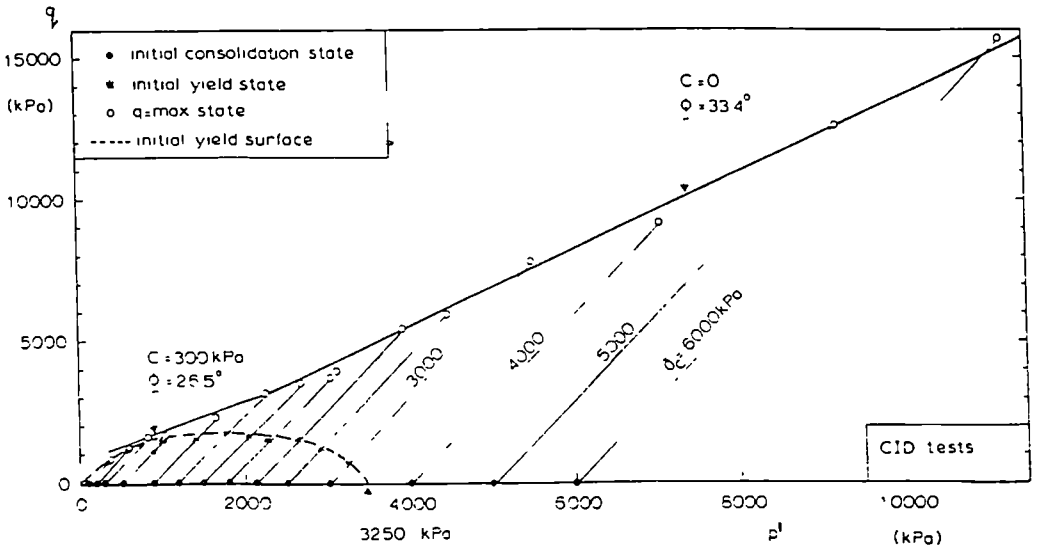

Figure 2.30 Stress paths for drained triaxial tests on a marl from the Corinth Canal (Anagnostopoulos et al., 1991).

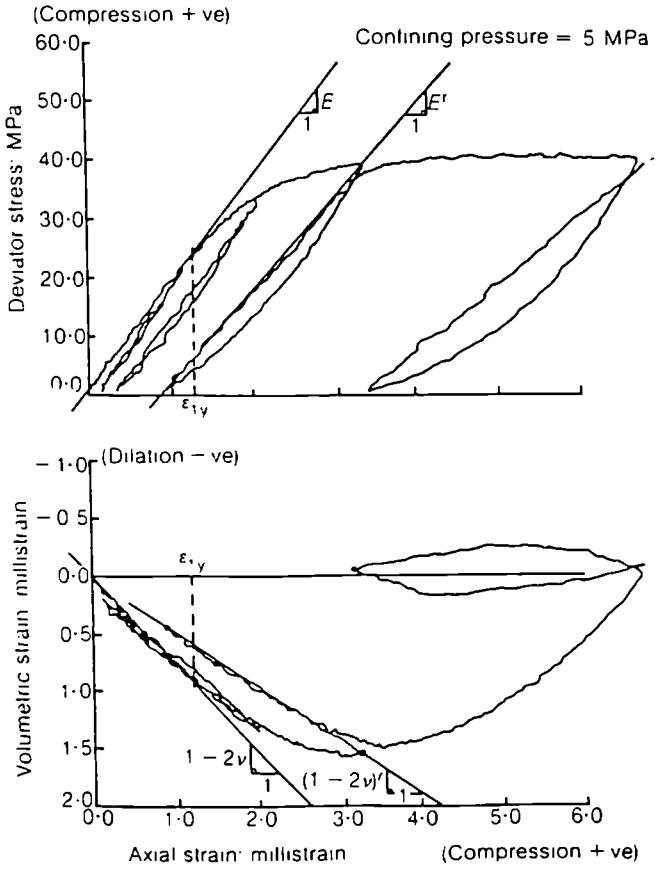

Figure 2.31 Determinations of the yield point for an oolitic limestone (after Elliott and Brown, 1985).

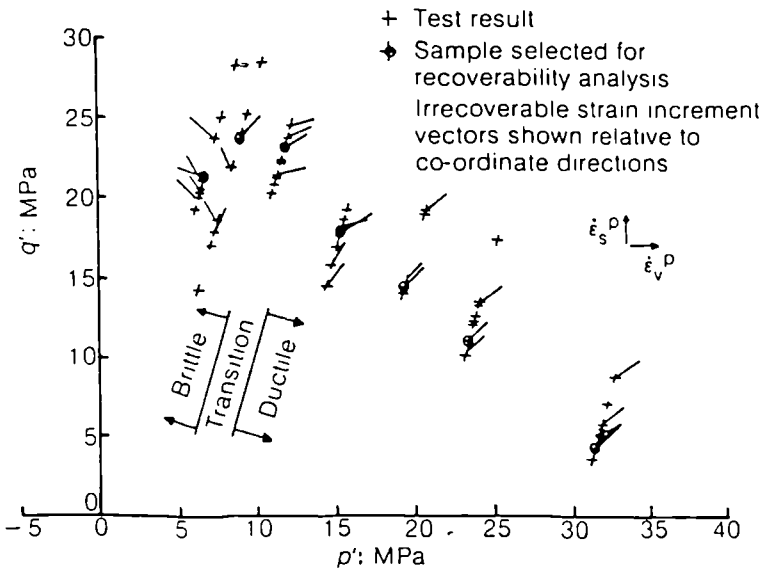

Figure 2.32 Stresses at yield for an oolitic limestone (after Elliott and Brown, 1985).

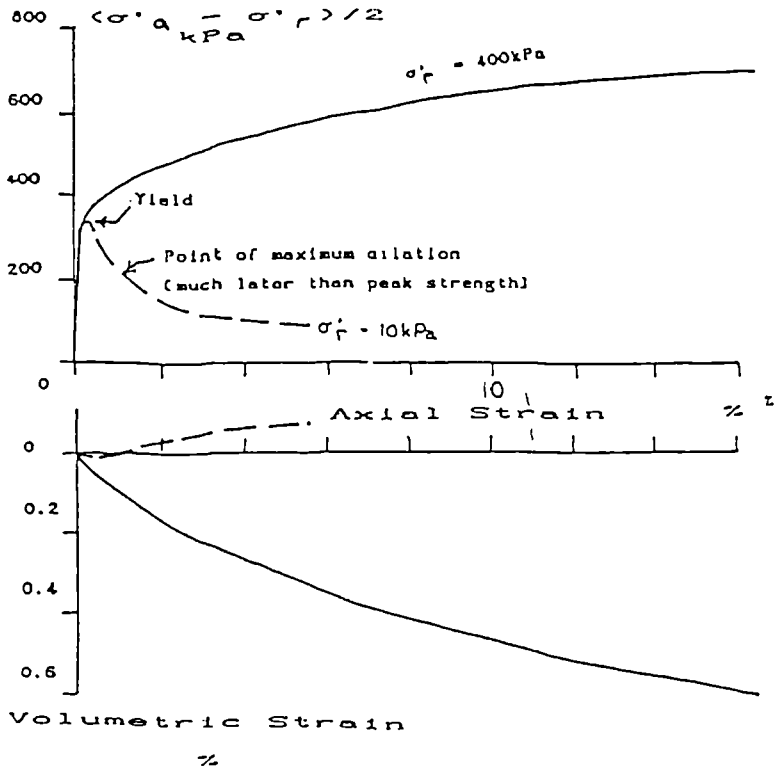

Figure 2.33 Drained triaxial tests on a residual soil from basalt (after Maccarini, 1987).

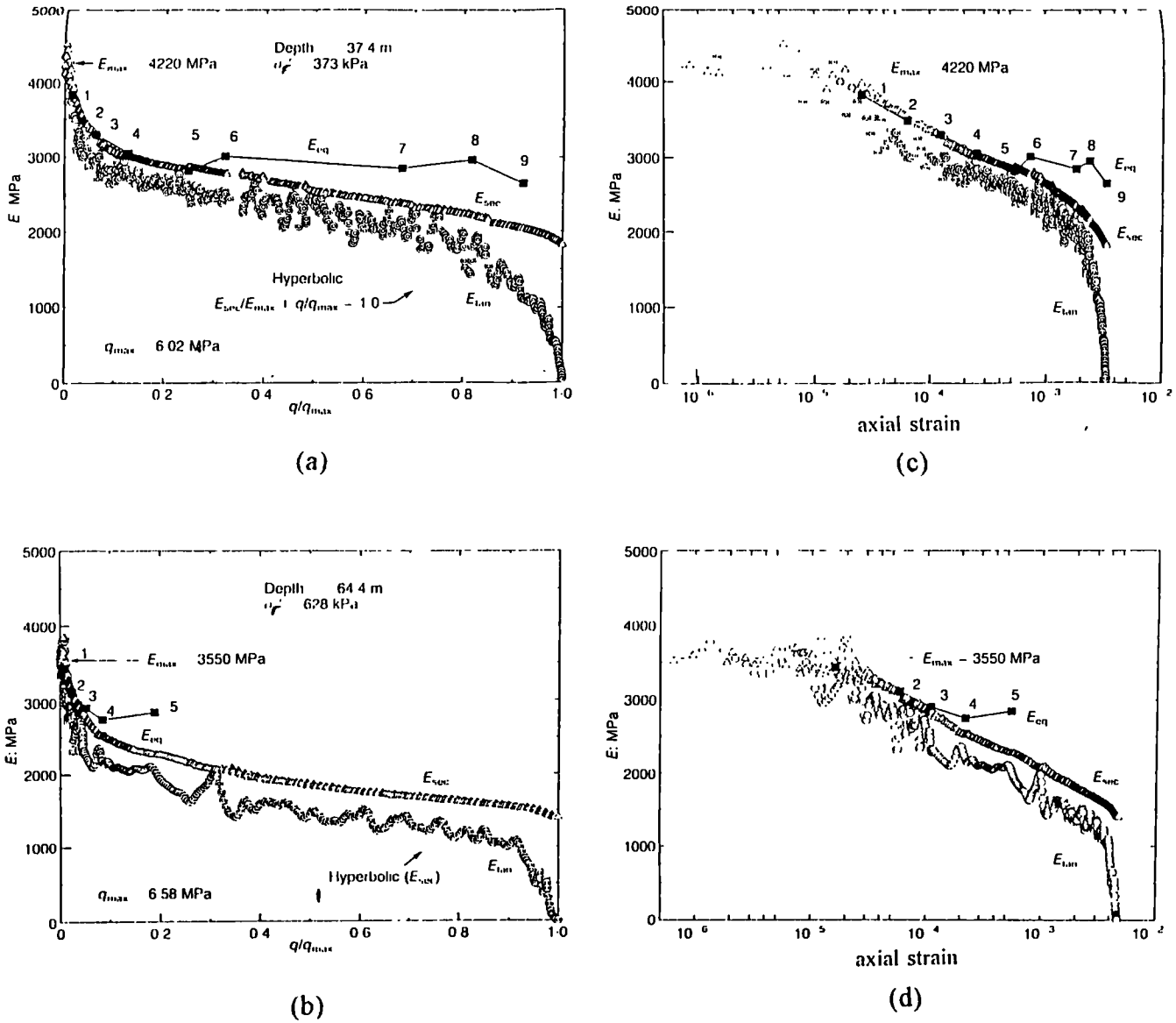

Figure 2.34 Variation of Young's moduli E_{sec}, E_{tan} and E_{eq} with: (a) and (b) q/q_{max}; (c) and (d) axial strains (after Kim et al., 1994).

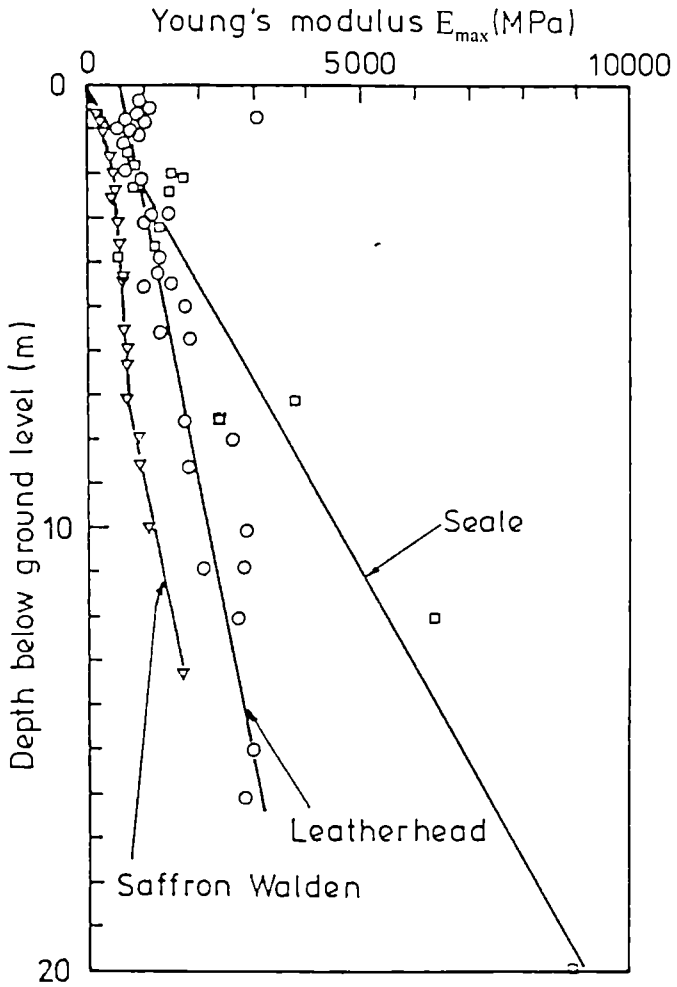

Figure 2.35 Variation of initial Young's modulus with depth for chalk at three different sites obtained from surface wave geophysics (Clayton, 1989).

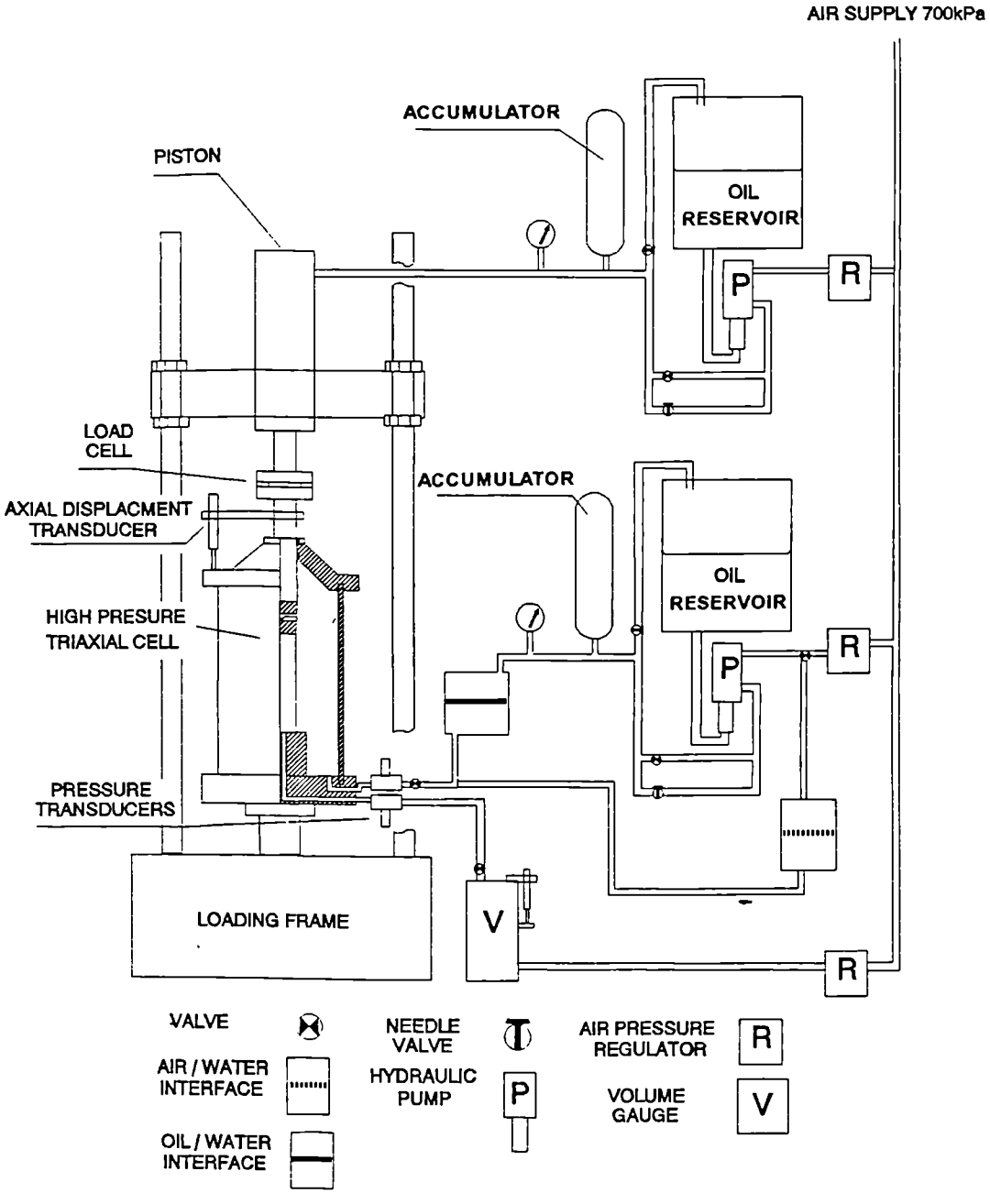

Figure 3.1 Schematic diagram of the high pressure system.

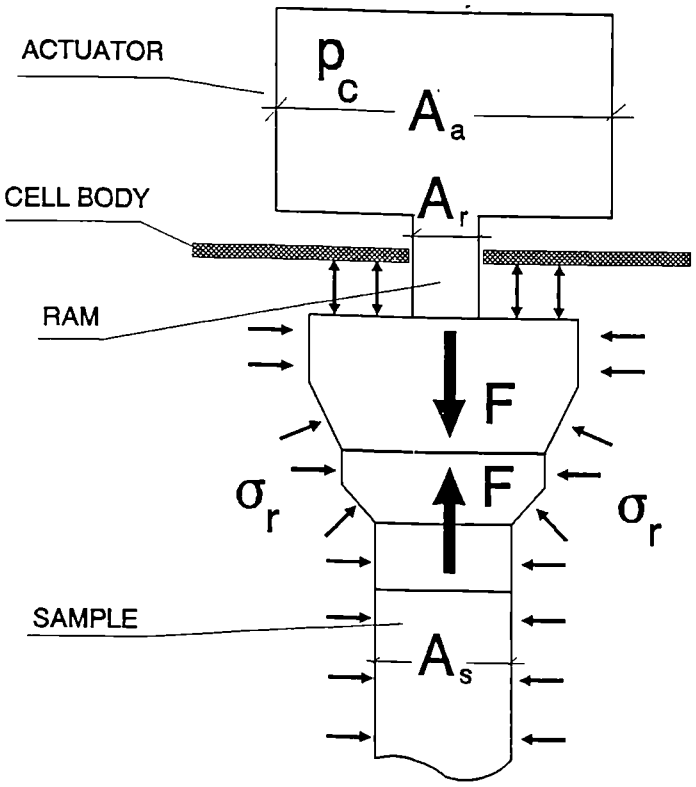

Figure 3.2 Schematic diagram of the axial loading system.

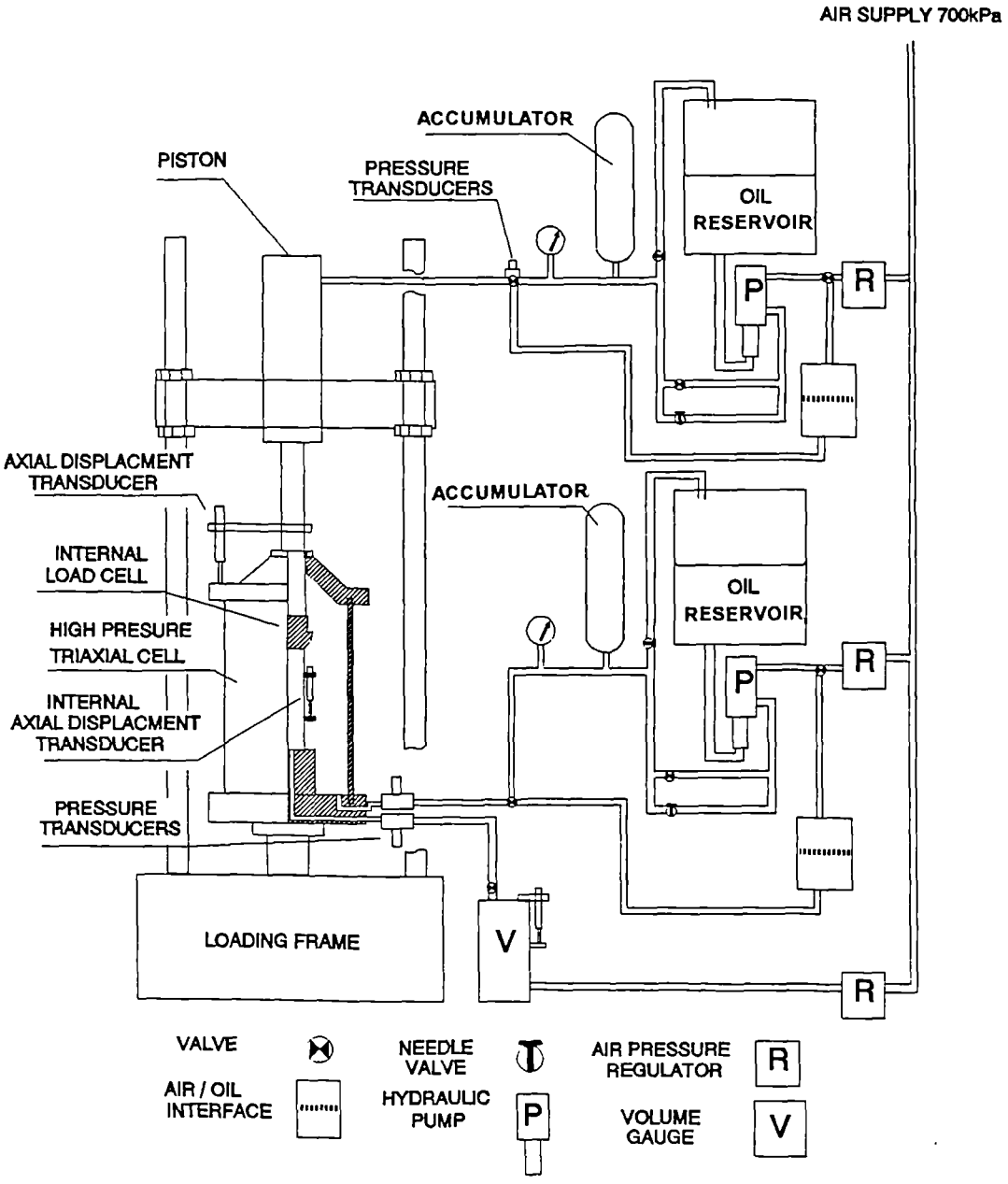

Figure 3.3 Schematic diagram of the 10 MPa triaxial system after modifications.

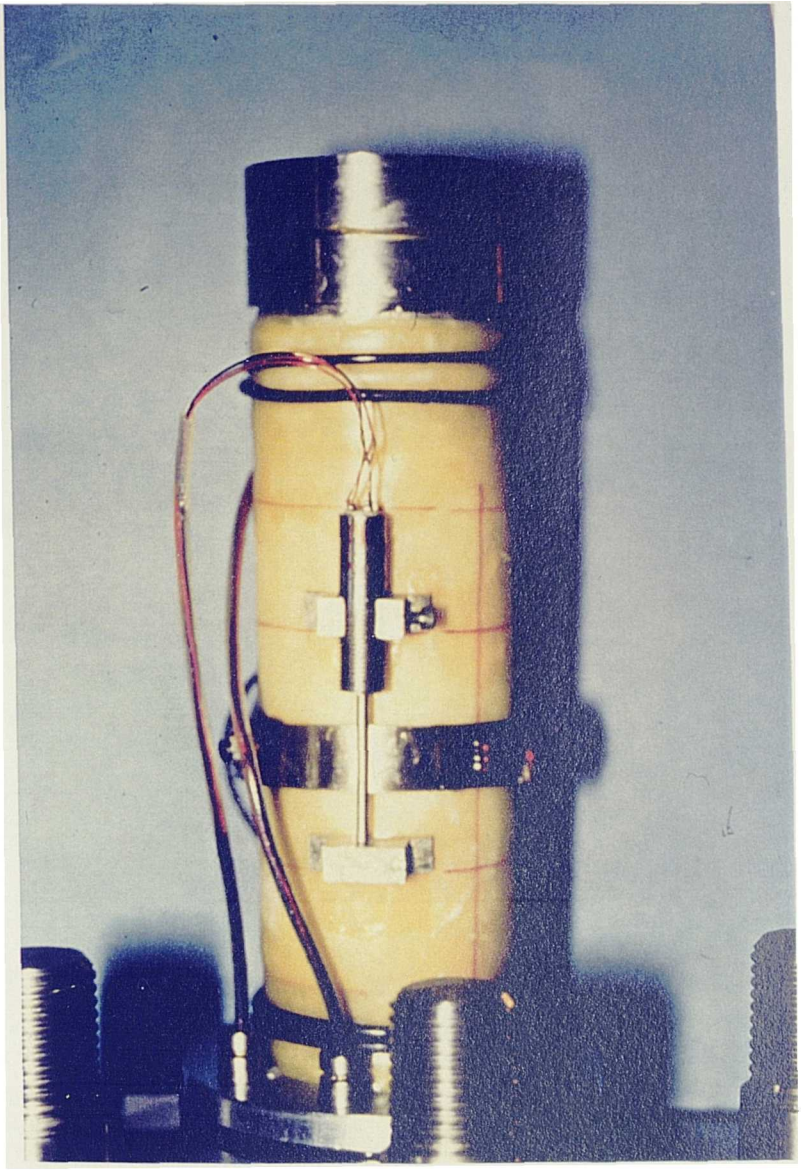

Figure 3.4 Arrangement of LVDTs and radial strain belt in the 70 MPa apparatus.

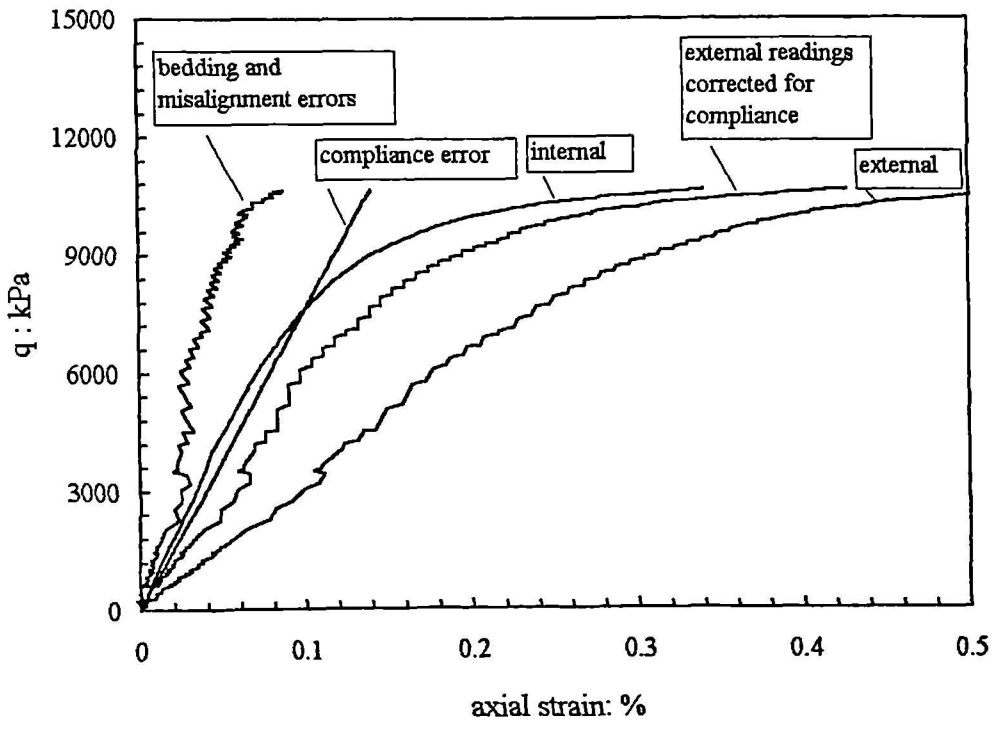

Figure 3.5 Errors affecting external axial strain measurements.

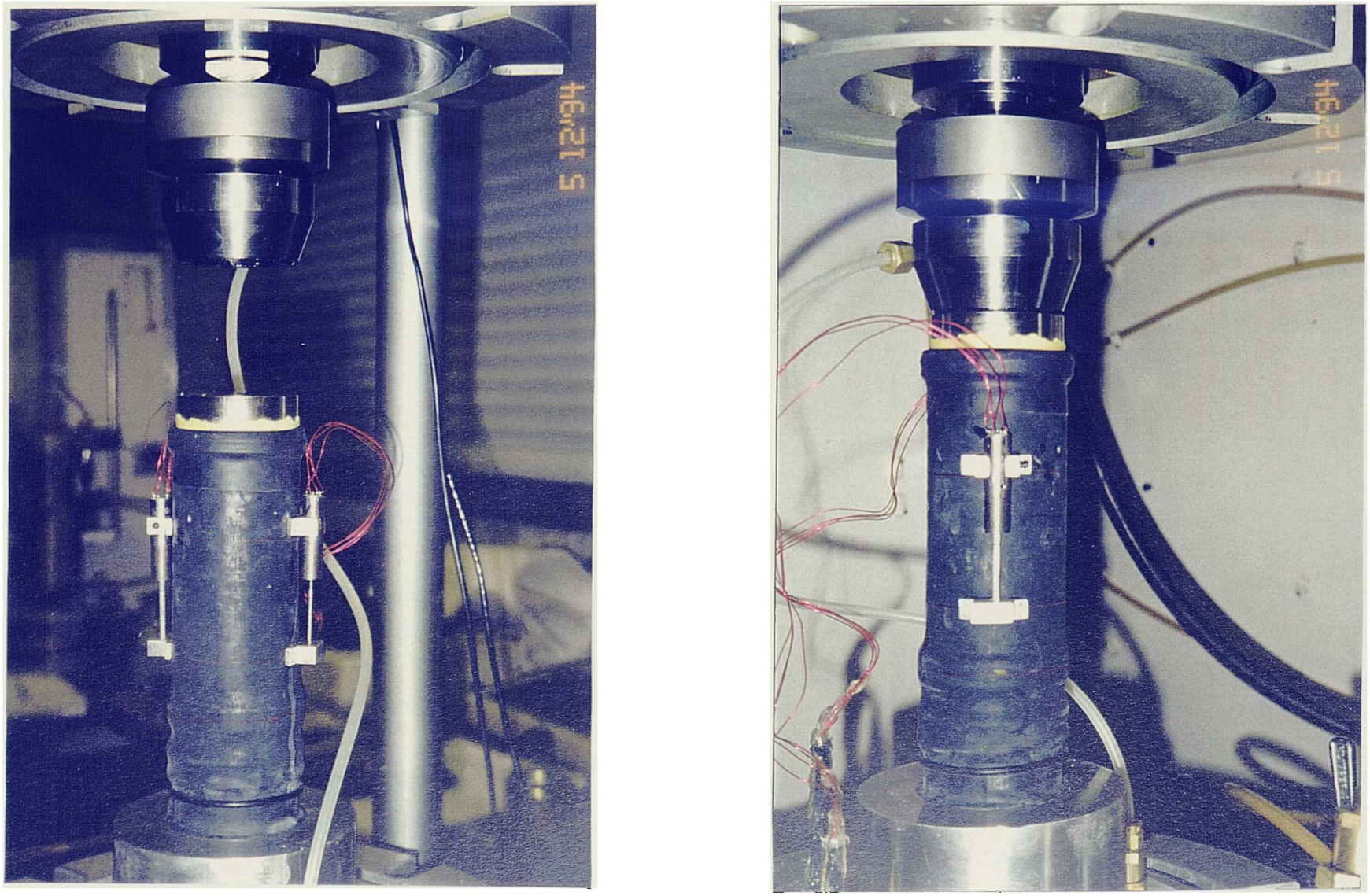

Figure 3.6 Arrangement of LVDTs in the 10 MPa apparatus.

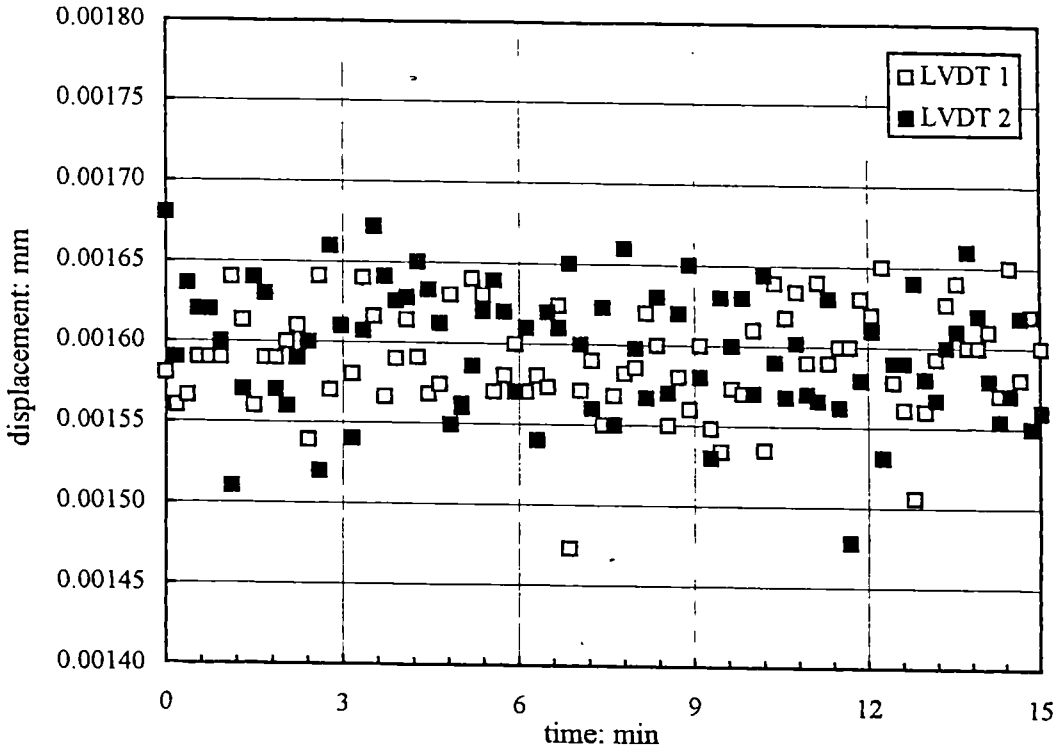

(a)

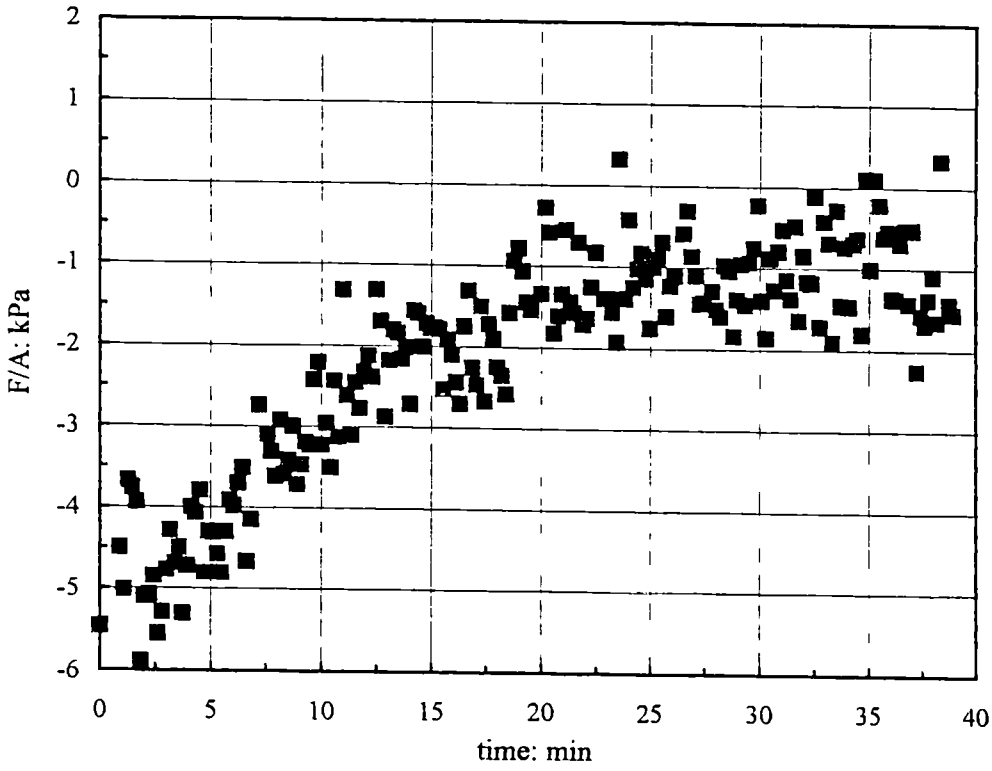

(b)

Figure 3.7 Noise from (a) LVDTs and (b) internal load cell.

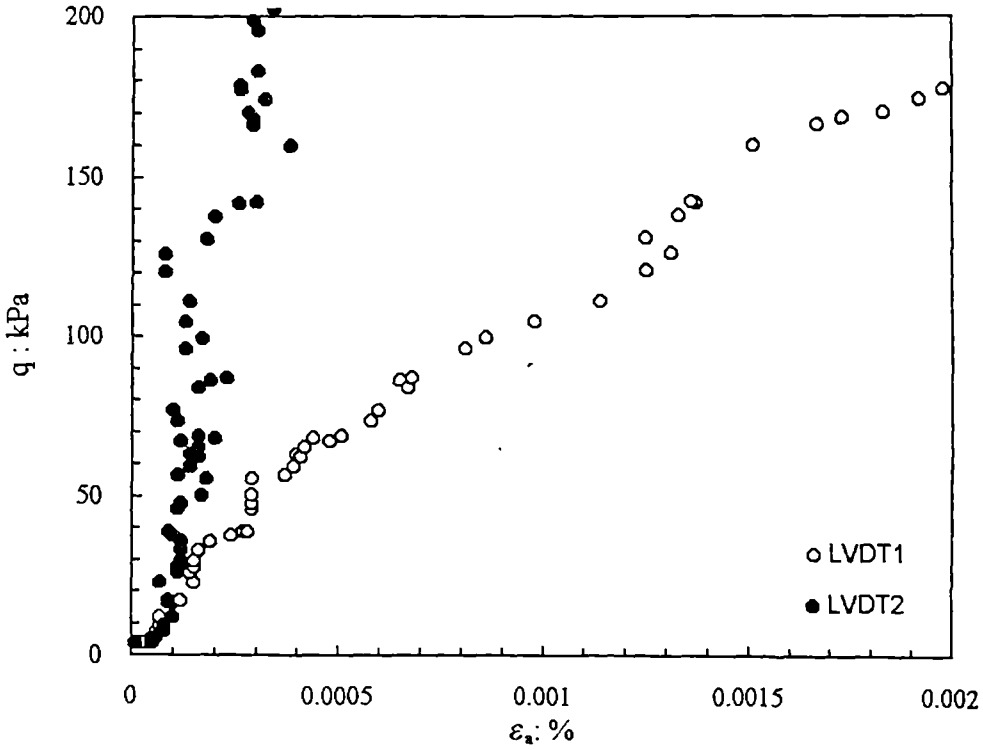

Figure 3.8 Stress-strain data showing non-uniformity of strains prior to changing the setting up and testing procedures.

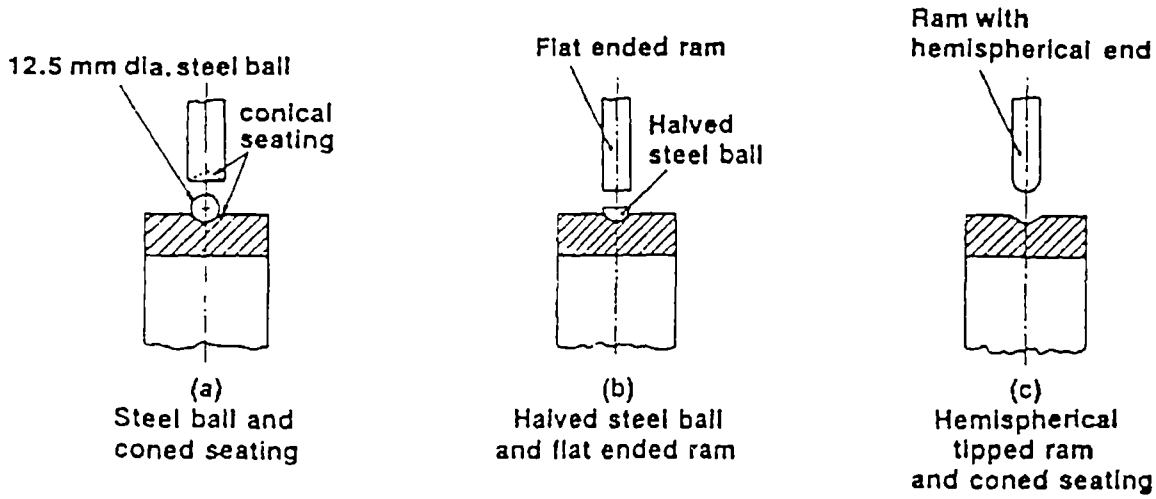

Figure 3.9 Connections between sample and load cell (after Baldi et al., 1988).

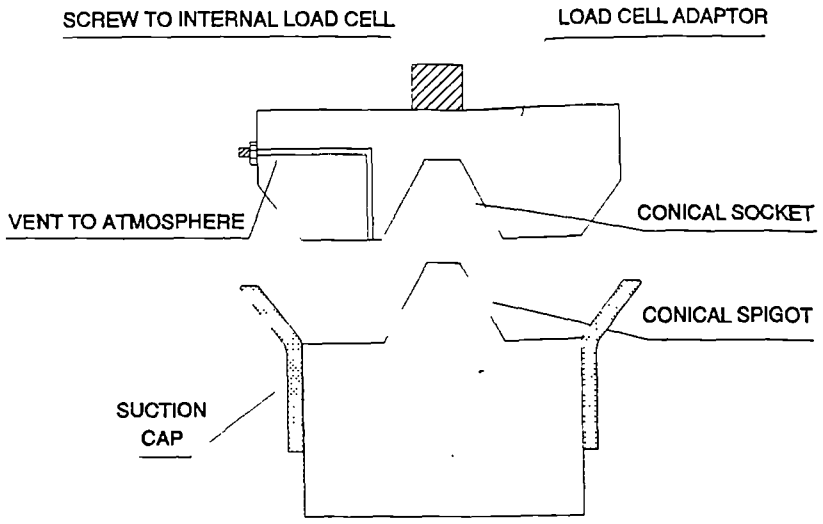

Figure 3.10 Conical connection between the sample and the internal load cell.

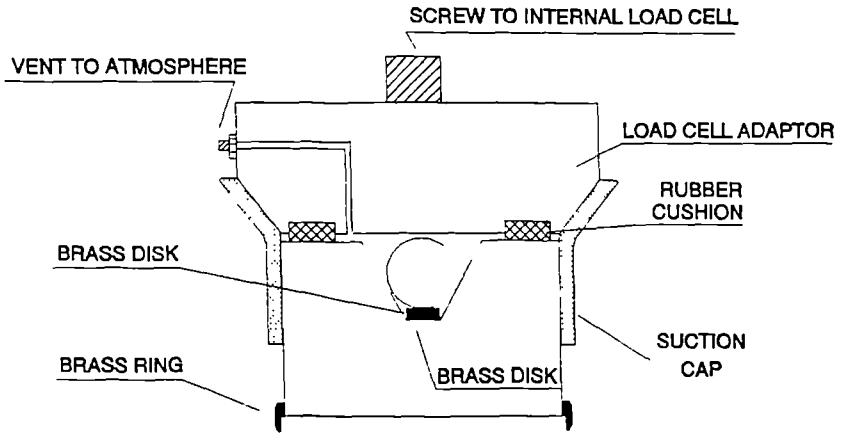

Figure 3.11 Redesigned connection between the sample and the internal load cell.

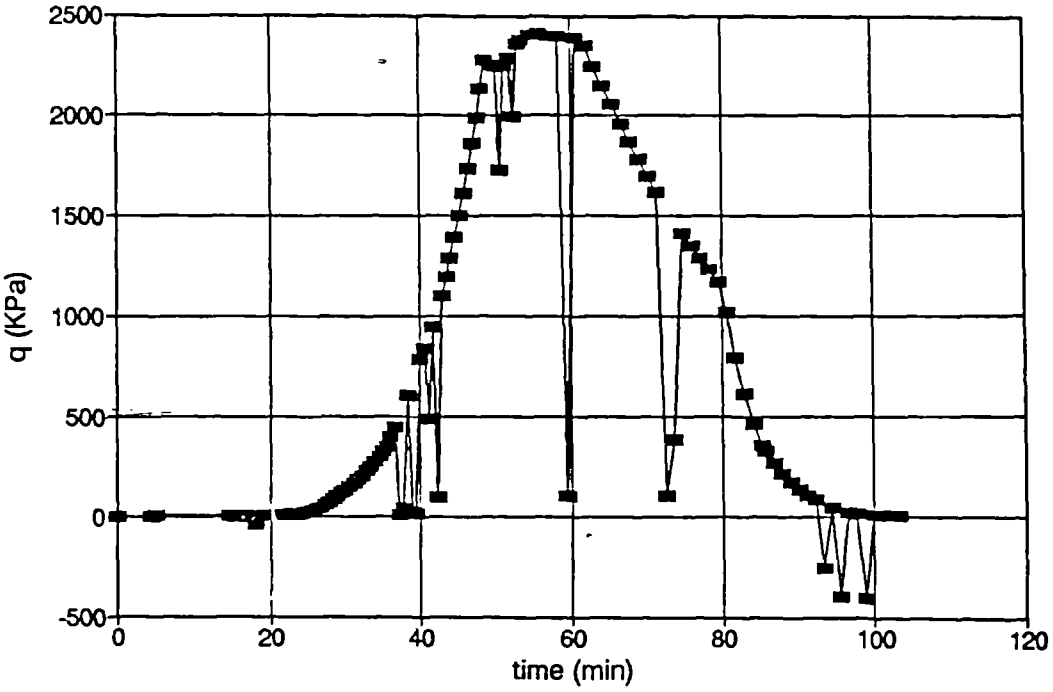

(a)

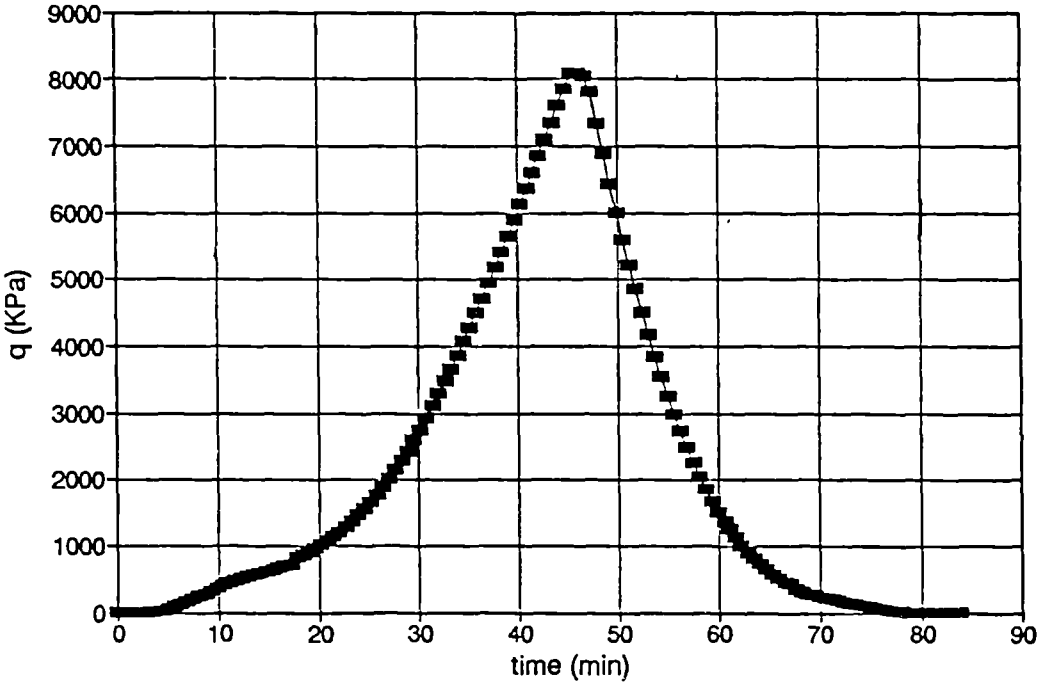

(b)

Figure 3.12 Variation of deviator stress with time for a dummy sample using the redesigned connection with (a) the initial and (b) final configurations.

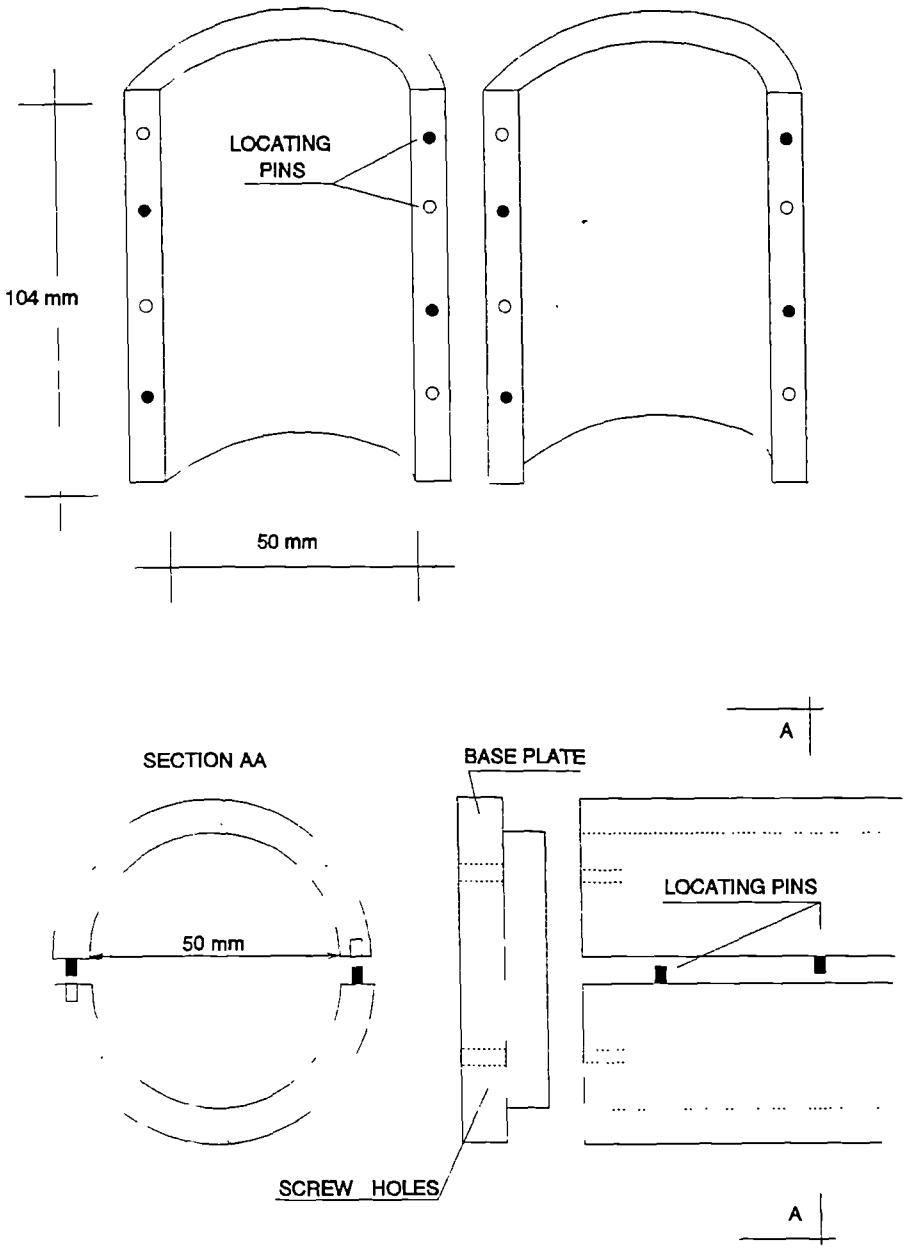

Figure 3.13 Mould for trimming the ends of the sample.

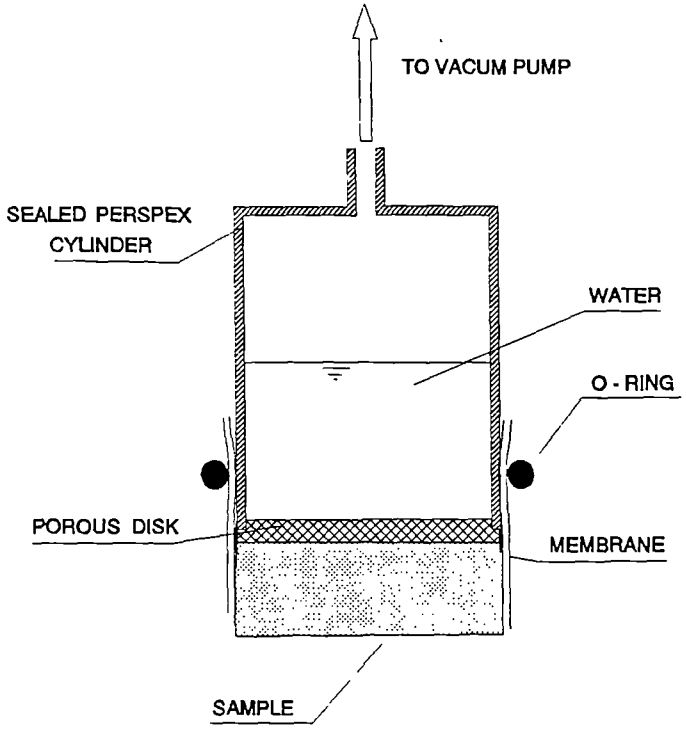

Figure 3.14 Device for the saturation of the sample.

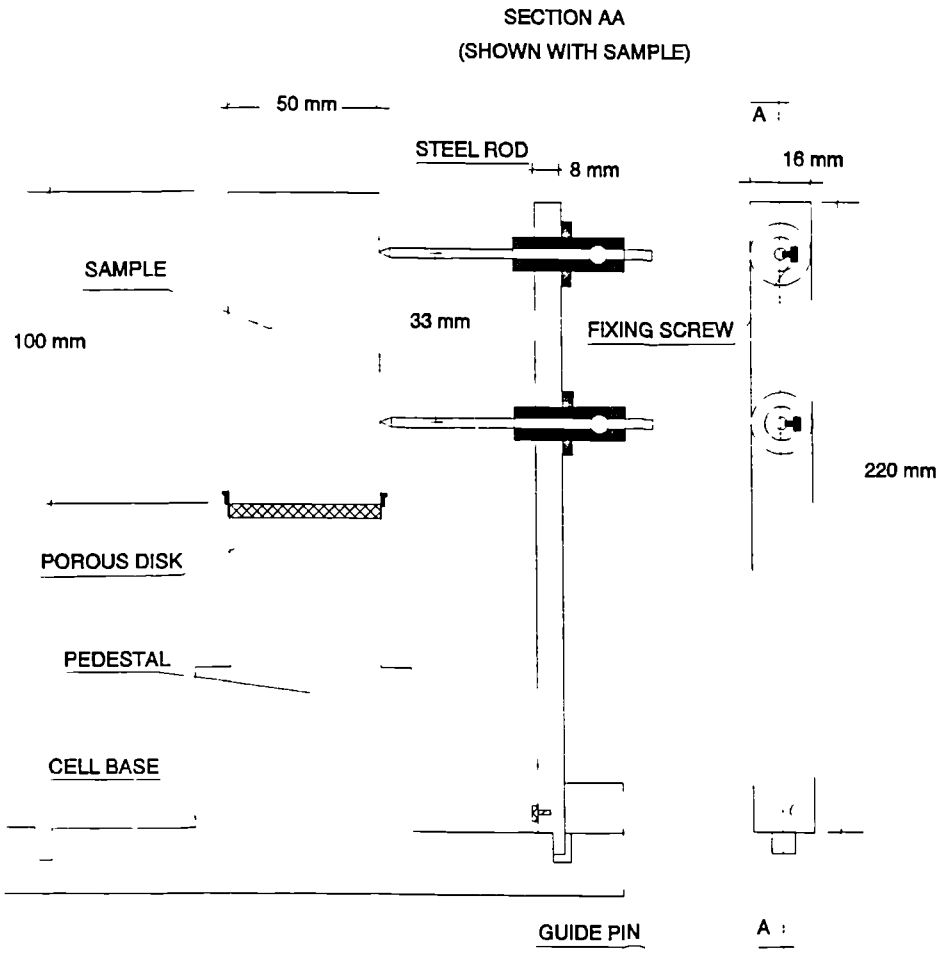

Figure 3.15 Device to check the sample centrality with respect to the apparatus axis.

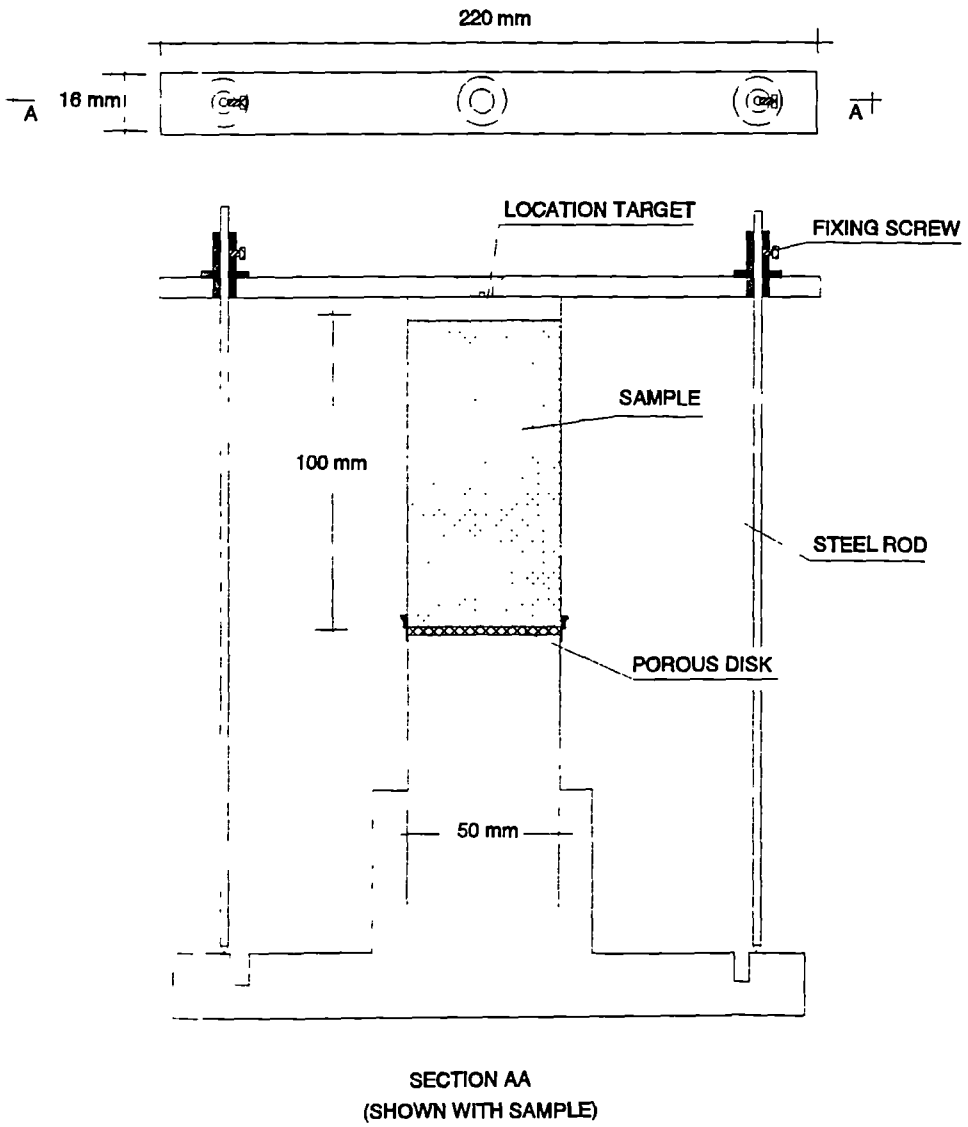

Figure 3.16 Device to check the perpendicularity of the ends of the sample with respect to the apparatus axes.

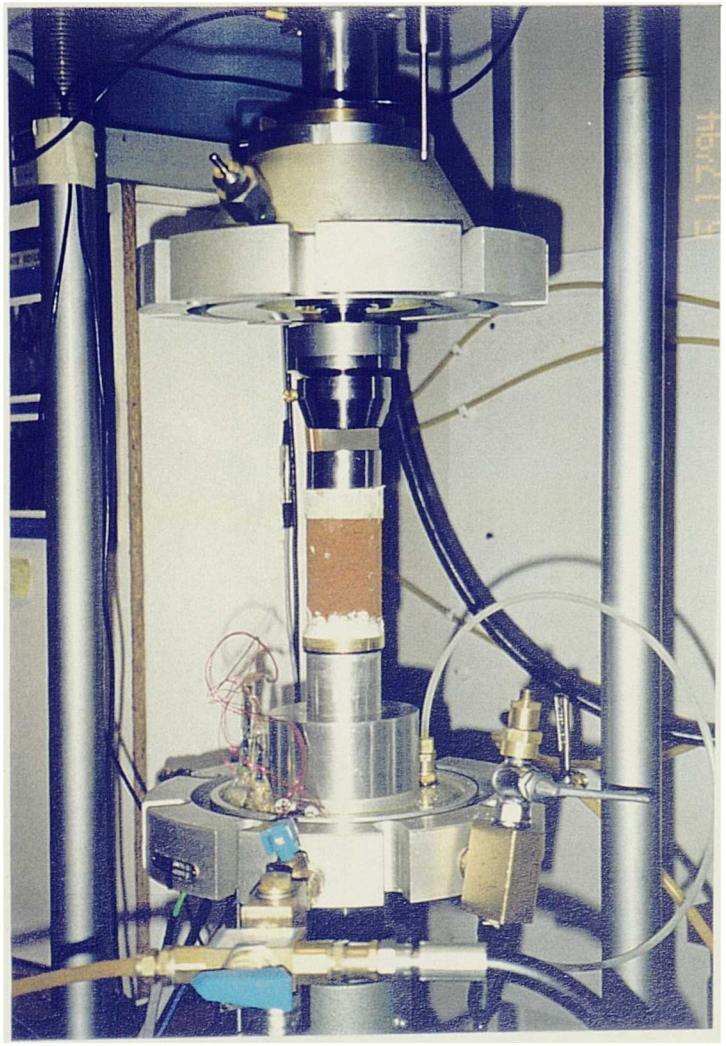

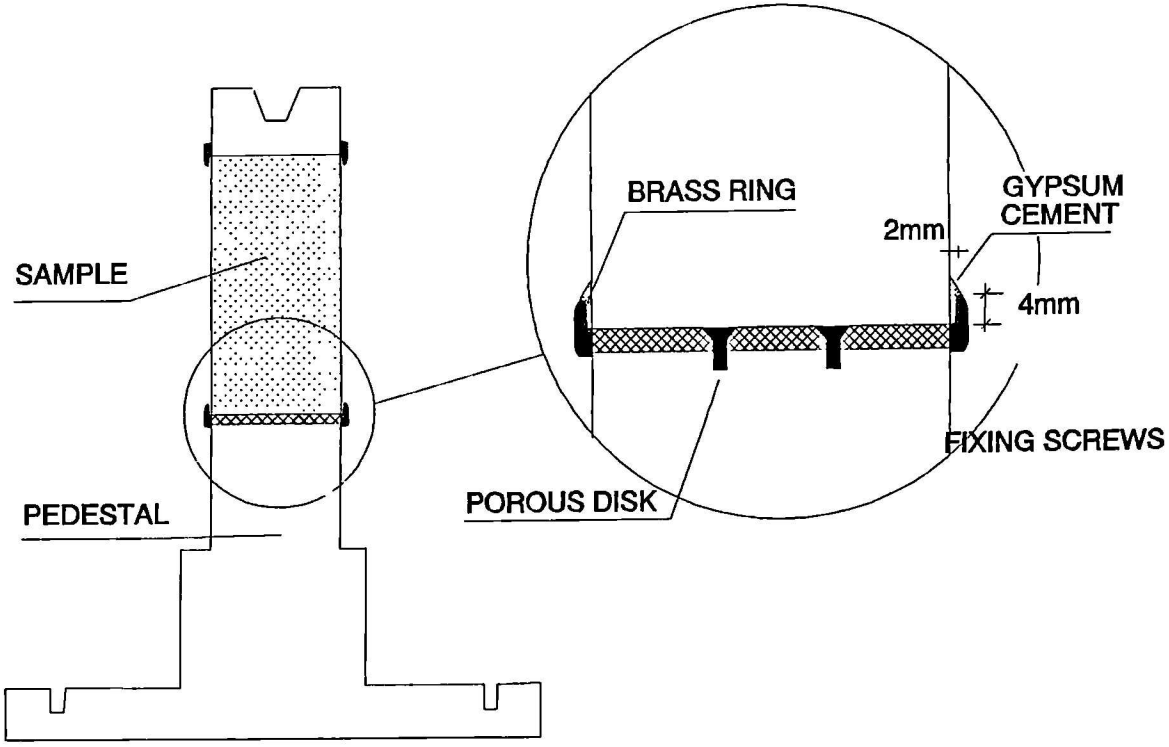

Figure 3.17 Installation of the sample in the 10 MPa apparatus.

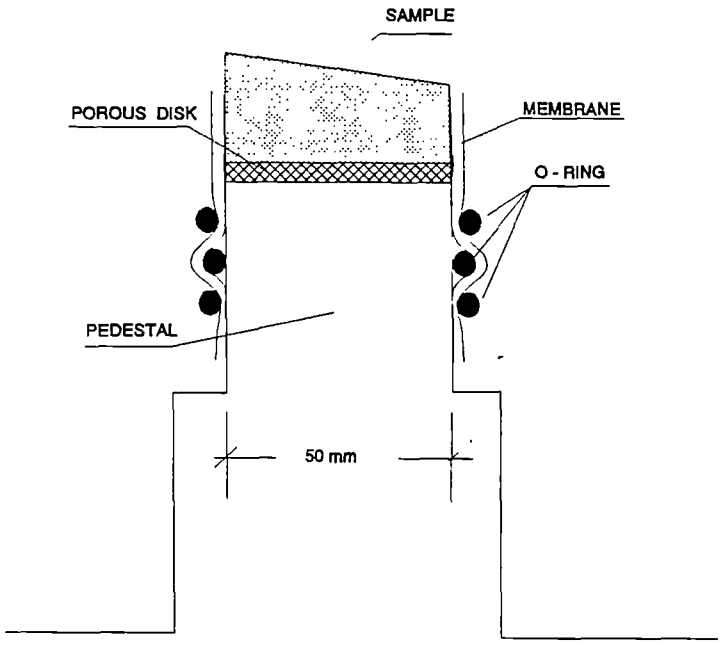

Figure 3.18 Configuration of 'O'-rings to seal the sample.

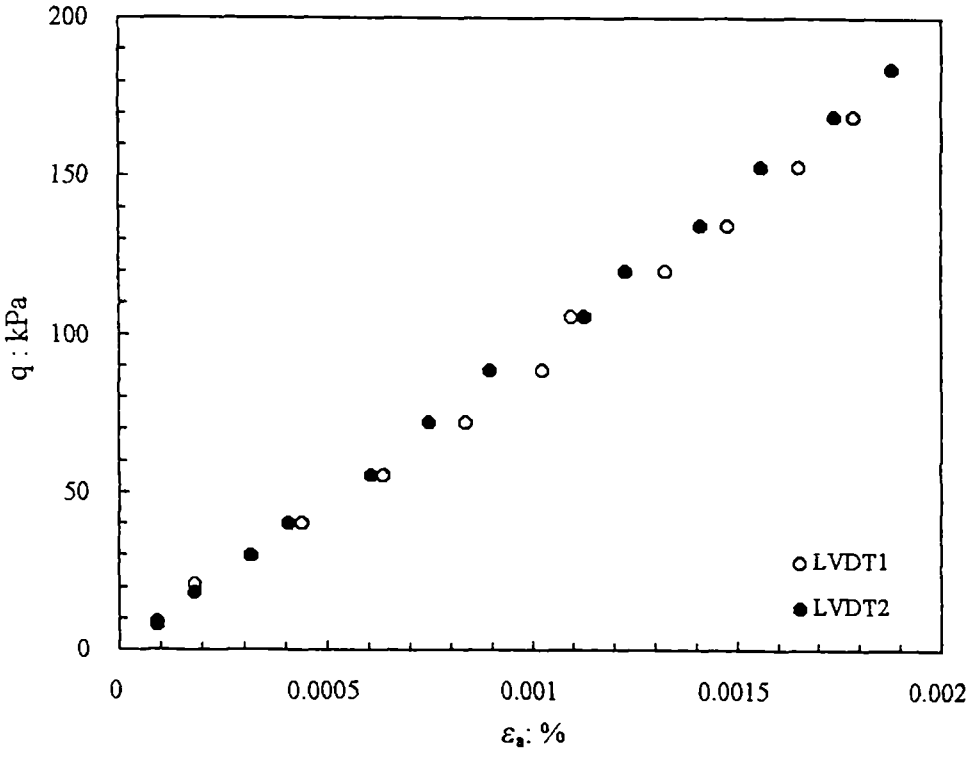

Figure 3.19 Stress-strain data showing the uniformity of strains after changing the setting up and testing procedures.

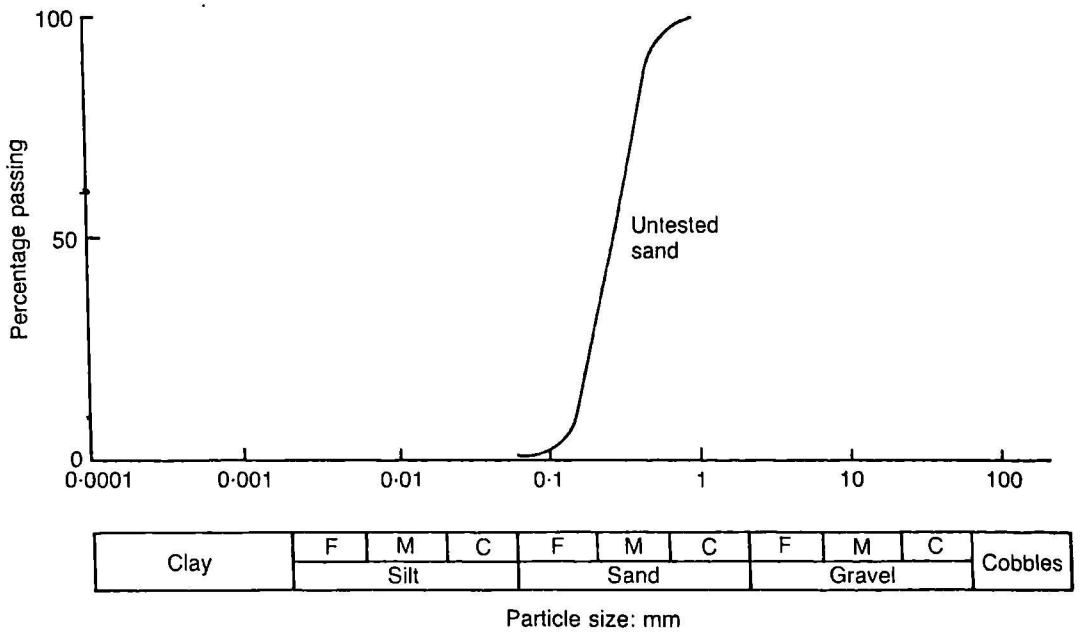

Figure 4.1a Grading curve of Dog's Bay sand (after Coop, 1990).

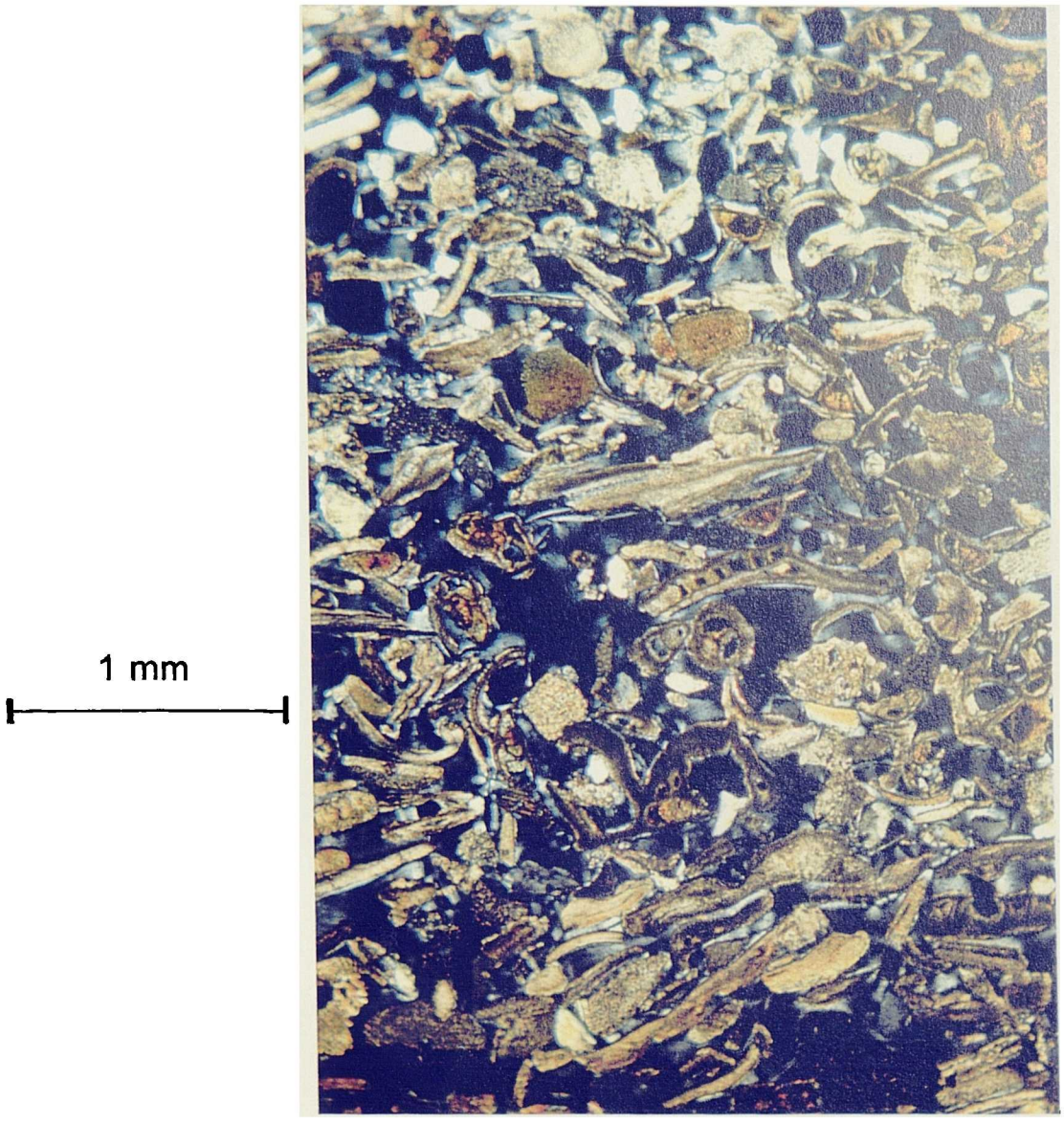

Figure 4.1b Thin sections of Dog's Bay sand under cross-polarised light.

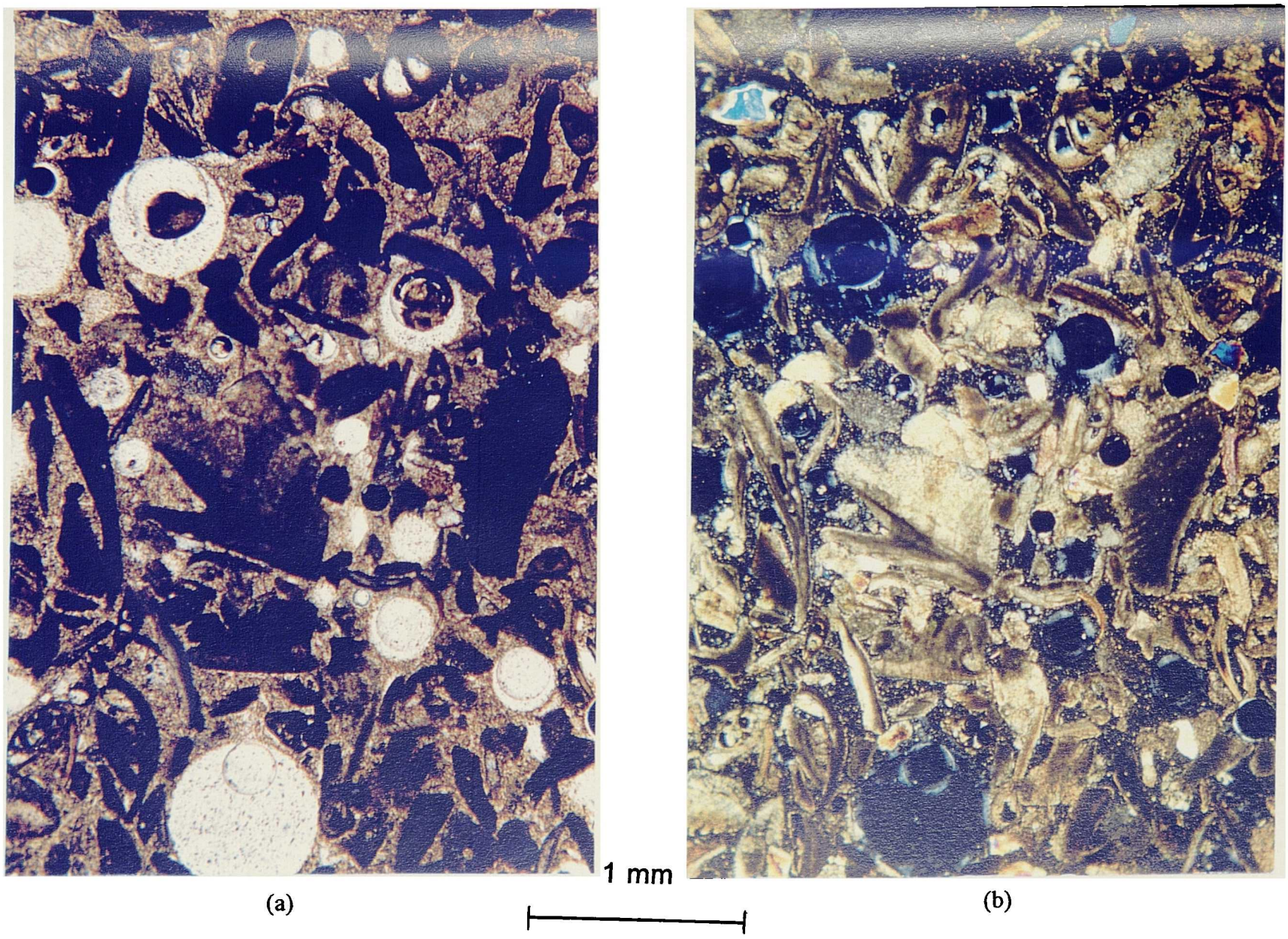

Figure 4.2 Thin section of the artificially cemented sand under: (a) plain white light; (b) cross-polarised light.

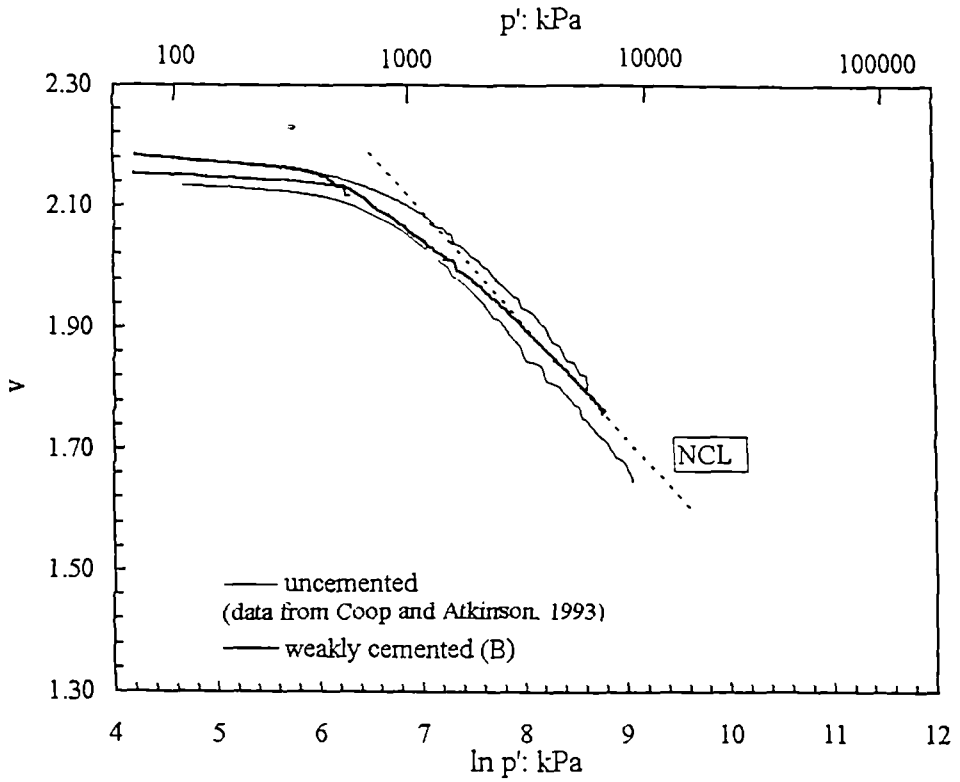

Figure 4.3a Isotropic compression of the weakly cemented sand prepared using method B and of the uncemented sand.

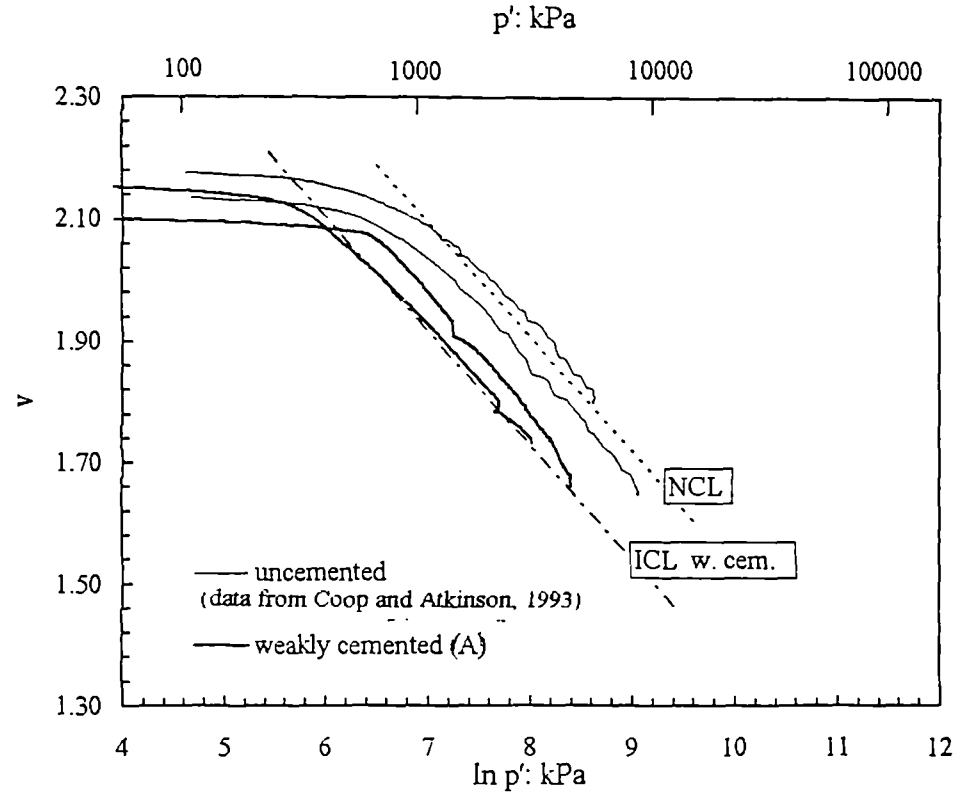

Figure 4.3b Isotropic compression of the weakly cemented sand prepared using method A and of the uncemented sand.

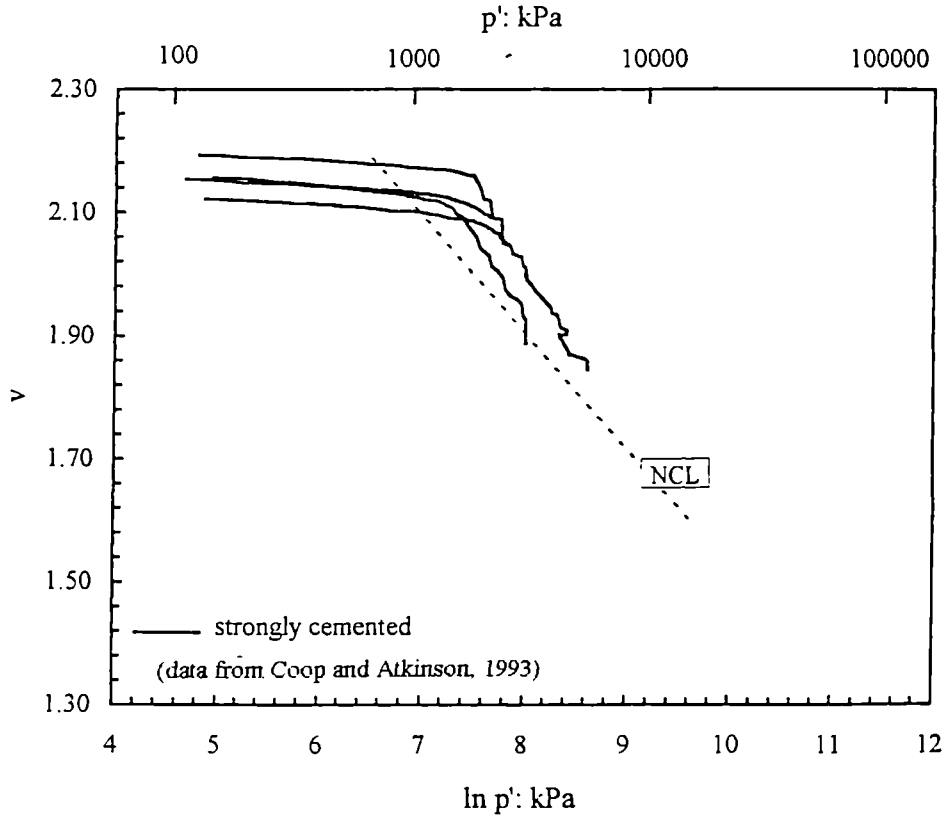

Figure 4.4 Isotropic compression of the strongly cemented sand.

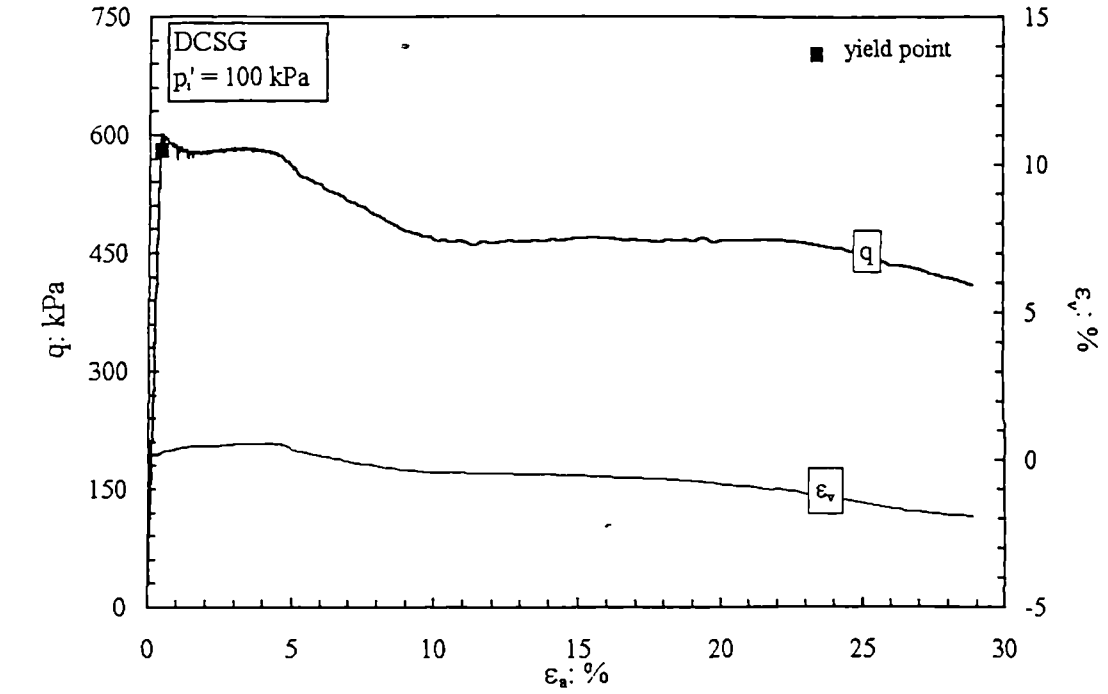

(a)

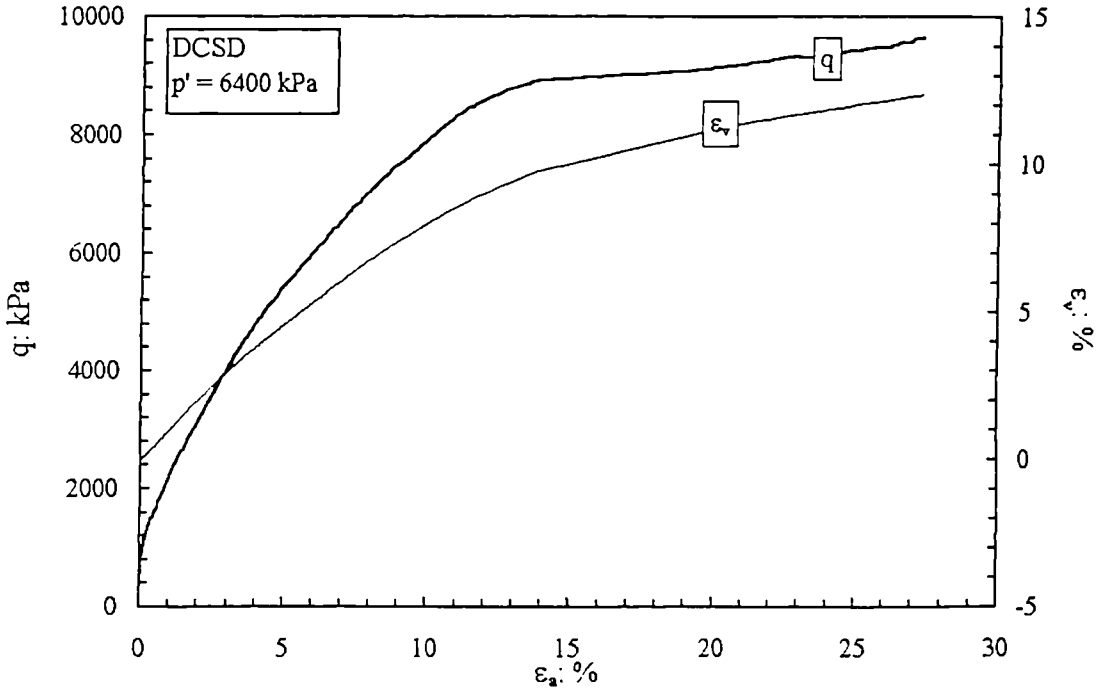

(b)

Figure 4.5 Stress-strain curves of the weakly cemented sand prepared using method B: (a) at low confining pressures; (b) at high confining pressures.

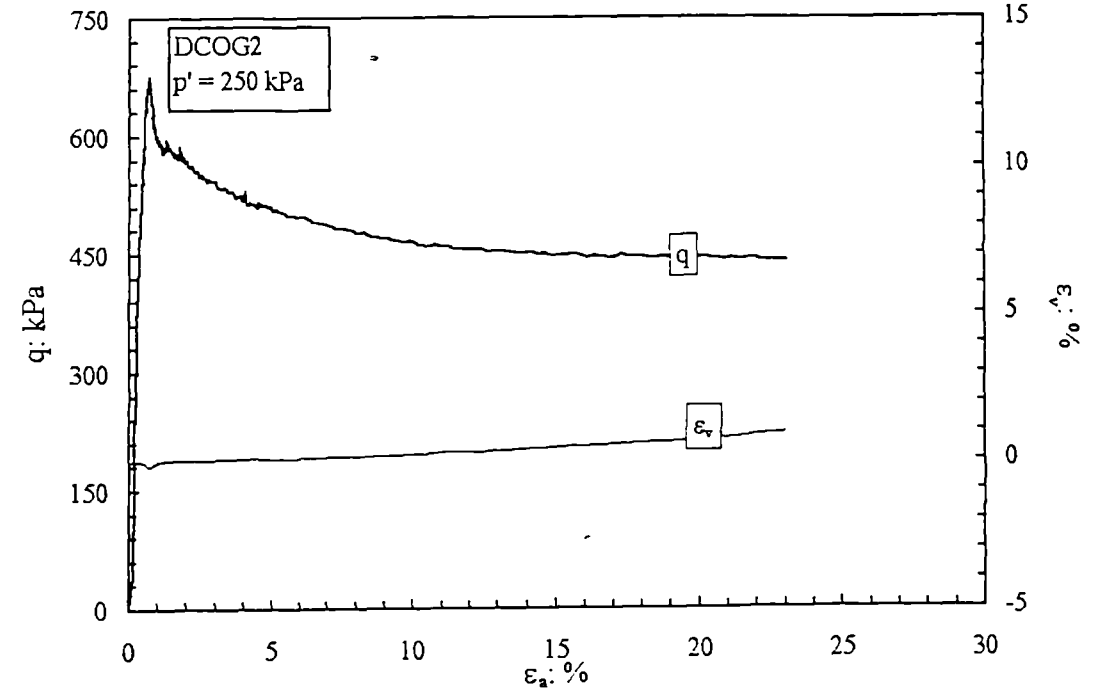

(a)

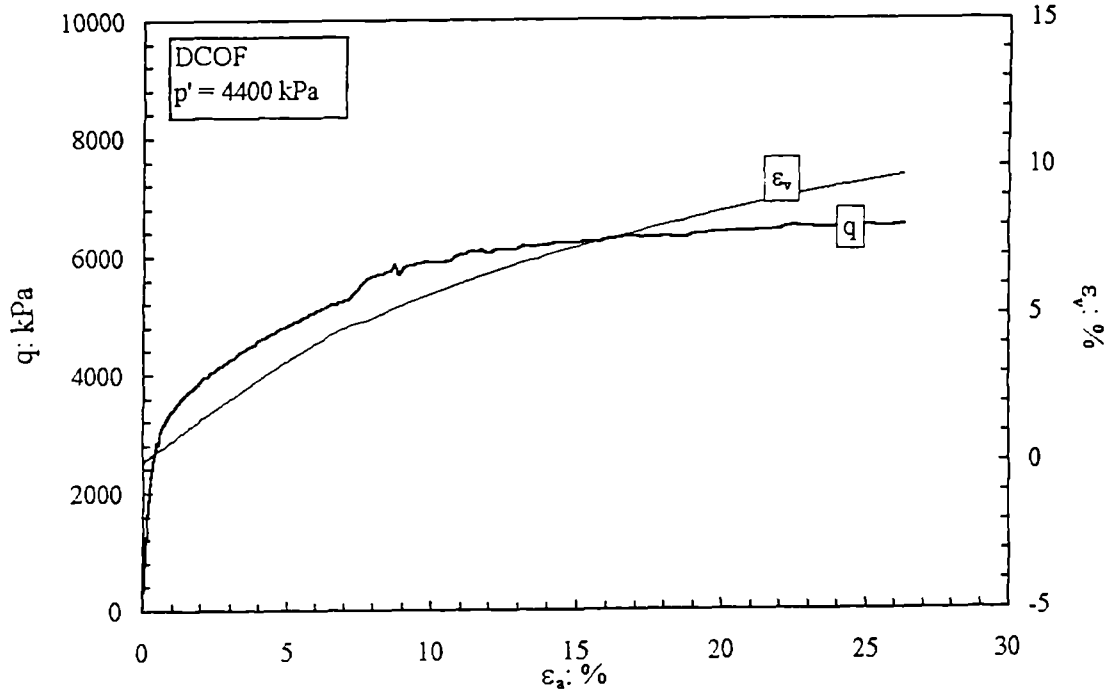

(b)

Figure 4.6 Stress-strain curves of the weakly cemented sand prepared by method A: (a) at low confining pressures; (b) at high confining pressures.

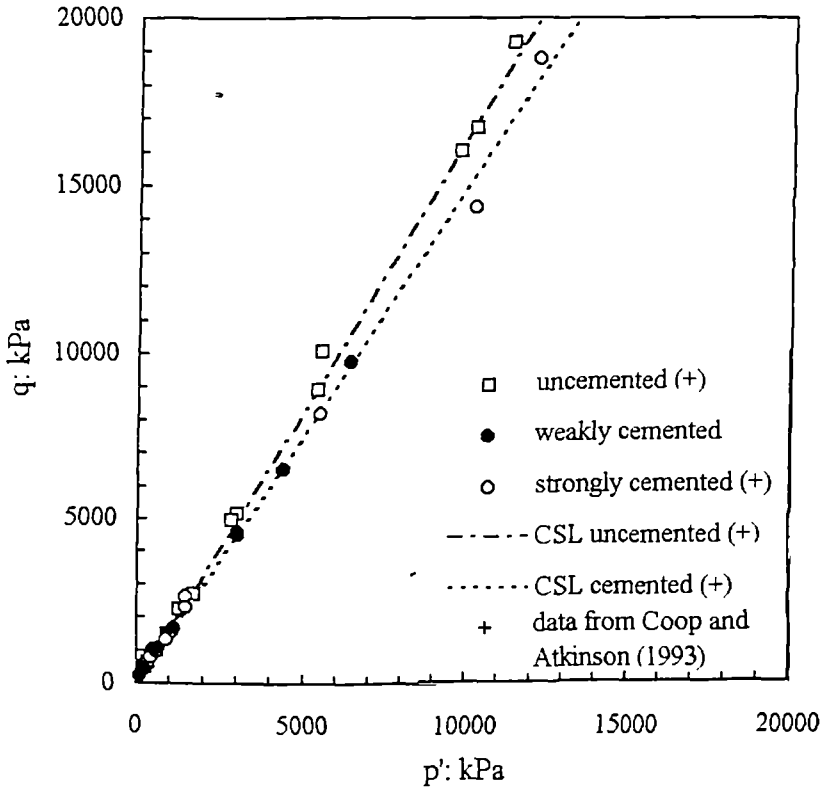

Figure 4.7 Ultimate states for the uncemented, weakly and strongly cemented samples.

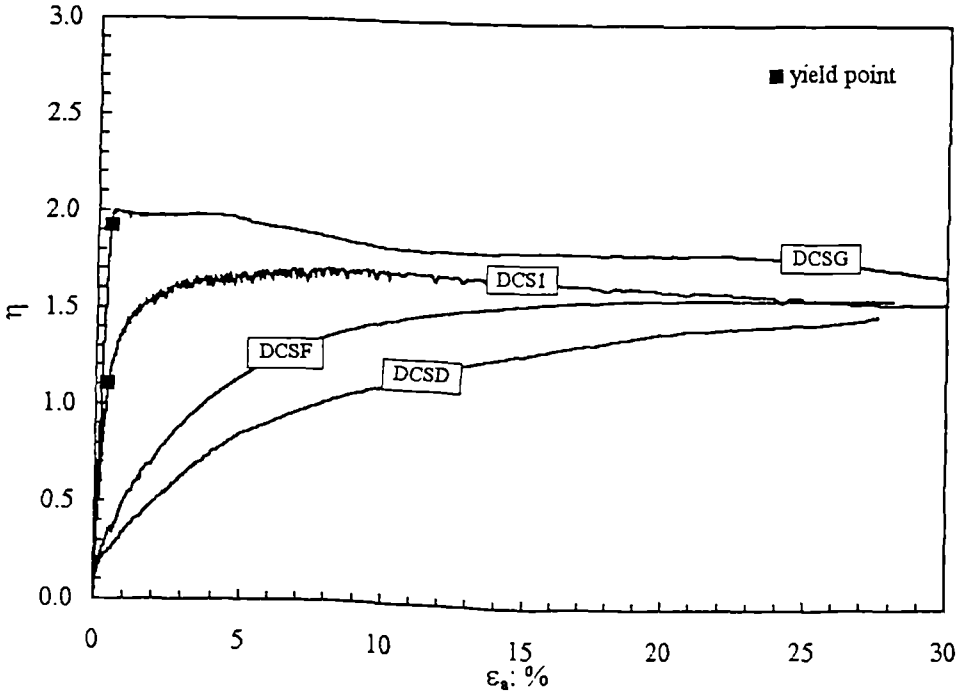

Figure 4.8 Stress ratios during shearing for all the weakly cemented samples prepared using method B.

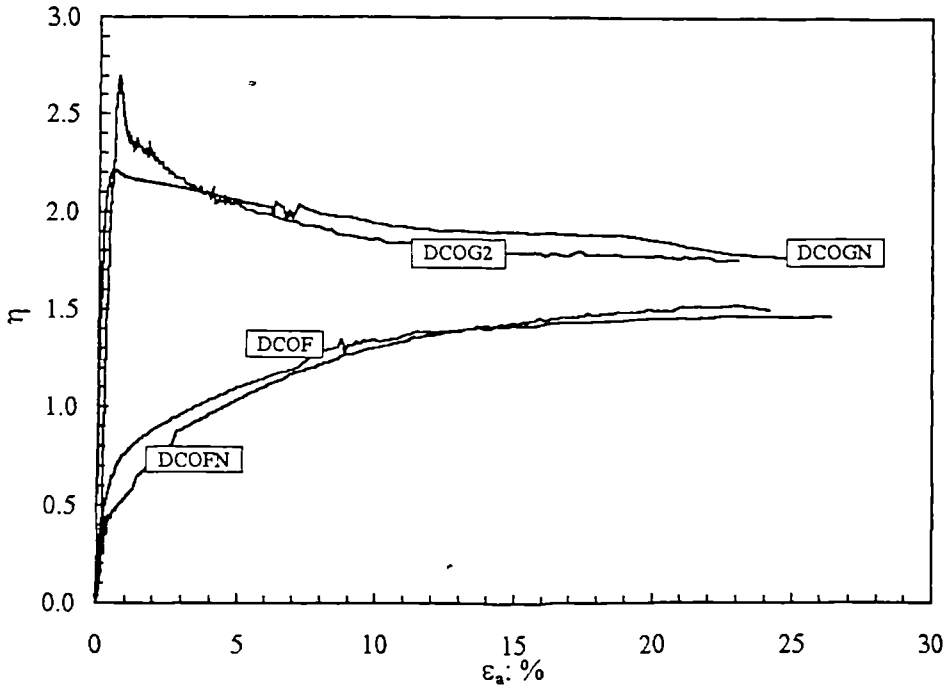

Figure 4.9 Stress ratios during shearing for all the weakly cemented samples prepared using method A.

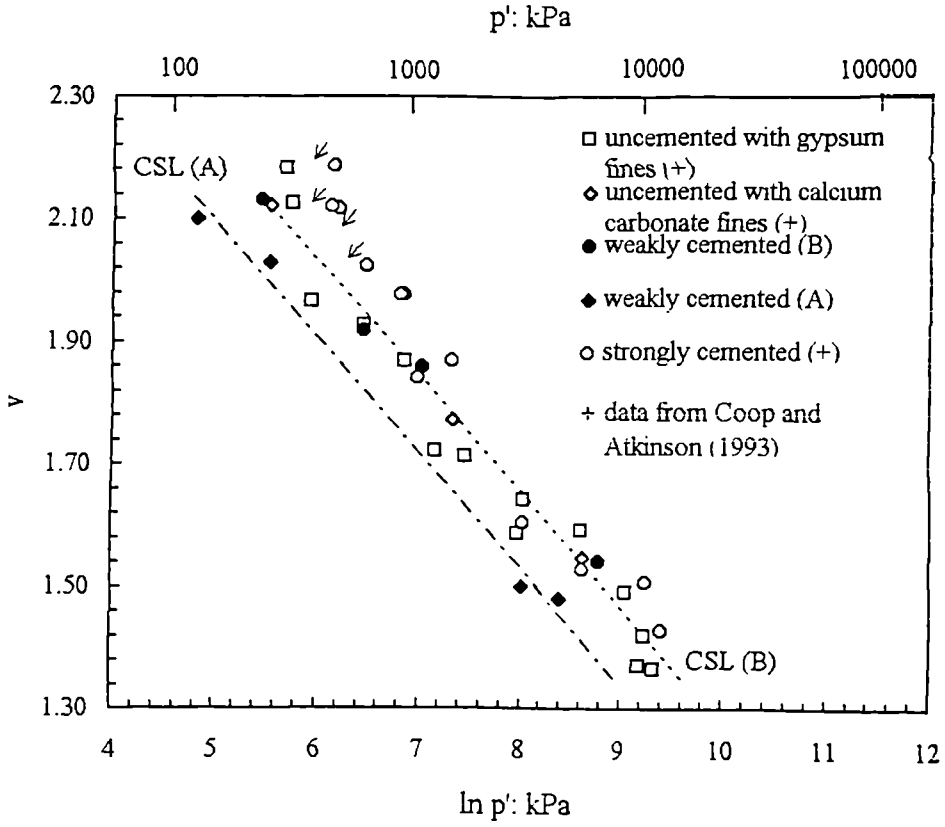

Figure 4.10 States at the end of shearing for uncemented, weakly and strongly cemented samples.

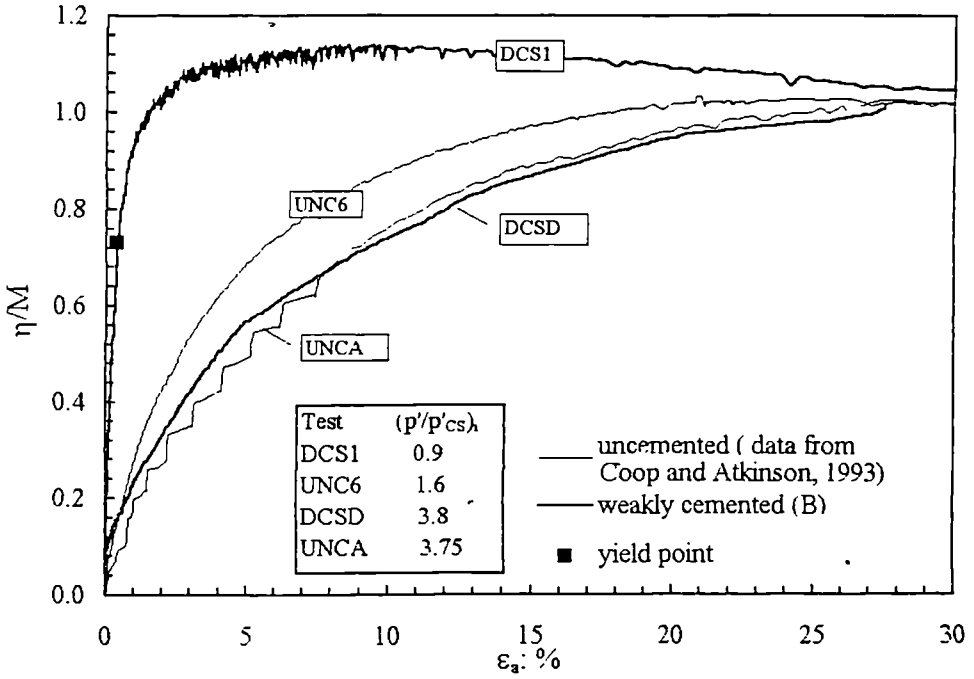

Figure 4.11 Shear behaviour of the weakly cemented samples (type B) and uncemented samples tested from similar initial values of p'/p'_{cs} at intermediate and high confining pressures.

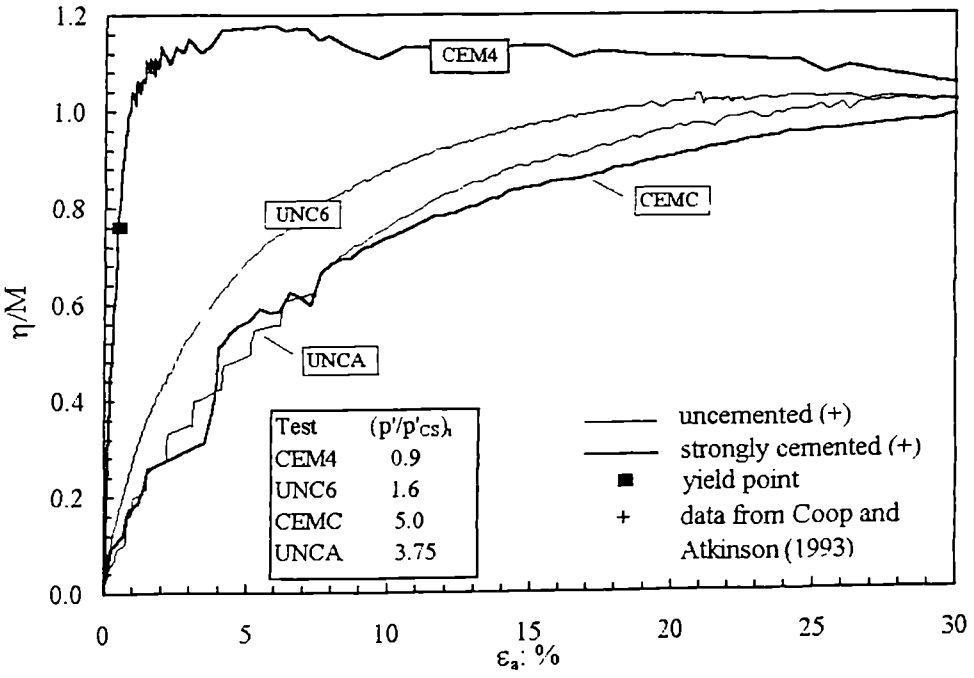

Figure 4.12 Shear behaviour of the strongly cemented and uncemented samples tested from similar initial values of p'/p'_{cs} at intermediate and high confining pressures.

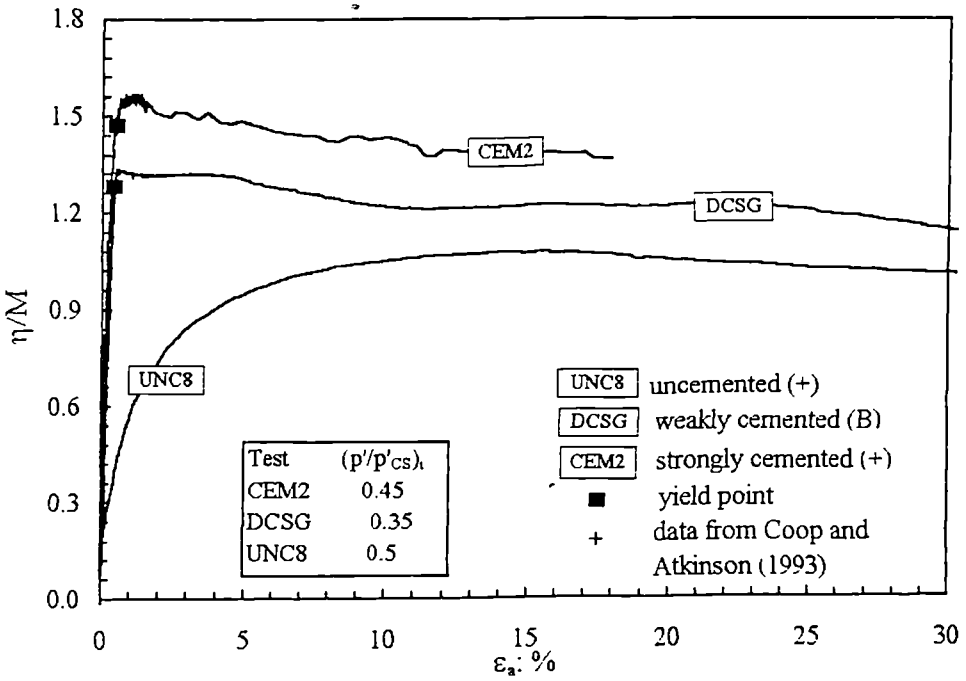

Figure 4.13 Shear behaviour of the strongly cemented, weakly cemented (type B) and uncemented samples tested from similar initial values of p'/p'_{cs} at low confining pressures.

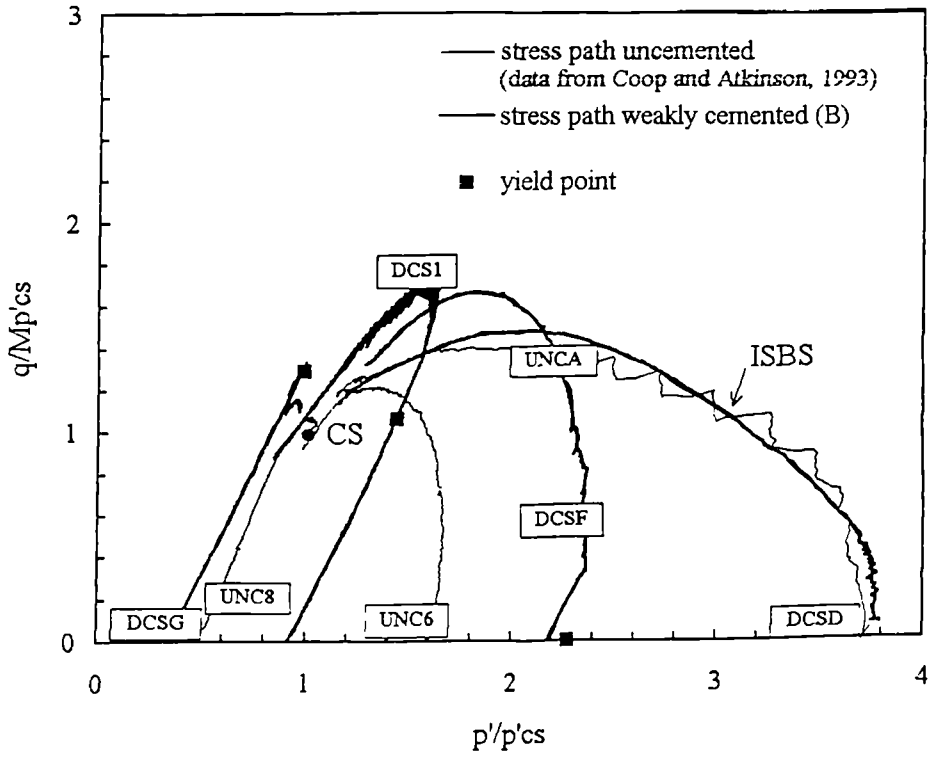

Figure 4.14 Normalized stress paths for the weakly cemented samples prepared using method B compared with those for the uncemented samples.

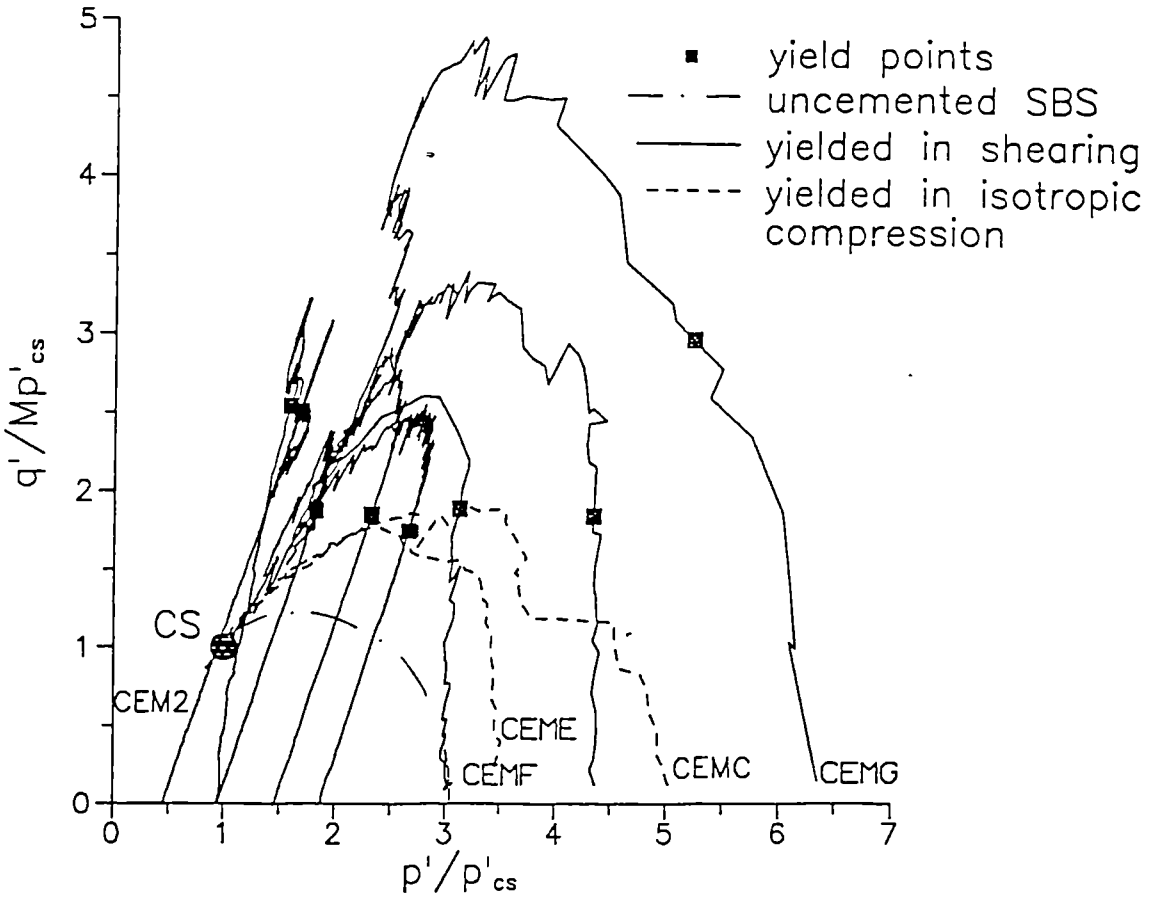

Figure 4.15 Normalized stress paths for the strongly cemented samples (after Coop and Atkinson, 1993).

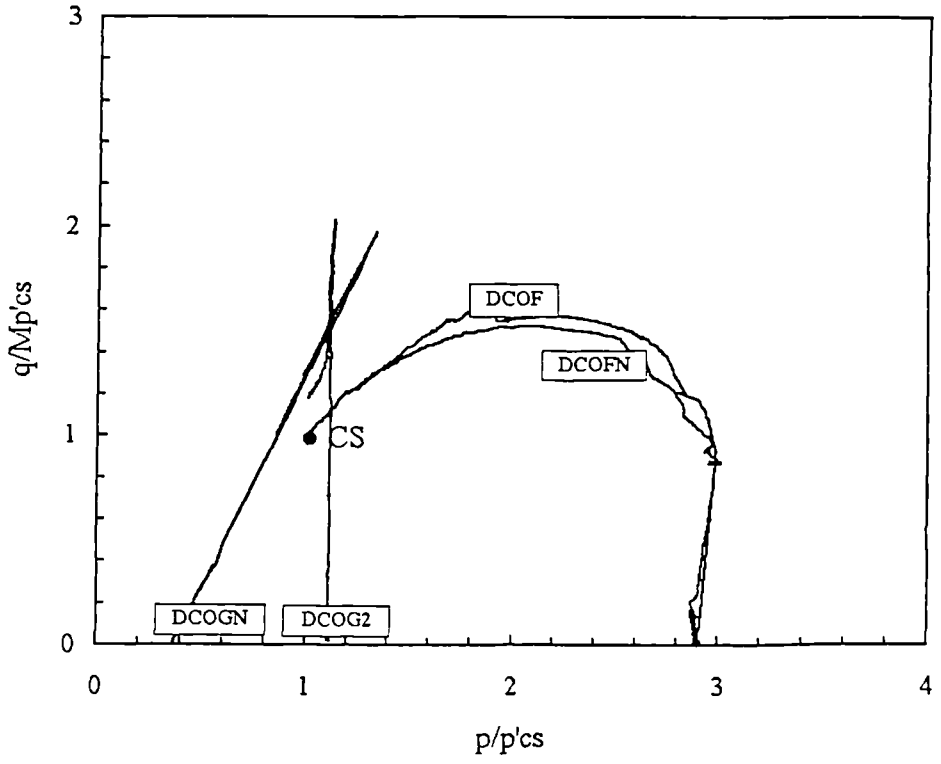

Figure 4.16 Normalized stress paths for the weakly cemented samples prepared using method A compared with those for the uncemented samples.

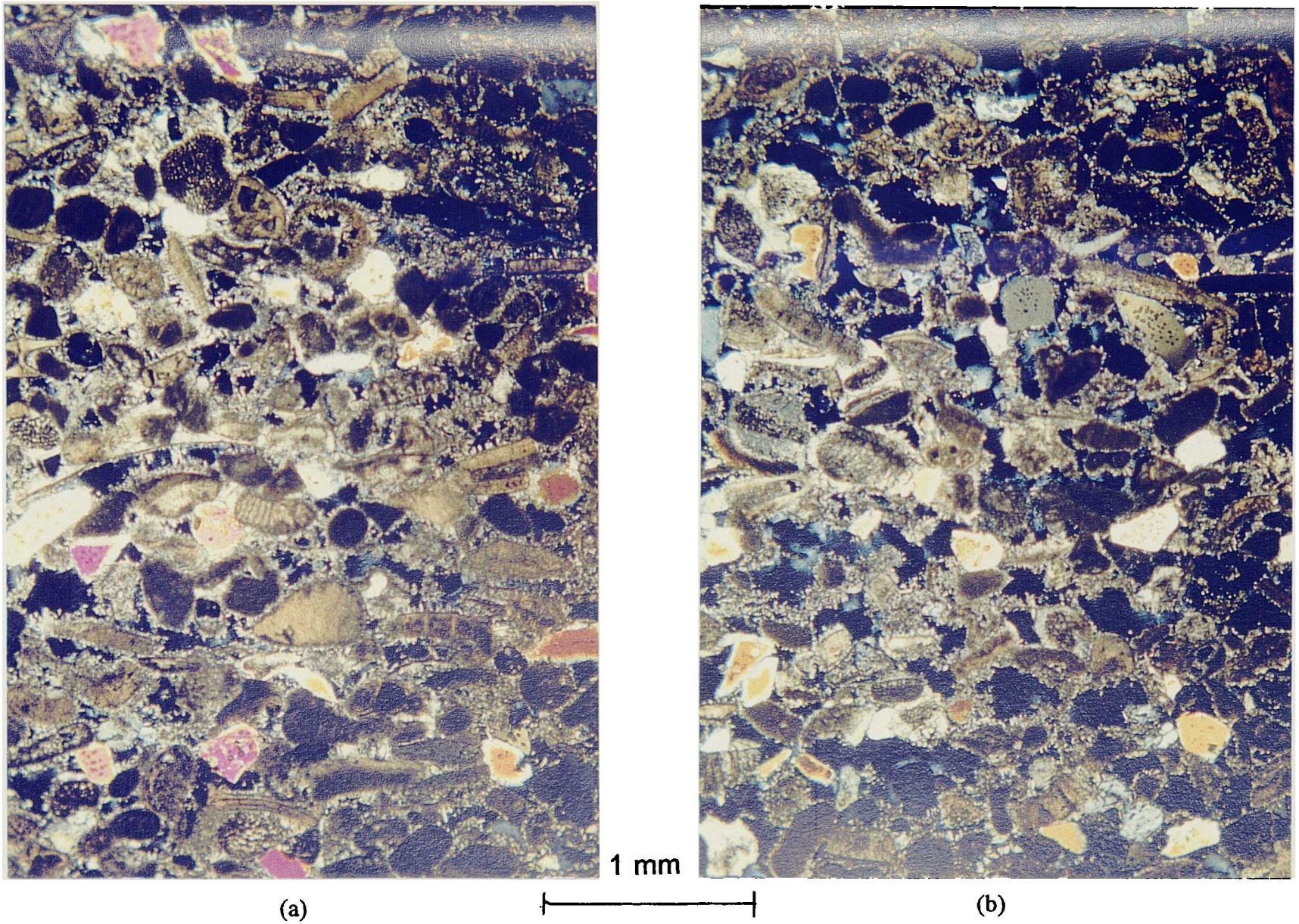

Figure 5.1 Thin sections under cross-polarised light for two calcarenite samples retrieved from borehole B2-6 at (a) 132.5 m and (b) 139.2 m depth below the sea bed.

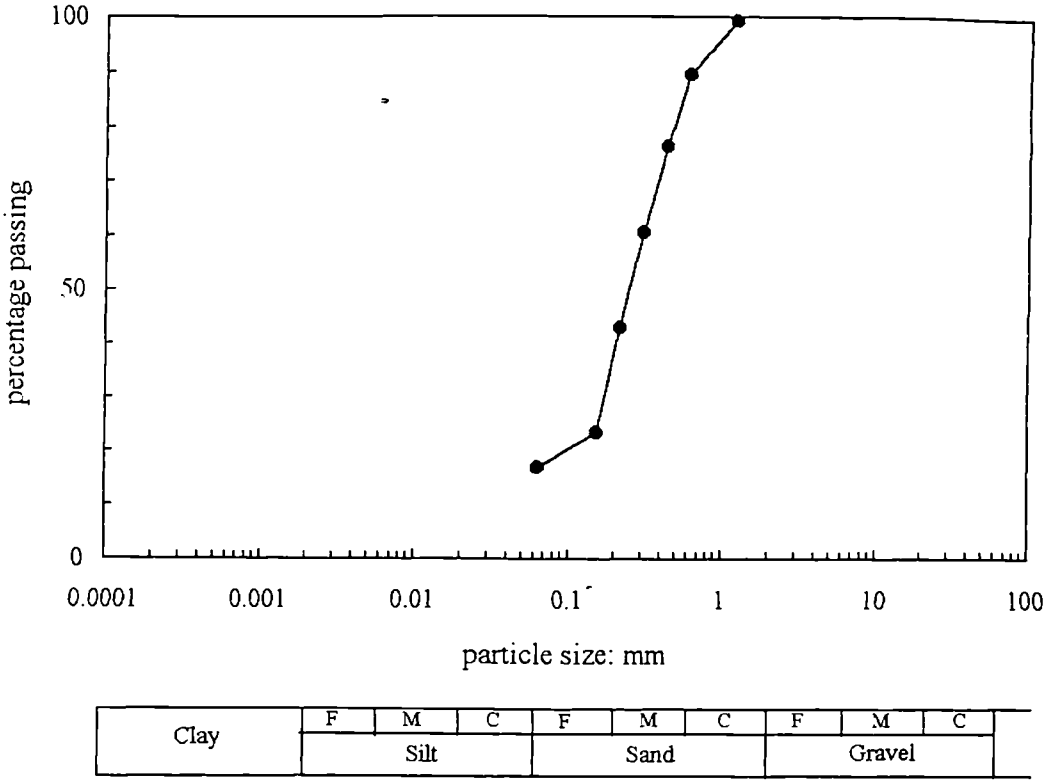

Figure 5.2 Grading curve determined for the reconstituted calcarenite.

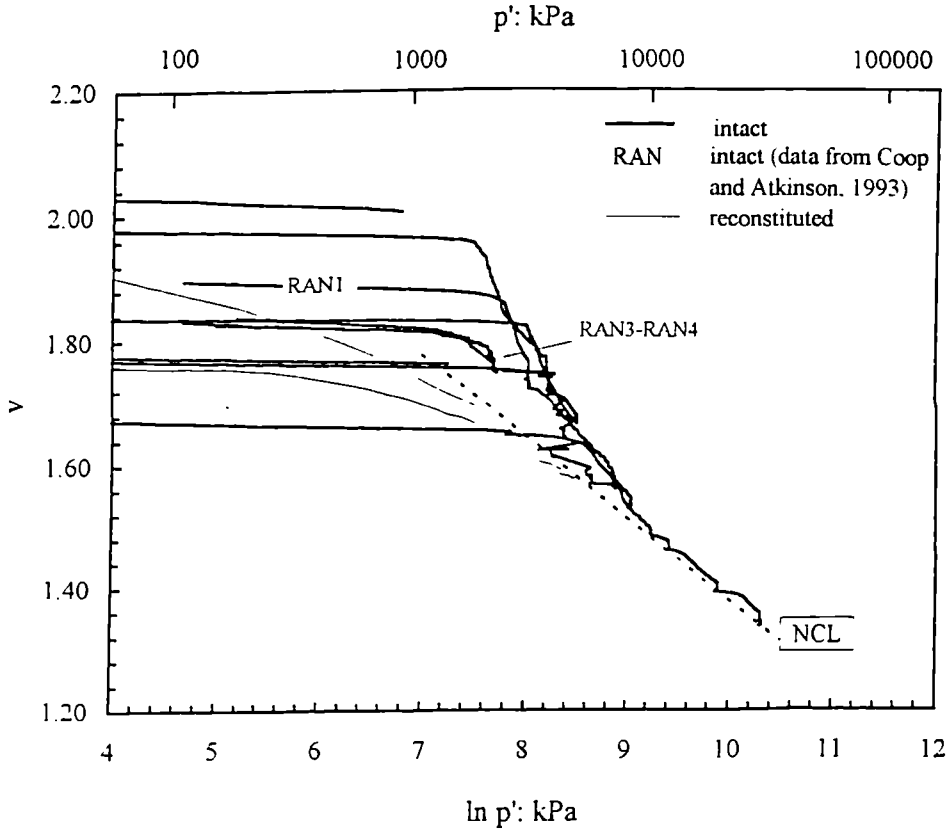

Figure 5.3 Isotropic compression of intact and reconstituted samples of calcarenite.

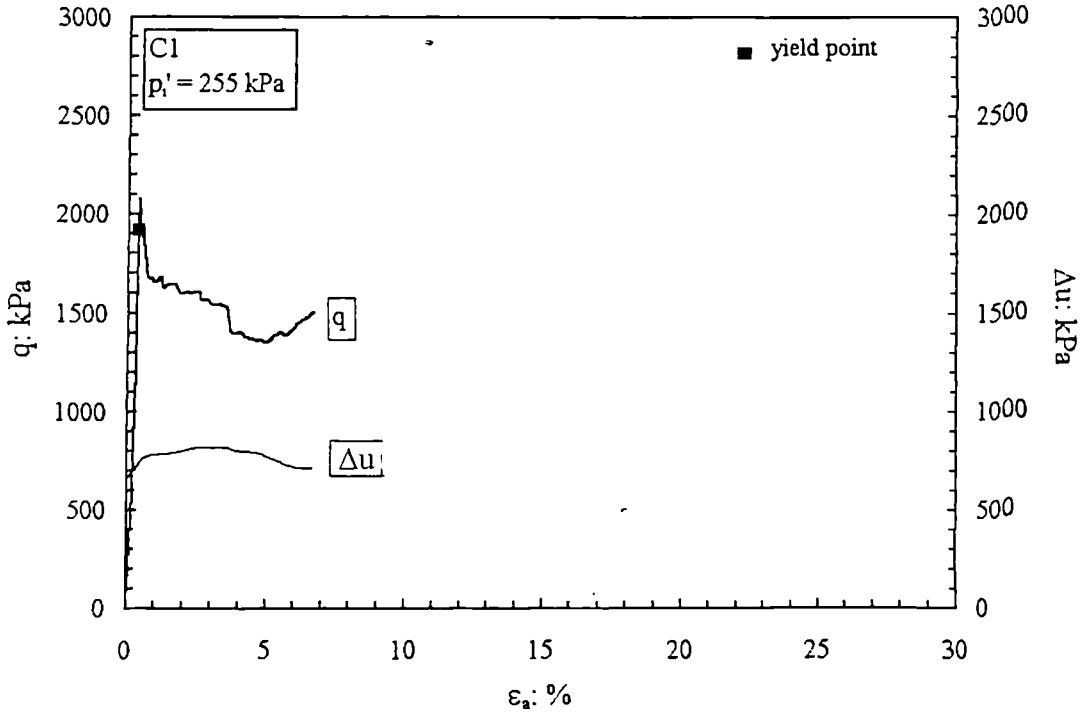

(a)

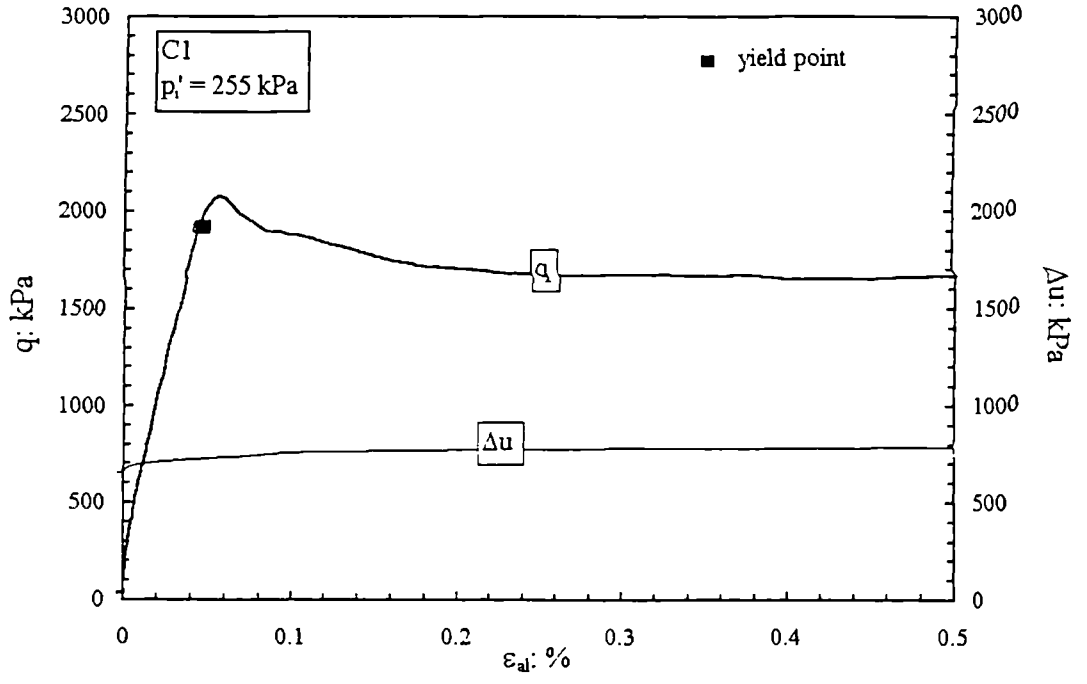

(b)

Figure 5.4 Stress-strain curves from an undrained test performed on the calcarenite at low confining pressures: (a) complete test; (b) local axial strains (ϵ_{al}) up to 0.5 %.

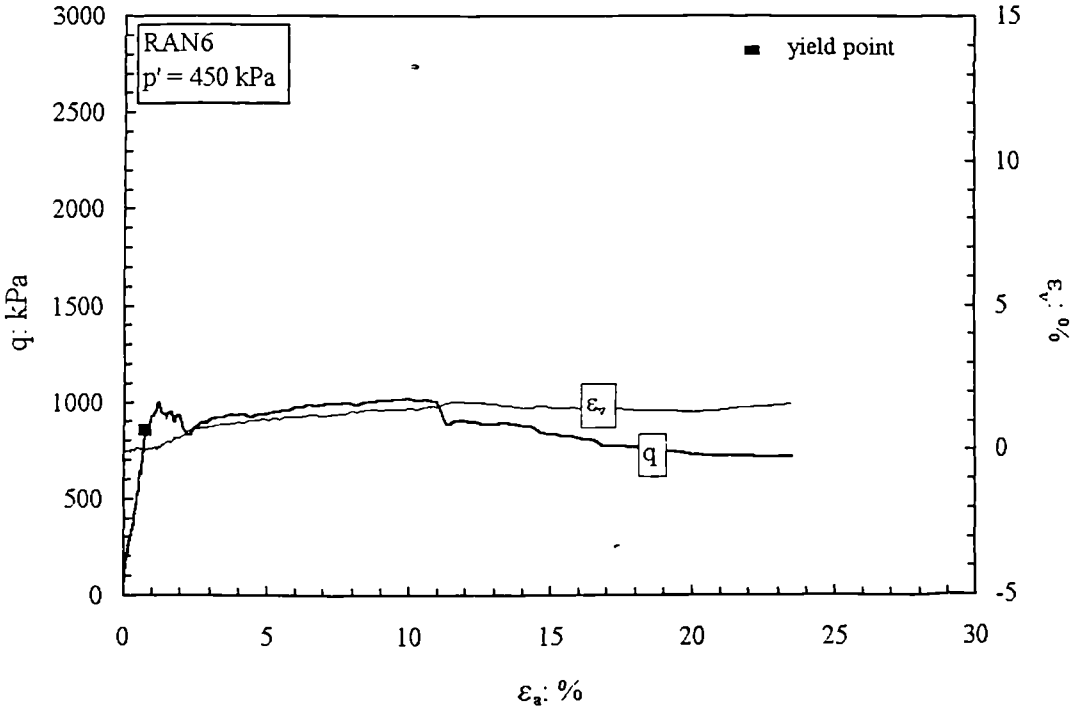

Figure 5.5 Stress-strain curve from a drained constant p' test performed on the calcarenite at low confining pressures (after Coop and Atkinson, 1993).

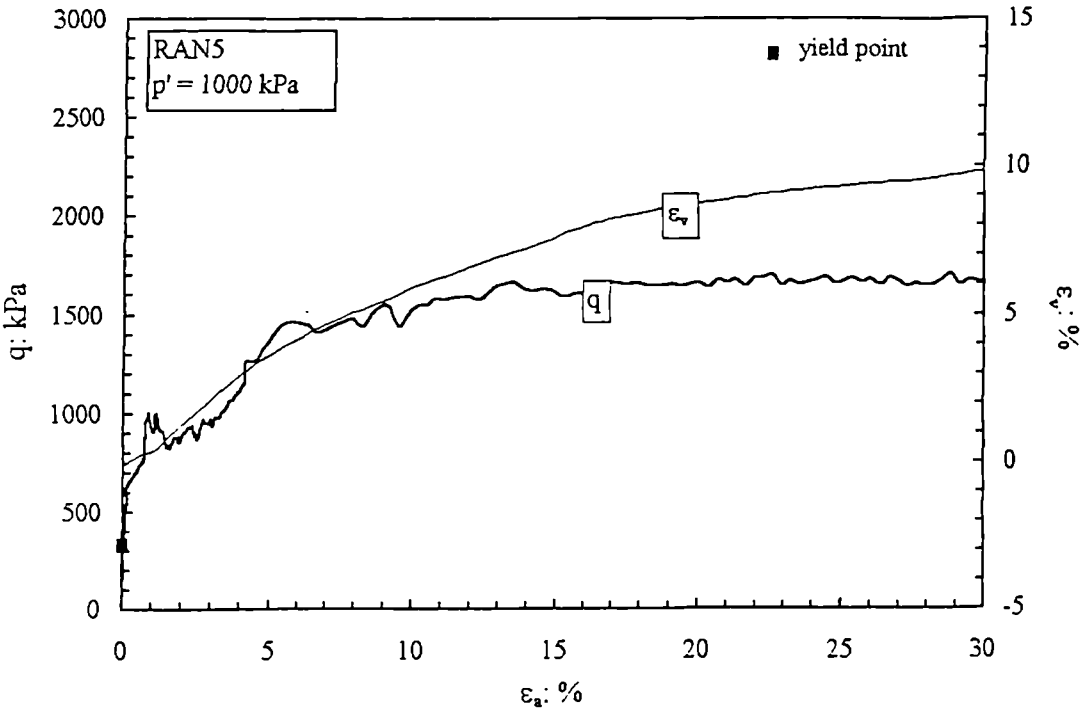

Figure 5.6 Stress-strain curve from a drained constant p' test performed on the calcarenite at intermediate confining pressures (after Coop and Atkinson, 1993).

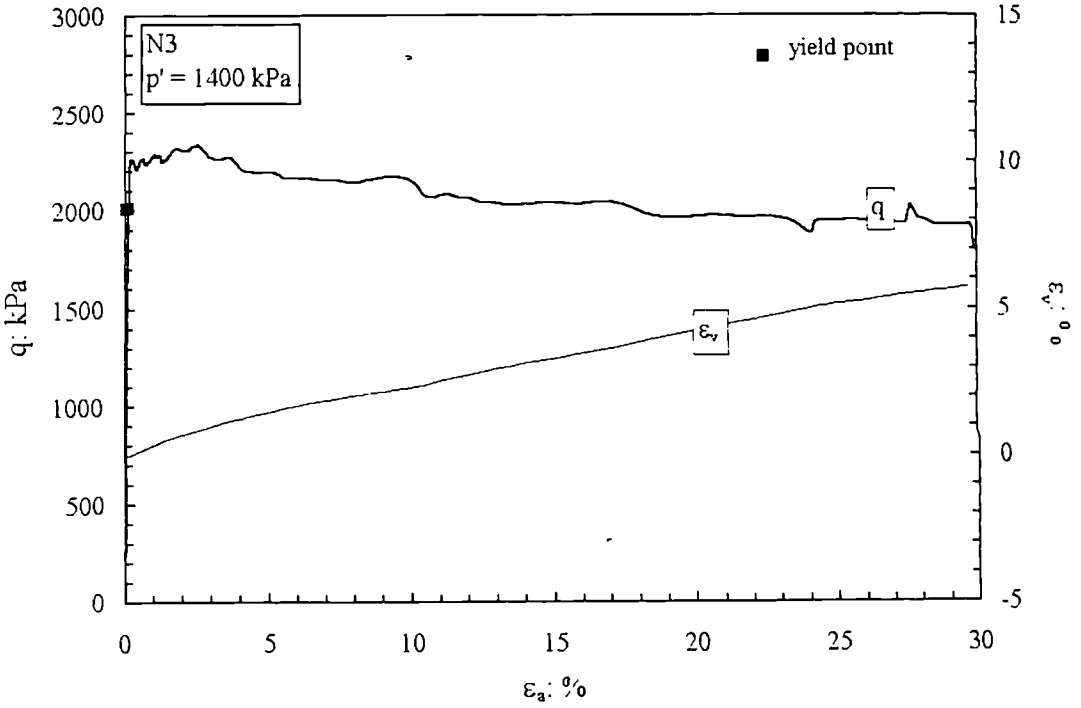

(a)

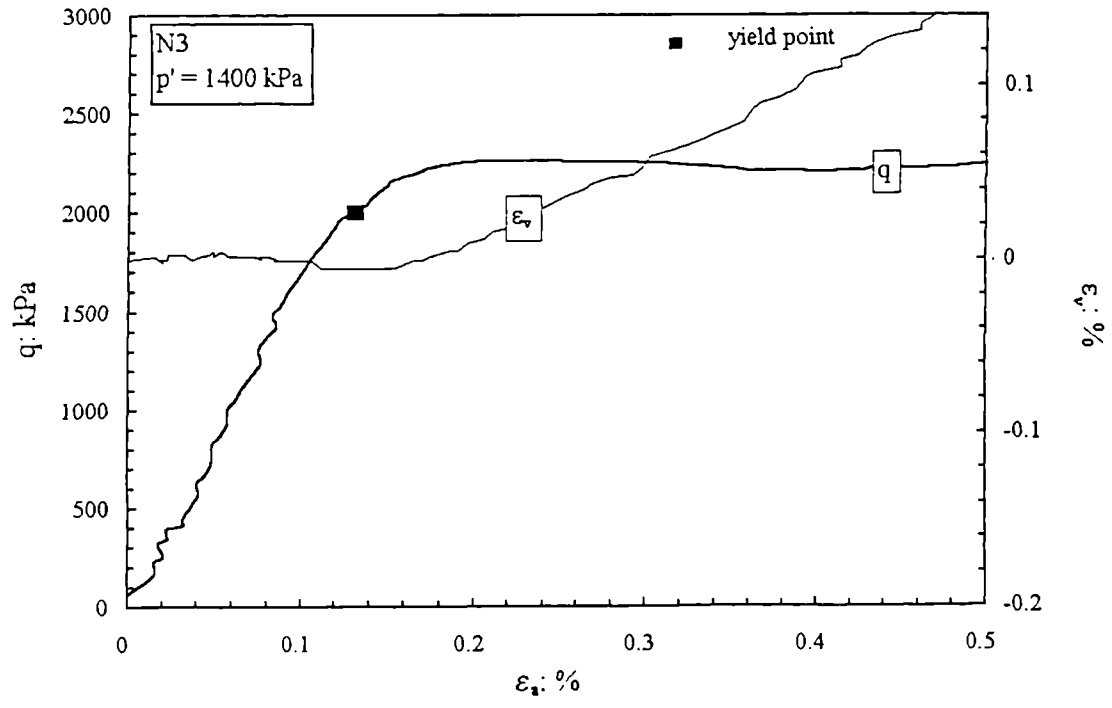

(b)

Figure 5.7 Stress-strain curves from a drained constant p' test performed on the calcarenite at intermediate confining pressures for: (a) the complete test; (b) external axial strains up to 0.5 %.

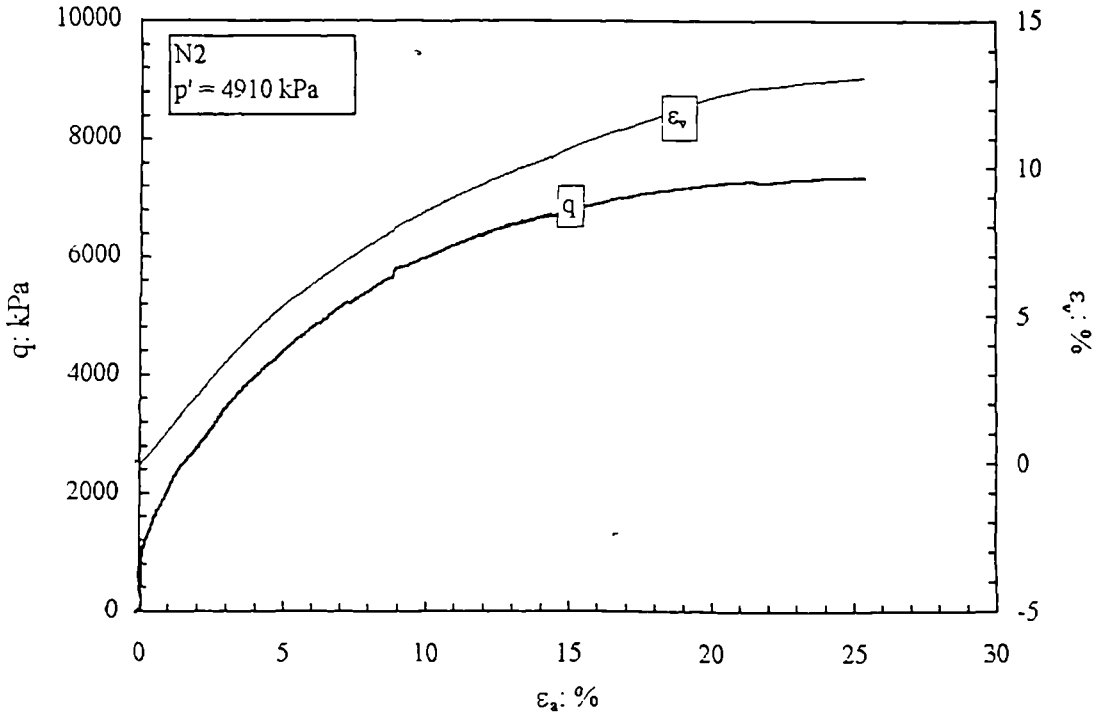

Figure 5.8 Stress-strain curve from a drained constant p' tests performed on the calcarenite at high confining pressures.

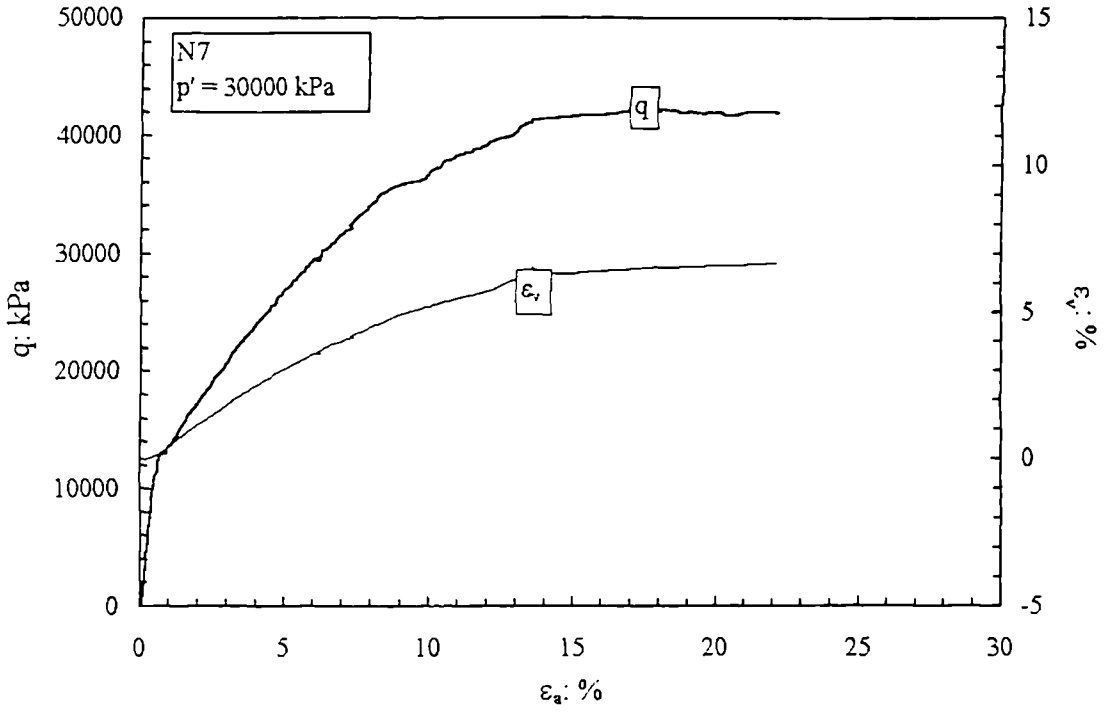

Figure 5.9 Stress-strain curve from a drained constant p' tests performed on the calcarenite at very high confining pressures.

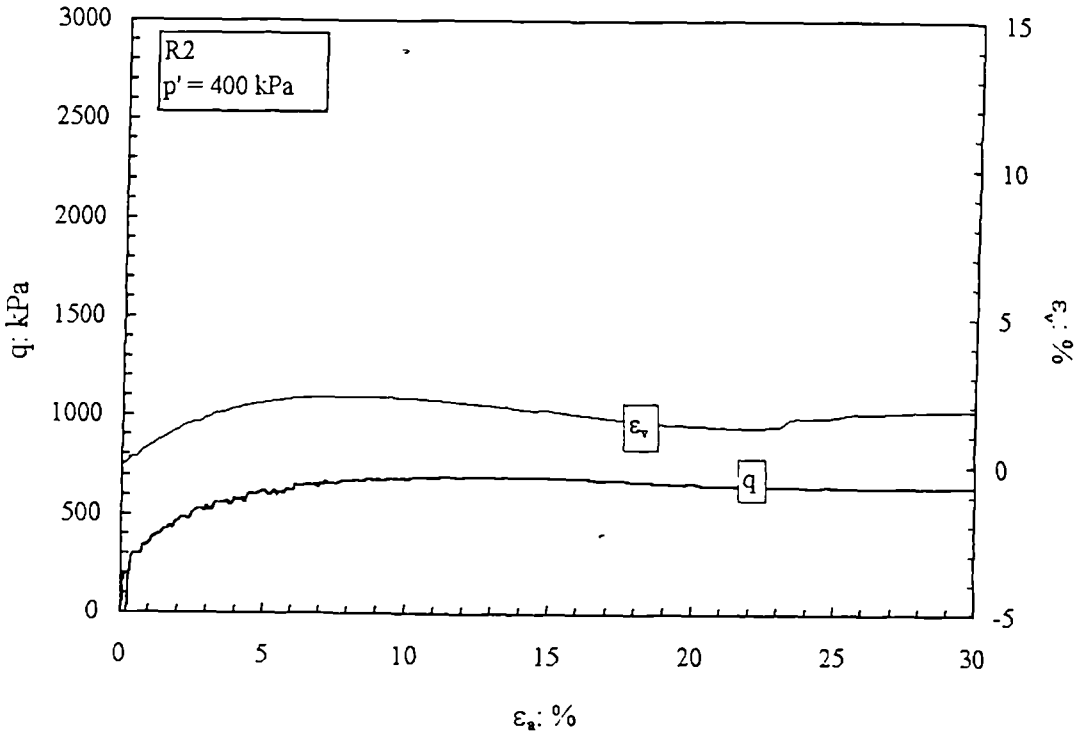

Figure 5.10 Stress-strain curve from a drained constant p' tests performed on reconstituted soil of calcarenite at low confining pressures.

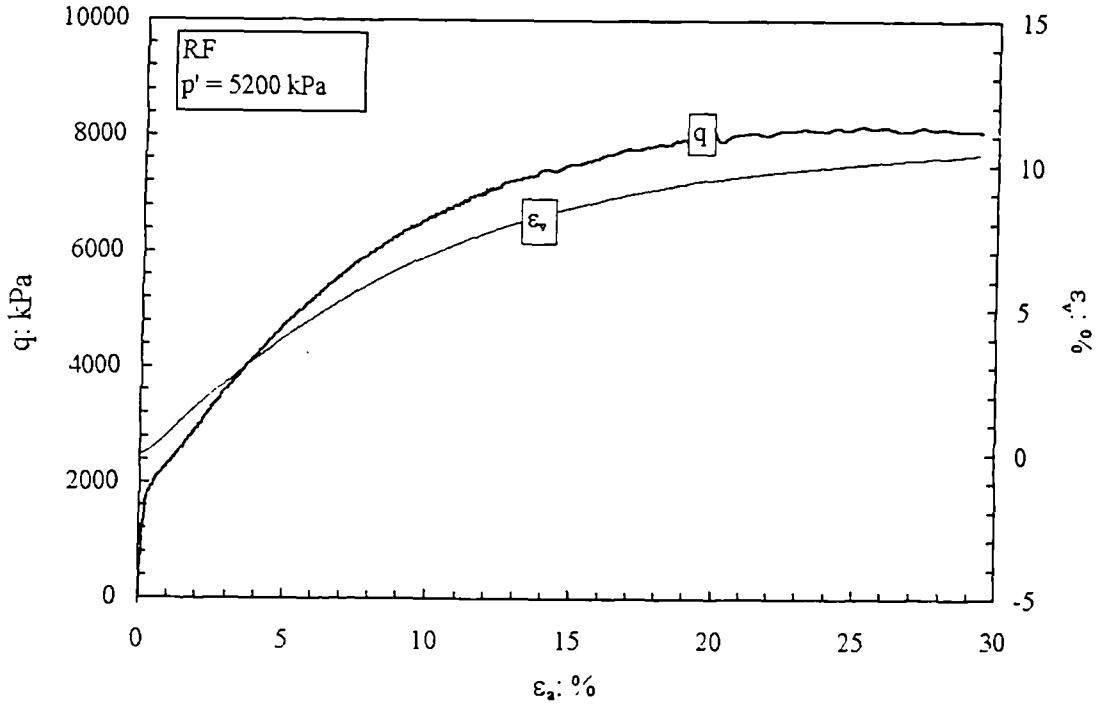

Figure 5.11 Stress-strain curve from a drained constant p' tests performed on reconstituted soil of calcarenite at high confining pressures.

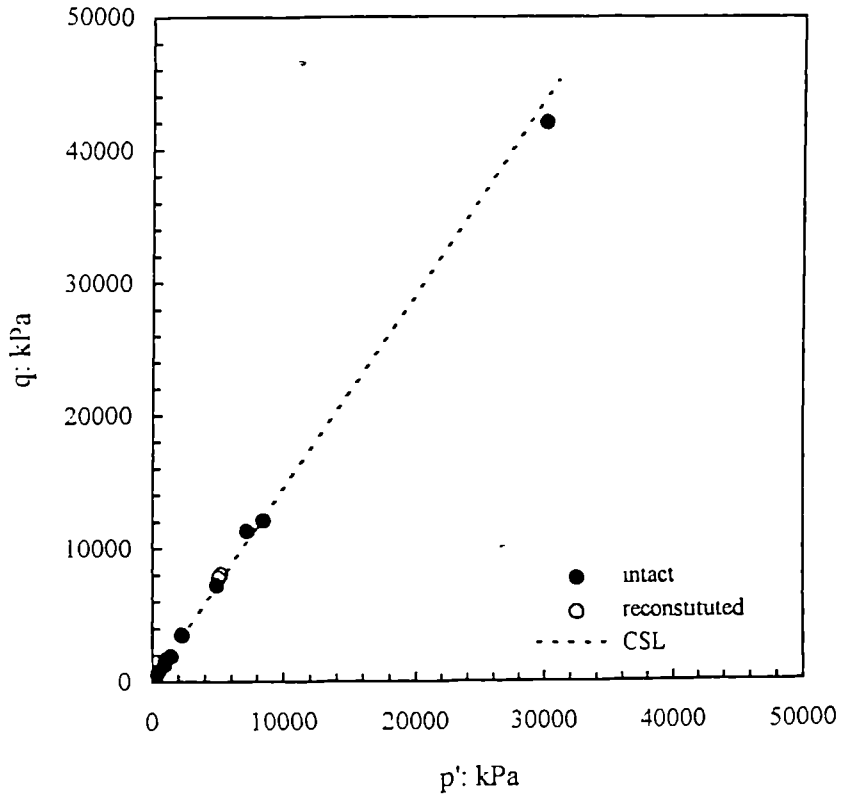

Figure 5.12 Ultimate states of intact and reconstituted samples of calcarenite.

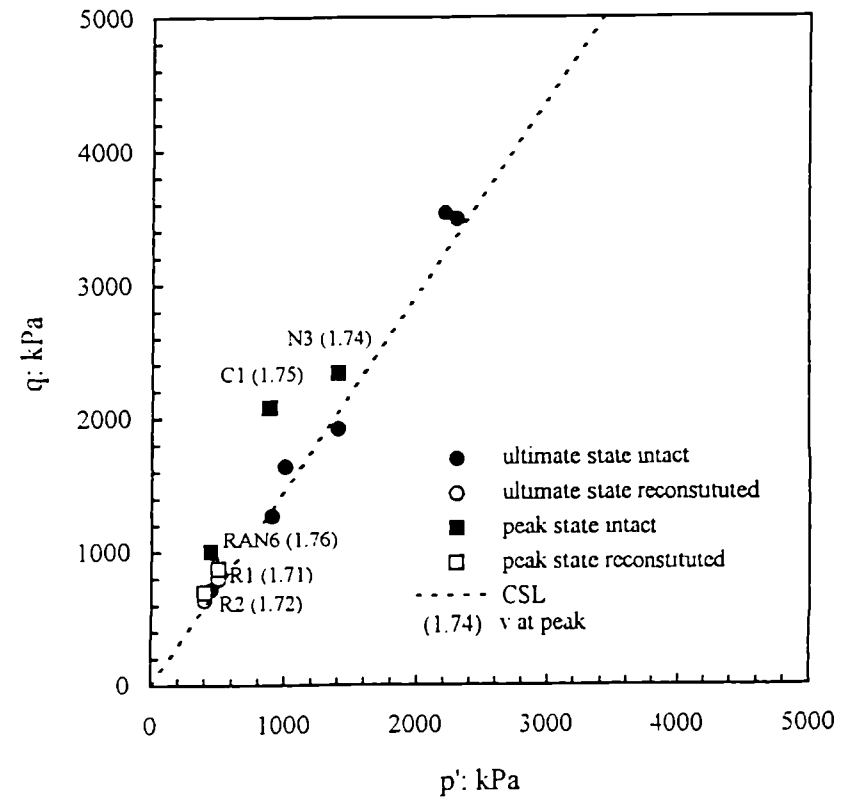

Figure 5.13 Ultimate states and peak states of intact and reconstituted samples of calcarenite.

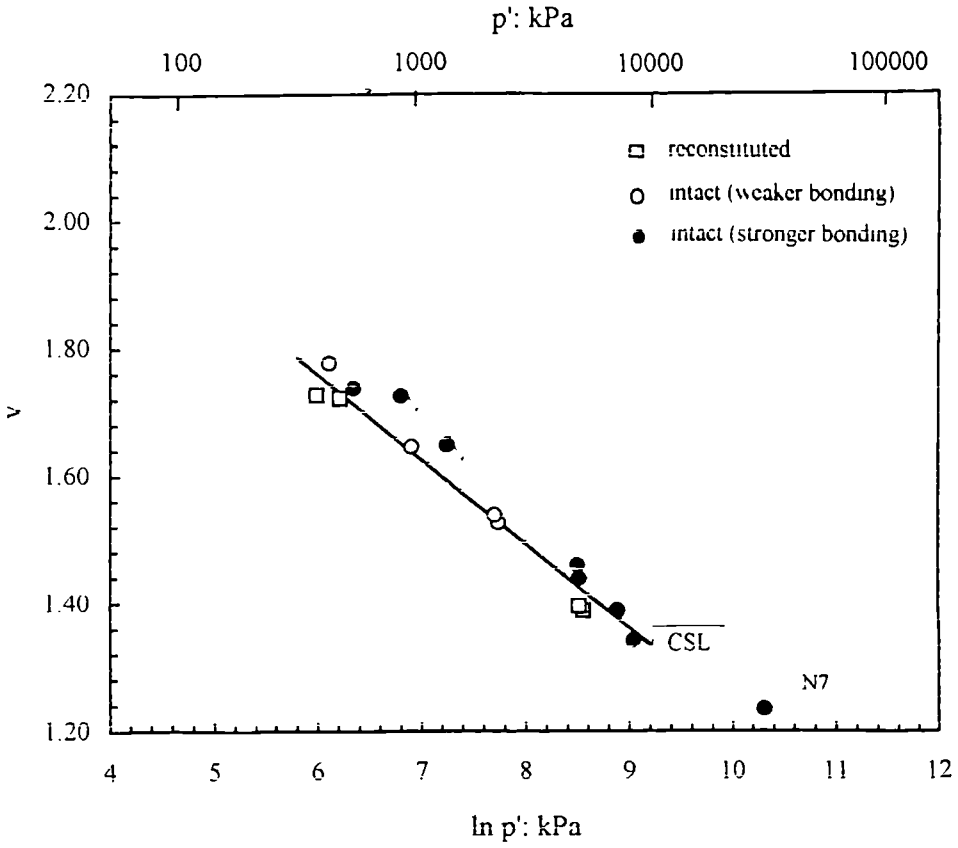

Figure 5.14 States at the end of shearing for intact and reconstituted samples of calcarenite.

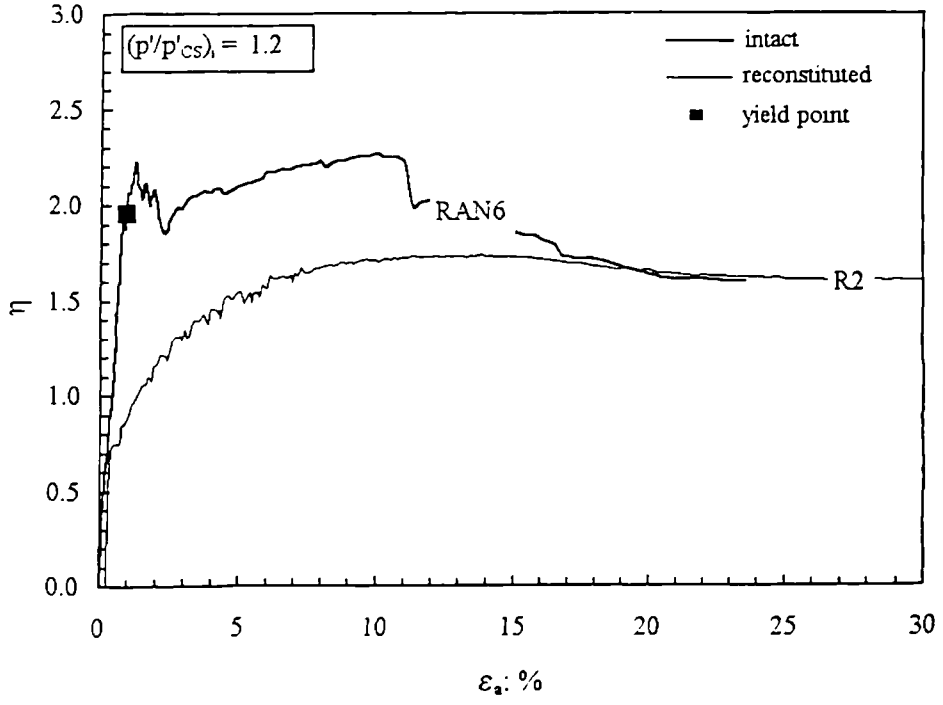

Figure 5.15 Shear behaviour of intact (after Coop and Atkinson, 1993) and reconstituted samples of calcarenite tested from similar initial values of p'/p'_{cs} at low confining pressures (constant p' tests).

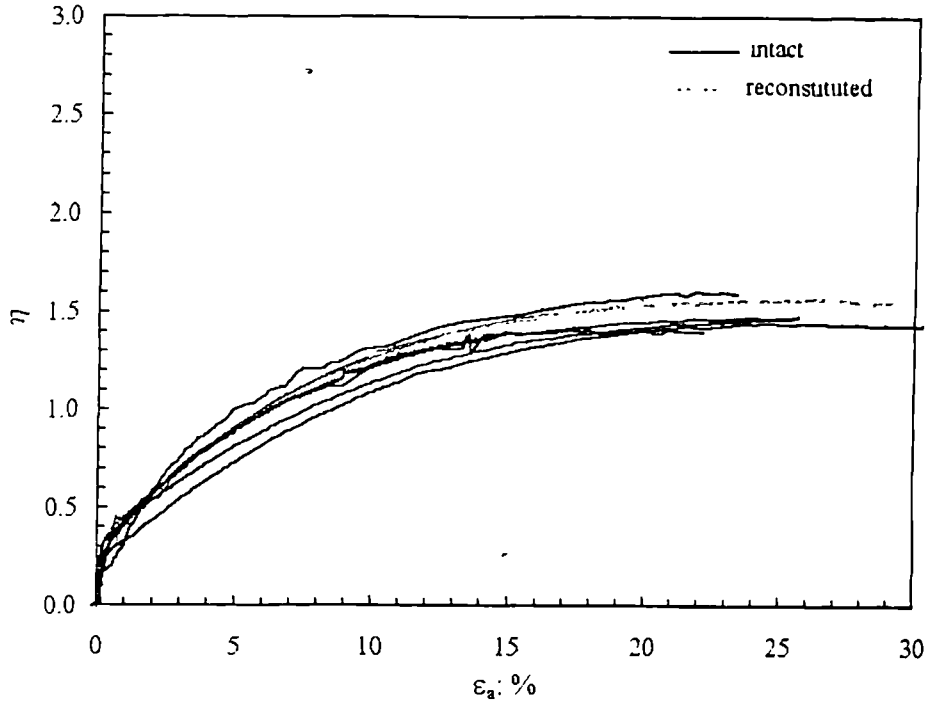

Figure 5.16 Shear behaviour of reconstituted and intact samples of calcarenite which yielded in isotropic compression (constant p' tests).

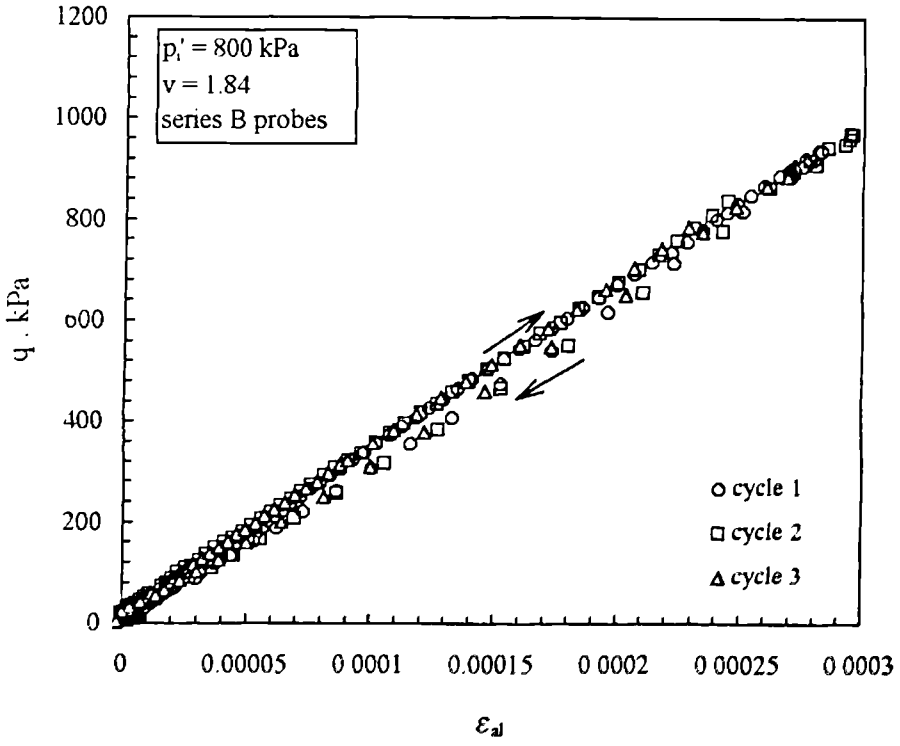

Figure 5.17 Pre-yield stress-strain relationships for undrained cycles performed on the calcarenite.

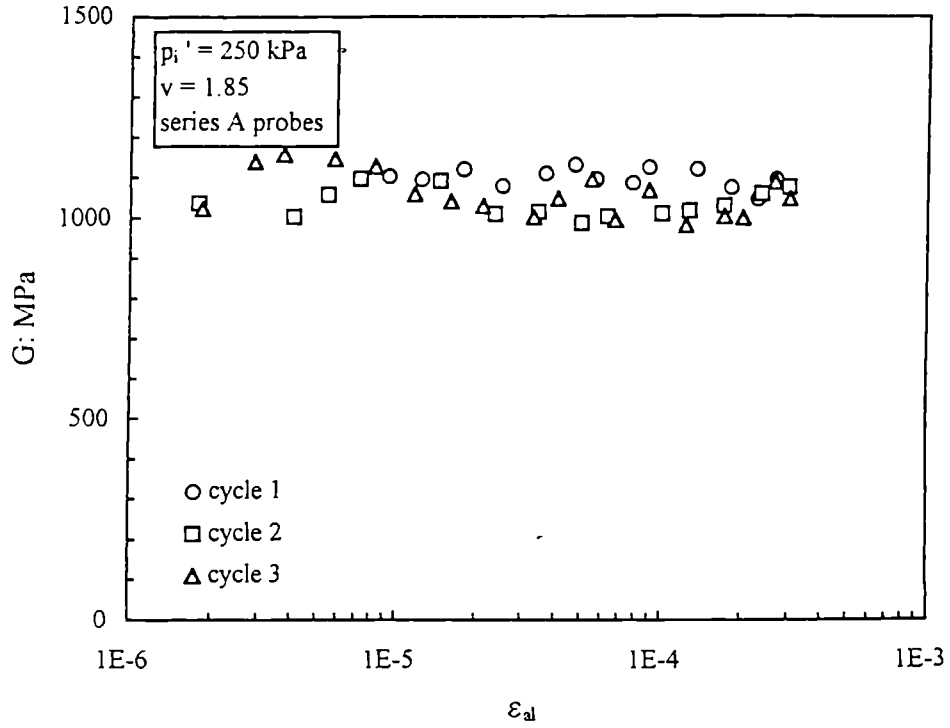

(a)

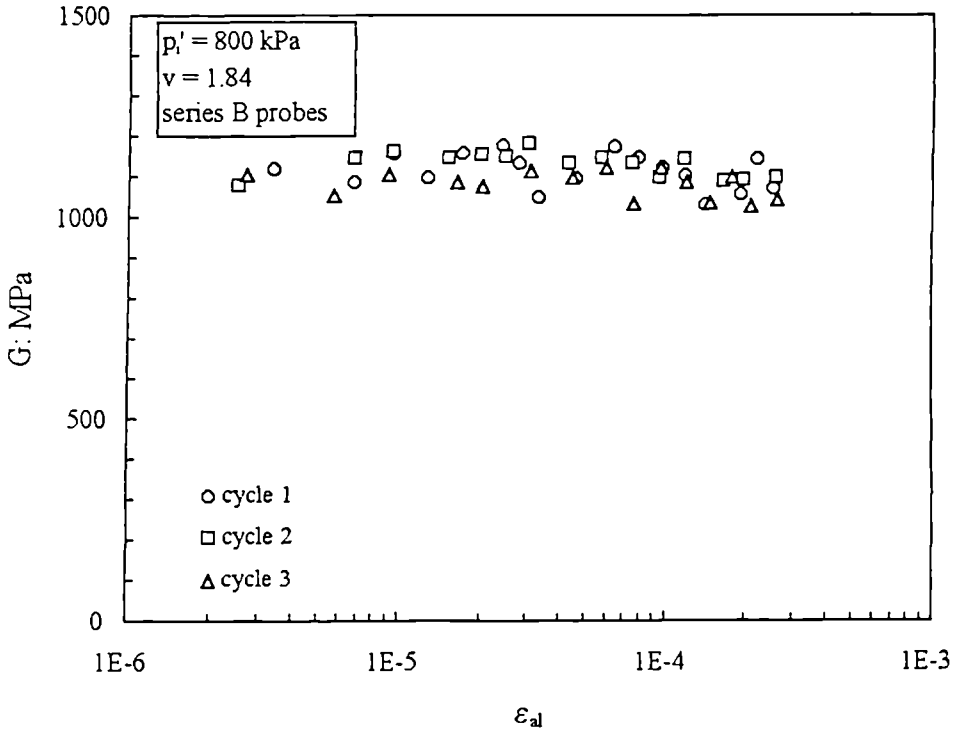

(b)

Figure 5.18 Pre-yield tangent shear moduli in two series of undrained cycles performed at low values of p'.

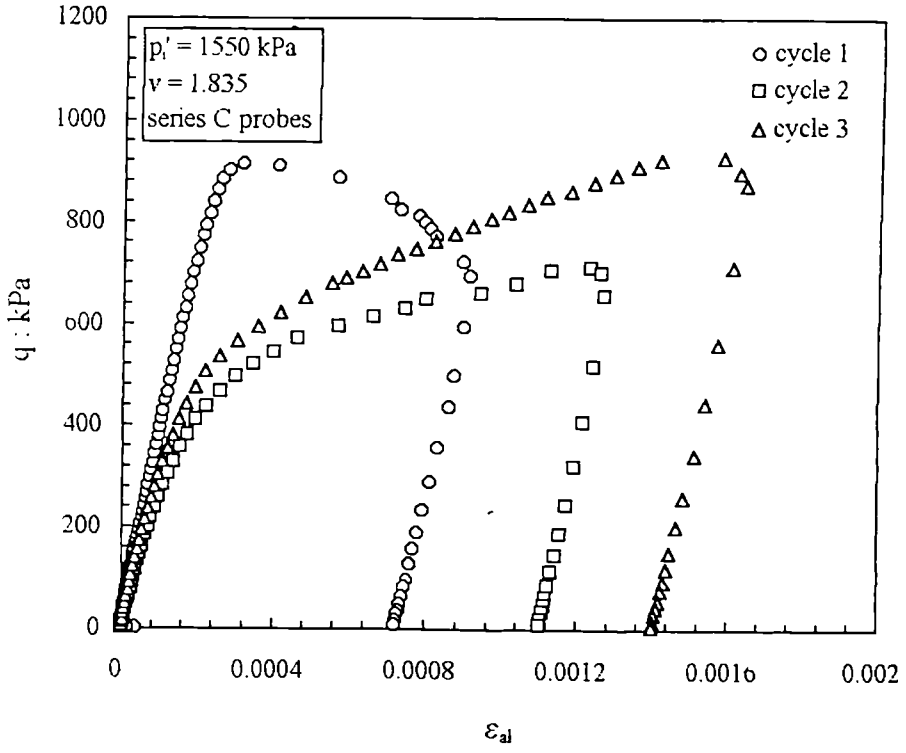

Figure 5.19a Stress-strain relationships for undrained cycles performed on the calcarenite at intermediate values of p'.

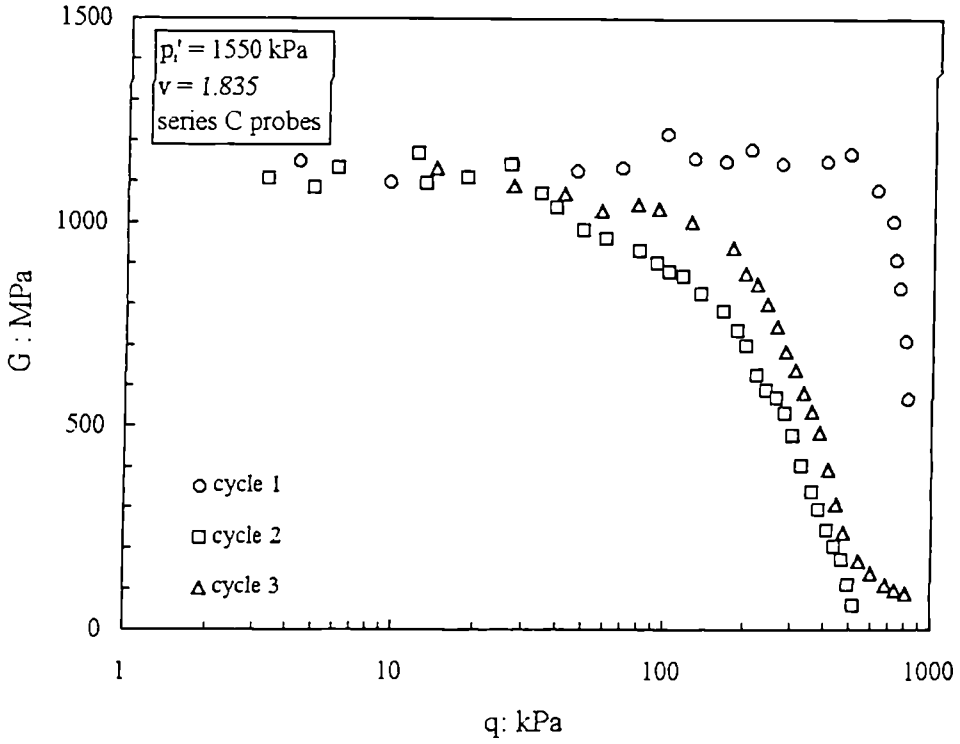

Figure 5.19b Variation of the tangent shear moduli with deviator stress for undrained loading probes performed on the calcarenite at intermediate values of p'.

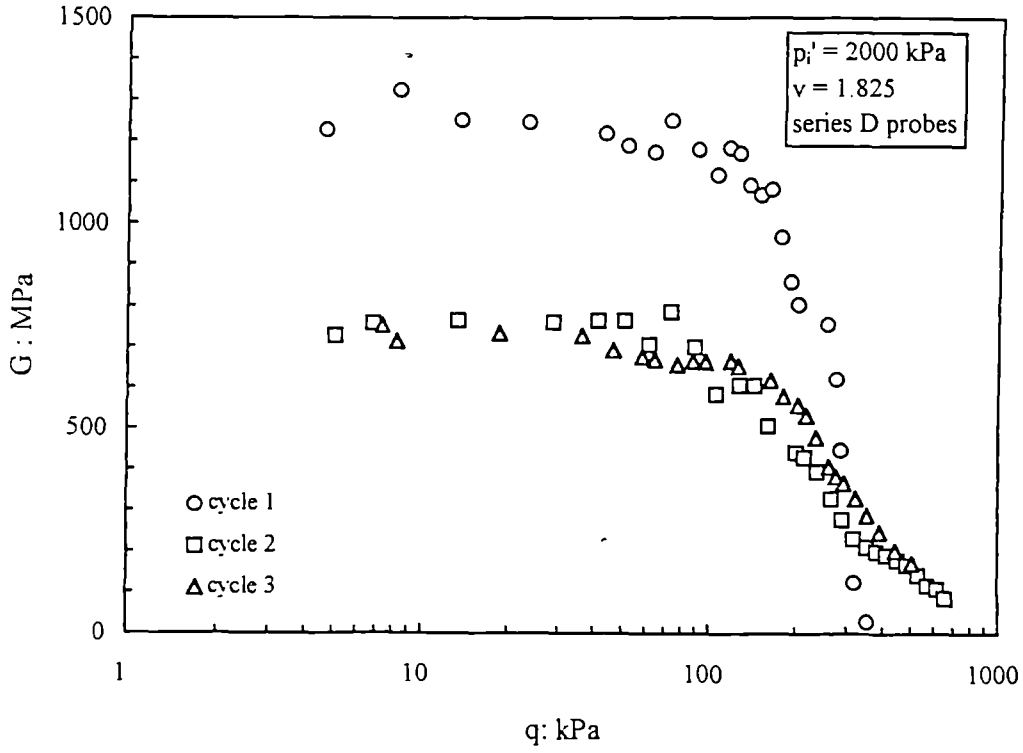

Figure 5.20 Variation of the tangent shear moduli with deviator stress for undrained loading probes performed on the calcarenite at intermediate values of p'.

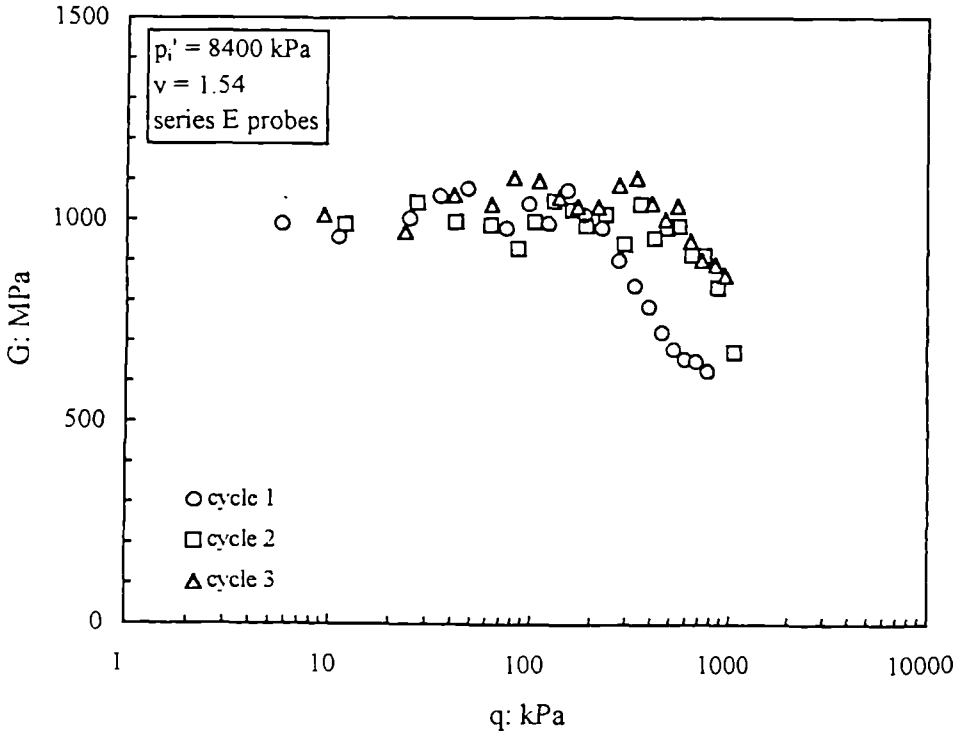

Figure 5.21 Variation of the tangent shear moduli with deviator stress for undrained loading probes performed on the calcarenite at high values of p'.

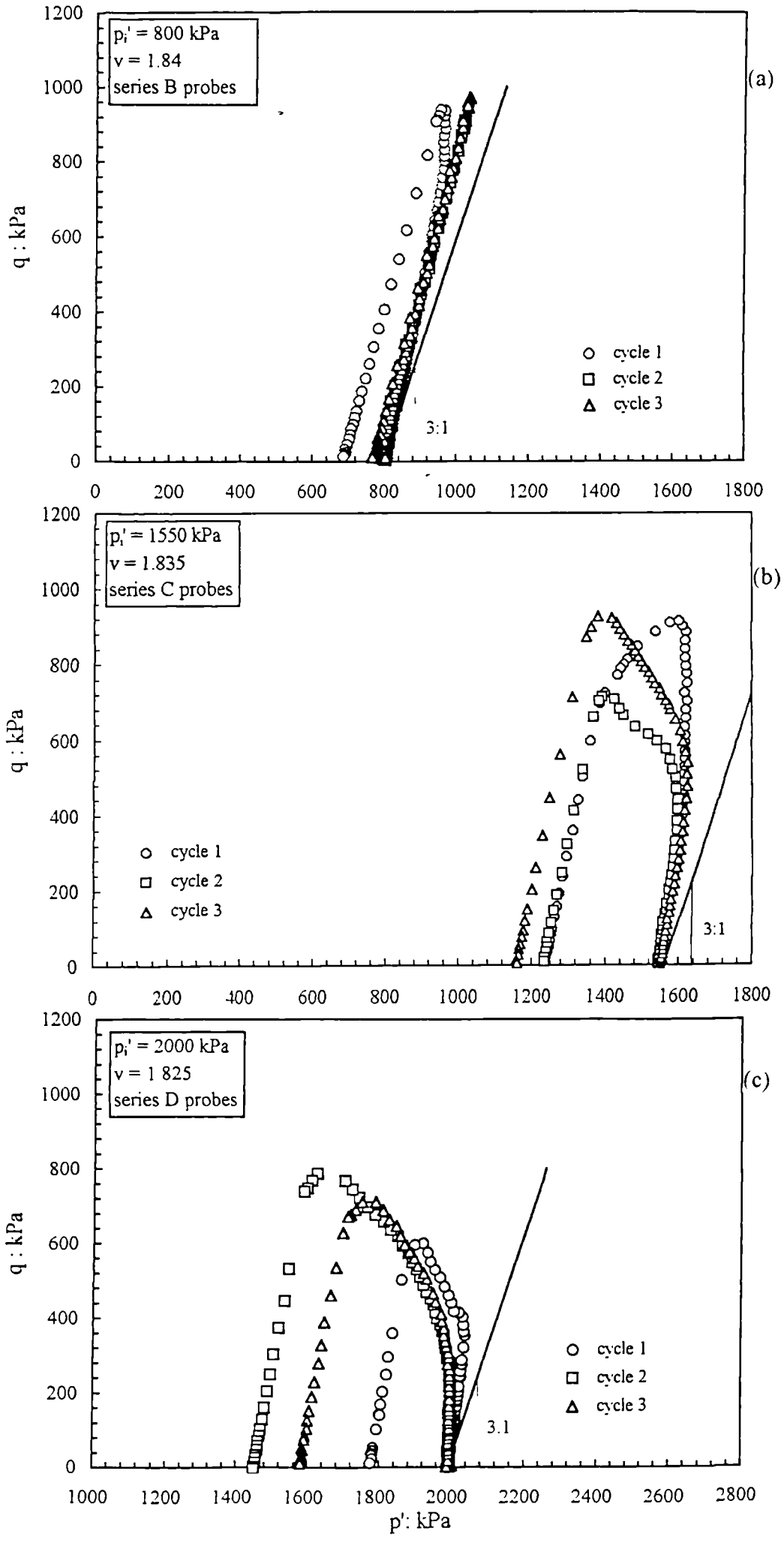

Figure 5.22 Effective stress paths for undrained cycles performed on the calcarenite for different values of p'.

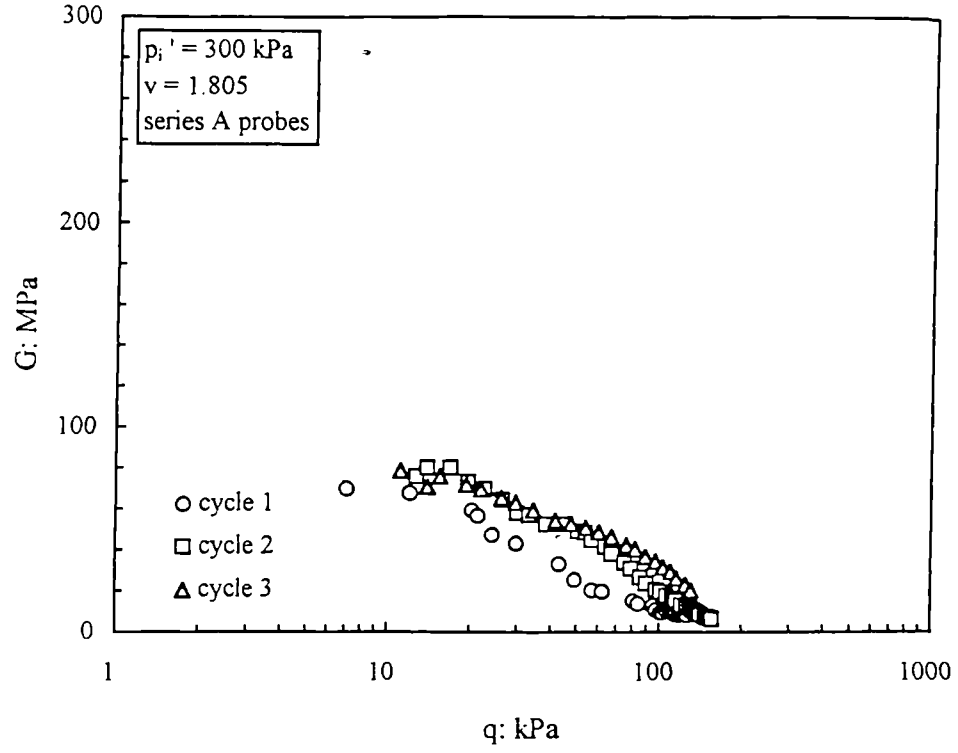

(a)

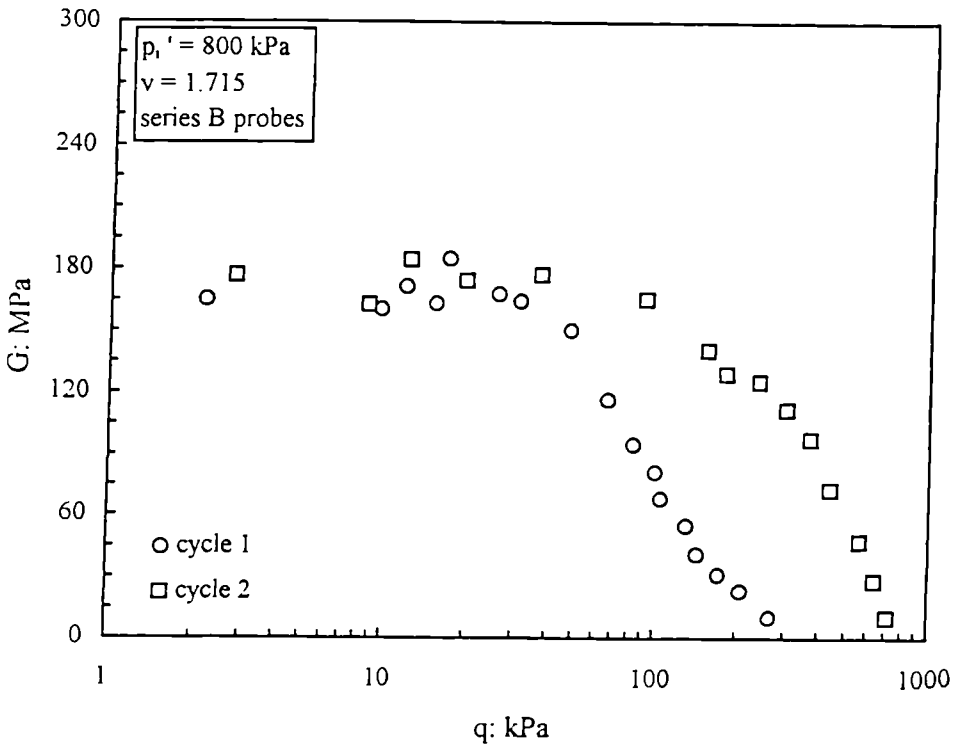

(b)

Figure 5.23 Variation of the tangent shear moduli with deviator stress from undrained loading probes on a reconstituted sample of calcarenite performed for different values of p'.

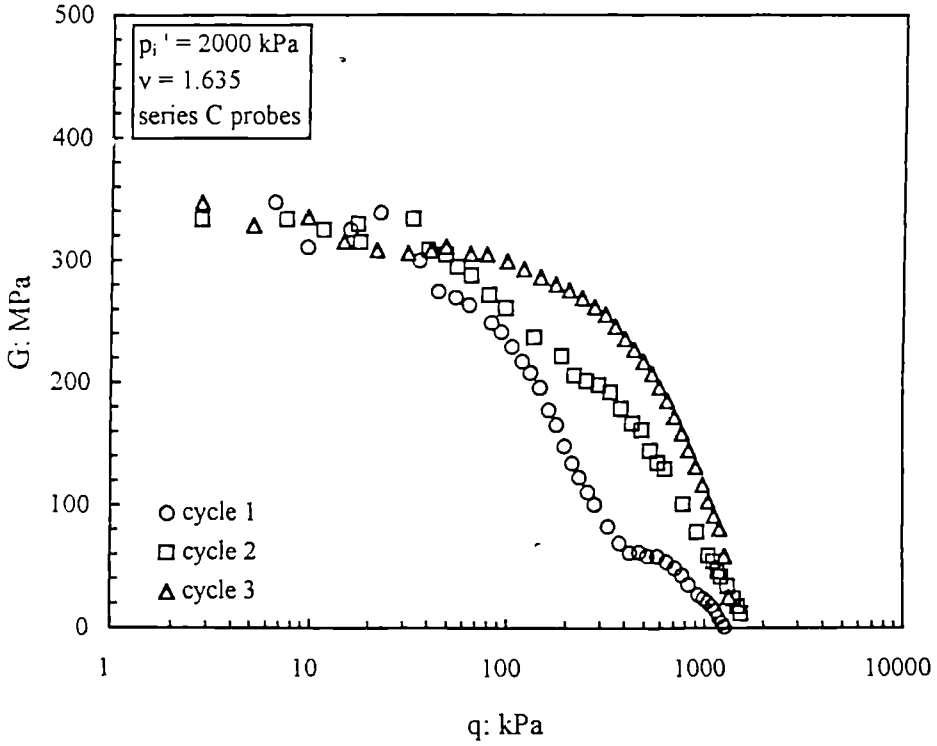

(c)

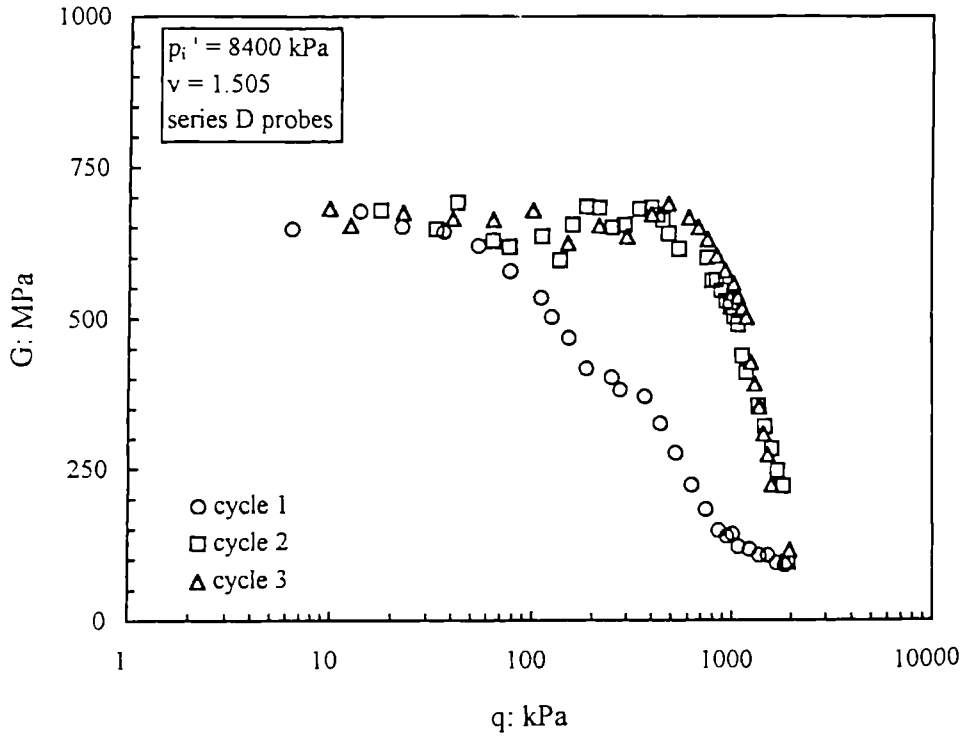

(d)

Figure 5.23 Variation of the tangent shear moduli with deviator stress from undrained loading probes on a reconstituted sample of calcarenite performed for different values of p'.

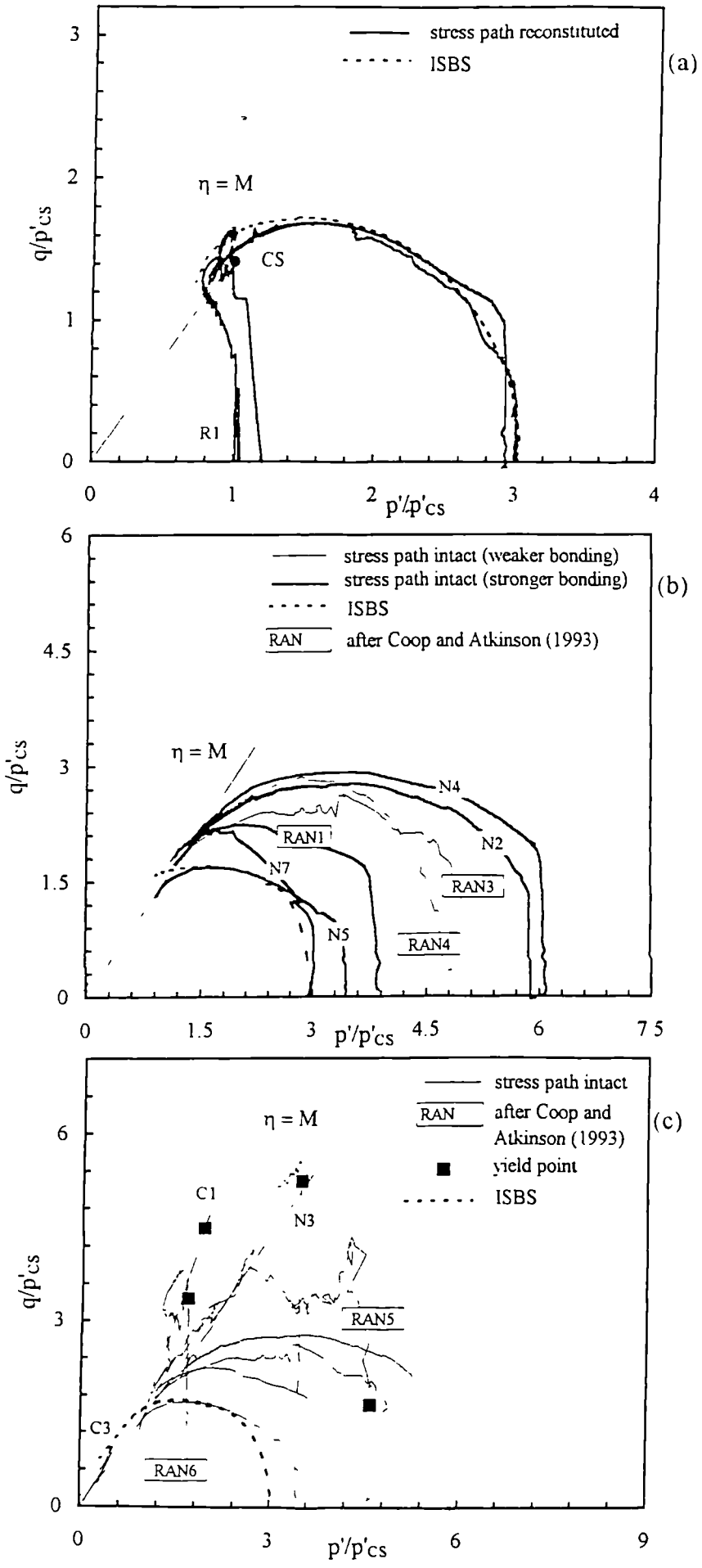

Figure 5.24 Normalized stress paths for the calcarenite: (a) reconstituted samples; (b) intact samples which yielded in isotropic compression; (c) intact samples which did not yield in isotropic compression and comparison with some of the tests in (b).

		ft	in.
"Gault, blue micaceous clay passing down into			
"Carstone, 72 ft 9 ins.	Brown clayey grit, becoming more sandy below; small scattered pebbles, and a line of pale phosphatic concretions made up of grit and grains of iron oxide 9 feet from the top	10	3
	Pebbly band, with small quartzites	0	6
	Brown sand with many scattered quartzite pebbles, and phosphatic concretions as above at several horizons. Wavy lines of iron oxide, and some beds with many grains of oxide	60	0
	Loose brown sand and grit	2	0
"Sand-rock Series, base uncertain, about 93 ft 6 ins.	White sand and blue clay interlaminated	12	0
	Do. with occasional lines of blue clay	32	0
	Striped sand and clay	9	0
	Do. chiefly clay and very sulphury	4	0
	Seam of iron oxide	0	6
	Bright-yellow and white sand, with ferruginous band at base	31	0
	Grey striped sand and clay	2	0
	White sand	3	0
"Ferruginous Sands, about 367 ft 6 ins.	Blue and striped sandy clay (? = 40 feet clay of Blackgang)	21	0
	Hard brown sandstone	3	6
	Grey sand, 'soot-coloured'	6	0
	Pebbly bands, containing small quartzites, phosphates, and iron oxide	2	0
	Dark-green or bluish clay and sand	1	0
	Ferruginous pebbly band with small phosphates and pebbles of iron oxide	1	6
	Soft yellow sand	6	6
	Dark clayey sand	6	0
	Pebbly band, containing many rolled phosphatic casts of ammonites and bivalves	0	4
	Pale-brown ferruginous sand	3	0
	Pebbly band, with small quartzites and numerous flakes of iron oxide	0	2
	Pale-brown sand with flakes of iron oxide	11	0
	Brown pebbly grit with small quartzites and grains and flakes of iron oxide	1	0
	Loose pale-green sand	17	0
	Greenish grit with many wavy seams of iron oxide	3	0
	Brown and green gritty sand	3	0
	Dark-green or nearly black clayey sand	6	0
	Brown sand with flakes and grains of iron oxide	68	0
	Greensand, with a vivid green streak; lines of clay occasionally; a layer of broken oysters nine feet from the base. Forms a smooth vertical wall	60	0
	Brown and reddish brown sandstone with grains of iron oxide very abundant about 20 feet from the top; forms the cliff on which [the remnant of] Redcliff Fort stands	114	0
"Ferruginous Sands, about 367 ft 6 ins.	Green sandy clay with wood and a line of large nodules	2	0
	Fine and very clayey sand with wood; lines of nodules in the upper part, and veins of iron oxide	14	0
	Seam of brown iron oxide	0	5
	Fine grey clayey sand	2	0
	Band of blood-red iron oxide	0	1
	Fine grey clayey sand	10	0
	Fine white clayey sand	2	0
"Atherfield Clay, 83 ft 4 ins.	Pale-blue clay with pale-blue nodules, weathering brown	77	0
	Perna Beds, 6 ft 4 ins. — Calcareous and ferruginous grit with many fossils, 1 ft 6 in. to	2	0
	Perna Beds, 6 ft 4 ins. — Passing down into pale-blue sandy clay with fossils	3	6
	Perna Beds, 6 ft 4 ins. — Impersistent grit, with scales and bones of fish, and phosphatic pebbles, some of which are rolled ammonites and bivalves; about	0	3
	Perna Beds, 6 ft 4 ins. — Pale-blue sandy clay with fossils	0	6
	Perna Beds, 6 ft 4 ins. — Grit, as above	0	0½
		617	1"[1]

Figure 6.1 Section of the Lower Greensand at Redcliff (after Osborne Wight, 1921).

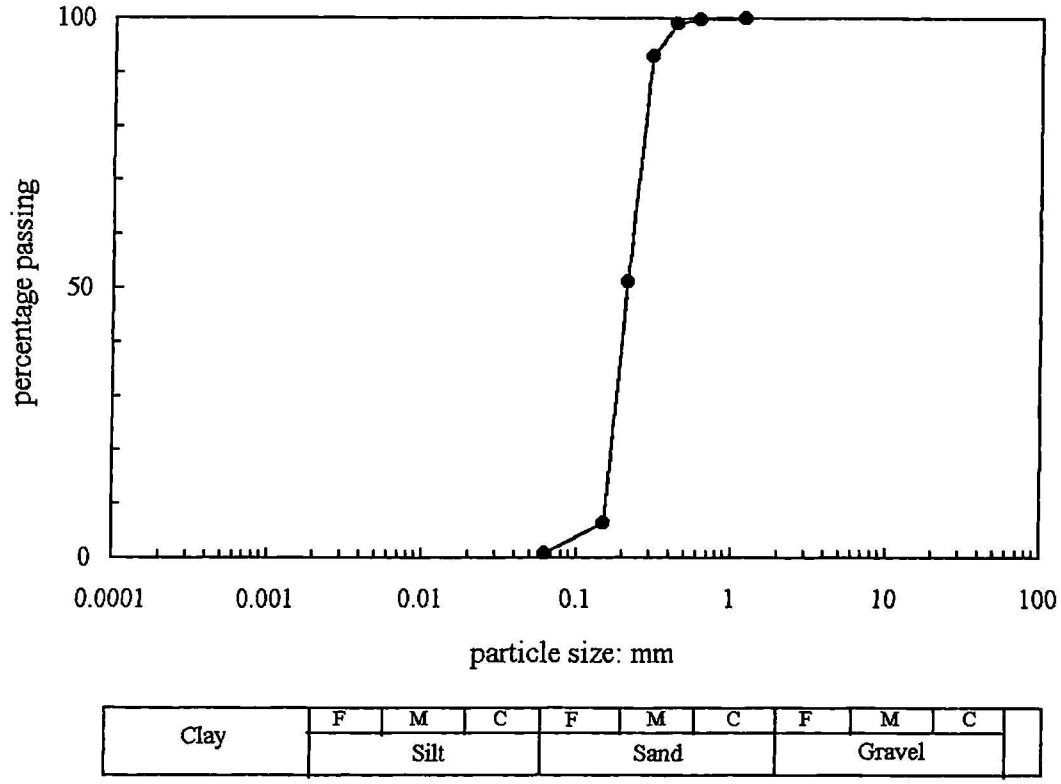

Figure 6.2 Grading curve of the reconstituted soil obtained from the silica sandstone.

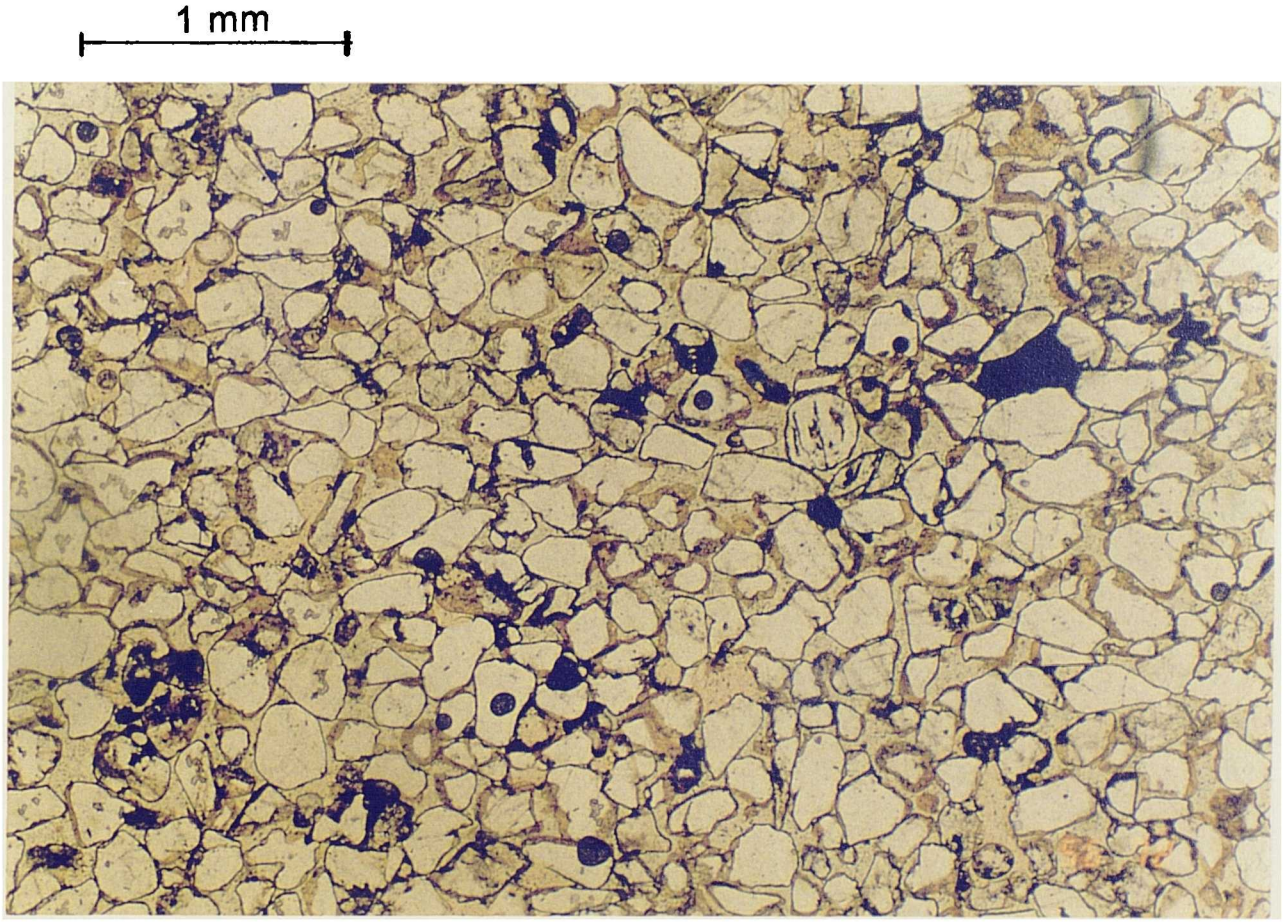

Figure 6.3 Thin section of the silica sandstone under plain white light.

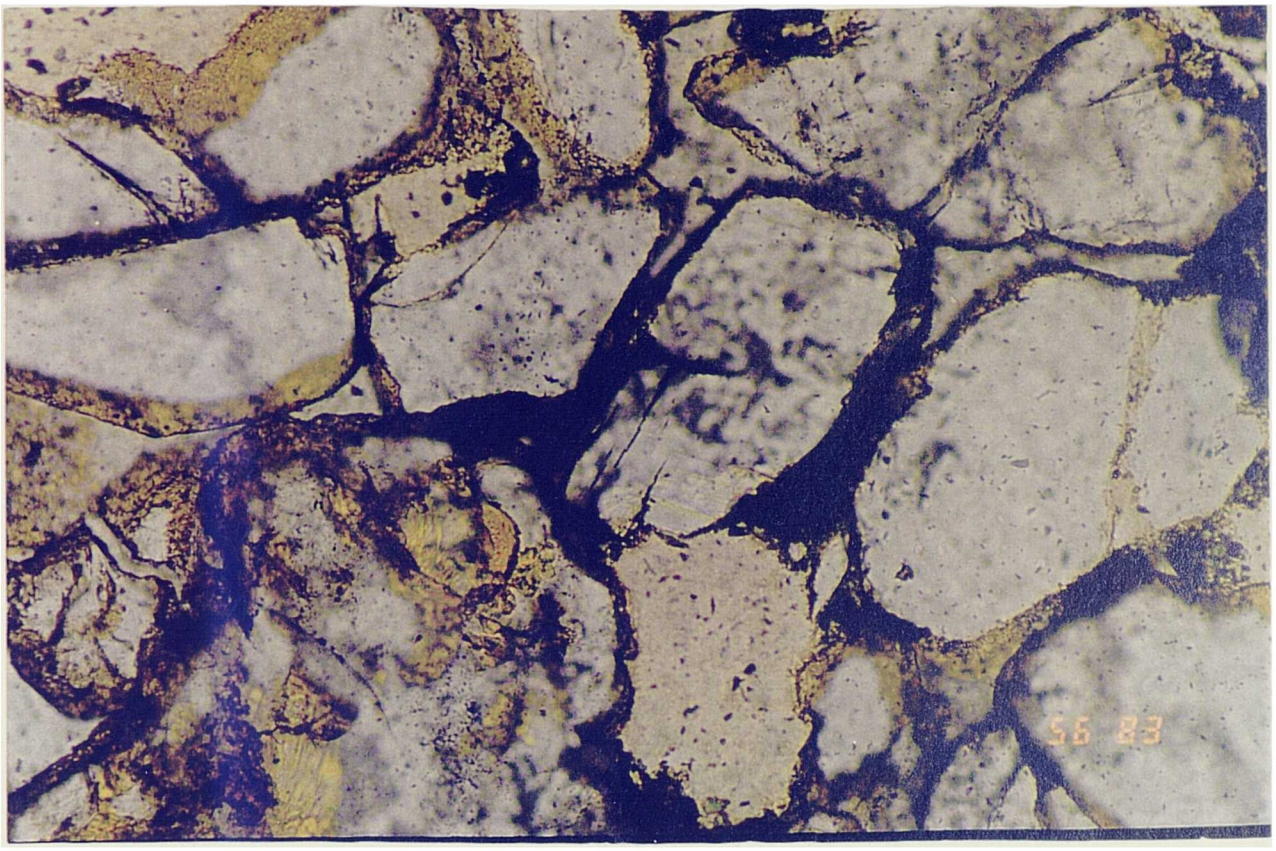

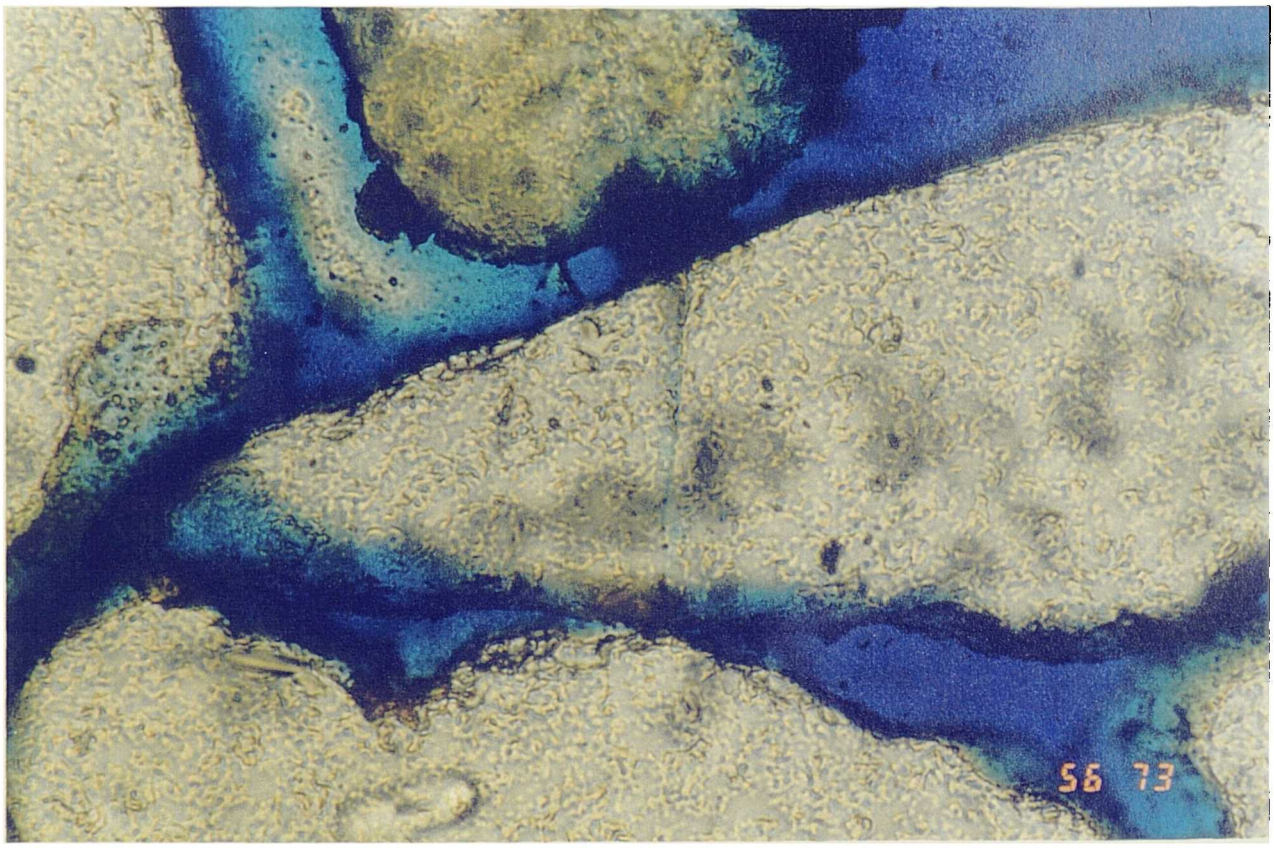

Figure 6.4 Thin sections of the silica sandstone under: (a) plain white light; (b) plain polarised light

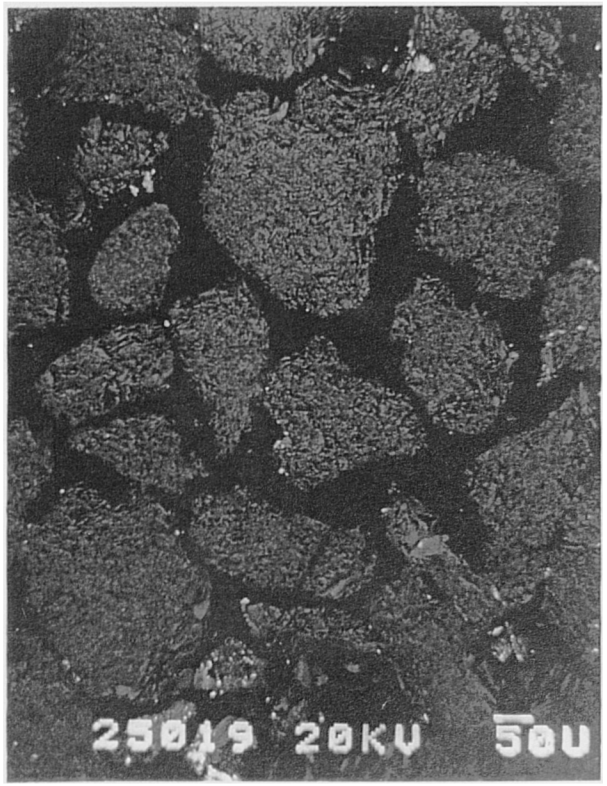

(a)

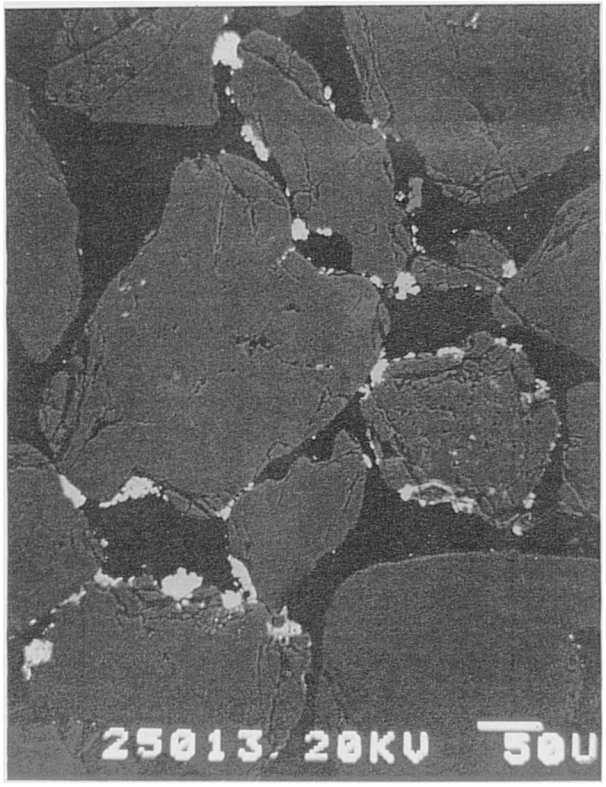

(b)

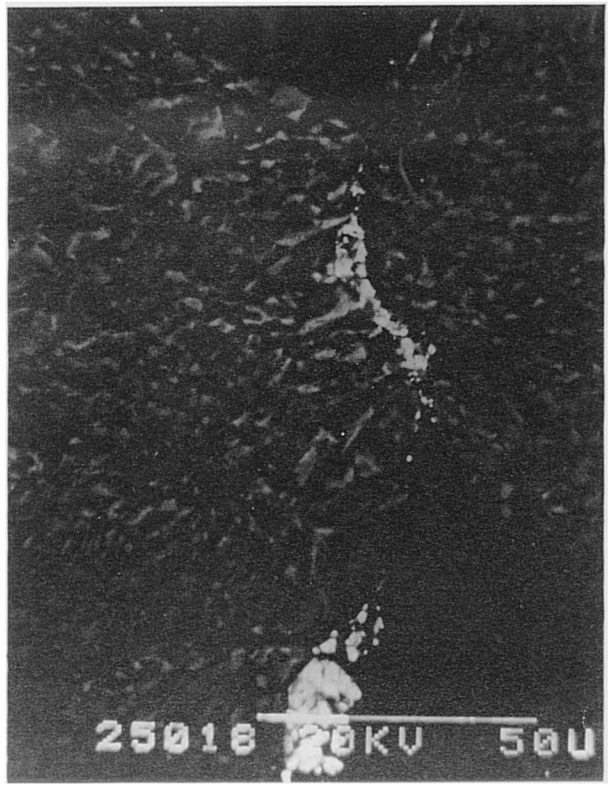

(c)

Figure 6.5 Scanning electron micrographs of the silica sandstone with different degrees of magnification: (a) and (c) samples with unpolished surfaces; (b) polished thin section.

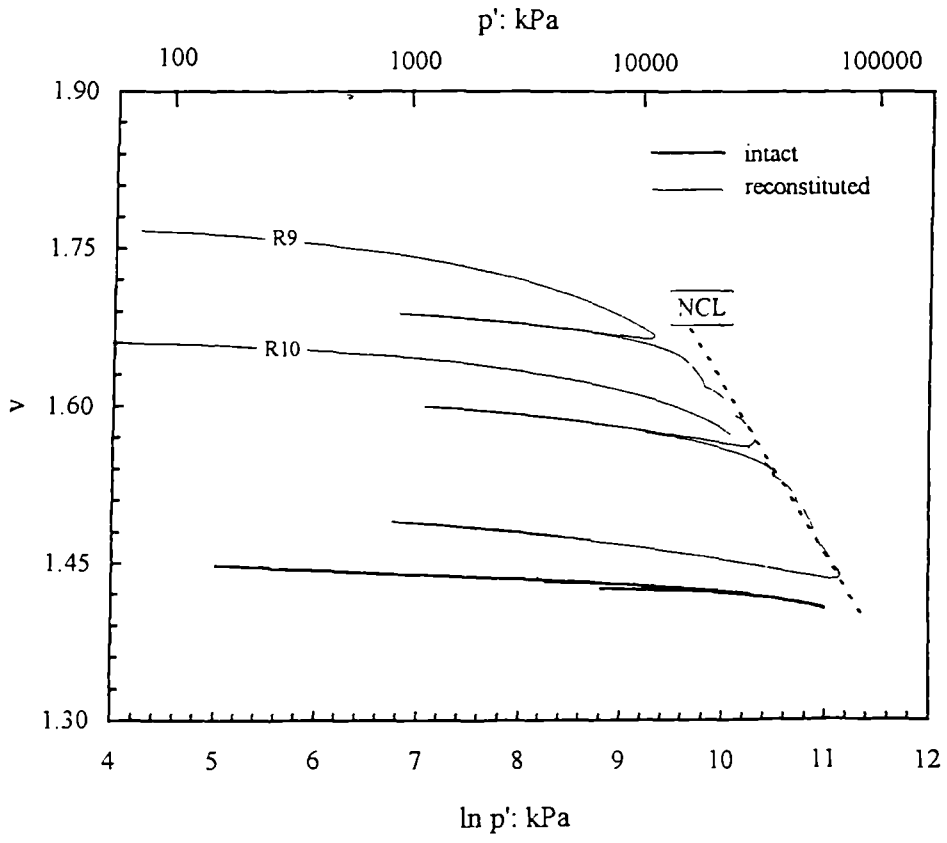

(a)

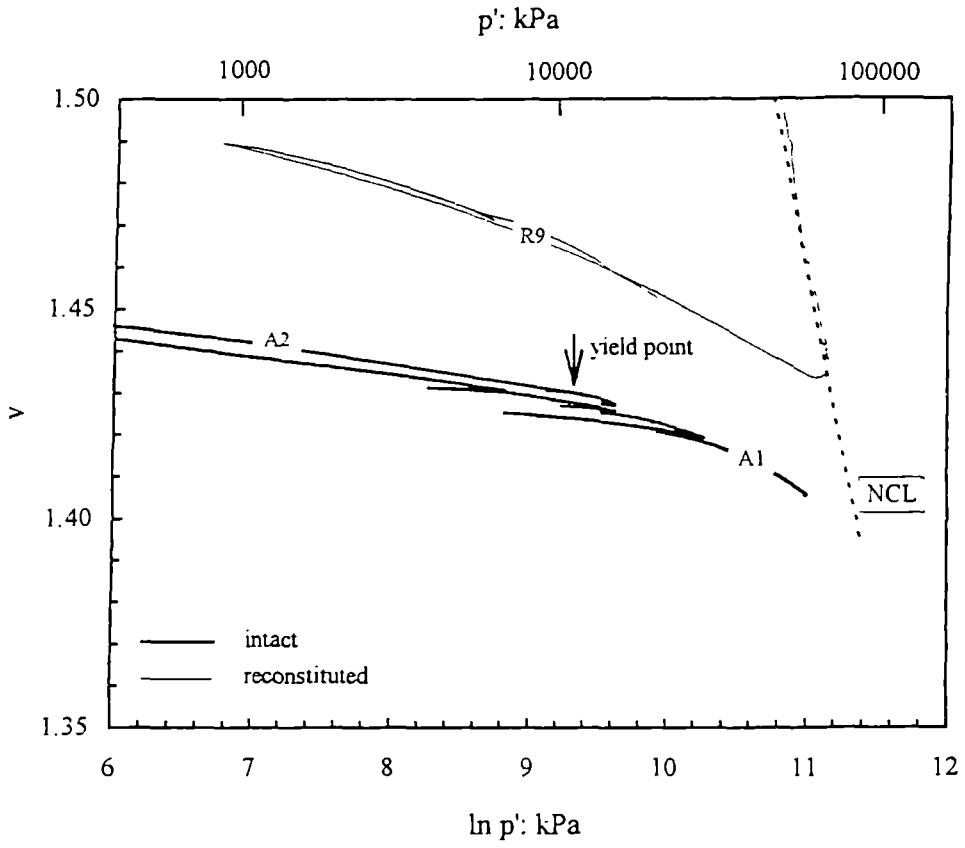

(b)

Figure 6.6 Isotropic compression of intact and reconstituted samples of silica sandstone.

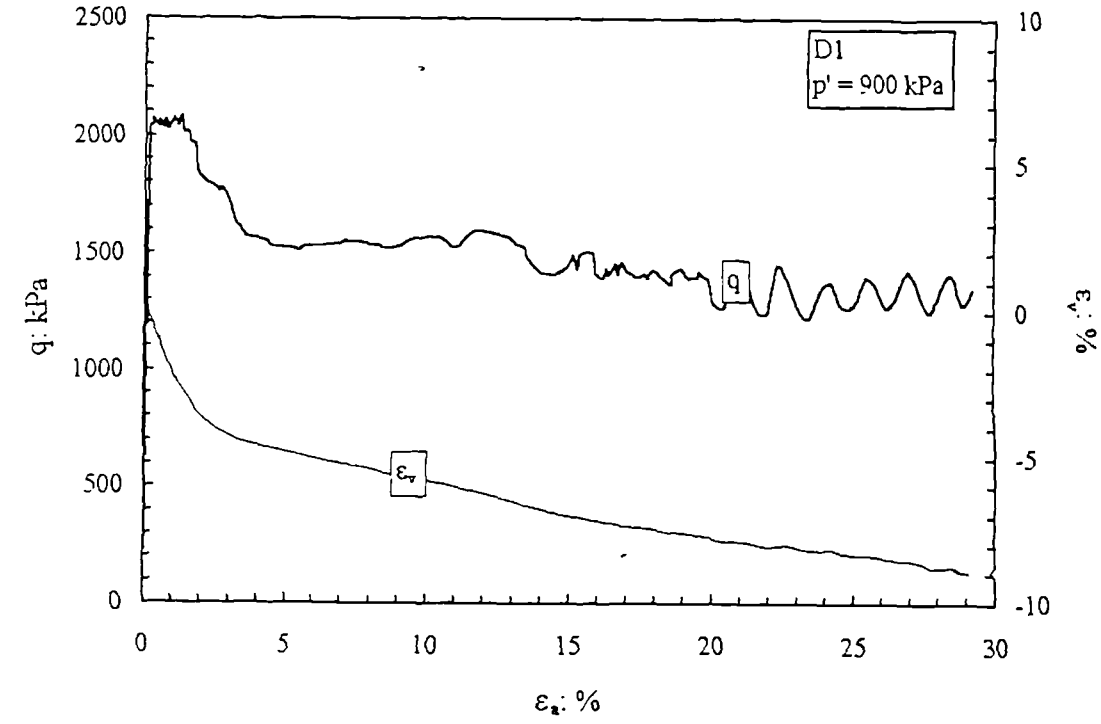

(a)

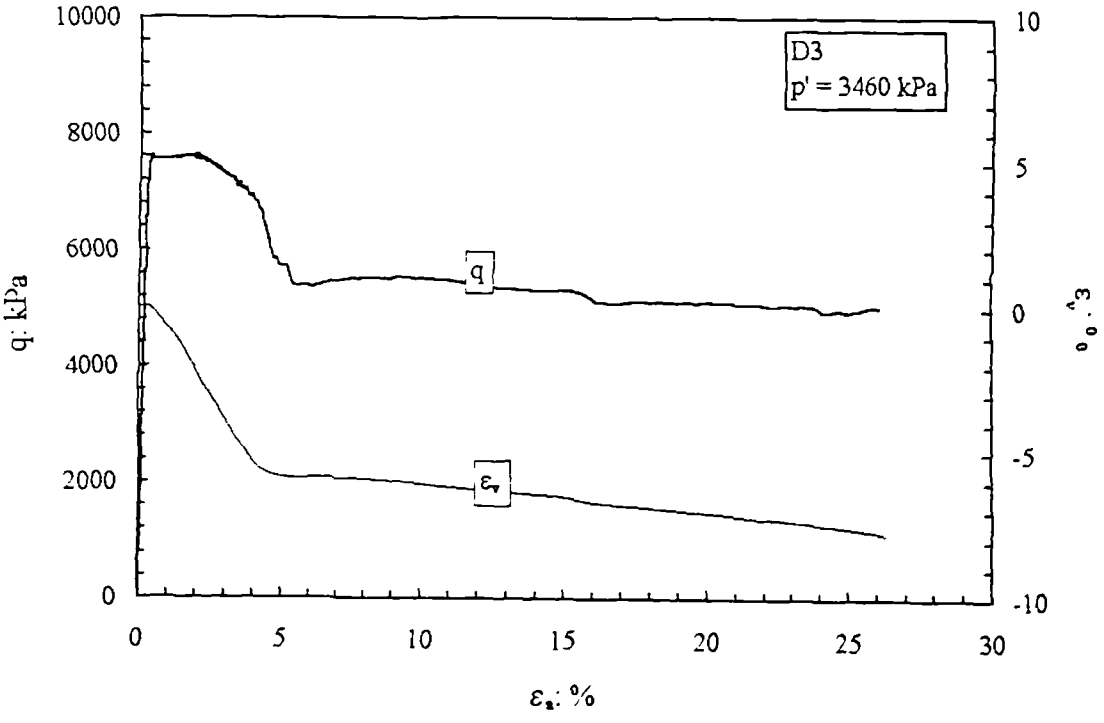

(b)

Figure 6.7 Stress-strain curves from drained constant p' tests performed on the silica sandstone at relatively low confining pressures.

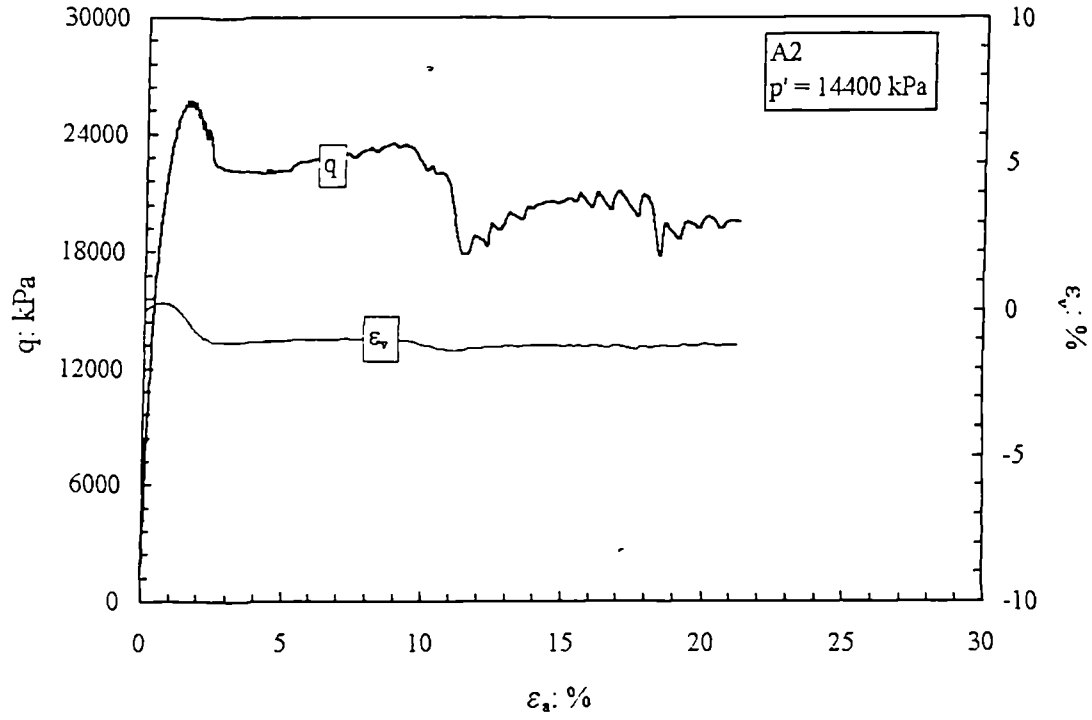

(a)

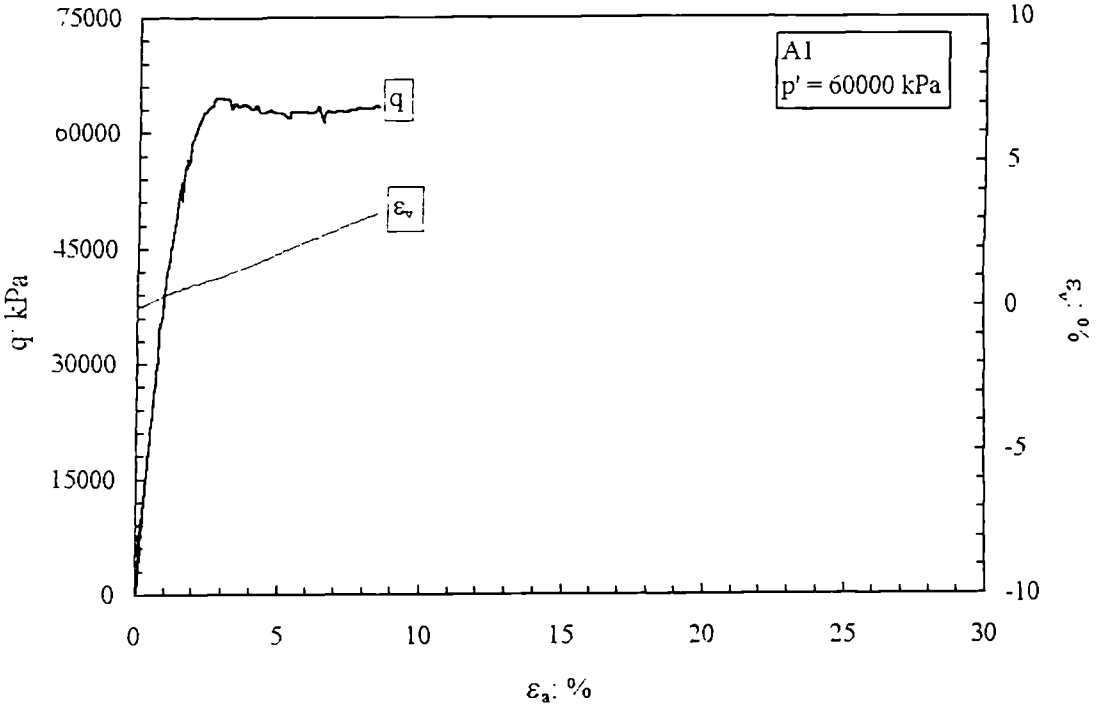

(b)

Figure 6.8 Stress-strain curves from drained constant p' tests performed on the silica sandstone at high confining pressures.

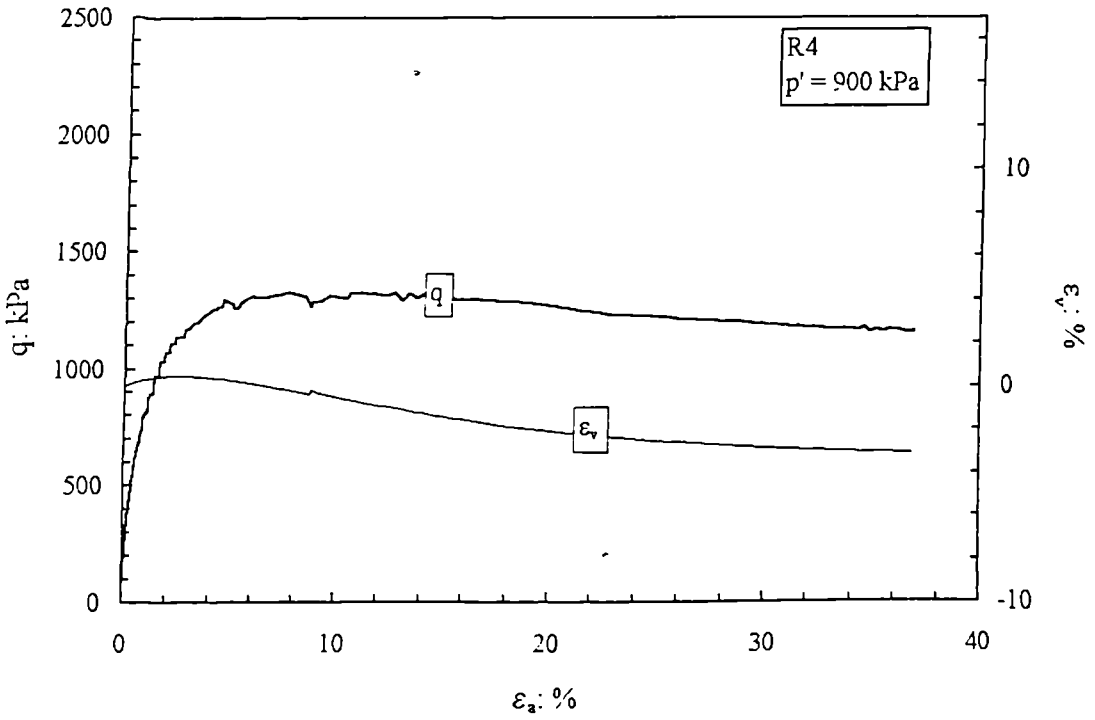

(a)

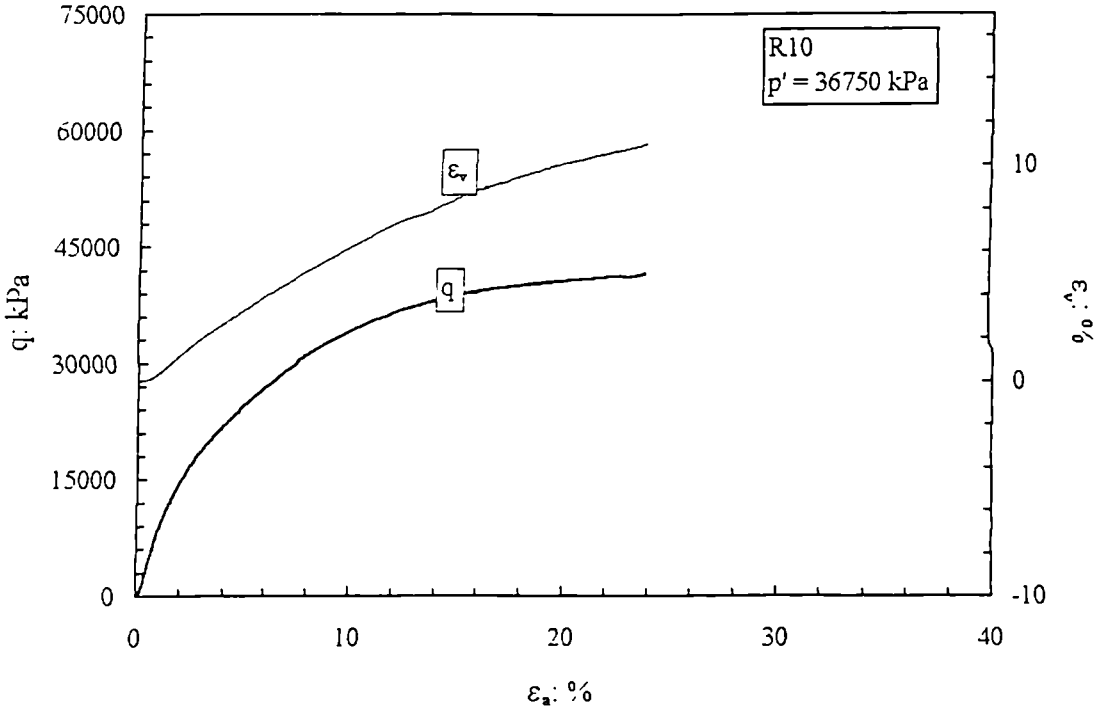

(b)

Figure 6.9 Stress-strain curves from drained constant p' tests performed on reconstituted samples of silica sandstone (a) at the lowest and (b) at the highest confining pressures.

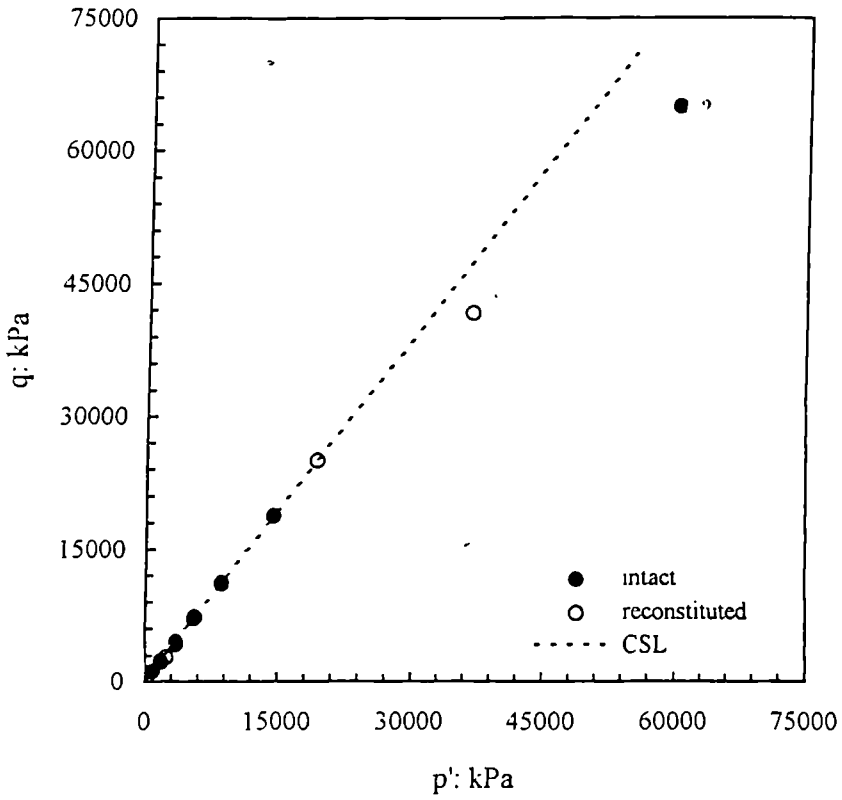

Figure 6.10 Ultimate states of intact and reconstituted samples of silica sandstone.

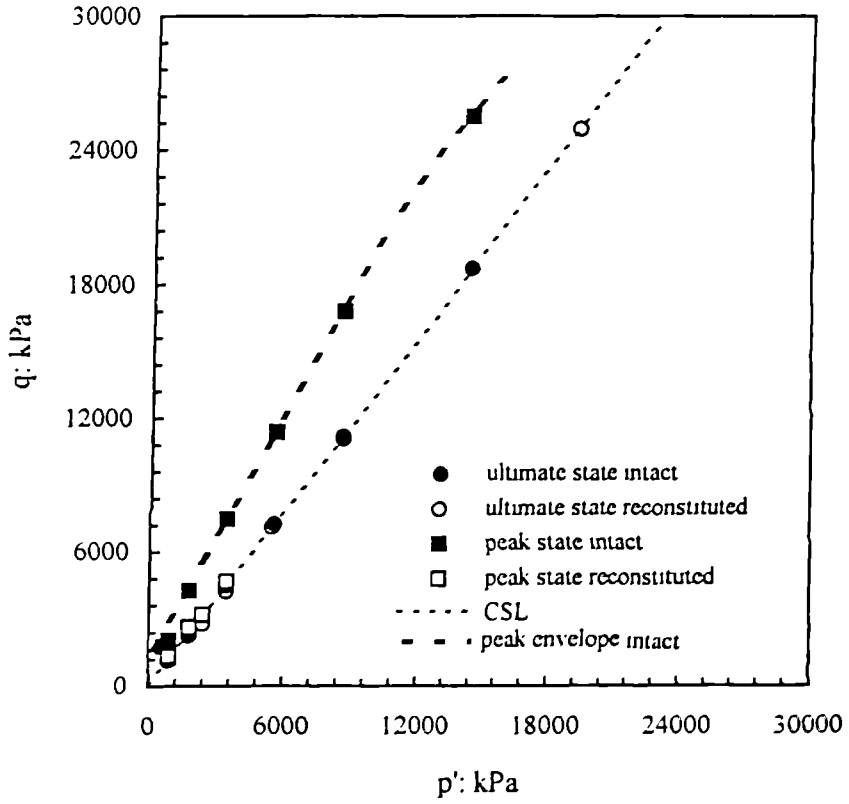

Figure 6.11 Ultimate states and peak states of intact and reconstituted samples of silica sandstone.

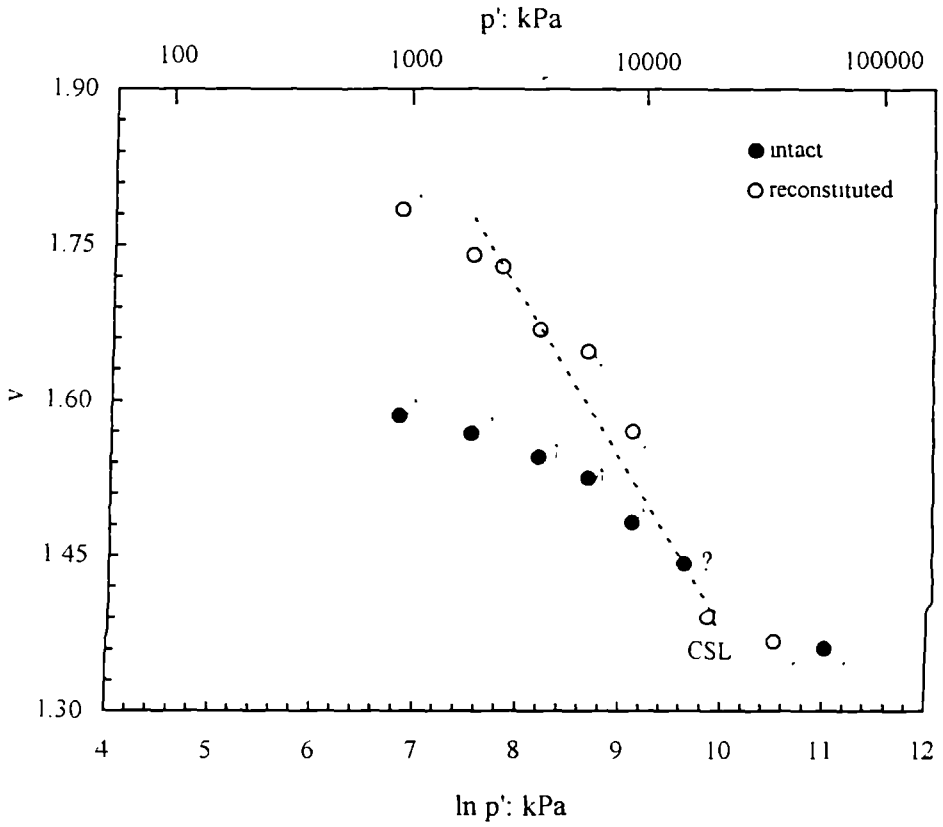

Figure 6.12 States at the end of shearing for intact and reconstituted samples of silica sandstone.

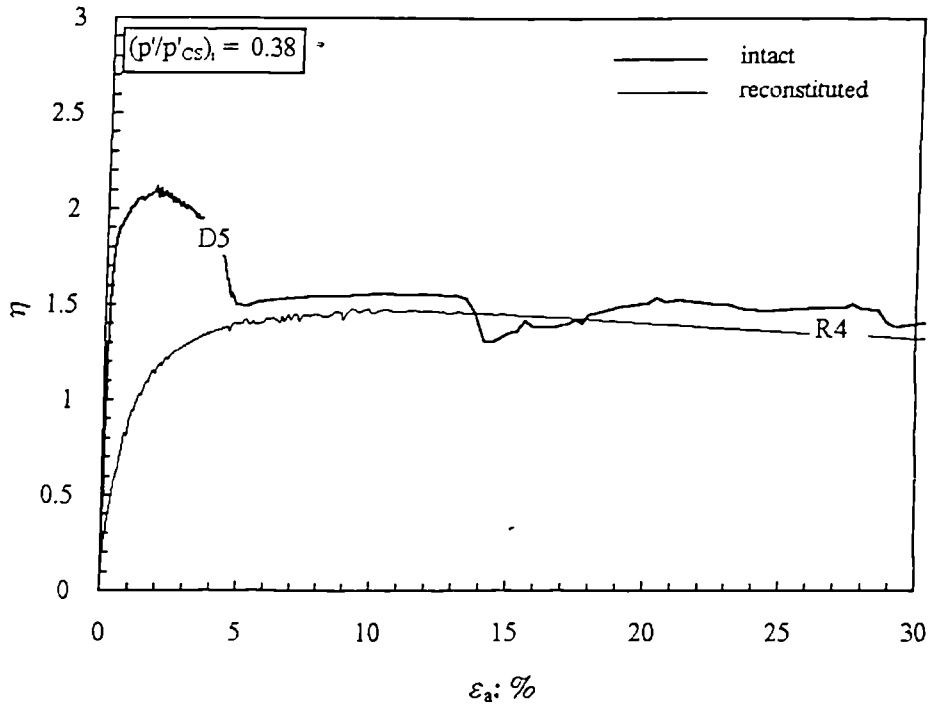

(a)

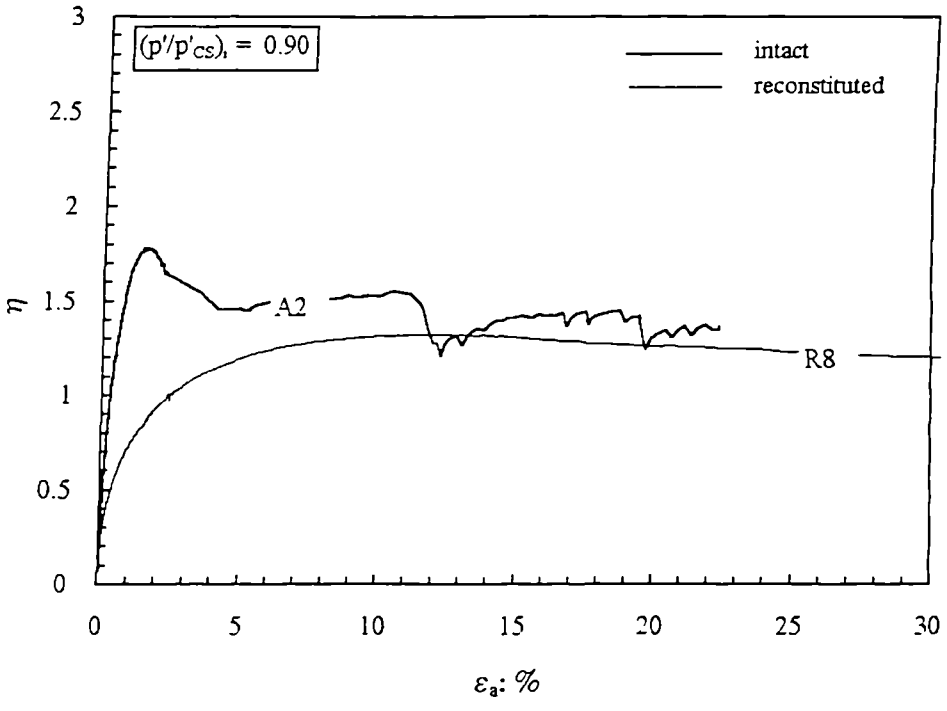

(b)

Figure 6.13 Shear behaviour of intact and reconstituted samples of silica sandstone tested from similar initial values of p'/p'_{cs} at (a) relatively low and (b) high confining pressures (constant p' tests).

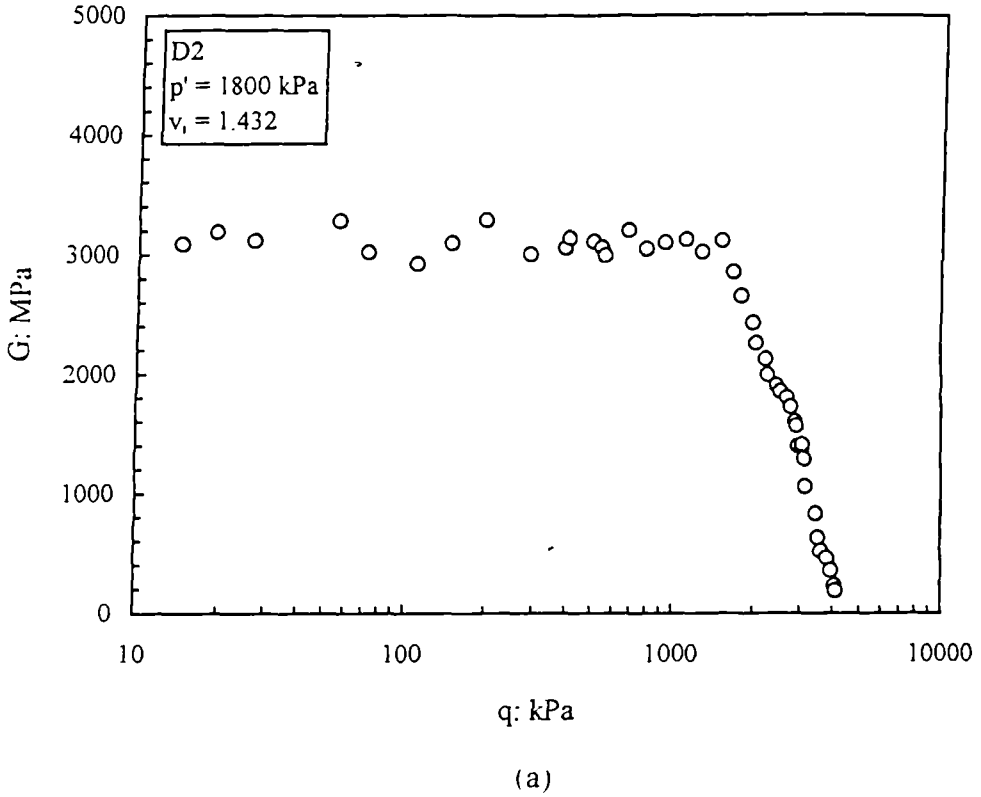

(a)

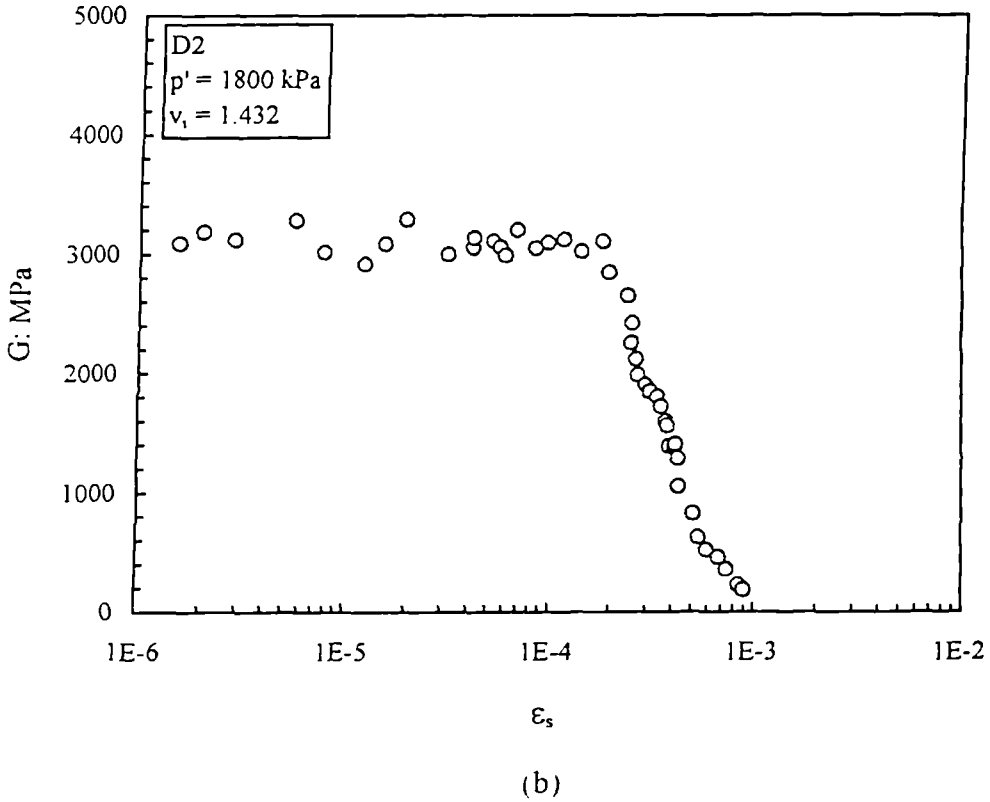

(b)

Figure 6.14 Tangent shear modulus as a function of (a) deviator stress and (b) shear strain for a constant p' test performed at relatively low confining pressures.

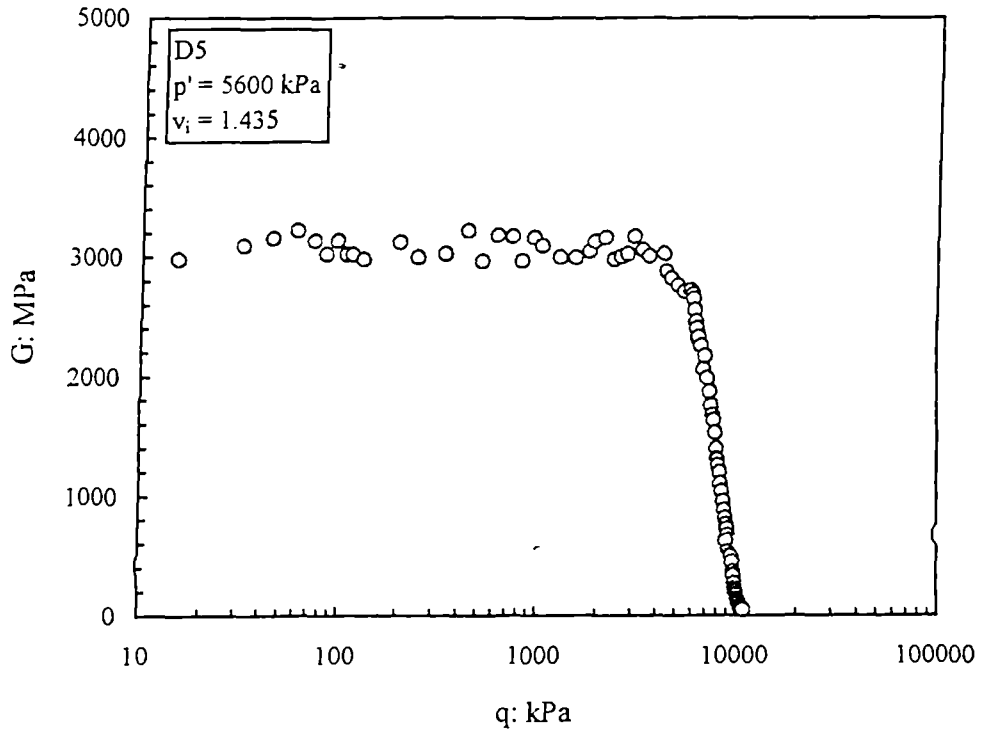

Figure 6.15 Tangent shear modulus as a function of deviator stress for a constant p' stress path test performed at intermediate confining pressures.

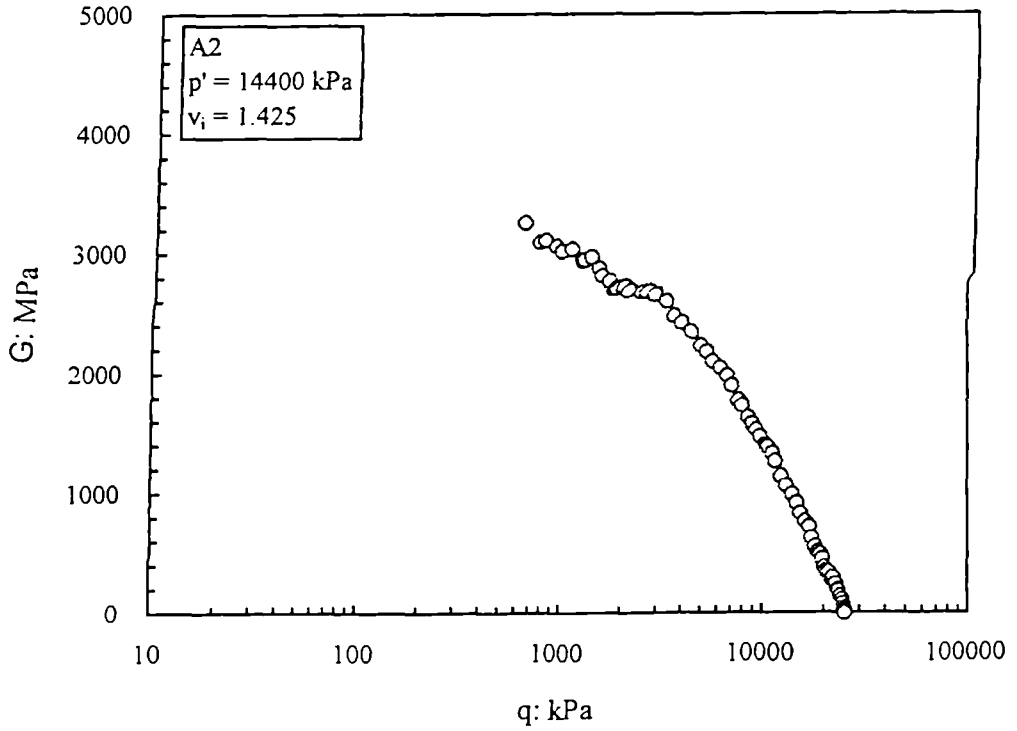

Figure 6.16 Tangent shear modulus as a function of deviator stress for a constant p' stress path tests performed at high confining pressures.

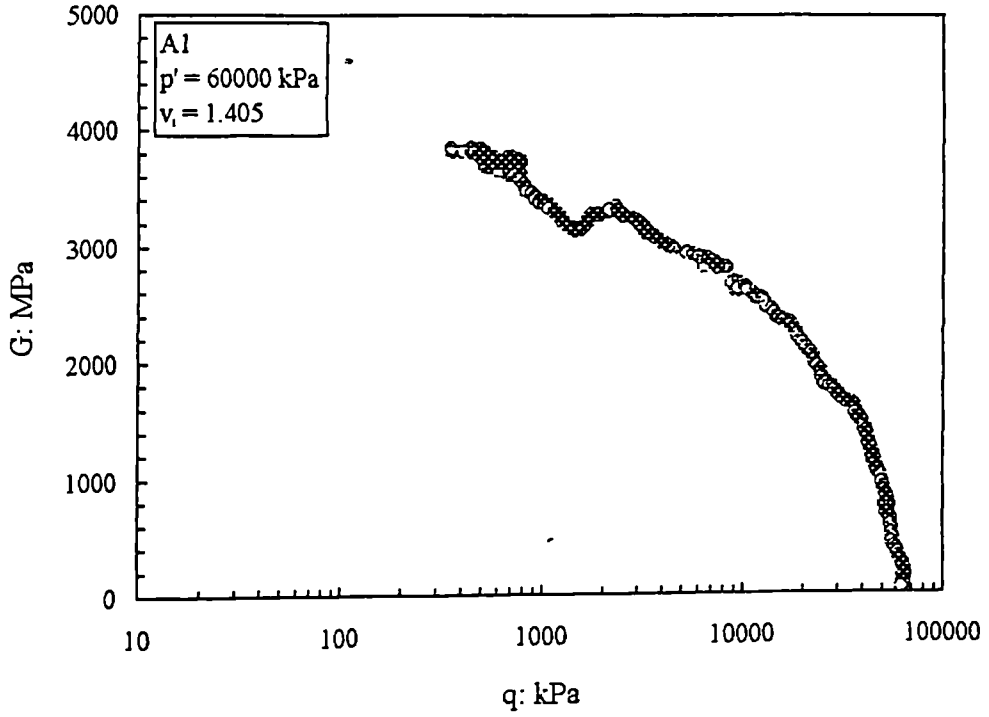

Figure 6.17 Tangent shear modulus as a function of deviator stress for a constant p' stress path tests performed at very high confining pressures.

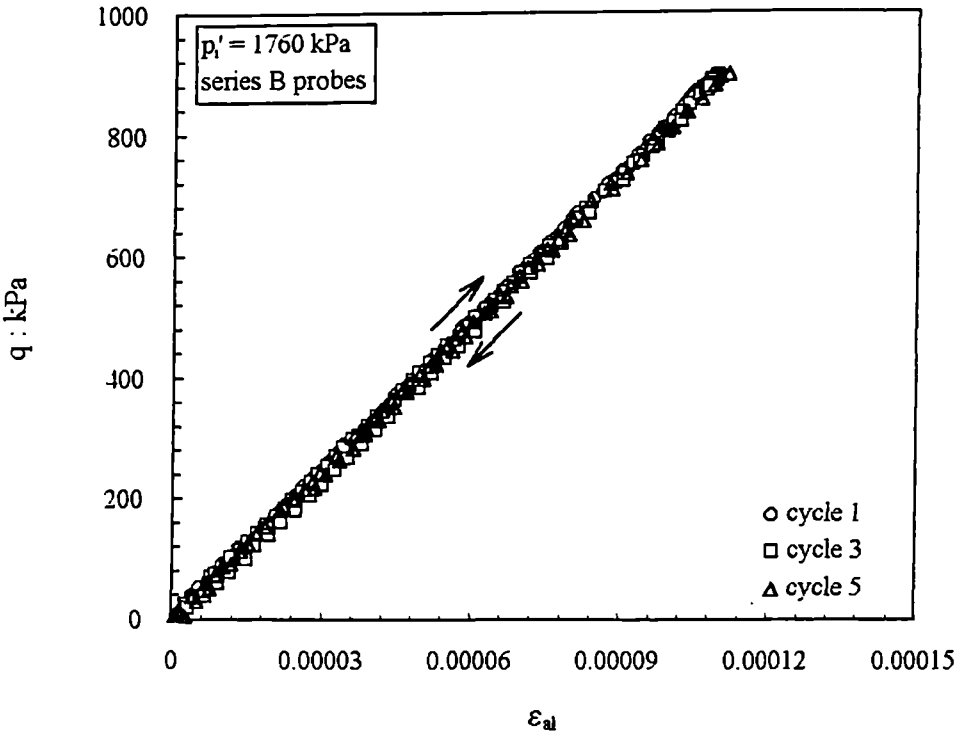

Figure 6.18 Pre-yield stress-strain relationships for undrained cycles performed on the silica sandstone.

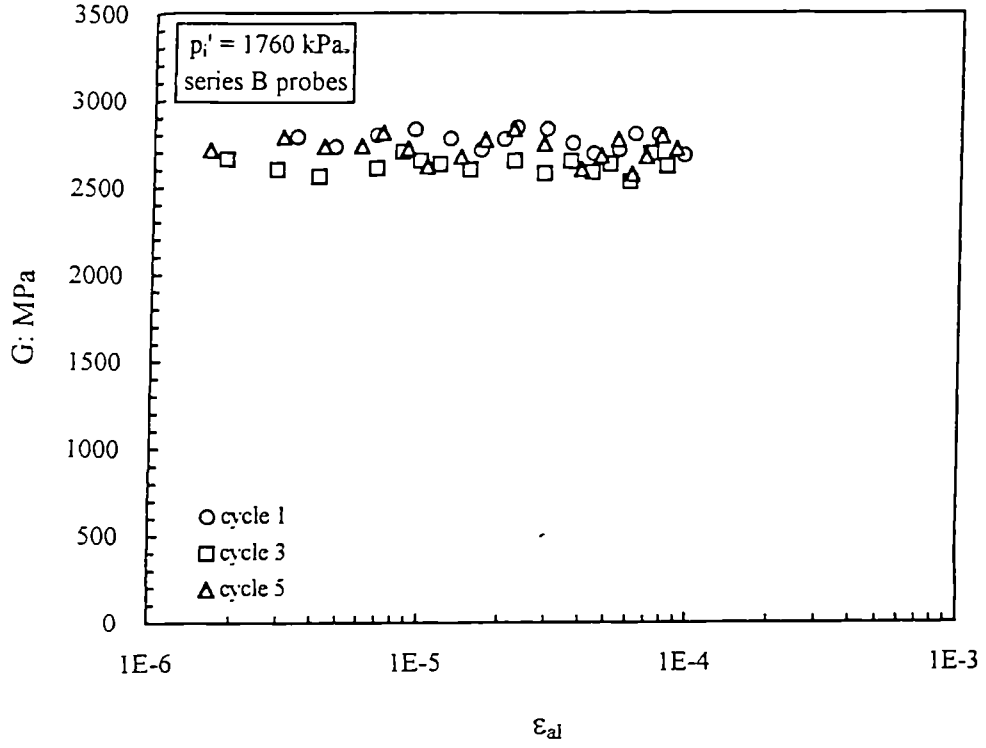

(a)

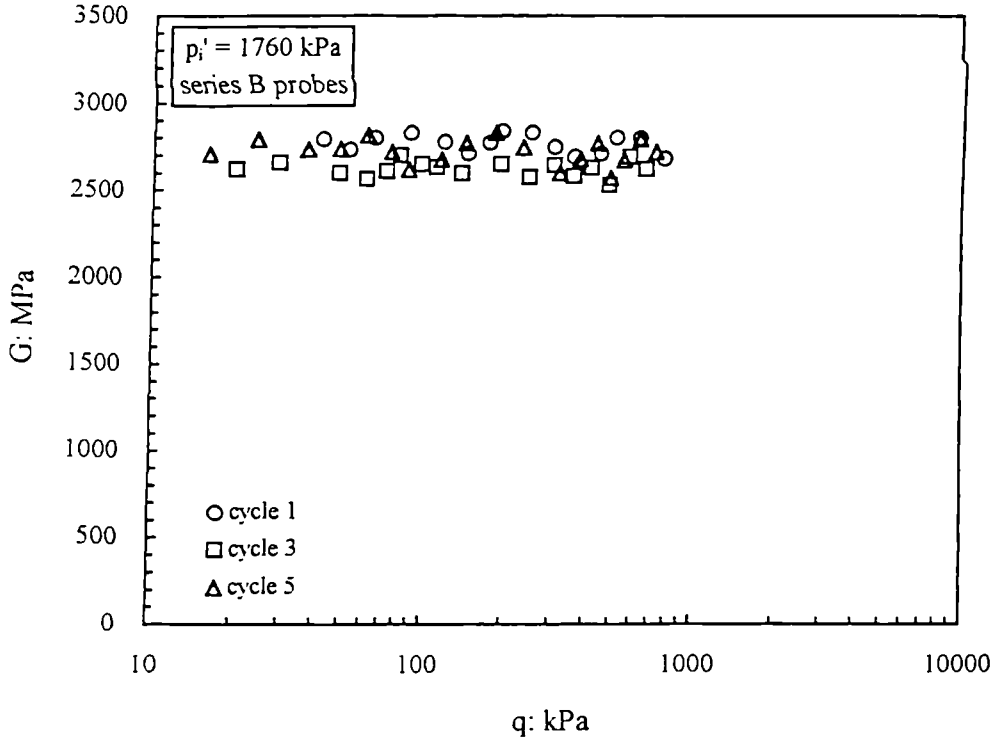

(b)

Figure 6.19 Tangent shear moduli as a function of (a) axial strain and (b) deviator stress obtained from undrained loading probes performed on the silica sandstone (q_{max} = 800 kPa).

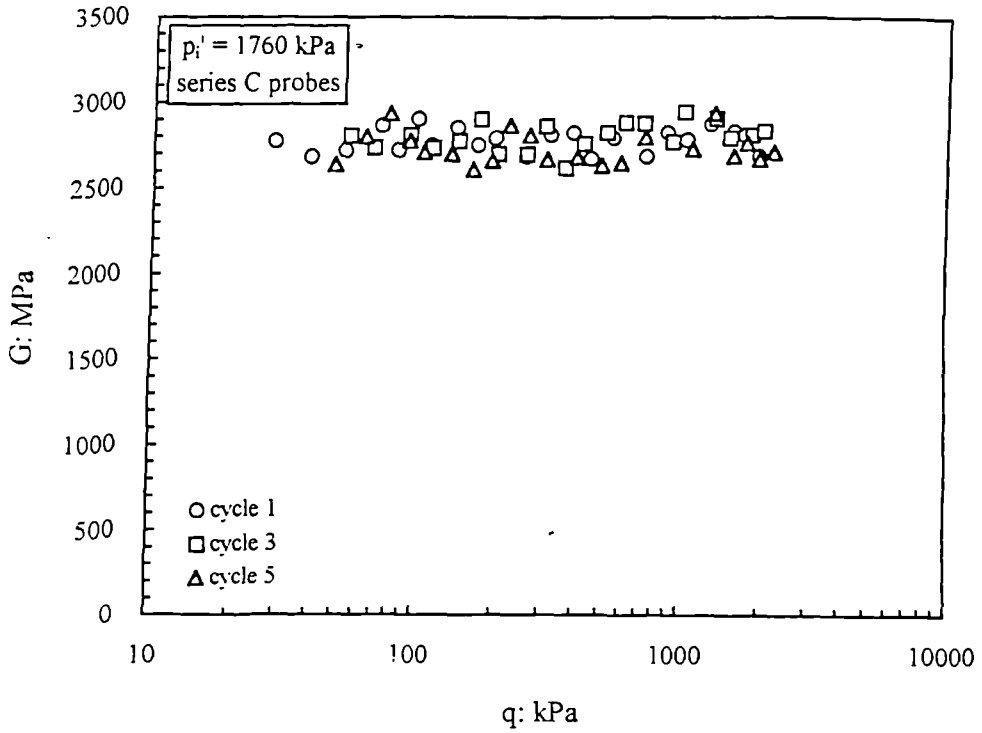

Figure 6.20 Tangent shear modulus from undrained probes performed on the silica sandstone (q_{max} = 2100 kPa).

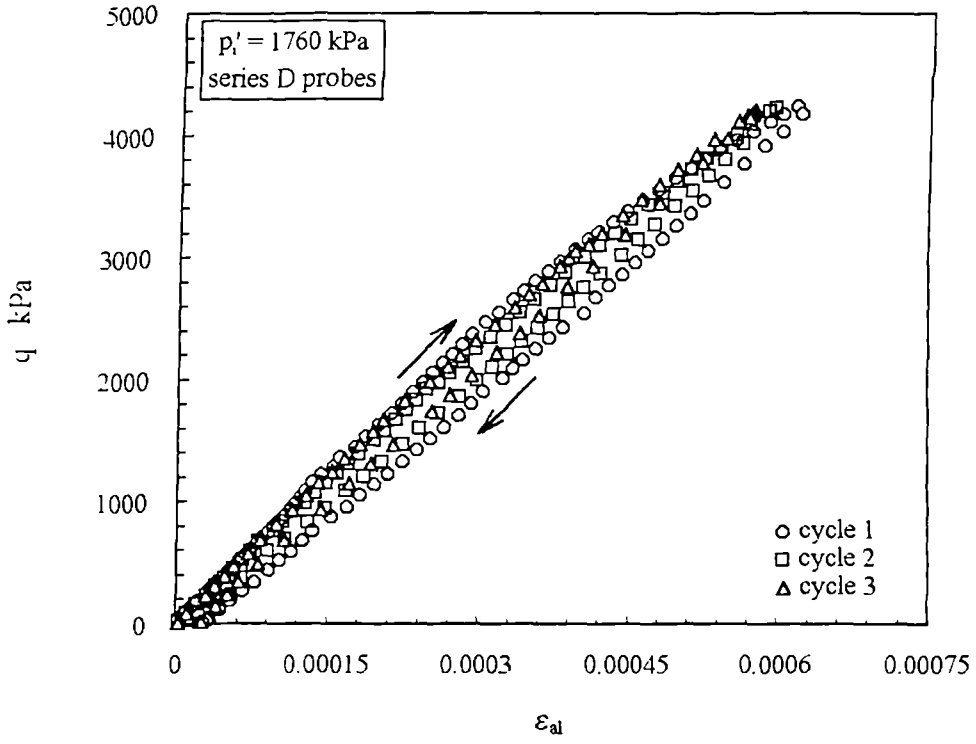

Figure 6.21 Stress-strain relationships from undrained loading probes performed on the silica sandstone (q_{max} = 4200 kPa).

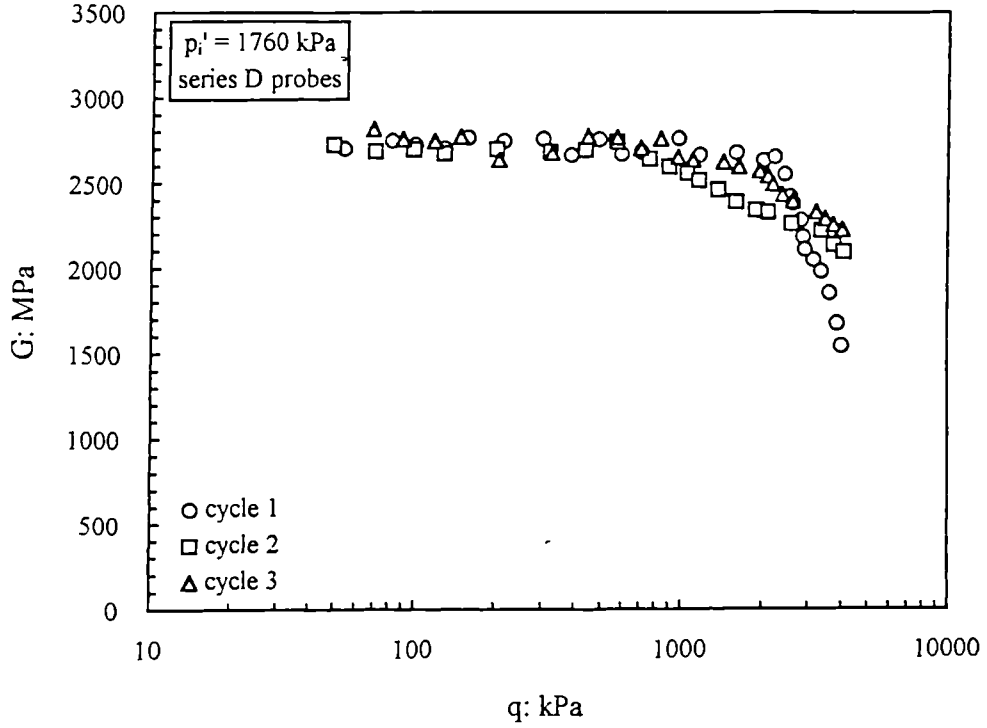

Figure 6.22 Tangent shear moduli from undrained loading probes performed on the silica sandstone (q_{max} = 4200 kPa).

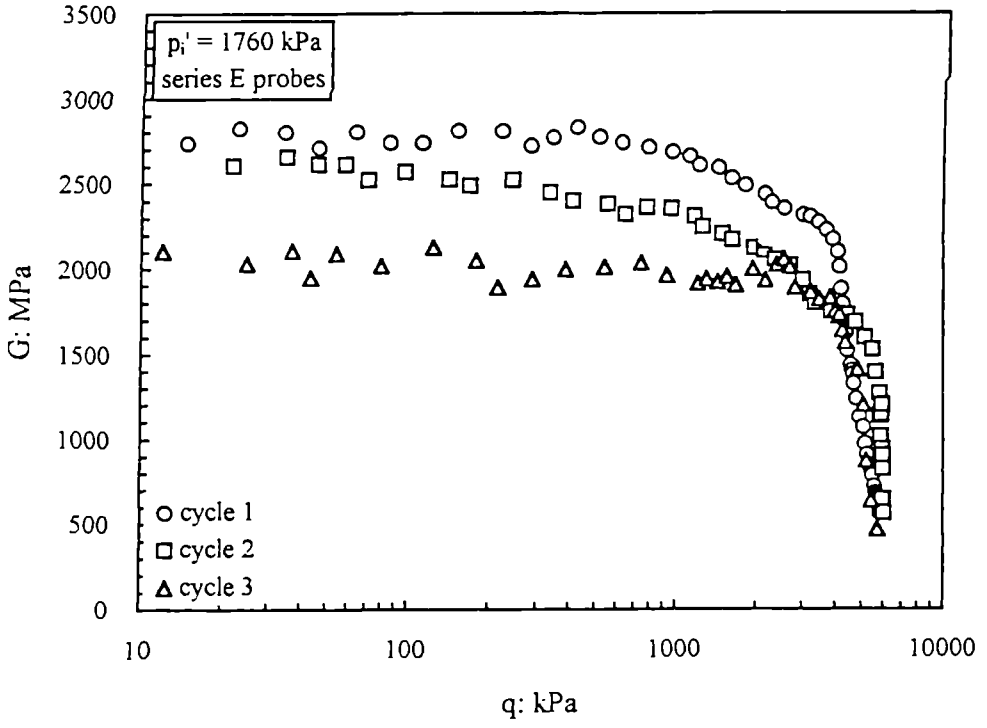

Figure 6.23 Tangent shear moduli from undrained probes performed on the silica sandstone (q_{max} = 6000 kPa).

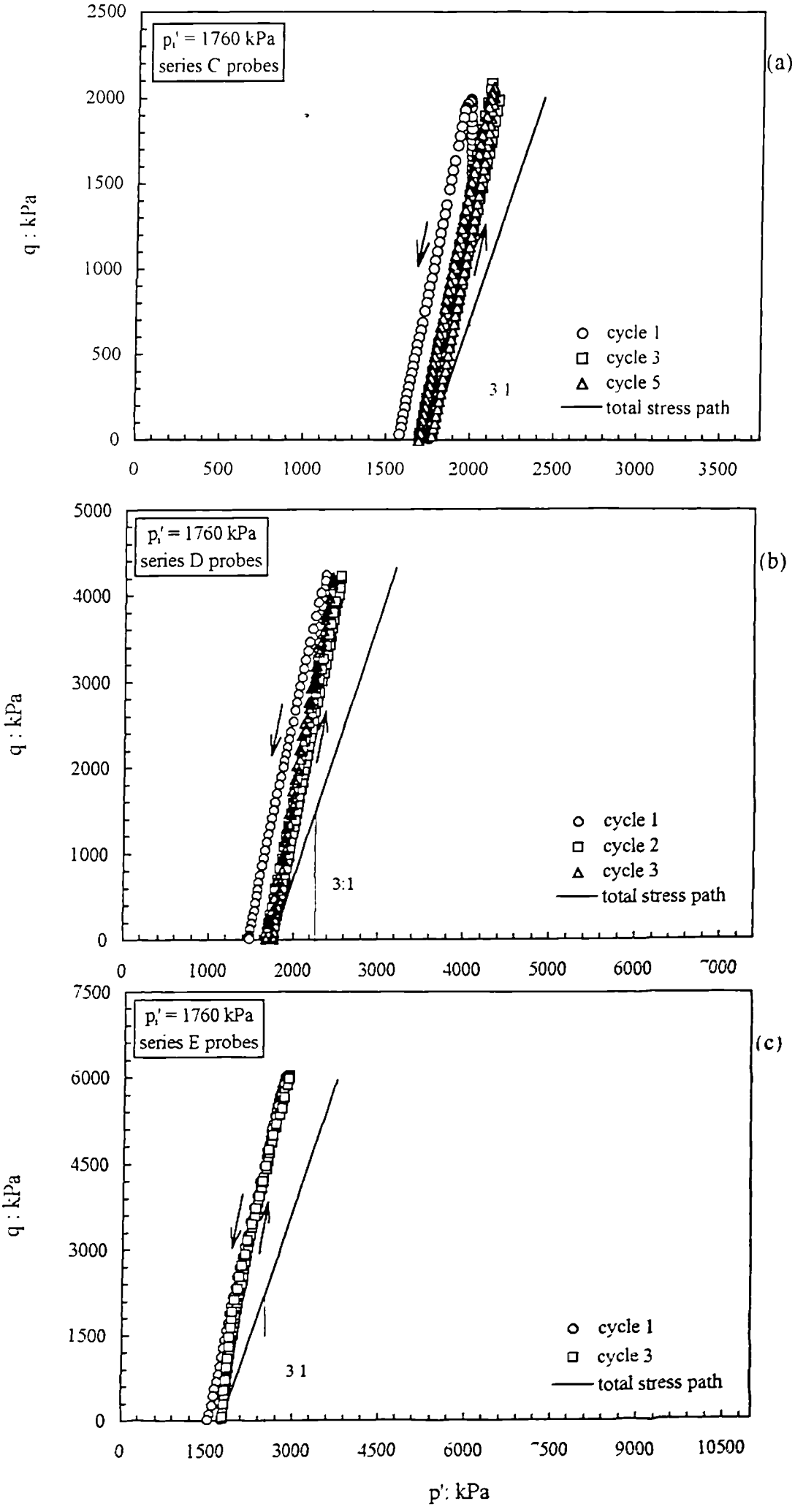

Figure 6.24 Effective stress paths for undrained cycles performed on the silica sandstone from the same isotropic state but up to different maximum deviator stresses.

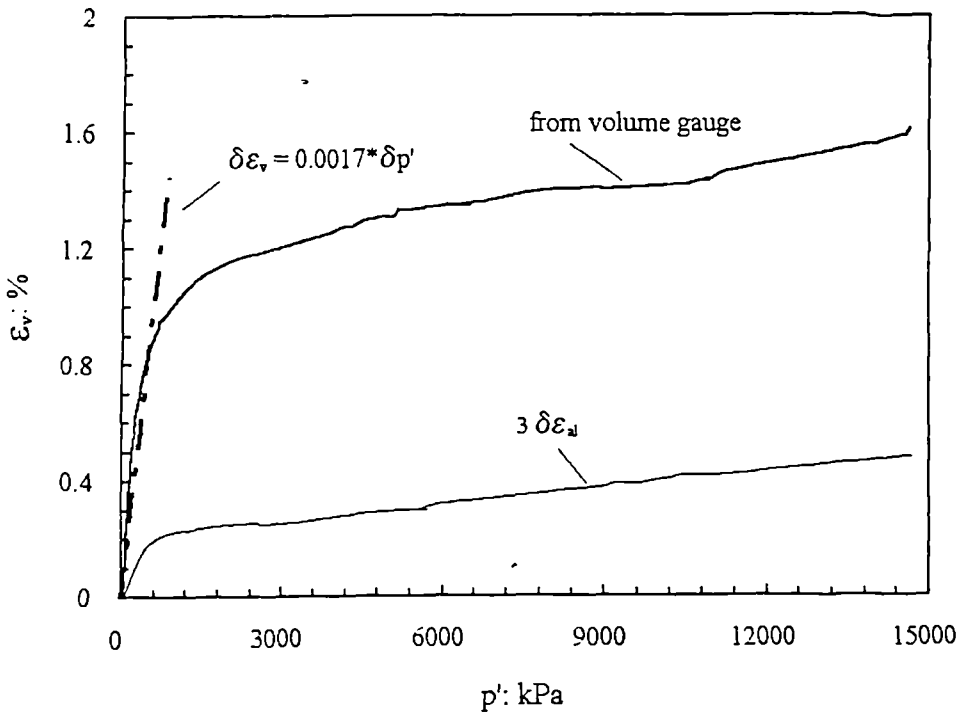

Figure 6.25 Comparison between the volumetric strains measured by the volume gauge and those determined from the local axial transducers in isotropic compression.

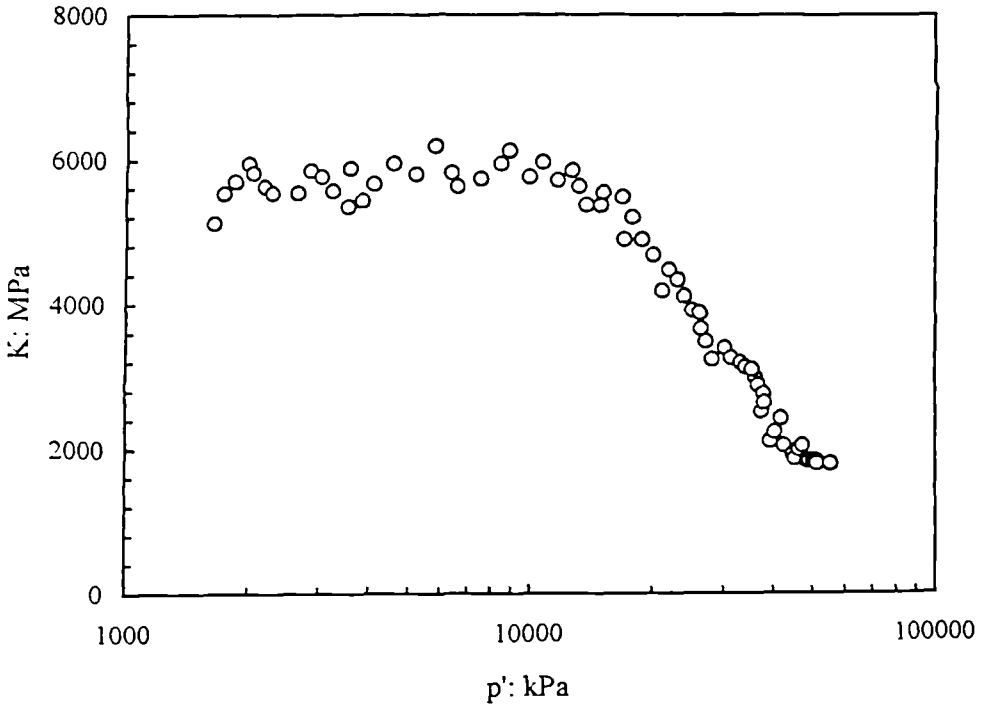

Figure 6.26 Variation of the bulk modulus of the silica sandstone with mean effective stress.

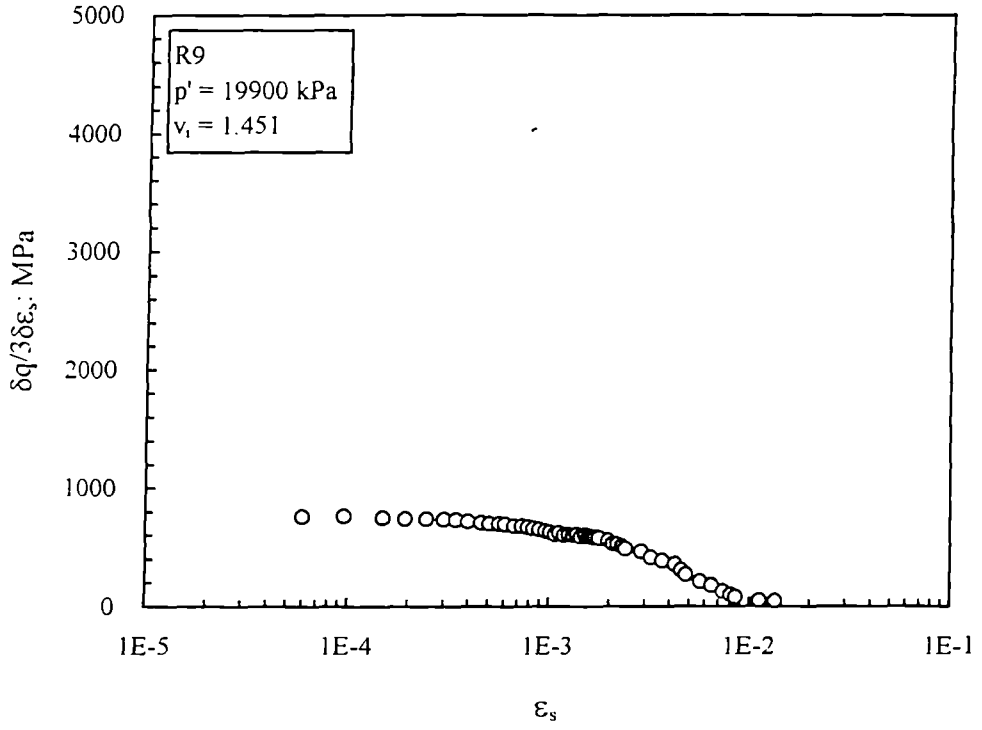

Figure 6.27 Tangent shear modulus as a function of shear strain for an overconsolidated reconstituted sample of the silica sandstone sheared at a constant value of p'.

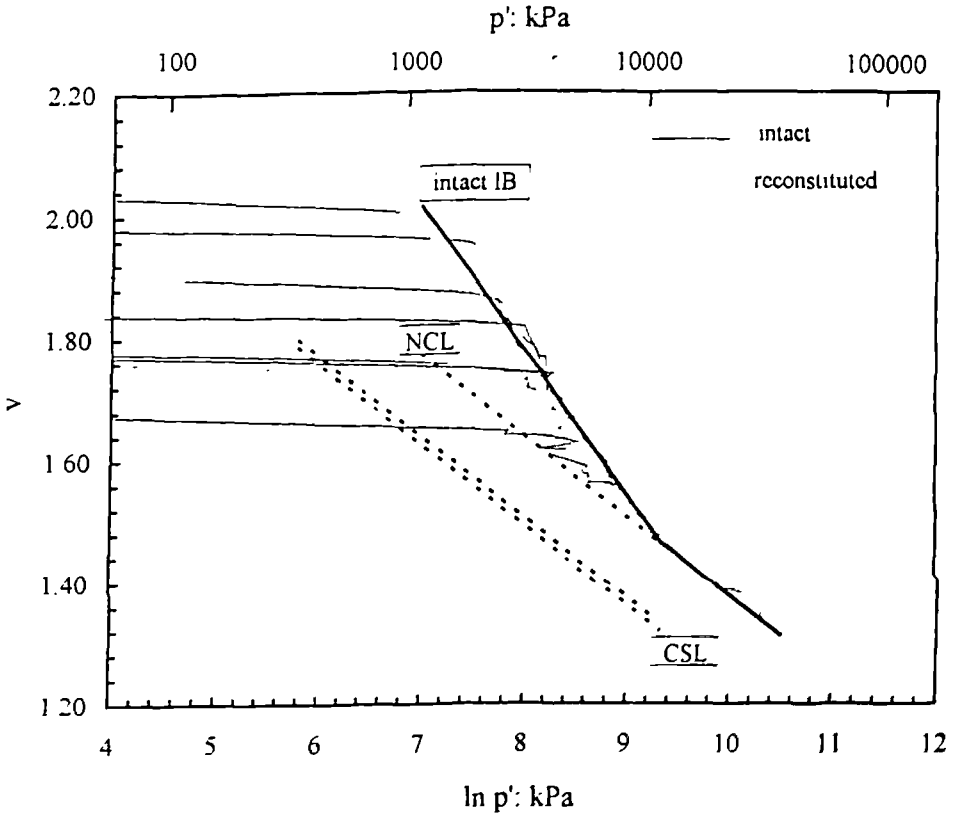

Figure 7.1 Isotropic boundary for the intact samples of calcarenite.

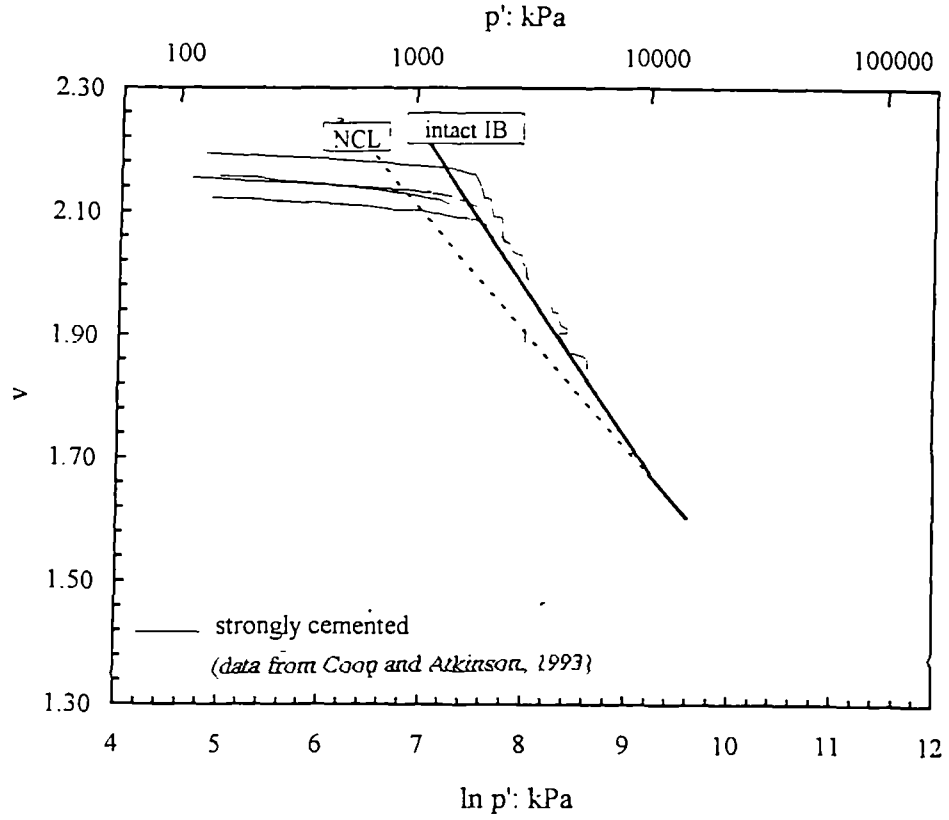

Figure 7.2 Isotropic boundary for the artificially cemented carbonate sand with strong bonding.

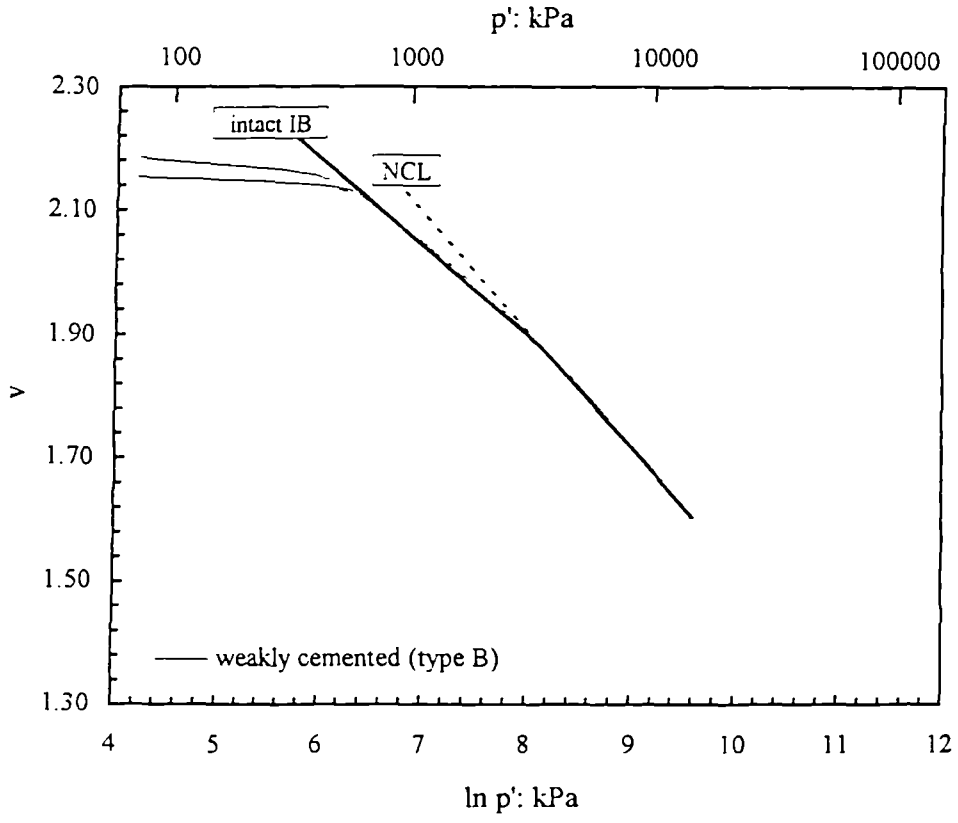

Figure 7.3 Isotropic boundary for the artificially cemented carbonate sand with weak bonding.

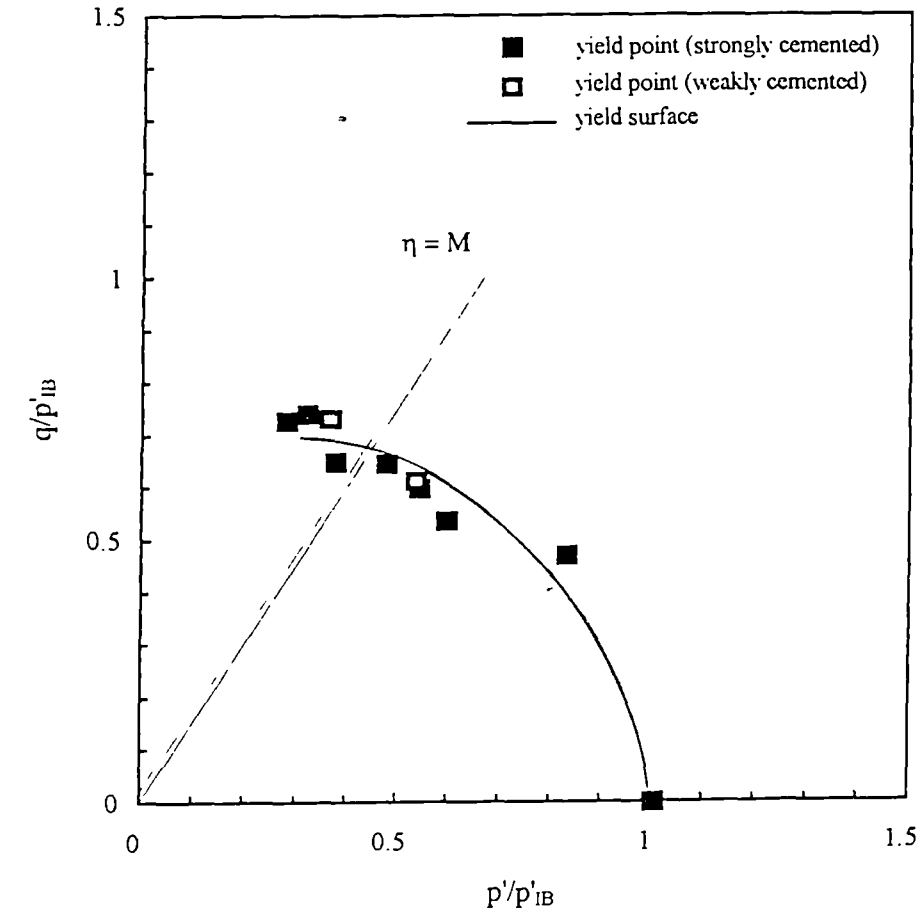

Figure 7.4 Yield surface for the artificially cemented carbonate sand.

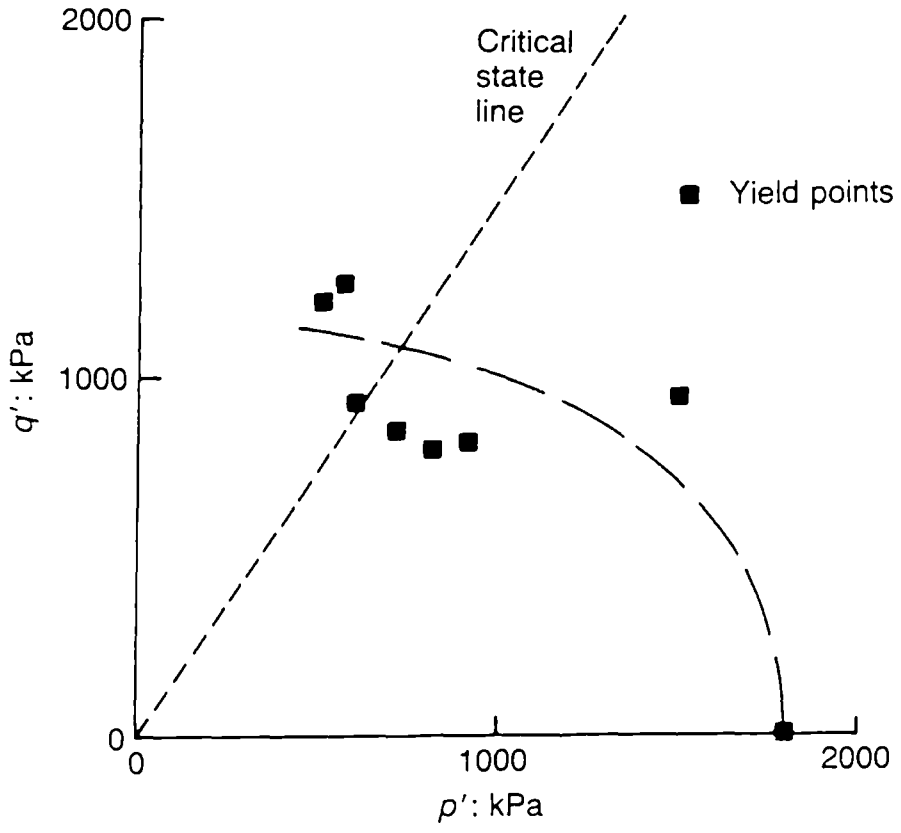

Figure 7.5 Stress states at yield for the artificially cemented carbonate sand with strong bonding (after Coop and Atkinson, 1993).

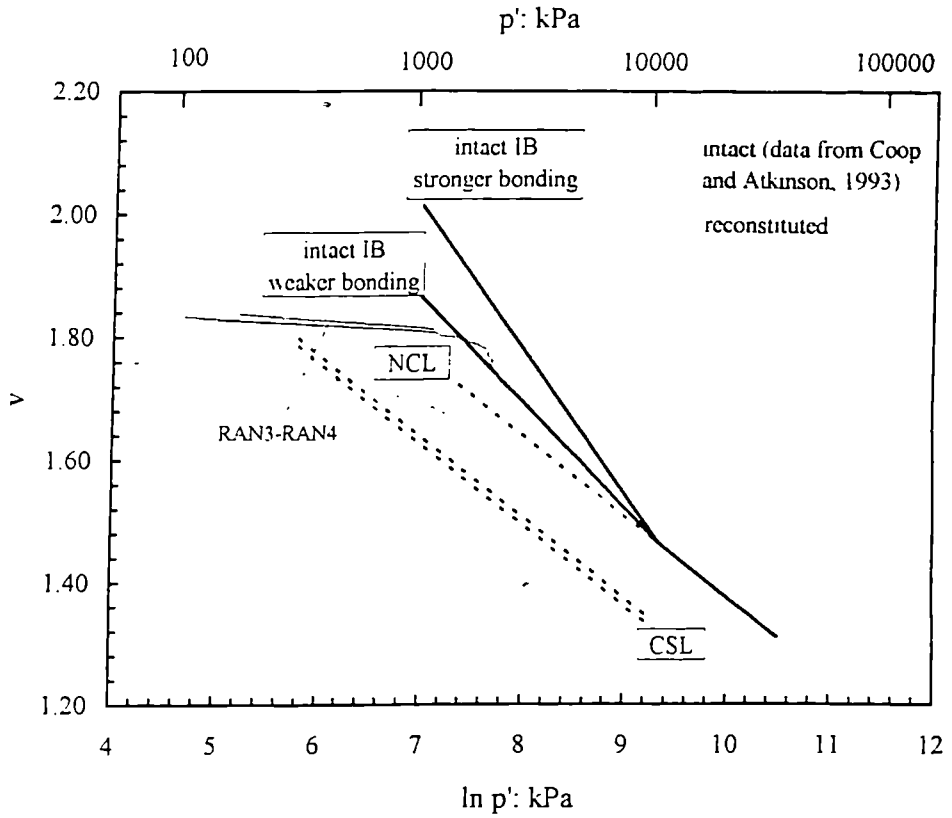

Figure 7.6 Isotropic boundary for the intact samples of calcarenite with weaker bonding.

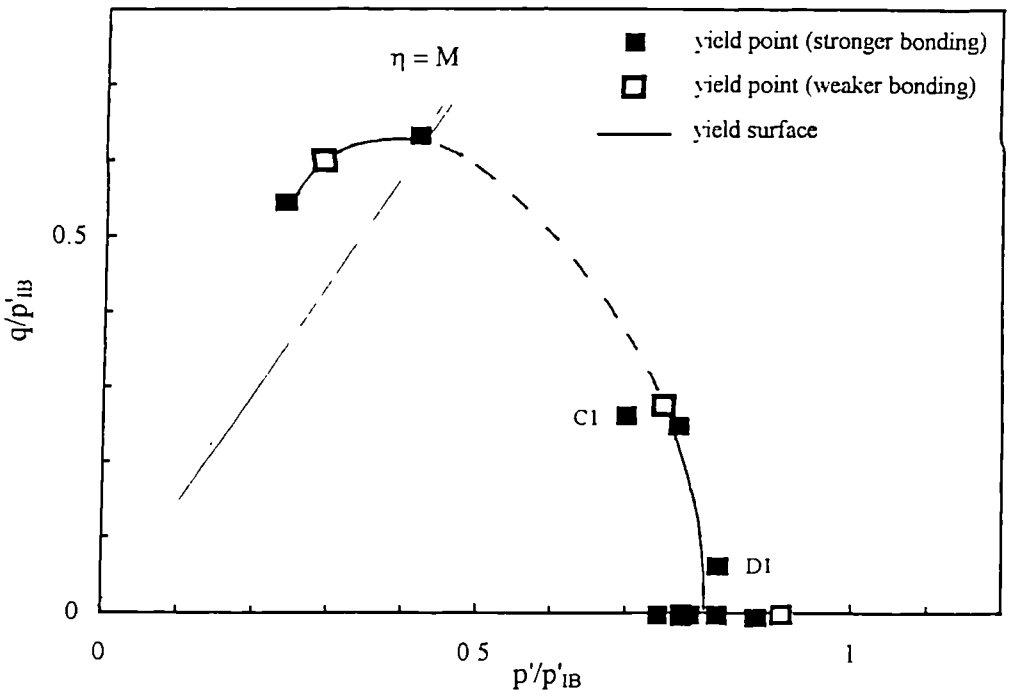

Figure 7.7 Yield surface for the calcarenite.

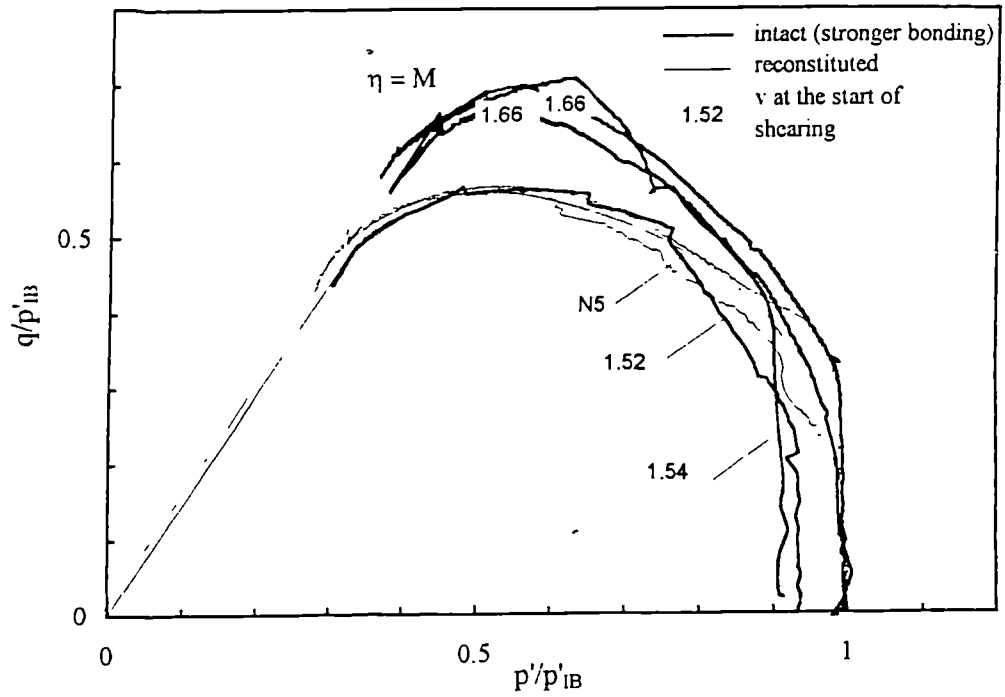

Figure 7.8a Normalized stress paths for reconstituted and intact samples of calcarenite with stronger bonding sheared after isotropic yielding.

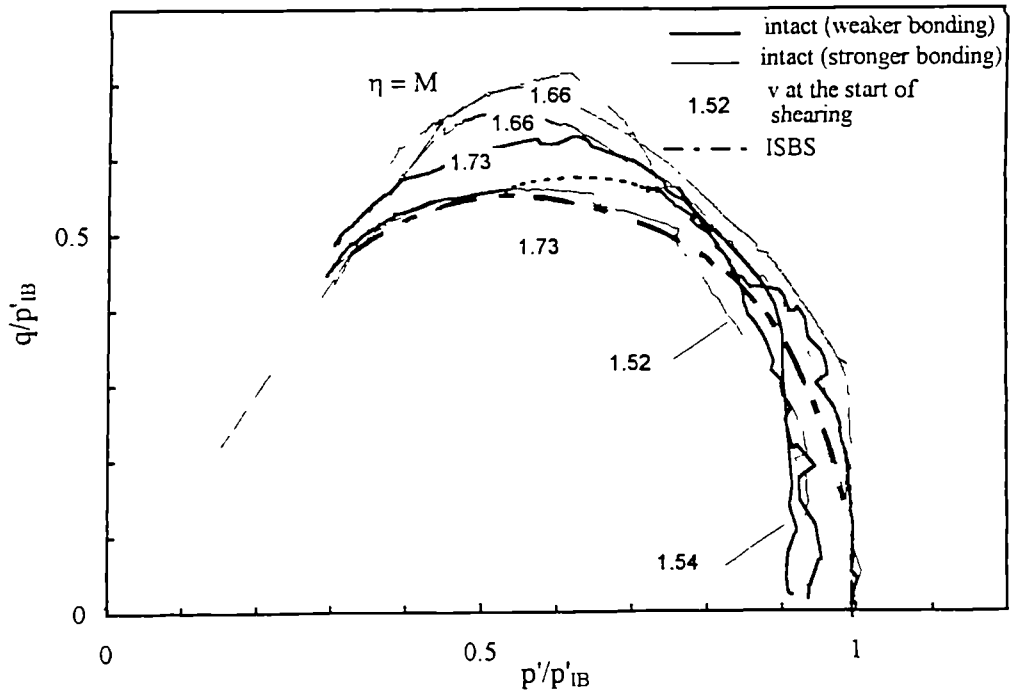

Figure 7.8b Normalized stress paths for intact samples of calcarenite with weaker and stronger bonding sheared after isotropic yielding.

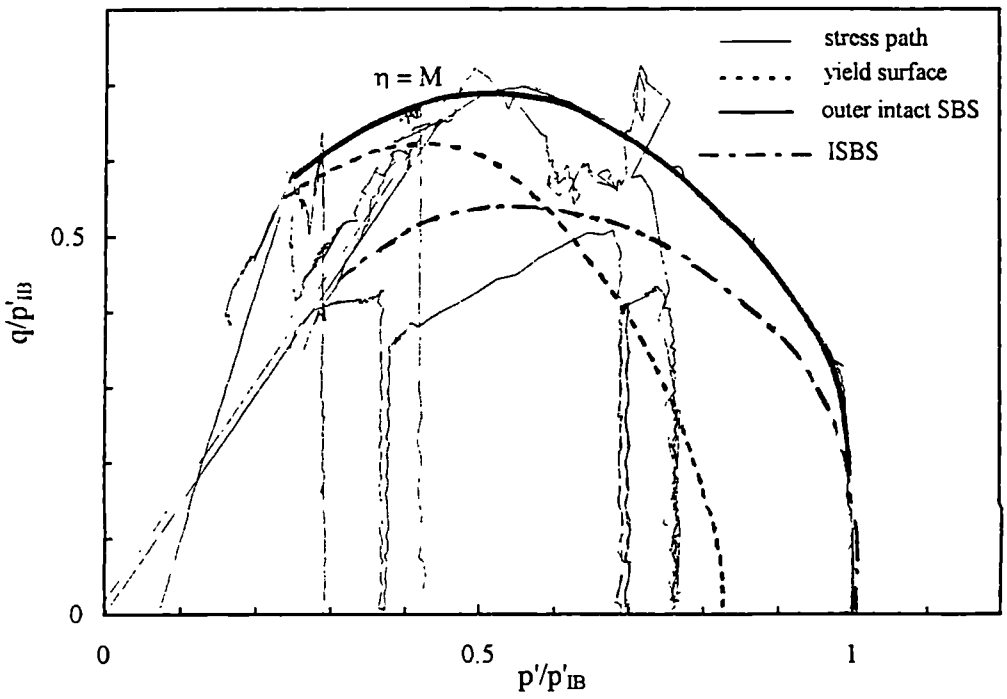

Figure 7.9 Shear behaviour of the calcarenite with identification of the yield surface, outer intact state boundary surface and intrinsic state boundary surface.

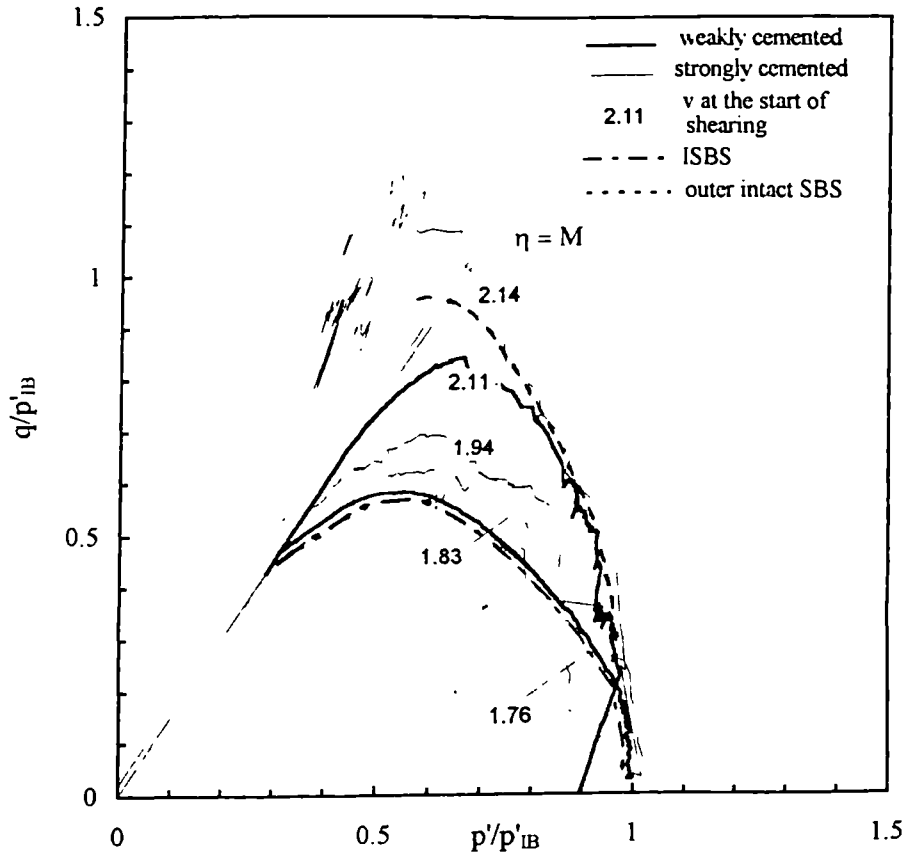

(a)

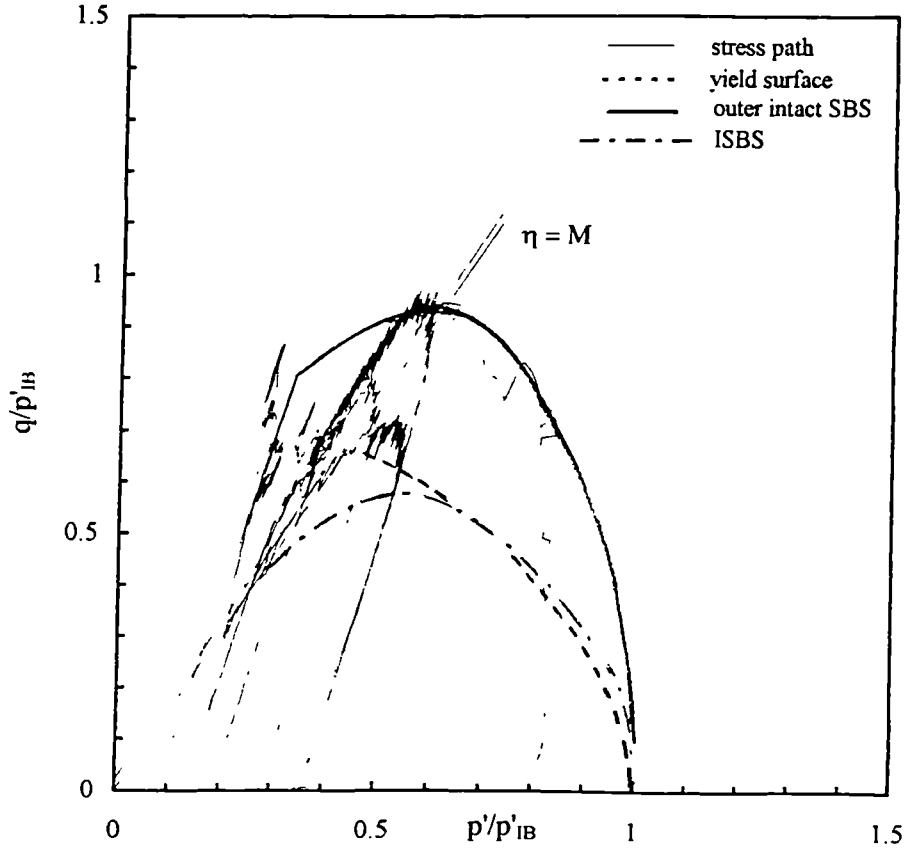

(b)

Figure 7.10 Shear behaviour of the artificially cemented carbonate sand: (a) normalized stress paths for samples sheared after isotropic yielding; (b) identification of the yield surface, outer intact state boundary surface and intrinsic state boundary surface.

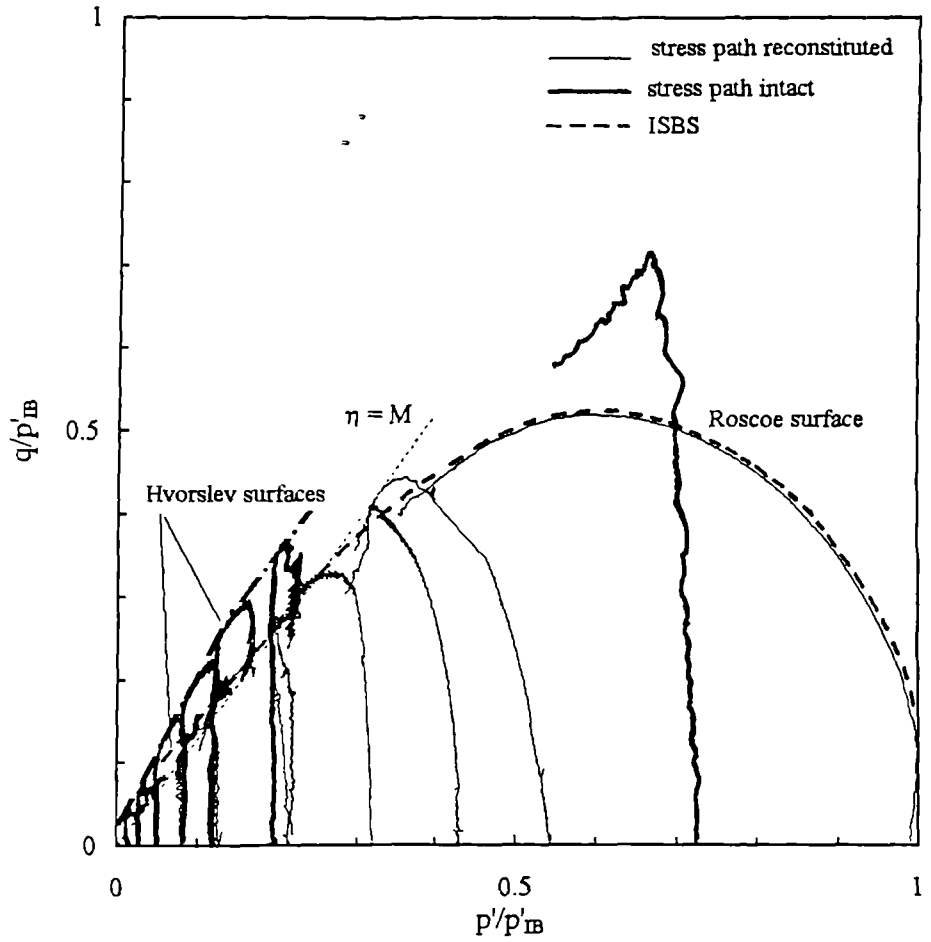

Figure 7.11 Normalized stress paths for intact and reconstituted samples of silica sandstone.

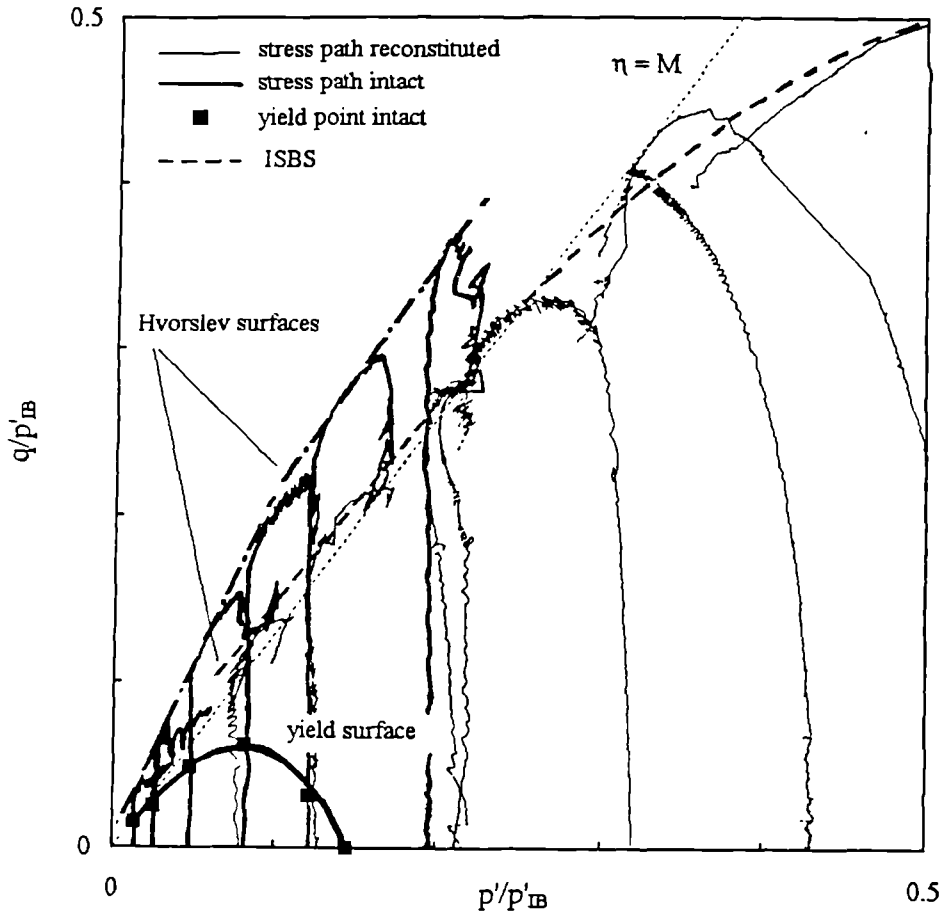

Figure 7.12 Magnification of Figure 7.11 showing the yield surface for the silica sandstone.

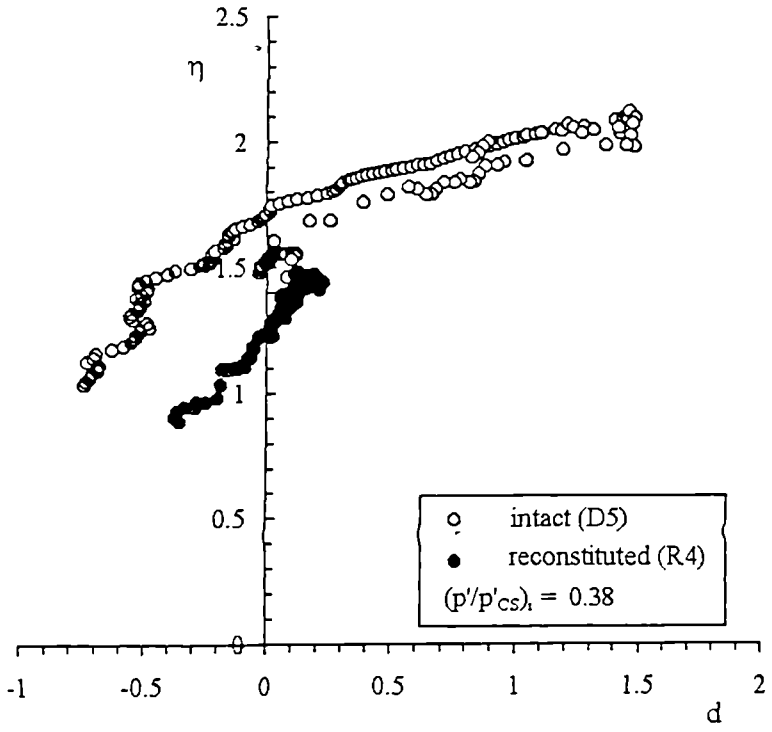

Figure 7.13 Stress-dilatancy relationships for constant p' tests performed on intact and reconstituted samples of silica sandstone with similar initial values of p'/p'_{cs}.

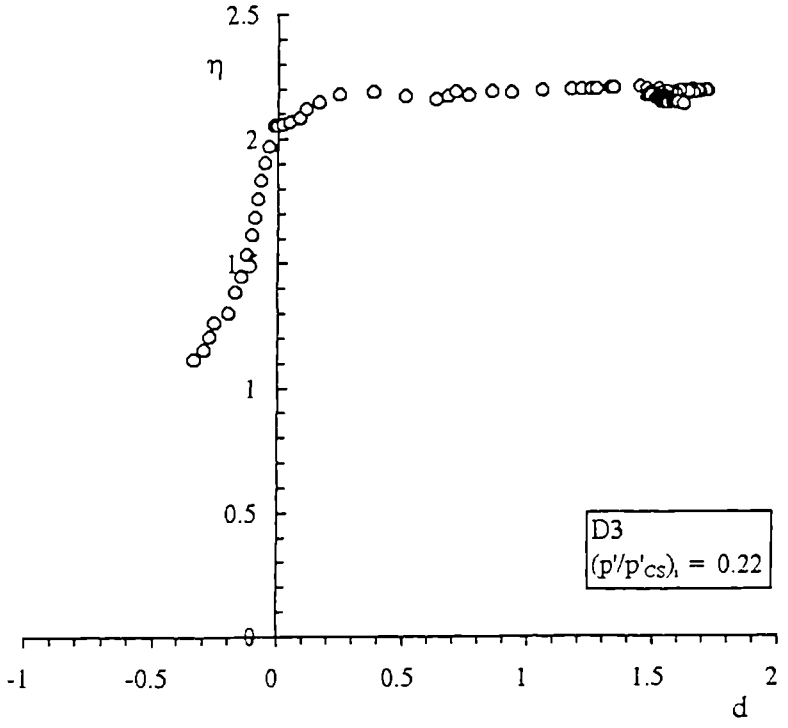

Figure 7.14 Stress-dilatancy relationship for an intact sample of silica sandstone sheared at a constant p' from a low value of p'/p'_{cs}.

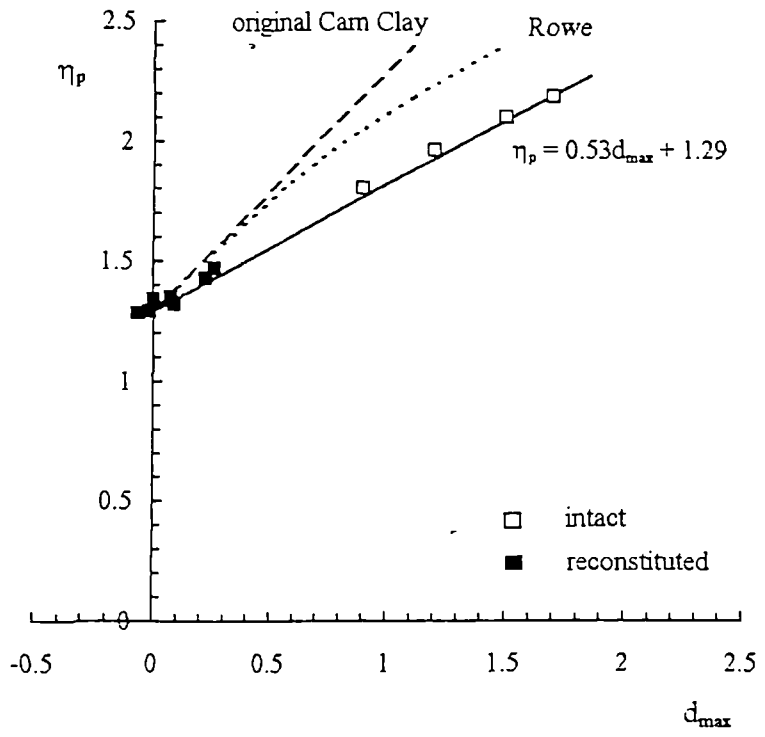

Figure 7.15 Peak stress ratio as function of maximum rate of dilation for intact and reconstituted silica sandstone.

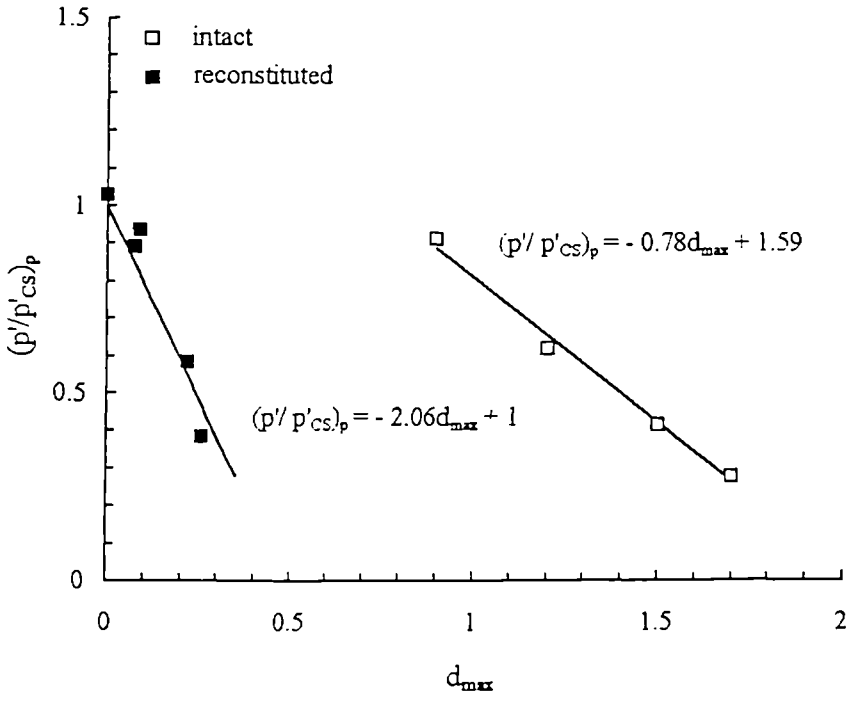

Figure 7.16 Normalized states at peak for reconstituted and intact samples of silica sandstone referred to the CSL of the reconstituted soil.

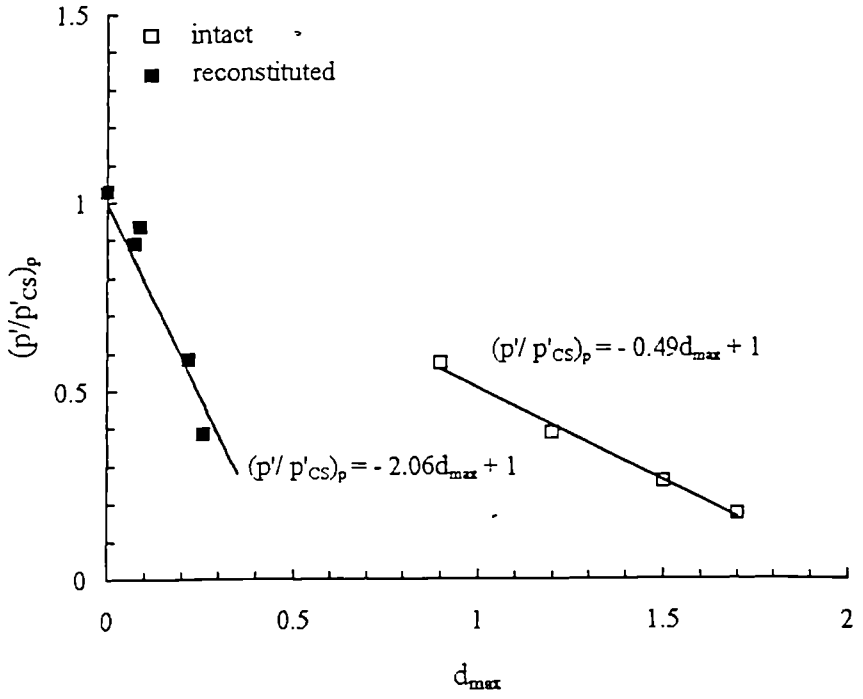

Figure 7.17 Normalized states at peak for reconstituted and intact samples of silica sandstone referred to the appropriate CSLs.

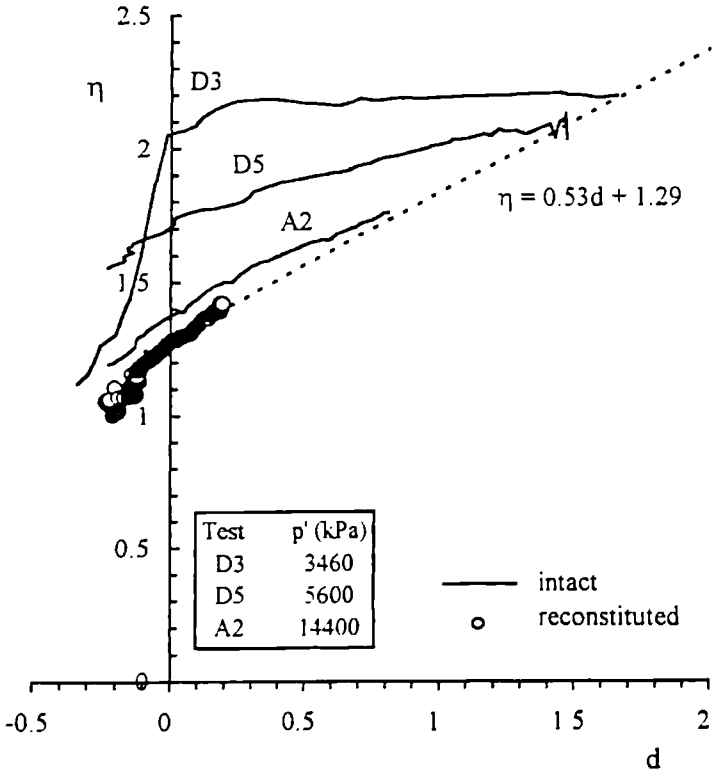

Figure 7.18 Comparison between the stress-dilatancy relationships of intact and reconstituted samples of silica sandstone sheared at different mean effective stresses.

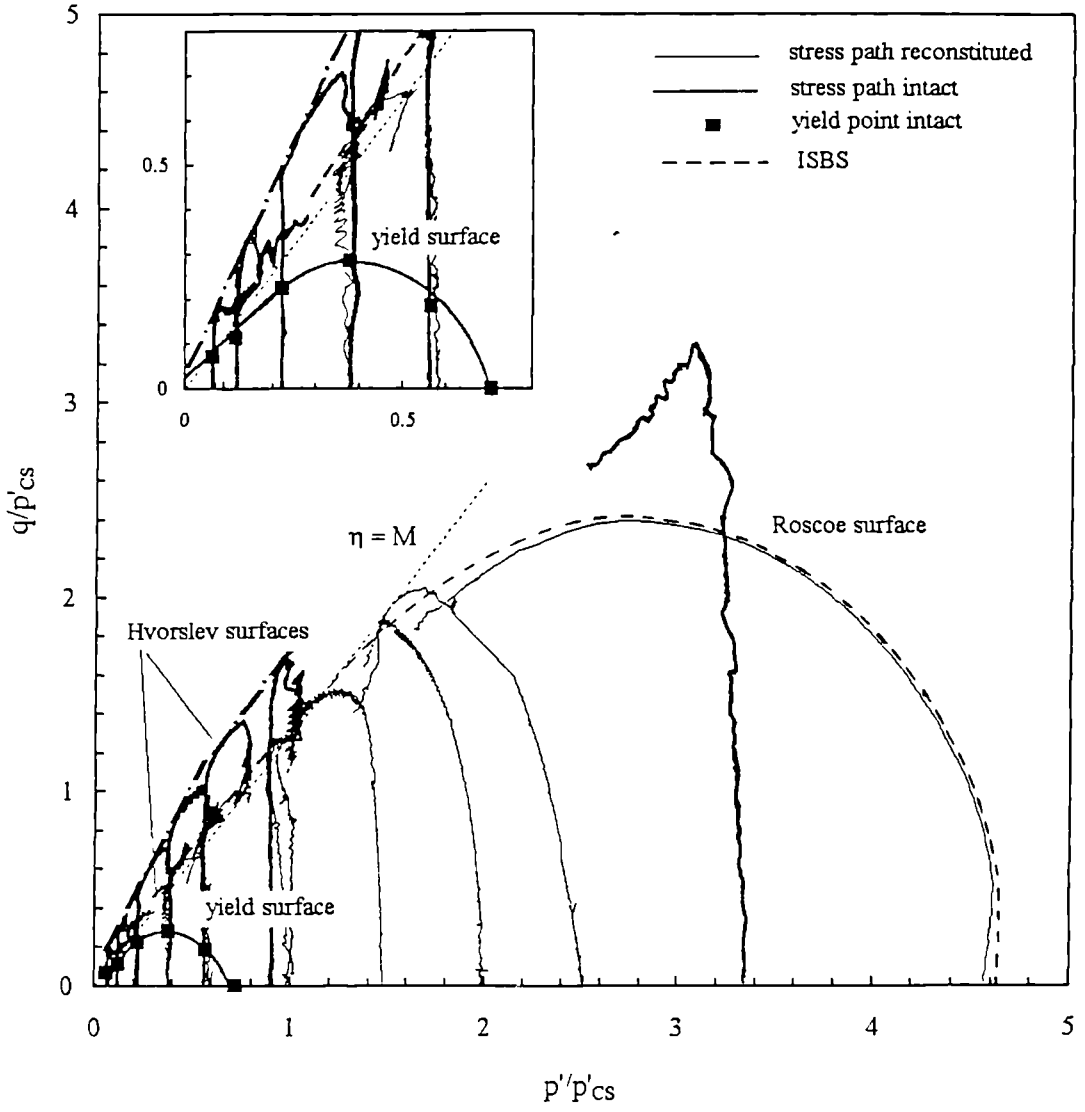

Figure 7.19 Shear behaviour of the reconstituted and intact silica sandstone referring the normalization of the intact soil to the CSL of the reconstituted soil.

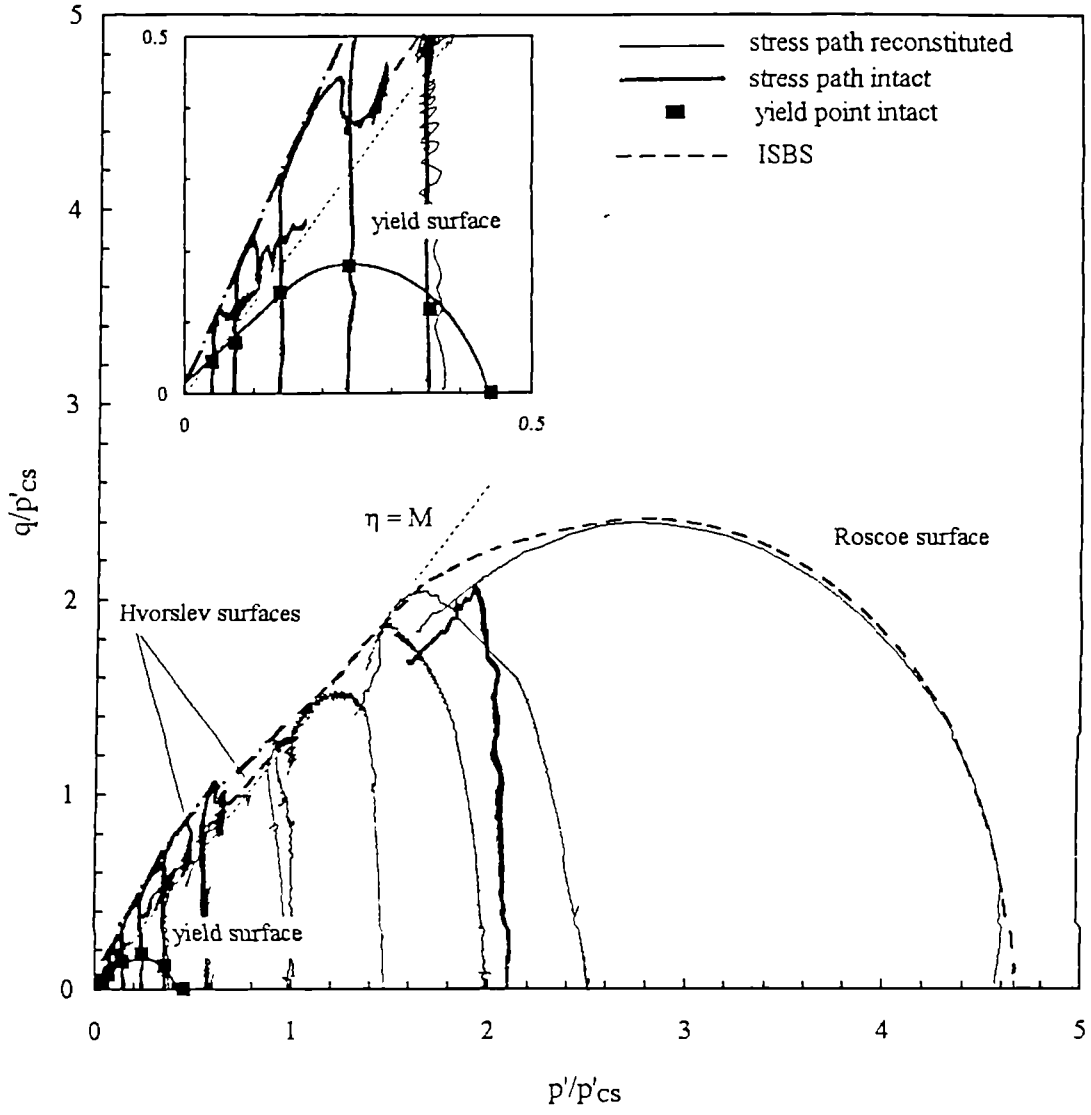

Figure 7.20 Shear behaviour of the reconstituted and intact silica sandstone referring the normalization of the intact soil to a CSL as indicated by Figure 7.16.

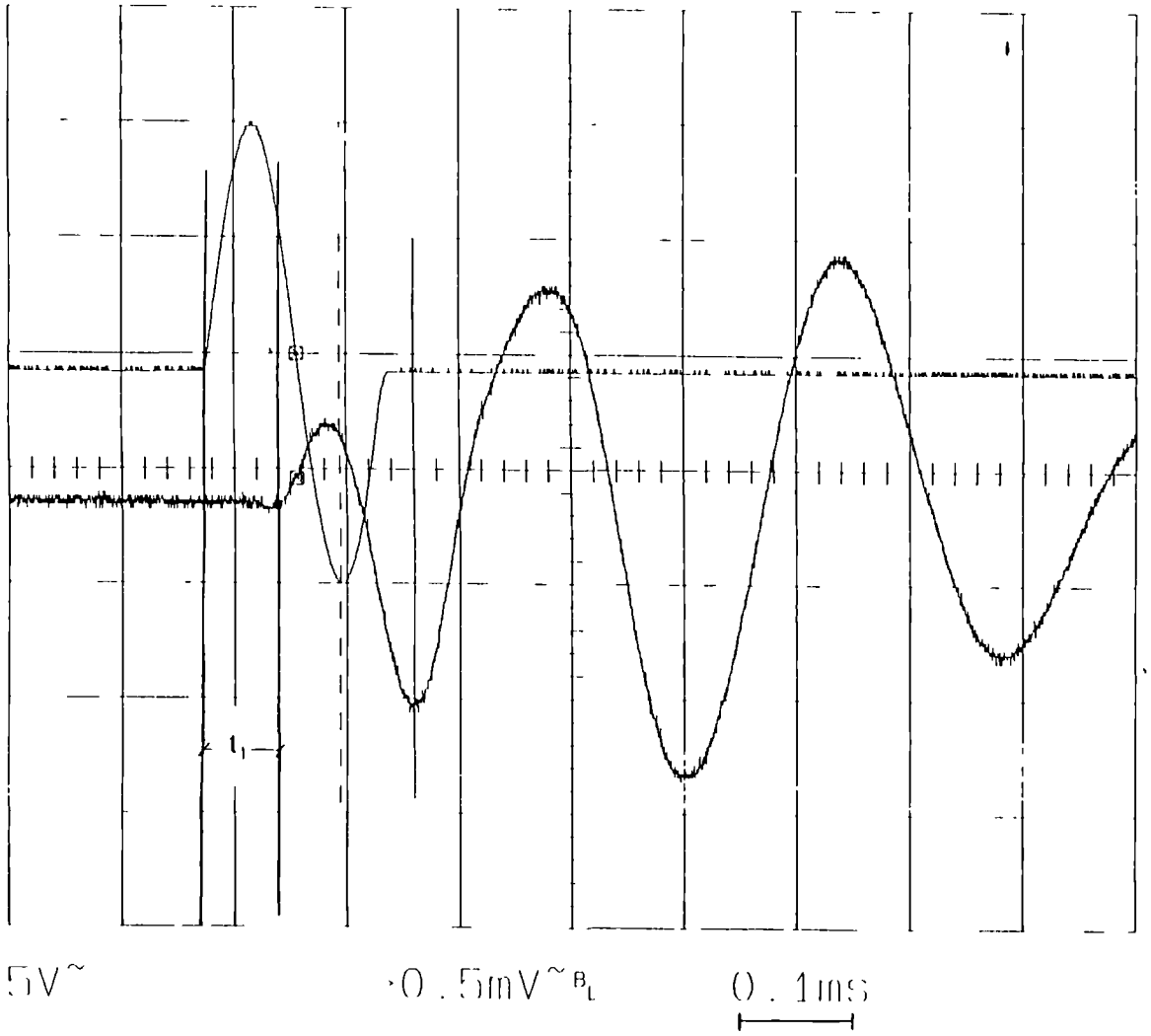

specific volume	1.45
specific gravity	2.66
density (ρ)	2144 Kg/m^3
sample hight	76.2x10^{-3} m
bender protrusion	3x10^{-3} m
First arrival t_1	64.9x10^{-6} s

$G_{max} = \rho V_s^2 = 2500$ MPa

where V_s is the shear wave velocity

Figure 7.21 Transmitter and receiver signals for a bender element test performed on the silica sandstone at low confining pressures.

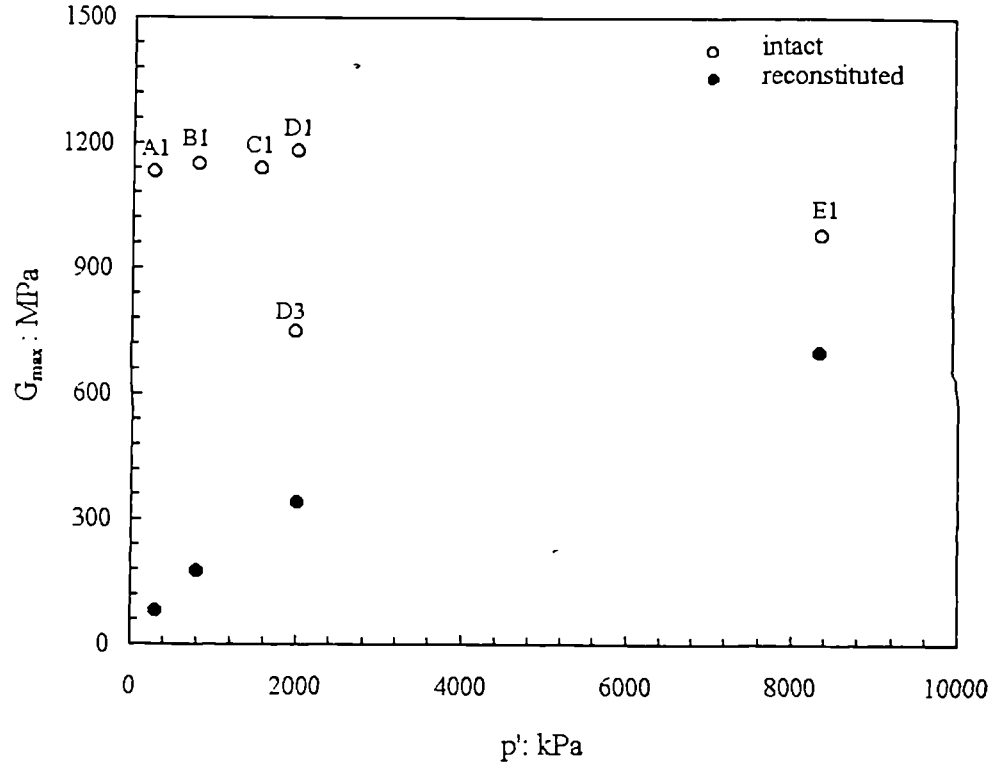

(a)

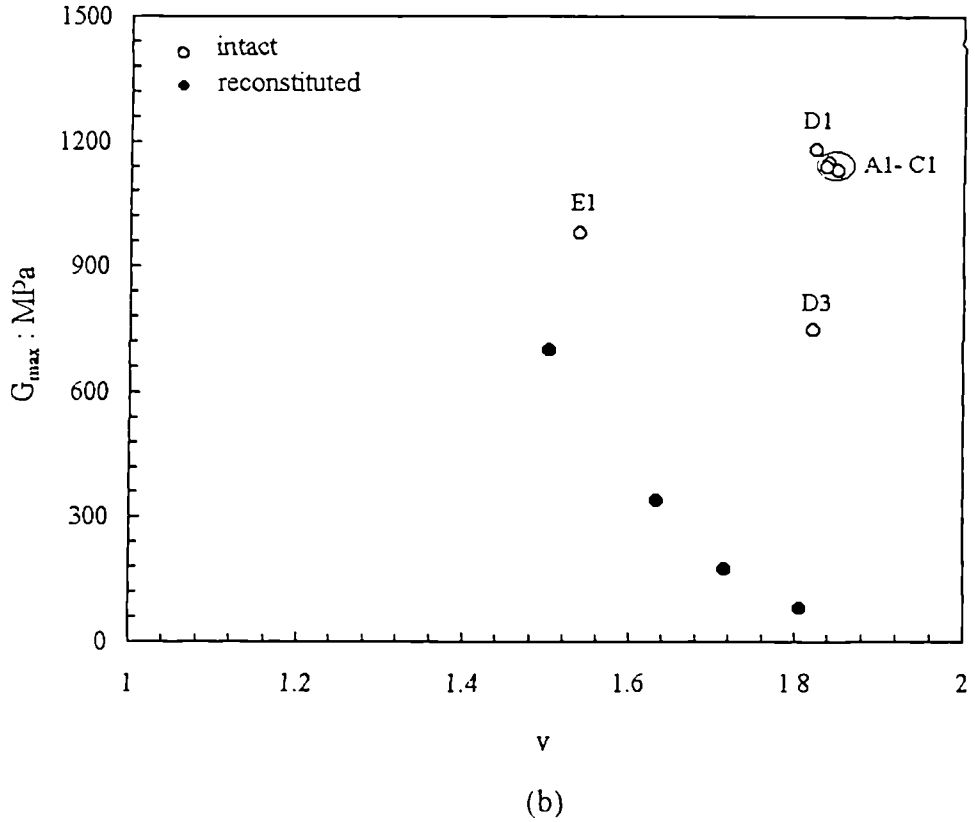

(b)

Figure 7.22 G_{max} for intact and reconstituted calcarenite as a function of (a) mean effective stress and (b) specific volume.

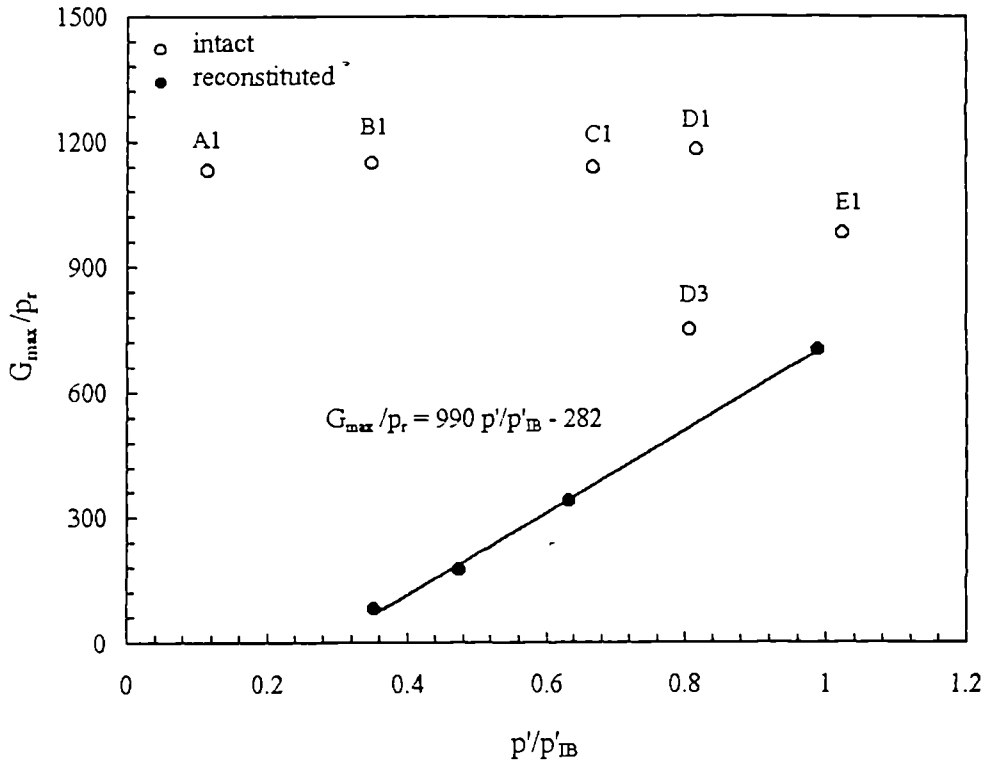

Figure 7.23 G_{max} for intact and reconstituted calcarenite as a function of the normalized state p'/p'_{IB}.

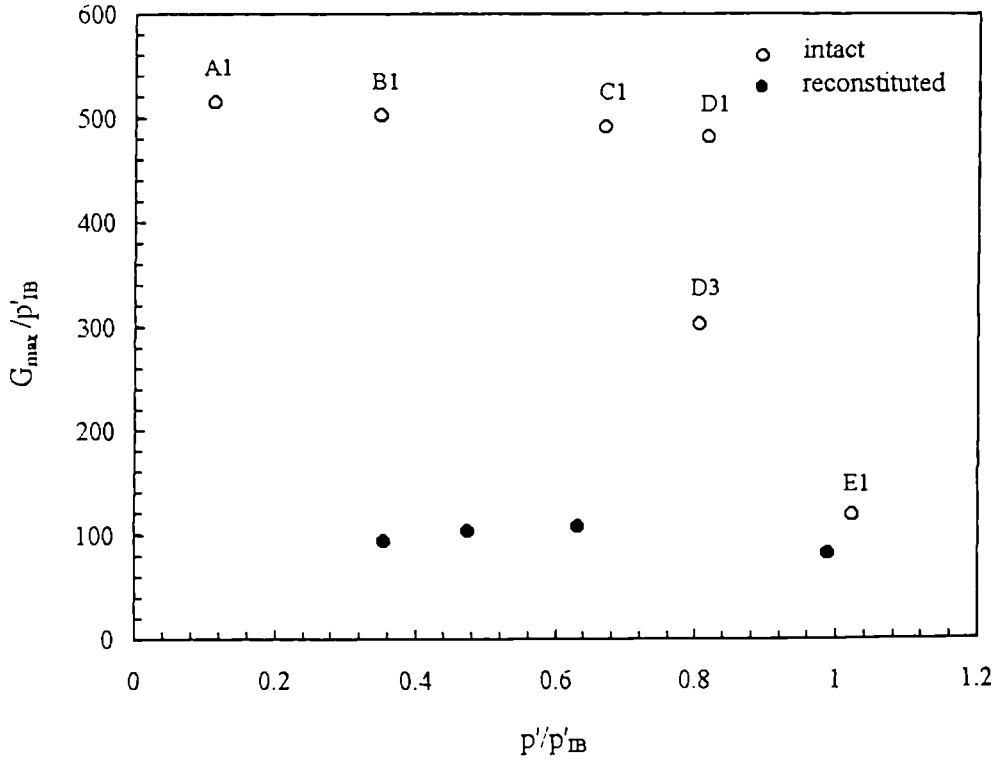

Figure 7.24 Comparison between the normalized maximum shear moduli of intact and reconstituted calcarenite as a function of the normalized state p'/p'_{IB}.